NMR Imaging Investigations of Swelling-Controlled Drug Delivery

by

Almira Blazek

B.Sc., University of Victoria, 1992

A thesis submitted in partial fulfilment of
the requirements for the degree of

Doctor of Philosophy

in

the Faculty of Graduate Studies
Department of Chemistry

We accept this thesis as conforming
to the required standard.

THE UNIVERSITY OF BRITISH COLUMBIA

July 31, 1998

In presenting this thesis in partial fulfilment of the requirements for an advanced degree at the University of British Columbia, I agree that the Library shall make it freely available for reference and study. I further agree that permission for extensive copying of this thesis for scholarly purposes may be granted by the head of my department or by his or her representatives. It is understood that copying or publication of this thesis for financial gain shall not be allowed without my written permission.

Department of CHEMISTRY

The University of British Columbia
Vancouver, Canada

Date Aug. 4 1998

DE-6 (2/88)

Abstract

Important current developments in pharmaceutical science are in the area of formulation technology where the ultimate goal is to control the rate and duration of drug release. Swelling-controlled drug delivery systems utilize the swelling of a hydrophilic polymer to control drug release. NMR spectroscopy and NMR imaging are presented as non-invasive and non-destructive techniques that can provide both chemical and spatial information during the swelling of such controlled release systems.

The tablet system chosen for this study contained hydroxypropylmethylcellulose (HPMC) as the hydrophilic polymer and one of two fluorinated compounds, trifluprom azine-HCl or 5-fluorouracil, as model drugs. The geometry for the tablet swelling was chosen to simplify the system to one where the transport processes were one-dimensional. Water distributions were determined by one-dimensional ^{1}H NMR imaging. HPMC distributions were not measured directly but were calculated from the calibration of the T_2 relaxation times of the water as a function of HPMC concentration. The presence of air bubbles in the swollen tablet resulted in experimentally determined polymer distributions which contained up to 45% more HPMC than the known weight of HPMC in the tablet. When the air in the tablet was removed under vacuum prior to the imaging experiment, the total weight of HPMC from the experimental distributions was much closer to the actual weight of HPMC in the tablet.

The comparison of the polymer distribution and the drug distributions, obtained from one-dimensional ^{19}F NMR imaging investigations of tablets containing model drugs, showed that most of the trifluprom azine-HCl remained within the swollen polymer tablet while more of the 5-fluorouracil was able to escape. The critical condition for drug release

from the tablet was the relationship between the diffusivity of the drug and the expansion rate of the tablet. For trifluprom azine-HCl, the required rate of diffusion was not reached until the region of tablet erosion. In contrast, the diffusion coefficient of 5-fluorouracil in 30% HPMC was large enough that the drug diffused faster than the polymer expanded.

Preliminary modelling calculations assuming Fickian diffusion and a segmented-tablet model were performed.

Contents

List of Tables

List of Figures

List of Abbreviations

5flu	5-Fluorouracil
FID	Free Induction Decay
G	Gauss
HPMC	2-Hydroxypropylmethylcellulose
i.d.	inner diameter
MRI	Magnetic Resonance Imaging
NMR	Nuclear Magnetic Resonance
o.d.	outer diameter
rf	radiofrequency
$\mathbf{T}_E$	The time-to-echo in a spin-echo pulse sequence, the time from the middle of the 90° pulse to the maximum amplitude of the echo.
TGA	Thermal Gravimetric Analysis
$\mathbf{T}_R$	The repetition time, the delay between repeats of an NMR experiment.
triflu	Triflupromazine-HCl

Acknowledgments

I would like to extend my gratitude to Prof. Colin A. Fyfe for the opportunity to join his research group and work with NMR. His guidance and support during the course of my Ph. D. research and the preparation of this thesis have been invaluable. I also wish to thank Drs. Hiltrud Grondey, Stephanie Isbell and Zhiming Mei for their knowledge and patience during the early stages of my research.

I wish to thank the members of the Electrical and Mechanical Engineering Services at UBC Chemistry, especially Mr. Tom Markus and Mr. Oskar Greiner, for their much needed assistance. Dr. Ping Gao of UpJohn-Pharmacia is thanked for the gift of the HPMC and Dr. Robert Miller and Mr. Randy Oates of the Department of Pharmaceutical Sciences are thanked for their help with the preparation of the HPMC tablets. I would also like to thank Dr. Mark Welsh of Retrologic Systems for developing software (listed in Appendix A.2) which greatly reduced the time spent on data processing.

I wish to thank the past and present members of the Fyfe group for making my time at UBC memorable. The past few years would not have been as much fun without their friendship and support. I also appreciate the support of friends, many of whom have completed or are in the process of completing their own Ph. D. programs.

I thank my mother, Maria, and my two brothers, Robert and Dennis, for their love and support throughout my academic career. My greatest thanks go to Mark, my best friend since the day we met, who has always encouraged me to be my best.

Chapter 1

Introduction

1.1 Controlled Release Formulations

1.1.1 Advantages of Controlled Drug Release

Oral ingestion of solid dosage forms such as tablets and capsules has historically been the most convenient and commonly used mode of drug delivery [1, 2]. In the 1980s, for example, more than half of the $200 billion US drug market consisted of solid oral dosage forms [1]. The many reasons drugs are given in tablet and capsule form rather than as a liquid include the ease of use by the patient, the predetermined unit dose of the drug, the greater stability of the drug in the solid versus the liquid state and the relative ease, when necessary, of protecting the drug from the stomach or *vice versa* through the use of coatings [2]. Although easy to administer, these dosage forms are still only effective when used properly. A 1979 study estimated that 50% of the 1.8 billion prescription medications dispensed annually in the US are not taken correctly [3]. Such noncompliance with instructions has a negative impact on the treatment outcomes and may result in disease complications that lead to hospitalization or even death [4].

The negative effects associated with incorrect use of medications are related to the overdose-underdose cycle of drug concentration that conventional, rapid-release formulations produce in the body [1, 2, 5, 6]. After ingestion of the solid dosage form, the drug concentration in the body increases rapidly, in some cases to a toxic level. As the drug is consumed or de-activated by the body, the concentration decreases and enters the range where the therapeutic effects of the drug are observed. The drug concentration continually

decreases and eventually drops below therapeutic levels, rendering the drug treatment ineffective. At this time another dose is required and the cycle begins again. As can be seen in Figure 1.1, the drug levels in the body depend strongly on the regularity of the dosing. Infrequent dosing would decrease the effectiveness of the drug if the concentrations are not maintained at therapeutic levels while too-frequent dosing would lead to highly toxic drug levels resulting in harmful effects. The dosing profile will vary for different medications depending on the biological half-life of the drug. One negative aspect of conventional drug delivery is the inability to use agents that are degraded too quickly by the body. Conventional methods result in the exclusion of a large number of attractive synthetic drugs and almost the entire family of mammalian biochemicals [2].

Within the past 30 years pharmaceutical research has become increasingly focussed on the development of novel systems for drug delivery that overcome the disadvantages of conventional methods of drug treatment. A controlled release device, designed to release enough drug initially to reach therapeutic levels and then continue releasing at a constant rate to replace used or de-activated drug, would reduce or eliminate the overdose-underdose cycle in the drug concentration and maximize the efficiency of the drug. Targetted or site-specific release in the body would also improve the efficiency of treatment and limit drug exposure to unnecessary areas that may result in side-effects [1, 5]. Also, controlled release devices provide a protective barrier to the metabolic processes in the body, thus enabling the delivery of the short half-life drugs that were previously unusable with conventional methods. In addition, new delivery methods may circumvent the oral administration route for drugs and provide constant drug release from implantable devices.

The use of controlled release formulations in disease treatment provides several advantages over rapid-release counterparts. Patients generally exhibit fewer side effects because the drug concentrations are kept under the toxic levels that cause adverse reactions [1, 5, 7]. The disease treatment is often more effective because therapeutic drug levels are maintained for longer periods of time compared to conventional methods [1, 5, 7]. Also, the activity of a drug can be extended throughout the night allowing the patient to sleep

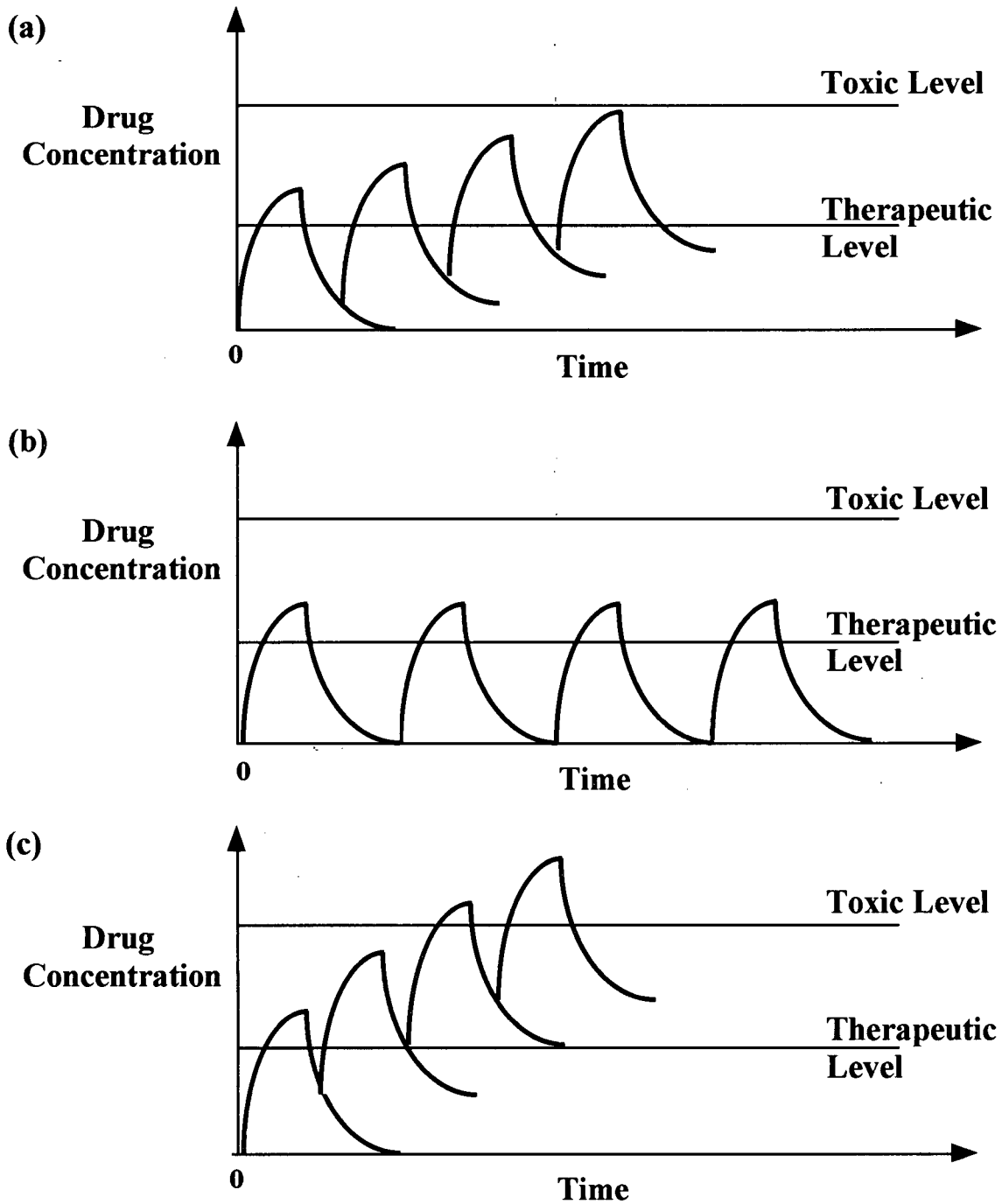

Figure 1.1: The variation of drug concentrations in the body with conventional drug delivery methods. Four hypothetical doses are administered at (a) the prescribed intervals, (b) longer intervals and (c) shorter intervals. The beneficial effects are observed when the drug concentration remains in the therapeutic range as in (a) and (c). However, harmful effects are observed when the drug concentration reaches toxic levels as in (c).

undisturbed [7]. The decrease in the frequency of dosing, from tablets every few hours for conventional medication to typically one daily dose with a controlled release formulation, leads to better patient compliance with the medication regimen [1, 5]. Also, the development of implantable devices for a particular medication removes the issue of patient compliance altogether.

Controlled release technology also provides potential economic benefits for the pharmaceutical industry, the patient, and the healthcare system. Although the development of a controlled release formulation is typically more costly than a conventional formulation, improving the efficiency of a current drug is generally less expensive than developing an entirely new one [8]. The ability to maintain market share and prolong the effective period of patent protection for a given drug by reformulation of the drug as a controlled release or targetted delivery system has been recognized as an important reason for the interest of the pharmaceutical industry in advanced drug delivery devices [9]. Although the cost per dose for a controlled release formulation is usually higher than for a conventional formulation, the treatment may be more economical for the patient and the healthcare system. The reduced adverse reactions that occur with the use of controlled drug delivery results in less hospitalization and fewer visits to the physician, a substantial saving in terms of time and money [4, 6]. The development of self-administered controlled release dosage forms for medications that would otherwise require professional assistance would reduce the time healthcare professionals spend on disease treatment, an additional saving for the healthcare system [4].

The ultimate goal for controlled release technology is to improve disease management by tailoring drug treatment to the needs of each patient or class of patients [7]. To achieve this aim, direct control over the rate, location and timing of drug release will be necessary. The solution involves the development of multicomponent systems in which the drug is but one component [2].

1.1.2 Methods of Attaining Controlled Drug Release

The various methods for controlling the release of drugs have been discussed elsewhere in great detail [1, 5, 6, 9, 10, 11]. A brief description of each technique, focussing on the mechanism of release control, will be provided here. Examples of the three main classes of delivery devices—diffusion-controlled systems, chemically-controlled systems and water penetration-controlled systems—are depicted in Figure 1.2. Each type uses polymers to provide some form of barrier to drug release. Polymers are uniquely suited as materials in controlled delivery systems because their properties can be modified and controlled [10].

The two types of diffusion-controlled systems, reservoir devices and monolithic devices, differ widely in their properties and performance. In reservoir systems, the active agent is surrounded by a permeable membrane. In monolithic systems, the drug is dissolved or dispersed in an insoluble polymer which is then formed into a tablet or slab. Drug release from a reservoir device depends on the rate of drug diffusion through the membrane and is constant as long as the concentration of drug in contact with the inner side of the membrane is constant. The release from a monolithic device declines with time and depends on the drug loading of the device. The mechanism of drug release from a monolithic device changes from diffusion through the polymer matrix at low drug loadings (<5% by volume) to diffusion of the drug through water-filled channels left behind by previously escaped drug at higher drug loadings (>20% by volume). The choice between the two diffusion-controlled systems depends on factors such as expense, safety and the desired drug-release profile. The rate of drug release from reservoir devices depends on the thickness, area and permeability of the membrane and the control of these factors in production leads to higher manufacturing costs. These devices are also susceptible to catastrophic failure if the membrane ruptures, leading to the immediate release of high concentrations of drug. The major advantage of reservoir devices is that they can provide long-term constant release profiles. On the other hand, monolithic systems release drugs at a declining rate but are inexpensive to manufacture and are relatively safe from dose-dumping. Diffusion-controlled devices are widely used as implants and in transdermal applications.

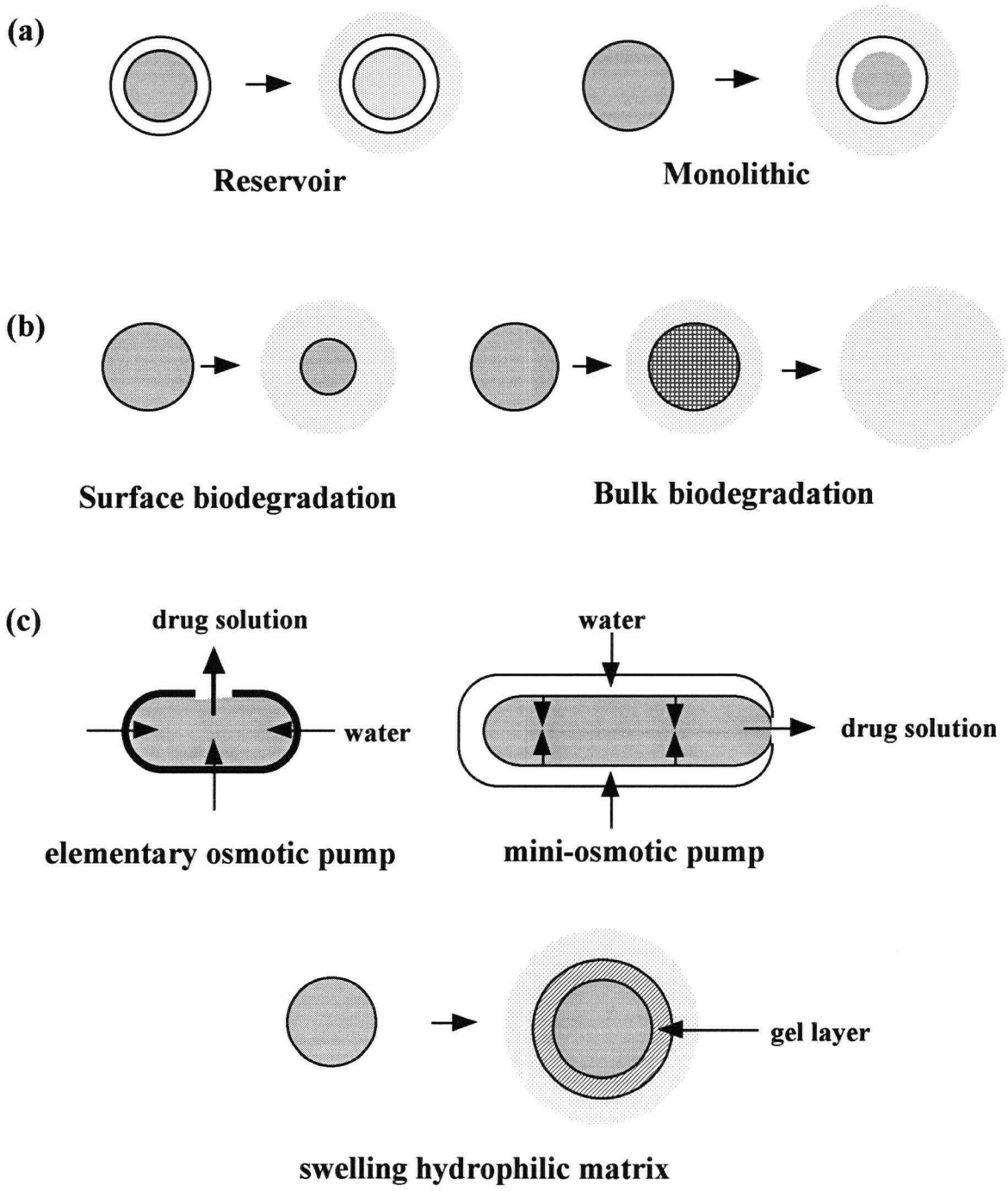

Figure 1.2: Schematic representations of the various methods of controlling drug release, (a) diffusion-controlled, (b) chemically-controlled, and (c) water-penetration controlled. The drug is represented by the dark colour and the lighter a region, the lower the drug concentration. The open-edged, dotted circles indicate drug released from the device.

Chemically-controlled systems release drugs by chemical processes such as polymer degradation or erosion. The earliest of these systems used slowly dissolving polymer coatings or matrices to retard the dissolution of the drug. Sustained release could be obtained by coating individual particles with polymer layers of varying thickness, thereby altering the dissolution rate for each particle and extending drug release over longer periods of time. Attempts were made to develop monolithic devices that released drug by controlled biodegradation of the polymer rather than dissolution. The hope was that the active agent in these systems would be released by slow surface, or heterogeneous, degradation of the polymer matrix. Unfortunately, the biodegradation of most polymers is not constant and is rarely confined to the surface of the polymer. Most polymers degrade by a homogeneous mechanism, where there is an initially slow bulk degradation and then at a critical stage when the entire polymer is degraded to the same extent, the polymer matrix quickly erodes. Often the release of active agent by diffusion prior to degradation is quite significant leading to complicated release patterns. Recently, biodegradable polymers have been used in conjunction with implantable diffusion-controlled devices to ensure that the spent reservoir or matrix degrades after drug release is complete.

Water penetration-controlled systems include osmotically driven and swelling systems. Osmotic systems utilize osmotic forces to pump drug out of a reservoir-like device. These systems contain osmotic agents surrounded by a membrane permeable only to water. As water penetrates and dissolves the osmotic agents, the osmotic pressure in the interior of the device increases and forces a drug solution out of the device. There are two types of osmotic devices, the elementary osmotic pump and the mini-osmotic pump. In the elementary device, the drug and osmotic agent form the core of the device which is coated with a semi-permeable membrane. As water penetrates and dissolves the interior core, osmotic pressure forces the drug solution out of the device through one or more small holes in the membrane. In the mini-osmotic pump, the osmotic agent and the drug are separated into two compartments by a movable partition. The water enters the osmotic agent compartment and the increased osmotic pressure moves the partition, forcing drug out of the drug

compartment. With constant reservoir volume, these devices deliver a volume of drug solution equal to the volume of osmotic water uptake within the same time interval. The rate of water influx and drug delivery will be constant as long as a constant thermodynamic activity is maintained across the membrane. In the mini-osmotic pump system, delivery of the drug can be zero-order because of the separate compartmental design. In the elementary pump system, the delivery is only constant as long as there is excess solid present. Osmotic delivery systems are capable of providing prolonged zero-order release at a delivery rate much higher than achievable by a diffusion mechanism. Elementary osmotic pumps are used as oral dosage forms whereas mini-osmotic pumps are often used as controlled release implants in experimental studies into the effects of continuous administration of drugs. Swelling hydrophilic matrices, the focus of this thesis, will be discussed in detail in the following section.

1.1.3 Swelling-Controlled Drug Delivery

The term swelling-controlled drug delivery is used to describe drug release from monolithic devices prepared with hydrophilic polymers whose dimensions change with the absorption of water [5]. These hydrophilic matrix tablets are primarily used in oral drug delivery. The tablet is ingested and as the hydrophilic polymer swells, a gel layer is formed around the tablet that inhibits the release of drug. The rate of drug release from the hydrophilic matrix is a function of water absorption, polymer hydration, and drug diffusion through the swollen polymer gel [5].

When water penetrates a hydrophilic polymer, relaxation of the polymer chains occurs once the water concentration is high enough to decrease the glass-to-rubber transition temperature of the system below the temperature of the experiment [12]. The mechanism of water penetration into the polymer will vary depending on the relative rates of the water diffusion and polymer-chain relaxation [5, 12, 13, 14]. When the diffusion rate of the water is the controlling factor in water uptake, the penetration behaviour follows Fick's laws of diffusion. When the rate of water or solvent uptake is largely determined by the rate of swelling and relaxation of the polymer chains, then non-Fickian Case II diffusion

behaviour is observed. The time-dependence, t^n, of the penetration front in a matrix slab is a convenient method of determining the nature of the diffusion process. The diffusion process is Fickian when the front movement is proportional to the square-root of time (n=0.5) but, if the front changes are linear with time, then the penetration process follows Case II diffusion [13]. A time-dependence of the penetration front between n=0.5 and 1 suggests that there is a mixture of the two penetration mechanisms. The drug release behaviour also varies with the mechanism of water penetration [5]. In the case of Fickian water diffusion, the drug release will depend on the rate of drug diffusion through different polymer concentrations. In systems that exhibit Case II water diffusion, drug release follows the swelling of the matrix. The rate of relaxation of the polymer chains is affected by parameters such as polymer orientation, molecular weight, molecular weight distribution and temperature [14]. Thus, the water diffusion mechanism and subsequent drug release behaviour for a controlled release system will depend on the nature of the polymer used in the formulation.

Cellulose ethers are a broad class of polymers commonly used in hydrophilic matrix tablets [15]. These derivatives of cellulose have functional group substitutions such as methyl, ethyl, hydroxypropyl and carboxymethyl, and their chemical properties can be tailored by the choice and degree of substitution of the cellulose chain. Cellulosic polymers, such as hydroxypropylmethylcellulose (HPMC), are chosen because of their wide availability, cost-effectiveness, compatibility with conventional techniques and low toxicity [12, 15]. The hydrophilic matrix formulation is prepared by mixing the drug with the polymer and pressing the mixture into a tablet or capsule. Water penetration into the polymer leads to the formation of a gelatinous layer containing regions that vary in polymer concentration [15]. In the area near 100% polymer, the gel is a wetted mass of powders that have swollen. Towards the outside of the tablet, as the polymer concentration decreases, the layer consistency becomes one of a true gel. At very low concentrations, the polymer chains dissolve and the erosion of the hydrophilic matrix in these regions is an additional mechanism of drug release.

1.1.4 Analytical Methods for Investigating Swelling Polymer Systems

This section is a representative review of the analytical methods that have been used to investigate swelling-controlled release systems. The techniques have been divided into three categories—bulk measurements, dissection, and imaging—based on the approach used to study the polymer device and drug release behaviour. Many researchers have used a combination of techniques to provide an extensive description of the release system under study. Selected references are provided for each technique, however, in general, numerous other examples are available in the literature. The discussion here will focus on the data obtained from each method or class of methods and on possible limitations.

The analytical methods that fall into the classification of bulk measurements are those that determine overall changes in a species concentration rather than specific concentration distributions. In the study of tablet swelling, the rate of water uptake is monitored through the weight changes of the tablet [13, 16]. In a similar manner to that described in Section 1.1.3, the time-dependence of the weight increase is used to determine the nature of the water penetration process. A square-root time-dependence of the tablet weight is proof of Fickian diffusion whereas a linear dependence on time points to non-Fickian Case II diffusion [14]. The polymer behaviour is inferred from the dimensional changes of the swelling tablet such as an increase in the thickness or diameter of a tablet [17, 18]. Several researchers have used theories of polymer swelling based on water penetration to develop models to fit thickness changes in systems where the swelling is restricted to the axial direction [19, 20]. The most common bulk technique for studying drug release is the dissolution method outlined in the US Pharmacopeia [21]. The tablets are suspended in water baths, or flow-cells, and the drug concentration released into solution is monitored by UV-Vis spectrophotometry or other suitable technique [18, 22, 23, 24, 25]. When the fractional drug release is linear with the square-root of time then drug diffusion is the significant mechanism of release and the process is Fickian [26]. A fractional release that is linearly dependent on time indicates that the polymer relaxation is the controlling factor in the

drug release. Bulk measurements of swelling tablets are a general method of characterizing the tablet and drug release behaviours but are unable to directly detect concentrations of water, polymer or drug within the tablet.

The dissection of a swollen tablet is a basic technique used to obtain concentration distributions in a hydrogel. For each time point, a fresh tablet is left to swell for the required duration and then the gel is sliced into sections of known dimension. The water and polymer concentrations in each slice are determined by drying to a constant weight. The drug concentration in each slice is determined by a suitable assay that can detect the drug without interference from the polymer. In this manner, the time-dependent concentration distributions for each species in the swelling tablet can be determined. In one example of this method, the distributions for polymer, drug and water in a swelling HPMC tablet containing KCl were obtained by freezing the swollen gel prior to dissection to stop the diffusion of the KCl [27]. Another common use of the dissection technique is to determine the diffusion coefficient from the drug distribution within swollen gels of known polymer concentration [28]. The advantages of the dissection method, low expense and ease of execution, are countered by the labour-intensive nature of the experiment. There is also the added risk of experimental variations due to the handling of the swollen tablet.

In situ imaging during the tablet swelling process allows for the detailed analysis of the system without disturbing the polymer gel layer. The various imaging techniques can be divided into two categories, those that provide only a pictographic record of the swelling hydrophilic matrix tablet and those capable of providing concentration distributions within the swollen polymer. The most basic form of imaging is photography which is useful to monitor the dimensional changes of the tablet during swelling [17, 18, 29]. Polarized-light microscopy, in conjunction with photography, permits the detection of the water penetration front and measurement of the gel layer thickness [14, 22, 23, 24], parameters that provide information on the nature of the water penetration process and polymer hydration. X-ray photography has also been used to monitor water penetration into HPMC tablets [30]. HPMC tablets containing sodium sulphate were placed in dissolution media

containing barium chloride resulting in the formation of X-ray opaque barium sulphate where water had penetrated the tablet. In the X-ray photographs, taken using dental film, dark rings indicated the swollen gel layer.

The information attainable with photographic methods is limited by the lack of concentration information for the water or the polymer in the swelling tablet. Also, these techniques cannot probe the drug release behaviour unless the loss of drug from the device leads to additional optical changes that can be detected apart from those caused by water penetration. Imaging techniques that can provide concentration information include optical imaging, confocal laser scanning microscopy, and NMR imaging. In one method of optical imaging, light scattering was used to obtain *in situ* optical images of the gel layer of a swelling HPMC tablet [31]. The intensity of the scattering, calibrated with respect to the HPMC concentration in HPMC-water mixtures, was used to calculate polymer concentration distributions at various times during the tablet swelling. This optical imaging technique could easily be applied in the study of other swelling polymer systems. The technique, unfortunately, does not provide drug concentration distributions but uses the dissolution method to determine drug release behaviour. Confocal laser scanning microscopy has been used to study both polymer swelling behaviour and drug release in monolithic devices [32, 33]. The technique produces spatially-resolved maps of a fluorescent species and can provide information on the concentration distributions of a fluorescent drug. NMR imaging has been used in several instances to study swelling-controlled controlled release systems. As the technique is the focus of this thesis, the experiments performed by other investigators will be discussed in detail in the following section.

1.1.5 NMR Imaging in the Investigation of Controlled Release Systems

The first experiments using an NMR method to obtain images were reported in 1973 where imaging was used to study two tubes of water [34] and a solid layered sample [35]. In both these experiments, a magnetic field gradient was applied to the sample and the resulting NMR 'spectrum', or one-dimensional image, showed frequency broadening related

to the position of the sample within the gradient. In the study of two tubes of water, magnetic fields were applied along various axes and the one-dimensional NMR images were mathematically back-projected into a two-dimensional image of the original sample. In the second study, a model sample consisting of plates of solid camphor was imaged using a magnetic field applied perpendicular to the plane of the plates. The spacings of the layers derived from the images were similar to the actual spacings of the sample within the 10% accuracy of the magnetic field calibration. The earliest reports of the use of NMR imaging to monitor solvent ingress into polymers were in the mid-1980s [36, 37, 38]. In recent years, numerous investigators have utilized this technique to monitor, for example, the NMR relaxation and diffusion properties of acetone and methanol in poly(methylmethacrylate) [39] and the absorption and desorption of water in Nylon 6,6 [40].

The number of reported NMR imaging investigations of drug delivery systems has been limited. The earliest application of the technique was in 1988 when the release of a paramagnetic contrast agent from an osmotic pump was monitored [41]. A later imaging study of osmotic pump tablets found that the degree of water penetration through the tablet membrane visible in the two-dimensional images, was greater for 'fast' release than for 'slow' release versions of the tablets [42]. NMR imaging of silicone oil within intact tablets was recently presented as a novel method of determining tablet porosity [43]. Other investigators have reported the use of NMR imaging in the development of drug release formulations. Researchers at Glaxo Wellcome Inc. changed the coat material of their regulated release tablets based on evidence from NMR images obtained in our laboratory that the process of water absorption in the coat was altering the expected drug release behaviour [44]. Proctor & Gamble modified the preparation of a tablet containing two active agents, from a monolayer tablet containing a mixture of the two drugs to a bilayer tablet where the drugs are separated, when NMR imaging experiments indicated that the mixture of drugs lead to the formation of a gel that hindered drug release [45].

The most extensive NMR imaging analysis has been performed on swelling hydrophilic matrix systems containing HPMC or similar polymers. During the course of this

thesis research, one group used two-dimensional imaging to determine the degree of tablet swelling, the gel layer thickness and the diffusivity of water in the polymer at various times during the swelling of an HPMC tablet [46, 47, 48]. Another imaging study of hydroxypropylcellulose capsules revealed that the rate of the hydration penetration front is not the rate-limiting step in drug release as determined by the dissolution method [49].

The work performed to date on hydrophilic matrix tablets has not exploited the advantages of NMR imaging. NMR imaging is a non-invasive, non-destructive technique that can provide quantitative concentrations distributions for species within the swollen polymer tablets, data useful in developing models to explain swelling and drug release. Also, other NMR active nuclei apart from ^{1}H can be imaged allowing for the independent monitoring of drug species in an aqueous environment. Although NMR imaging has been used to obtain concentration distributions to determine diffusion coefficients of a drug within a hydrogel [50], the technique has not been applied to monitor water, polymer and drug distributions from an initially dry hydrophilic matrix tablet until the work reported in this thesis [51, 52].

1.2 Nuclear Magnetic Resonance Spectroscopy

Nuclear magnetic resonance was first reported in 1946 [53, 54]. From 1949, with the discovery of the chemical shift effect, to the present day, NMR has proven to be one of the most important tools for investigating chemical structures. The theory of the phenomenon has been extensively discussed in several books [55, 56, 57, 58]. The description here will be a brief review of the basic concepts underlying the experiments of this thesis.

1.2.1 The NMR Phenomenon

Nuclei contain protons and neutrons which are both spin-$\frac{1}{2}$ species. The coupling of the angular momenta of the individual nucleons leads to a total nuclear spin that can have an integral, half-integral or zero value. A nucleus of spin I has (2I+1) spin states, m_I, which take on values -I, -I+1, up to +I. An I=0 nucleus has only one spin state and exhibits no NMR properties.

A moving charged body has an associated magnetic moment. For the nucleus, the magnetic moment, $\vec{\mu}$, is related to its angular momentum, $\vec{P}$, by γ, the nuclear gyromagnetic constant (Equation 1.1). In the absence of an external magnetic field, all the spin states of the nucleus are degenerate in energy. However, when a magnetic field B_0 is applied in the z-direction, as in the NMR experiment, the energy levels for the spin states separate in relation to the strength of the magnetic field, the value of γ, Planck's constant h over 2π ($\hbar$) and the spin state quantum number, m_I, as shown in Equation 1.2.

$$\vec{\mu} = \gamma \vec{P} \tag{1.1}$$

$$E = -\gamma \hbar m_I B_0 \tag{1.2}$$

For the simplest case of a spin-$\frac{1}{2}$ nucleus, there are two energy levels separated by a ΔE of $\mid \gamma \hbar B_0 \mid$. Transitions between these two states can be induced by an oscillating magnetic field when its frequency corresponds to ΔE, as in Equation 1.3. Often the strength of a magnet used in an NMR experiment is quoted in terms of the frequency for the ^{1}H transition in the magnet, *e.g.* 400 MHz rather than 9.4 T.

$$\Delta E = h\nu = \mid \gamma \hbar B_0 \mid \tag{1.3}$$

$$\nu = \mid \frac{\gamma}{2\pi} \mid B_0$$

Another method of regarding the NMR experiment is to use a vector formalism. The magnetic field, $\vec{B}$, exerts a torque on the magnetic moment vector, $\vec{\mu}$, causing it to precess about the axis of the main magnetic field, usually defined as the z-axis. The induced angular velocity, $\vec{\omega}$, of this Larmor precession is equal to $-\gamma \vec{B_0}$ and ν is equal to $\mid \gamma/2\pi \mid B_0$ as before. A sample under investigation contains an ensemble of spin-$\frac{1}{2}$ nuclei in one of the two possible spin states each representable by a vector as shown in Figure 1.3(a). The net magnetization in the systems depends on the population difference between the two energy states which can be determined from the Boltzmann equation. The resulting total

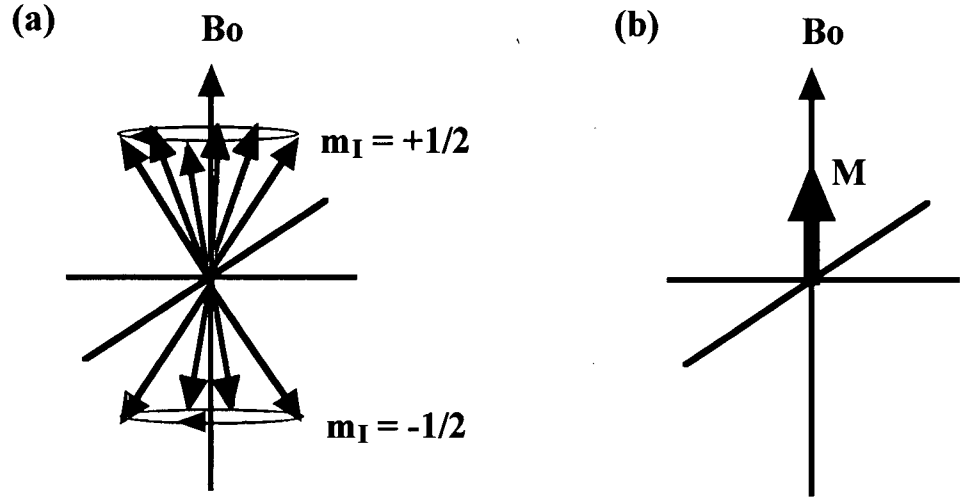

Figure 1.3: (a) Nuclear spins depicted as precessing vectors. Spins with m_I=+1/2 are at lower energy than m_I=−1/2 spins, hence the larger number of +1/2 vectors. (b) The net magnetization vector, $\vec{M}$, with magnitude given by Equation 1.4.

magnetization vector $\vec{M}$, shown in Figure 1.3(b), is directed along the z-axis and has the magnitude given in Equation 1.4 where N is the total number of spins, kT is the thermal energy and k is Boltzmann's constant.

$$M_0 = \frac{N(\gamma\hbar)^2 B_0}{2kT} \tag{1.4}$$

The diagnostic structural information available from NMR is due to the additional phenomenon of local electronic shielding. The motion of electrons in a magnetic field results in an induced magnetic moment opposed to the primary applied field. The decrease in the apparent magnetic field experienced by the nucleus causes a shift in the resonance frequency for that nucleus. An empirical database of chemical shifts for different nuclei in specific molecular environments has been developed over the past 50 years. This database makes possible structure determinations of unknown molecules from their NMR spectra .

1.2.2 Pulsed Fourier-Transform NMR and Relaxation Processes

The earliest manner of performing an NMR experiment was the continuous wave method where the sample was placed in a fixed magnetic field and the radiofrequency (rf) field was

scanned through a range of values (or *vice versa*). When the resonance frequency for each type of nucleus in the sample was matched, an absorption peak was observed in the NMR spectrum. Modern NMR experiments are performed with rf pulses that have a broad excitation range and simultaneously satisfy the resonance condition for all the different nuclei in the sample within that range. The NMR spectrum is obtained by observation of the decay of the excited state as the perturbed systems relax toward equilibrium. Fourier transformation of the signal intensity as a function of time yields the NMR spectrum, a map of intensity as a function of frequency.

The description of the effect of an rf pulse on the net magnetization is aided by the definition of a new frame of reference. In the laboratory frame, the axes are static and the nuclei and rf pulse move with respect to the axes. By defining a rotating frame, where only the z-axis is static and the x and y-axes rotate at the same frequency as the rf pulse, both the rf magnetization and the spin vectors can be static with respect to the frame. In the rotating frame, the $\vec{B}_1$ magnetic field generated by the pulse causes the net magnetization to rotate about the direction of the applied pulse. The angle of rotation depends on the strength and duration of the pulse and the gyromagnetic ratio of the nucleus. A '90°' pulse tips the magnetization from the z-axis into the x,y-plane. When the frequency of the pulse is exactly equal to the Larmor precession frequency, the net magnetization will be static with respect to the frame. The return to equilibrium will generate a free induction decay (FID) as in Figure 1.4(a). When the frequency of the pulse is not equal to the Larmor frequency, the result is an oscillating FID (Figure 1.4(b)) because the Larmor precession frequency is faster or slower than the rotating frame frequency which is defined by the frequency of the pulse. The FID is recorded by computer and multiple repetitions of the same experiment can be added together to improve the signal-to-noise ratio in the resulting NMR spectrum.

There are two relaxation times to consider when performing basic pulse FT-NMR experiments because an rf pulse disturbs the population balance in the spin states and generates a temporary phase-coherence in the spins. After the pulse, the system populations

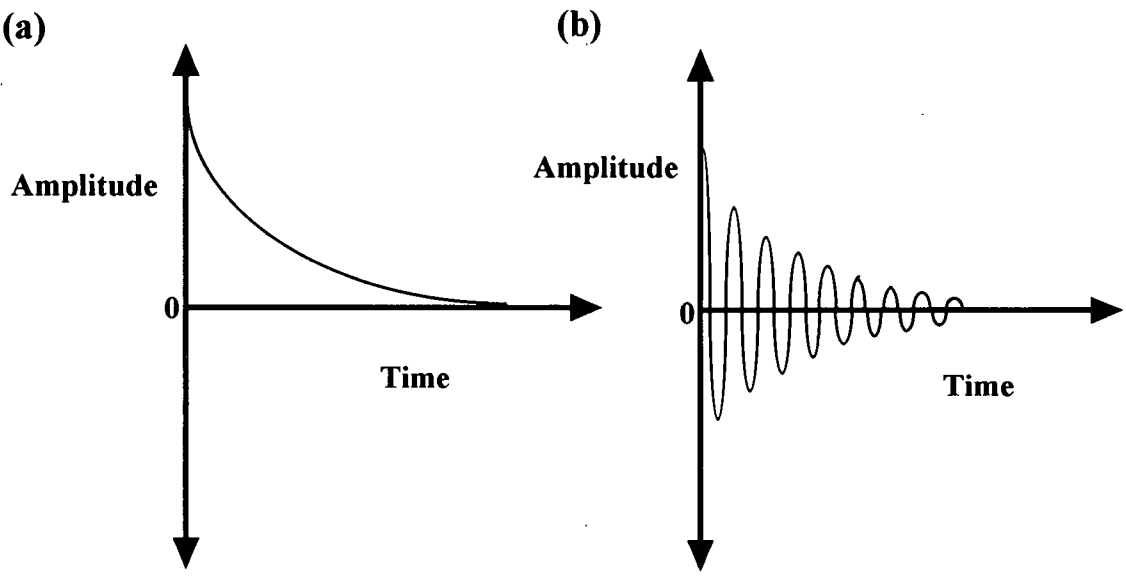

Figure 1.4: The free induction decay (FID) of a sample after an (a) on-resonance rf pulse and (b) off-resonance rf pulse.

will revert back to the Boltzmann equilibrium populations. This relaxation is described by the Bloch equation for Boltzmann relaxation, Equation 1.5, where T_1 is the spin-lattice, or longitudinal, relaxation constant. The second time, spin-spin or transverse relaxation, is responsible for the decay of the FID. The nuclear spins, phase-coherent during the rf pulse, begin to dephase again, resulting in a decrease from the maximum intensity. The time constant of the decay, as shown in Equation 1.6, is T_2, the spin-spin relaxation parameter. The T_1 and T_2 relaxation times are characteristic for a nuclear species in its environment. These parameters should be known prior to performing more complex NMR studies as their values will determine which experiments are feasible.

$$\frac{\partial M_z}{\partial t} = -\frac{(M_z - M_0)}{T_1} \tag{1.5}$$

$$\frac{\partial M_a}{\partial t} = -\frac{M_a}{T_2}, \quad a = x, y \tag{1.6}$$

The knowledge of the T_1 relaxation time is important for obtaining quantitative signals as the delay (T_R) between successive repetitions of a pulse sequence should be five times T_1 to ensure complete recovery to Boltzmann equilibrium. T_1 values are typically

measured by the inversion-recovery sequence shown in Figure 1.5 [59]. The 180° pulse inverts the magnetization from the +z to the -z directions and relaxation to Boltzmann equilibrium occurs during the τ delay. The 90° pulse tips the magnetization in the x,y-plane so that the sign and magnitude of the magnetization can be detected. The magnetization changes from $-M_0$ to $+M_0$ following Equation 1.7 which is the integrated form of the Bloch equation. Figure 1.5 shows plots of this equation with relatively short and long T_1 values.

$$M_z = M_o(1 - 2e^{-\frac{T_R}{T_1}}) \tag{1.7}$$

The T_2 relaxation time dictates the length of time that the magnetization can be manipulated and detected in an NMR experiment. Although T_2 relaxation causes the decay of the FID, additional factors, such as magnetic field inhomogeneities, increase the rate of the decay and thus, the true T_2 value cannot be measured directly from the FID envelope. The sequence used to measure this relaxation parameter, the spin-echo shown in Figure 1.6, refocusses the magnetic field inhomogeneities but has no effect on T_2 relaxation. The 90° pulse in the sequence tips the z-magnetization into the x,y-plane. The individual vectors fan out due to field inhomogeneities that cause Larmor precessional frequencies faster or slower than the average. After a duration τ the 180° pulse rotates the vectors to a new position so that the faster vectors lag behind the slower ones and the different precession frequencies cause the vectors to refocus after another τ delay. The refocussed vector, however, has decreased in magnitude as a result of true T_2 dephasing according to Equation 1.8 where the time-to-echo (T_E) is equal to 2τ.

$$M_{x,y} = M_o e^{-\frac{T_E}{T_2}} \tag{1.8}$$

The mechanisms for T_1 and T_2 relaxation are limited to those that produce fluctuating magnetic fields to induce transitions between nuclear spin levels. For spin-$\frac{1}{2}$ nuclei, there are a number of physical mechanisms which provide the appropriate conditions.

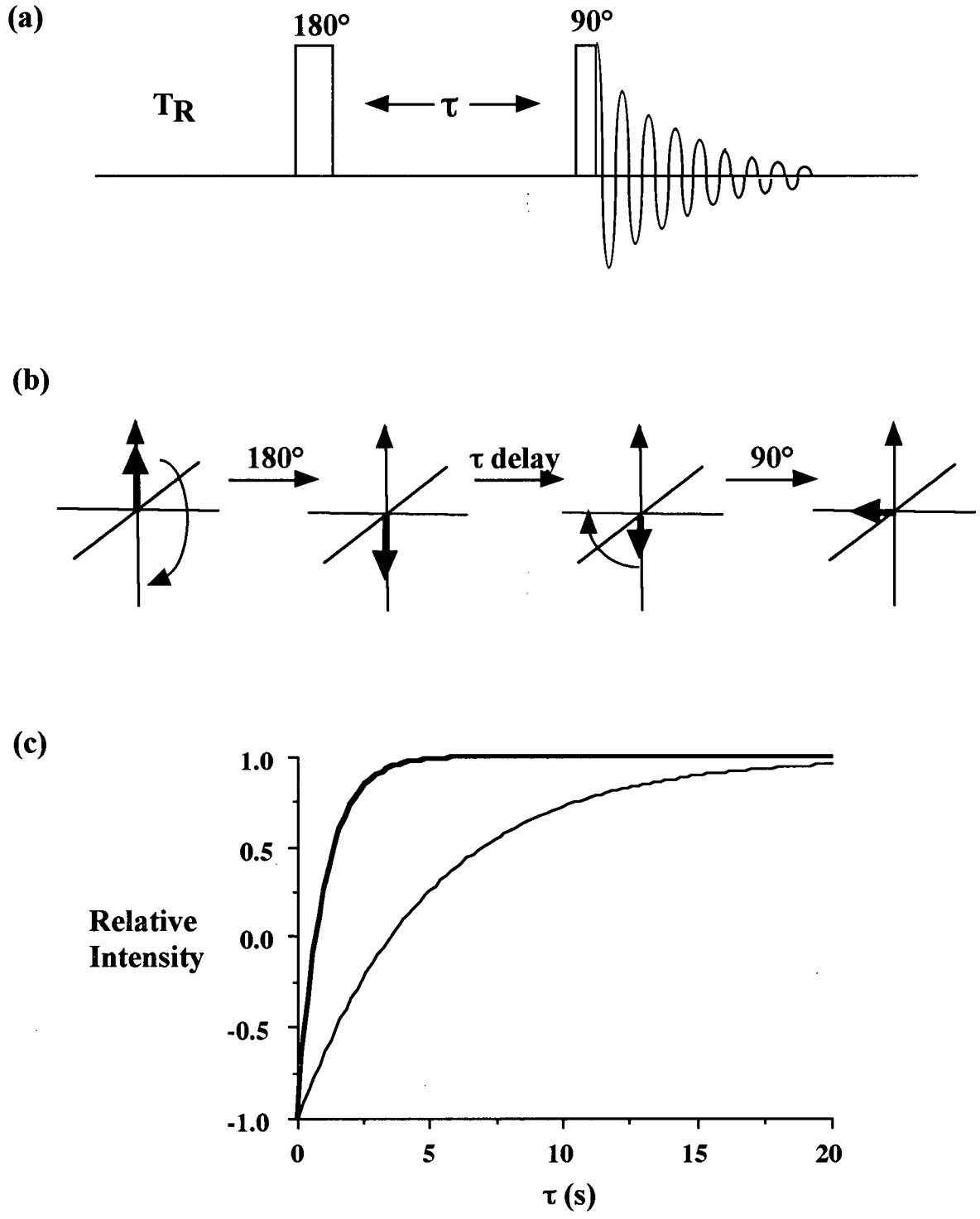

Figure 1.5: The inversion recovery experiment for measuring T_1, (a) the pulse sequence, (b) the vector description of the effect of (a) on the net magnetization vector, and (c) Equation 1.7 plotted with T_1 values of one second (thick line) and five seconds (thin line).

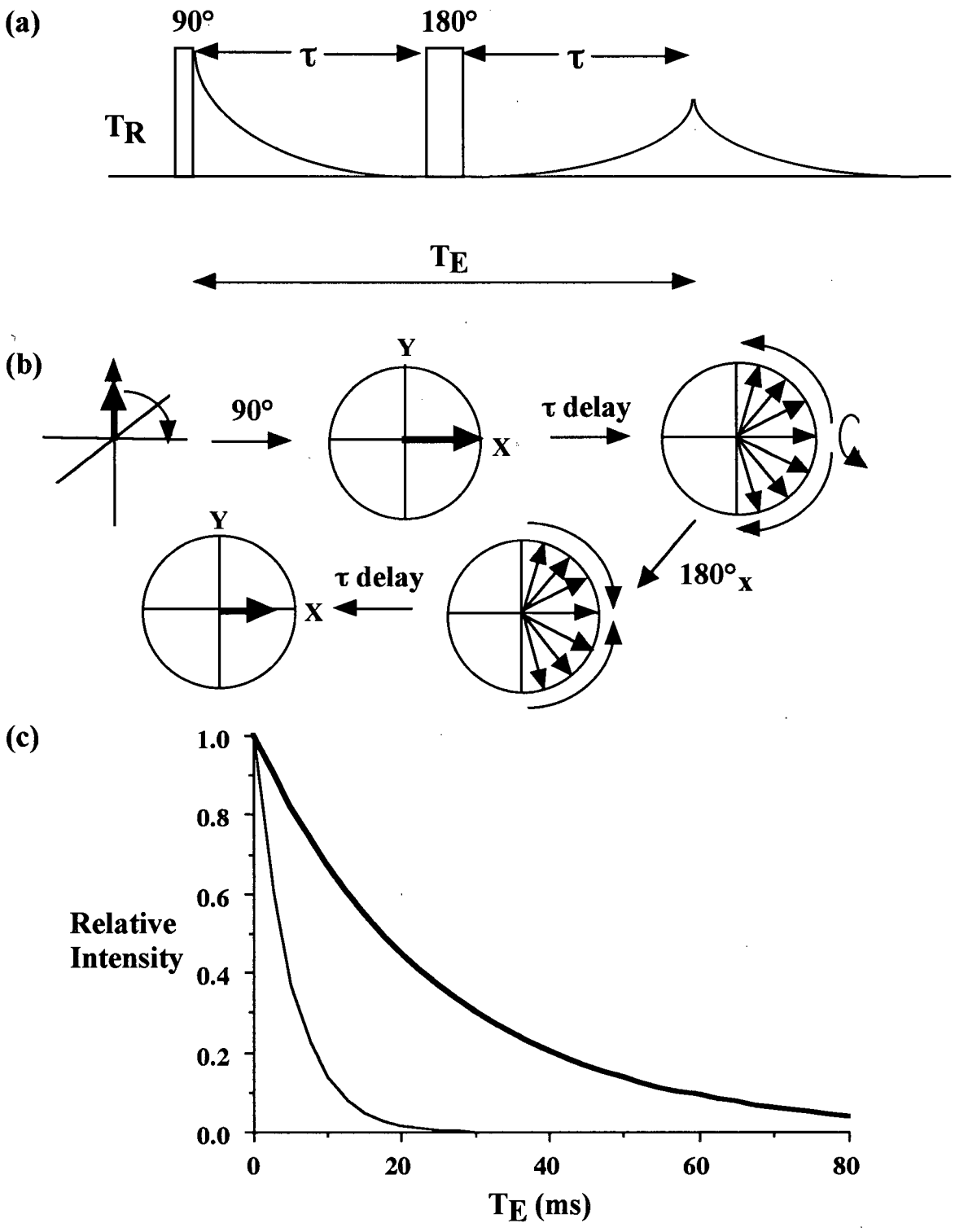

Figure 1.6: The spin-echo experiment for measuring T_2, (a) the pulse sequence, (b) the vector description of the effect of (a) on the net magnetization and on the individual magnetization vectors in the x,y-plane for an on-resonance experiment, and (c) Equation 1.8 plotted with T_2 values of five milliseconds (thick line) and twenty-five milliseconds (thin line).

Dipole-dipole interactions are the most important relaxation mechanism for molecules in solution. They may be modulated by molecular tumbling or by translational diffusion. Dipolar interactions with unpaired electrons are another relaxation mechanism which is often deliberately promoted by the use of paramagnetic salts, such as $CuSO_4$, to decrease the relaxation times. Dipolar interactions with electrons are much larger those with nuclei because the magnetic moments of electrons are very large in comparison to those of nuclei. Another mechanism of relaxation is through scalar coupling. When one spin, I, is coupled to another spin, S, there are two pathways which can lead to relaxation of the I spin. The Type 1 scalar relaxation mechanism for I occurs when the scalar coupling with S is time-dependent, such as in a rapid chemical exchange process, which results in the generation of a fluctuating field. The Type 2 scalar relaxation occurs when S has a very short relaxation time. A third mechanism of relaxation is chemical shielding anisotropy (CSA). As mentioned previously, electrons in a molecule shield the nucleus from the applied magnetic field. When the shielding is not symmetrical, molecular tumbling leads to fluctuating local magnetic fields and increased relaxation rates. Coherent molecular rotation can also generate a magnetic field, due to the motions of the electrons, which can couple with the nuclear spin and provide another relaxation pathway. The overall relaxation rate for a particular species is a sum of the reciprocal relaxation rates for the various mechanisms.

The dominant mechanism of relaxation for spin-$\frac{1}{2}$ nuclei, dipolar coupling, is modulated by reorientation due to molecular motions. The relaxation rates, $1/T_1$ and $1/T_2$, can be determined from this relaxation mechanism and are expressed in the Bloembergen-Purcell-Pound equations, 1.9 and 1.10 [60], where r is the internuclear distance, ω_0 is the precession frequency and τ_c is the characteristic correlation time, a measure of the rate of molecular reorientation. τ_c can be regarded as the "time between jumps" so as the molecular motion decreases, the value of τ_c increases. The two relaxation times exhibit different behaviours with respect to molecular motion changes in the system. In a log-log plot of the relaxation time as a function of the τ_c, the T_1 time exhibits a V-shaped behaviour with the minimum given by $\omega_0\tau_c \approx 0.62$. To the faster motion side of the minimum, T_1 increases

as the motion increases. However, on the slower motion side of the minimum, T_1 increases with decreasing motion. In contrast, the T_2 value decreases fairly regularly with decreasing motion.

$$\frac{1}{T_1} = \frac{3}{10}\frac{\gamma^4\hbar^2}{r^6}[\frac{\tau_c}{1+\omega_0^2\tau_c^2} + \frac{4\tau_c}{1+4\omega_0^2\tau_c^2}] \tag{1.9}$$

$$\frac{1}{T_2} = \frac{3}{20}\frac{\gamma^4\hbar^2}{r^6}[3\tau_c + \frac{5\tau_c}{1+\omega_0^2\tau_c^2} + \frac{2\tau_c}{1+4\omega_0^2\tau_c^2}] \tag{1.10}$$

1.2.3 Diffusion Measurements by NMR

The effect of diffusion in an inhomogeneous magnetic field on the spin-echo experiment was described in the pioneering work of NMR by Hahn [61], Carr and Purcell [62]. After a 90° pulse, the nuclear spins dephase due to a spread of Larmor precession frequencies caused by irregularities in the main magnetic field. The 180° pulse of the spin-echo experiment refocusses the magnetization but only for spins whose Larmor precession frequencies have remained constant for the duration of the experiment [63]. When a spin diffuses in an inhomogeneous magnetic field, it may enter a region where the local magnetic field is different and thus, its precessional frequency will change. The magnetization of this spin, and all others that have diffused in a similar manner, will not be refocussed completely by the 180° pulse and the overall echo amplitude will decrease as a result.

The effect of diffusion on the echo amplitude can be used to measure the self-diffusion coefficient in an experiment where a magnetic field gradient is deliberately applied to cause incomplete refocussing of the echo. The most efficient method, the pulsed-gradient spin-echo (PGSE) technique, was introduced in the mid-1960s [64]. In this experiment, shown in Figure 1.7, the magnetic field gradient is applied in two pulses. The spacing, Δ, and duration, δ, of the two pulses can be varied while maintaining a constant T_E, thus keeping the T_2 dephasing constant between experiments. Assuming a Gaussian model for diffusion, the echo attenuation at constant T_E is given by Equation 1.11 where $A_G(T_E)$ is the amplitude at T_E when the gradient is applied, $A_0(T_E)$ is the amplitude at T_E in

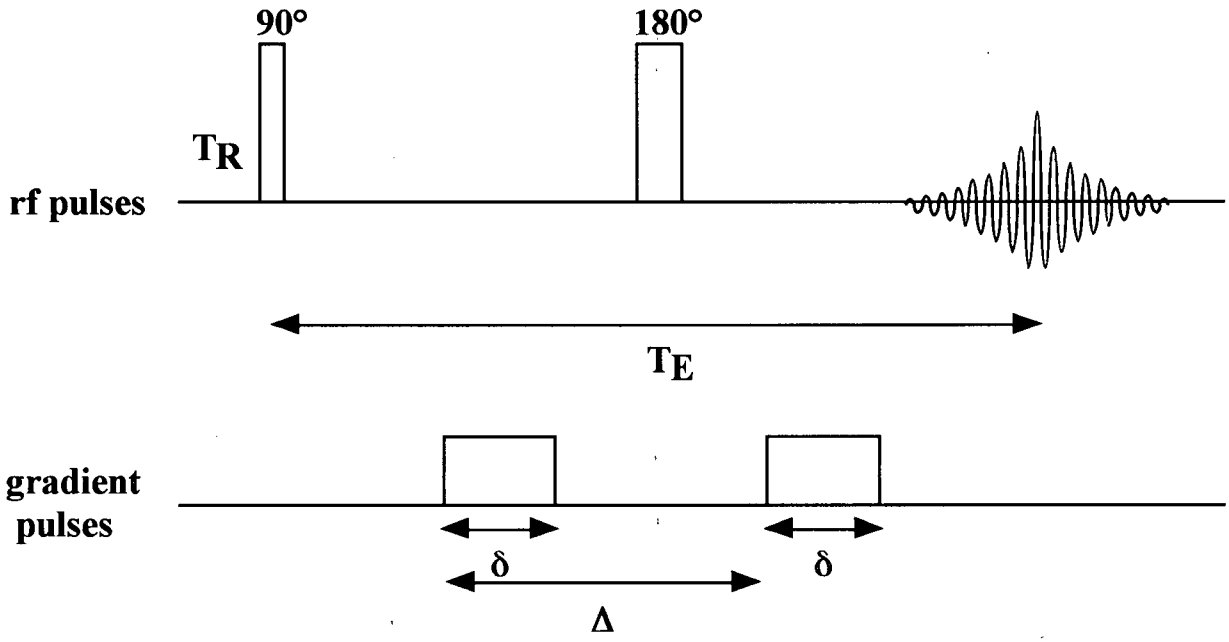

Figure 1.7: The pulse sequence for the PGSE experiment.

the absence of the gradient, G is the strength of the applied magnetic field gradient and D is the self-diffusion coefficient. The echo amplitude can be altered by changing any or all of Δ, δ, or G. The PGSE experiment determines the self-diffusion coefficient from the displacement of the spins in the direction of the magnetic field gradient during a diffusion time of $(\Delta - \delta/3)$ [63].

$$\frac{A_G(T_E)}{A_0(T_E)} = e^{-D\gamma^2\delta^2(\Delta - \frac{\delta}{3})G^2} \tag{1.11}$$

1.2.4 Z-Spectroscopy

NMR studies of polymers are difficult to perform because the rigid environment of the polymer chains leads to very broad spectral lines. Z-spectroscopy is a technique that utilizes dipolar coupling between the mobile protons of a liquid and the rigid protons of a semi-solid material to gain information about the material [65]. The pulse sequence, shown in Figure 1.8, has a long, weak rf pulse that saturates or partially saturates the protons of

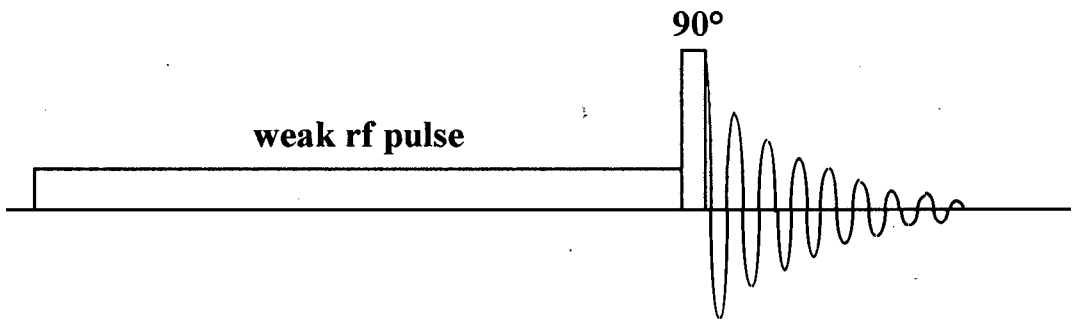

Figure 1.8: The pulse sequence for the z-spectroscopy experiment.

the semi-solid in the system. Because of the dipolar coupling between the protons of the liquid and the semi-solid, the amplitude of the spectrum of the liquid protons, acquired by the on-resonance 90° pulse, depends on the T_1 and T_2 relaxation times of the protons of the semi-solid, as well as on the ratio of the number of semi-solid to liquid protons and the magnetization transfer rate between them. The effect of the pulse on the spins of the semi-solid material will vary with the resonance offset of the preparation pulse and hence, the amplitude of the spectrum of the liquid spins will also vary. The z-spectrum is the plot of the normalized signal amplitude of the liquid component as a function of the off-set frequency. The inverse of the z-spectrum is similar in shape to the wide-line ^{1}H NMR spectrum of the solid-like component and reflects the internal mobility of the solid-like component in the sample [65].

The liquid-solid system can be modelled as a pair of spin baths, A and B, interacting via intermolecular dipole-dipole interactions. The system can be described in the rotating frame by a set of six coupled Bloch equations for spins in the presence of an rf field [66]. If the rf field is assumed to partially saturate the B spins without directly affecting the A spins, then the transverse components of A may be neglected. This assumption is only valid when the preparation pulse frequency is far from the A spin resonance frequency. The steady state solution of the remaining four equations is given by Equation 1.12 [66]. In these equations, Δ is the offset of the rf field from the A resonance, f is the ratio of the number of B spins to the number of A spins, ω_1 is the amplitude of the rf field of the preparation pulse, R_A and R_B are the spin-lattice relaxation rates for the A and B spins, R_{BA} is the rate of cross-relaxation between the A and B spins, and M_A^{Z0} is the equilibrium

longitudinal magnetization in the absence of any rf fields. In the limit where $R_{BA}/R_A \gg 1$, the equation can be reduced to Equation 1.13 which is very similar to the expression for steady state z-magnetization for the B spins except for the T_{1B}/fT_{1A} term. In the case where $fT_{1A} \gg T_{1B}$, $\overline{M}_A^Z$ is exactly the steady-state magnetization of spin B in an rf field. Thus, the z-spectrum would, under certain conditions, yield the spectrum of the B spin system [66].

$$\begin{aligned} \overline{M}_A^Z &= \frac{\alpha}{\beta+4\pi^2\Delta^2\gamma} \\ \alpha &= \frac{fR_{BA}T_{2B}\omega_1^2}{2R_AR_B} \\ \beta &= \frac{R_{BA}}{R_B} + f\left(\frac{R_{BA}}{R_A}+1\right)\left(\frac{T_{2B}\omega_1^2}{R_B}+1\right) \\ \gamma &= T_{2B}^2\left[\frac{R_{BA}}{R_B} + f\left(\frac{R_{BA}}{R_A}+1\right)\right] \\ \overline{M}_A^Z &= \frac{M_A^{Z0}-M_A^Z(t)}{2M_A^{Z0}} \end{aligned} \tag{1.12}$$

$$\overline{M}_A^Z = \frac{1}{2}\left\{\frac{\omega_1^2 T_{1B}T_{2B}}{(1+4\pi^2T_{2B}^2\Delta^2)(1+\frac{T_{1B}}{fT_{1A}}) + \omega_1^2T_{1B}T_{2B}}\right\} \tag{1.13}$$

1.3 Nuclear Magnetic Resonance Imaging

1.3.1 One-dimensional Imaging

One-dimensional NMR imaging was first introduced in 1973 [34, 35] as an extension of the NMR experiment where a magnetic field gradient was used to broaden the frequency of the NMR signal in the direction of the applied gradient. In Figure 1.9, an example with two tubes of water is presented. In the traditional NMR experiment, the magnetic field is homogeneous, and the NMR spectrum contains a single peak at the resonance frequency for water. In the one-dimensional imaging experiment, a linear magnetic field gradient is applied to the sample to introduce a controlled magnetic field inhomogeneity. The water

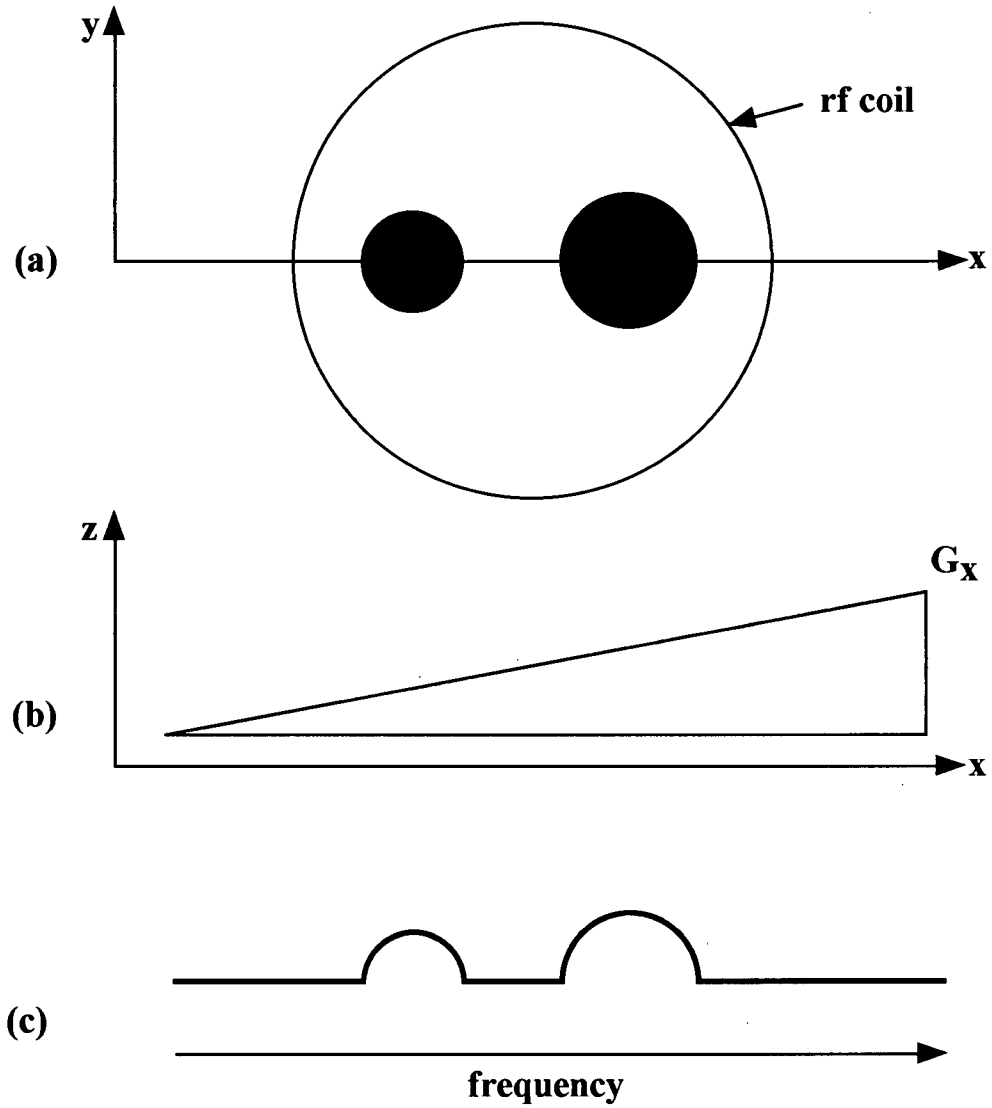

Figure 1.9: An example of a one-dimensional imaging experiment, (a) two tubes of water in the rf coil, (b) the applied magnetic field gradient, G_x, which adds to the main magnetic field and (c) the resulting NMR spectrum which reflects the position of the tubes in the gradient.

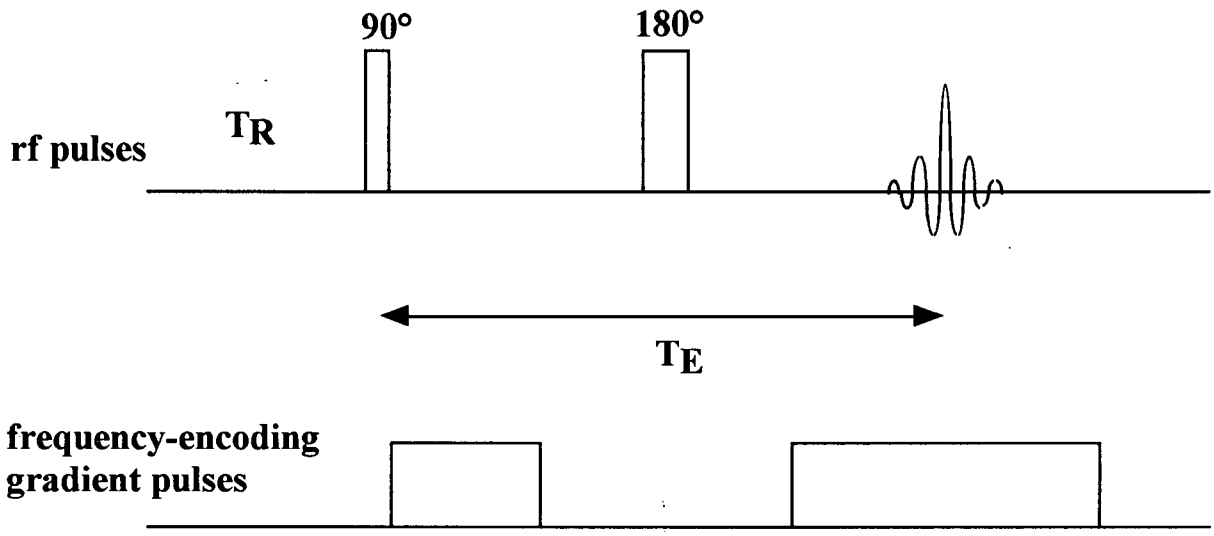

Figure 1.10: The spin-echo pulse sequence used to acquire one-dimensional images.

in each of the tubes now experiences different applied magnetic fields and the Larmor frequency for a particular water molecule in the sample varies as given by Equation 1.14, where ω_0 is the angular momentum generated by the main magnetic field, G_x is the gradient strength and x is the position in the gradient.

$$\omega = \omega_0 + \gamma G_x x \tag{1.14}$$

In early NMR imaging experiments, the magnetic field gradient was applied during the acquisition of the FID in a basic 90° pulse experiment. Recent methods have incorporated the spin-echo to separate data acquisition from the pulses and gradient switching positions. A typical sequence used to acquire one-dimensional images is shown in Figure 1.10. Because the sequence is symmetrical about the 180° pulse, the entire echo can be recorded rather than just the FID, resulting in a $\sqrt{2}$ gain in signal-to-noise. The relationship between the concentration of spins, $\rho(x)$ and the signal obtained with the imaging experiment, S(x), where x is the position in an x-gradient, is given in Equation 1.15. To obtain a quantitative NMR signal directly relatable to concentration, the experimental parameters T_R and T_E must be chosen such that $T_R \gg T_1(x)$ and $T_E \ll T_2(x)$ is true for the entire sample. In practice, the T_R time should be five times the maximum T_1 value present

in the sample and the T_E time should be as short as possible compared to the minimum T_2 value present in the sample. An imaging experiment can also be used to measure the T_2 (or T_1) distribution in a sample in the direction of the gradient by varying T_E (or T_R) with all other factors kept constant. As the frequency distribution in a one-dimensional image is described by a finite number of points, each point represents the signal from a region of width Δx, rather than a fixed position, x, in the sample. The parameter Δx is the resolution of the experiment and is a function of the number of points, the strength of the gradient and the gyromagnetic ratio of the nucleus.

$$S(x) = C\ \rho(x)\ (1 - e^{\frac{-T_R}{T_1(x)}})\ (e^{\frac{-T_E}{T_2(x)}}) \tag{1.15}$$

1.3.2 Slice Selection

Discussions of NMR imaging experiments, also known as magnetic resonance imaging (MRI), often include the concept of slice selection. These slices are not physical dissections of the sample but are selected planes of the sample from which the NMR signal intensity is measured.

Slice selection incorporates two components, a linear magnetic field gradient and a frequency-selective rf pulse. When the selective pulse is applied at the same time as the magnetic field gradient spreads out the resonance frequencies of the sample, a limited region of the sample, as shown in Figure 1.11, is excited by the rf pulse. A small negative gradient is used immediately after the slice-selection procedure to refocus the magnetization in the slice. Only the signal from this plane of the sample will be affected by further pulses and appear in the resulting NMR image. The slice thickness, usually quoted in micrometres, is calculated by dividing the excitation bandwidth of the pulse by the product of the gradient strength and the gyromagnetic ratio of the nucleus.

Traditional rf pulses, meant to excite a wide frequency range, are rectangular step functions where the rf power is switched on for microseconds and then switched off. There is a Fourier transform relationship between the shape and duration of a pulse and its excitation

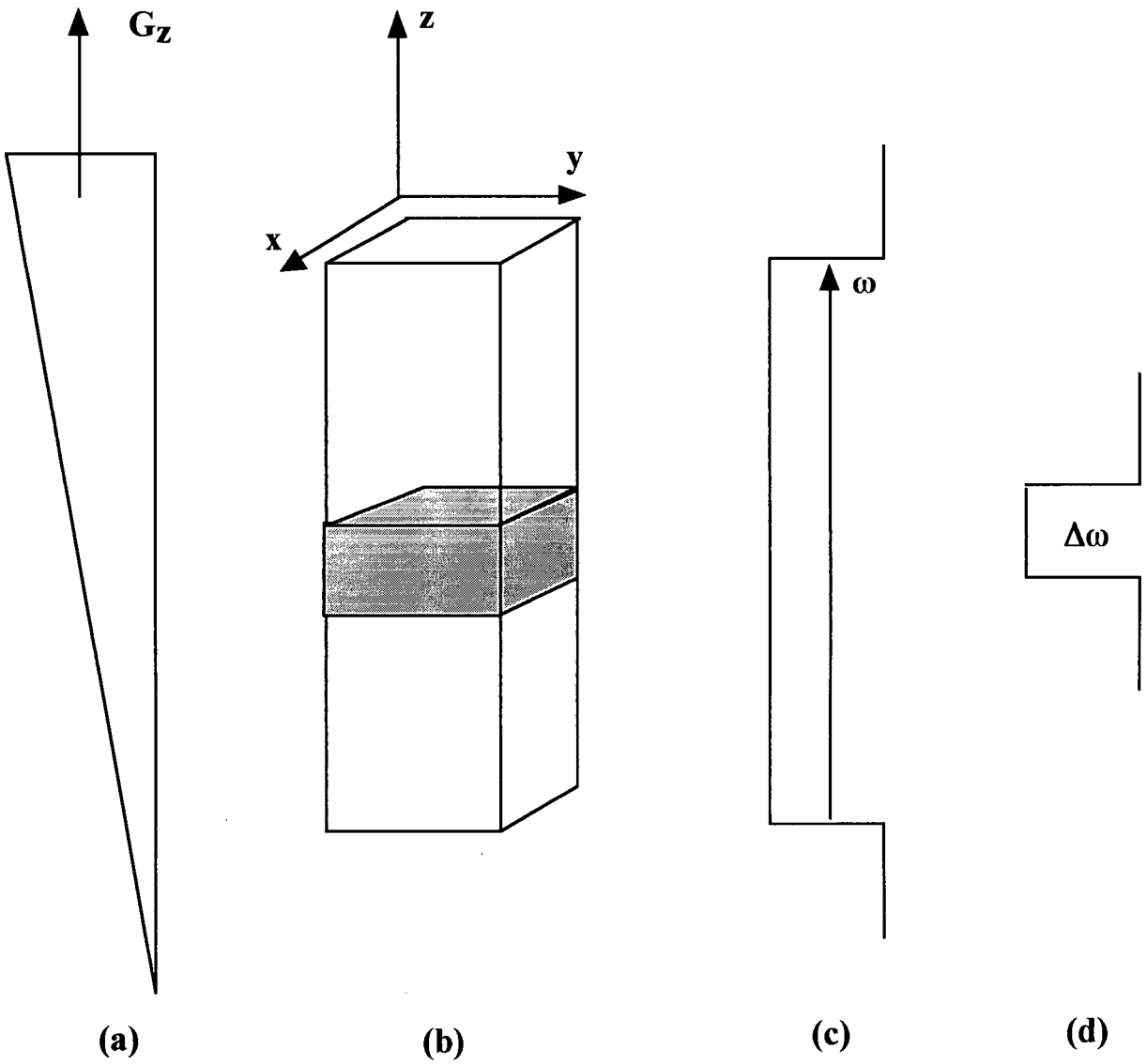

Figure 1.11: The slice-selection process in NMR imaging, (a) the applied z-gradient, (b) a sample in the gradient, (c) the spread of frequencies from sample (b) as a result of the applied gradient, and (d) the excitation width, $\Delta\omega$, of the selective pulse which corresponds to a particular region of the original sample, as indicated by the shaded box in (b).

frequency. A short rectangular pulse has a wide excitation range and a sinc shape (sinx/x) after Fourier transformation. By the same relationship, the original pulse must be long and shaped similarly to a sinc function to obtain a narrow rectangular excitation profile.

1.3.3 Two-dimensional Imaging

The first two-dimensional imaging technique was part of the pioneering work of NMR imaging [34] where the two-dimensional image of two tubes of water was obtained by the mathematical back-projection of a series of one-dimensional images taken along different axes. In contrast, the two-dimensional Fourier imaging technique, developed in 1975 [67], incorporated an additional magnetic field gradient directly in the pulse sequence to spatially resolve the NMR signal in a second dimension. In a one-dimensional imaging experiment, the gradient encodes spatial information in the frequencies of the detected signal and is therefore called a frequency-encoding gradient. The second gradient in the two-dimensional experiment encodes spatial information in the phase of the detected signal and is termed the phase-encoding gradient. The scheme in Figure 1.12 shows how the combined phase- and frequency-encoding can uniquely characterize a specific region of the sample. The phase angle acquired at a position in the sample is given by Equation 1.16 where ω_0 is the precessional frequency, G_y is the strength of a y-gradient, and y is the position within the gradient and t_1 is the duration of the gradient.

$$\phi = (\omega_0 + \gamma G_y y)t_1 \tag{1.16}$$

The second dimension of the NMR imaging experiment is obtained by modulating the phase angle in the experiment. The Fourier imaging method, shown in Figure 1.13, obtained the phase modulation by increasing the t_1 time in successive experiments. However, the method also introduced the problem of increased T_2 relaxation with increasing t_1. The spin-warp modification circumvented this problem by varying the gradient strength in Equation 1.16 while keeping the t_1 time constant [69]. A spin-echo was also introduced into the sequence for the same reasons as in the one-dimensional experiment, to move the

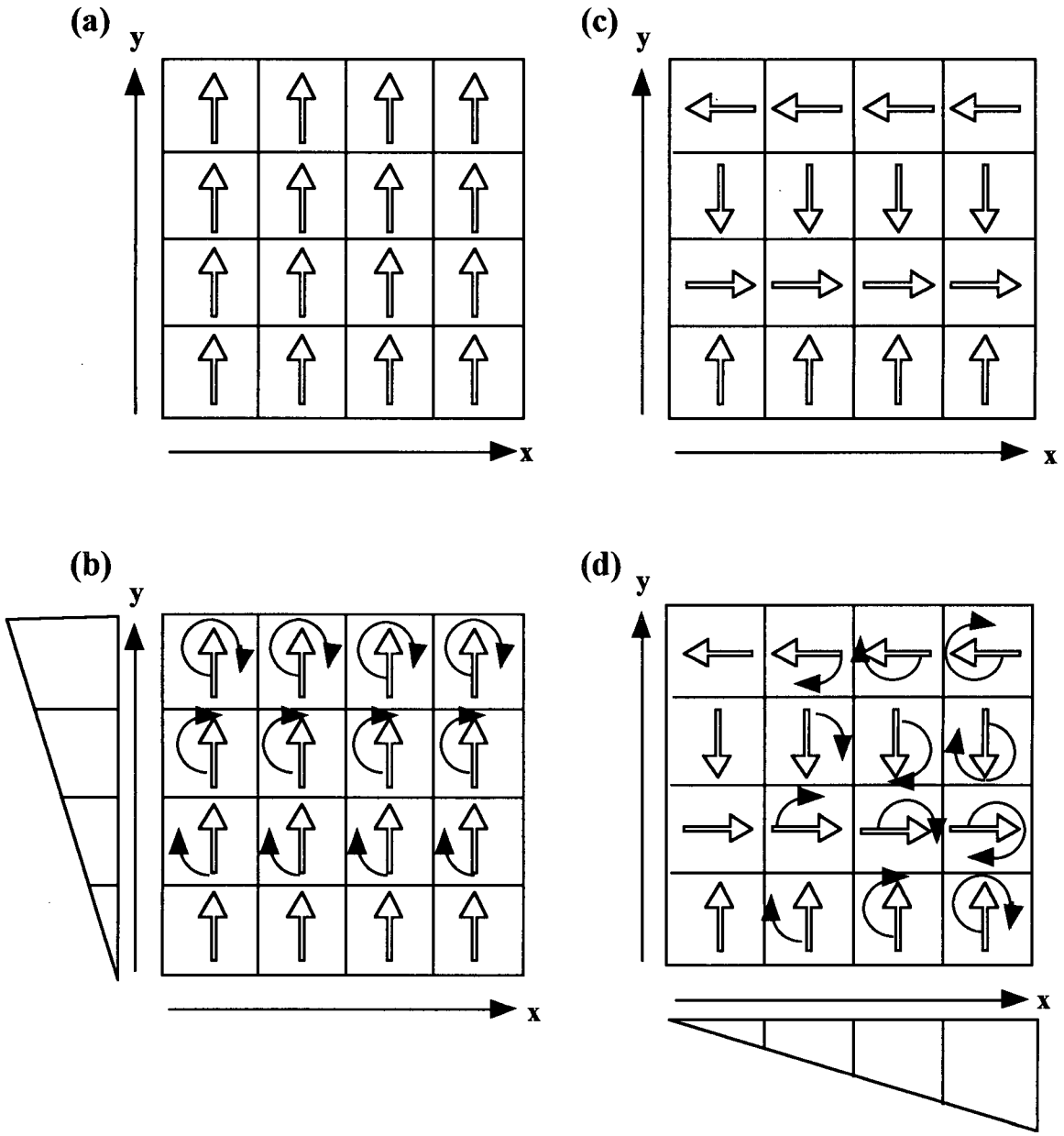

Figure 1.12: Phase and frequency encoding of a sample divided into 16 voxels, (a) the nuclear spins in the x,y-plane after the 90° pulse, (b) the differential precession of the spins during the application of the y-gradient, (c) the resulting phase-encoding of the voxels once the y-gradient is removed, and (d) the frequency-encoding of the spins as the x-gradient is applied. Each voxel in (d) is uniquely identified by the combined phase and precession frequency of the spin.

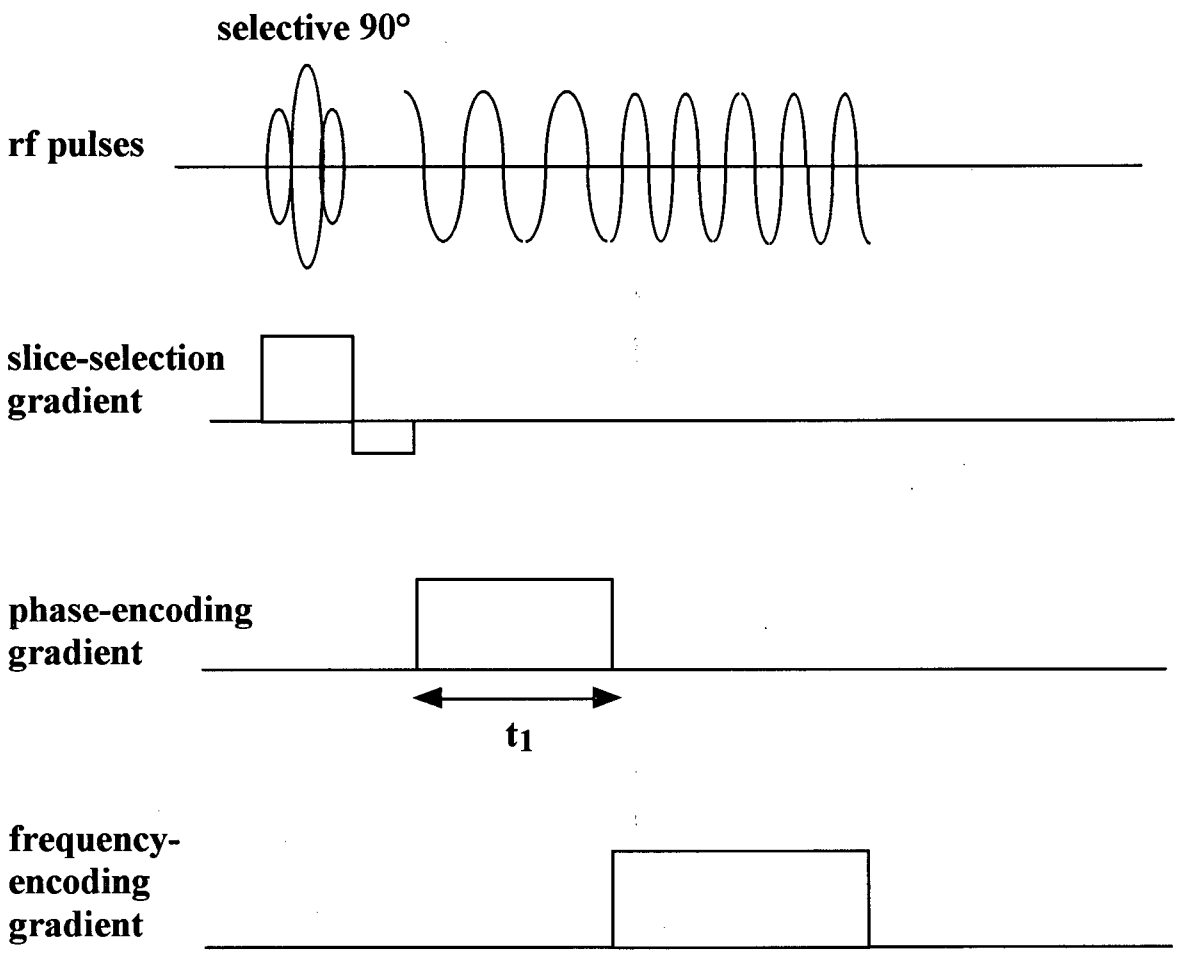

Figure 1.13: The pulse sequence for the two-dimensional Fourier imaging experiment. The FID reflects the local frequencies induced by each gradient [68].

acquisition away from the pulses and to increase the signal-to-noise ratio by $\sqrt{2}$. The final two-dimensional image is obtained by performing a Fourier transformation on both the frequency and phase domains of the two-dimensional dataset.

The spin-warp imaging pulse sequence, shown in Figure 1.14, is usually performed with a selective 90° pulse to obtain the image. The choice of gradient direction for each of the slice-selective, phase-encoding and frequency-encoding gradients depends on the region of the sample desired for the image. As in the one-dimensional imaging, the experiments are performed with a finite number of points in the frequency domain and an equal number of increments of the phase-encoding gradient producing an N x N pixel image. Each pixel contains the NMR signal from a volume element, or voxel, given by the product of the slice thickness and the square of the resolution. The signal intensity, S(x,y), from each voxel is also related to the concentration of spins, ρ(x,y), by Equation 1.15. The signal will be quantitative when $T_R \gg T_1$(x,y) and $T_E \ll T_2$(x,y). The variation of the T_R and T_E parameters can also be used to obtain a two-dimensional map of the T_1 and T_2 distribution in the slice.

1.4 Goals of the Thesis Research

The growing use of swelling-controlled drug delivery necessitates a detailed understanding of the swelling and drug release behaviour for these systems. NMR imaging, in combination with NMR spectroscopy, is presented as an ideal tool to gain new insight into the behaviour of swelling hydrophilic matrices. The ability of the technique to provide concentration information for different chemical species is fully exploited.

The hydrophilic matrix tablet chosen for the study contained HPMC as the hydrophilic polymer and one of two fluorinated compounds, trifluprom azine-HCl or 5-fluorouracil, as model drugs. Spectroscopic studies of prepared mixtures of the polymer, water, and drugs are presented in Chapter 2. These preliminary investigations provide a detailed understanding of the dependence of the diffusivity of the species and the T_1 and T_2 nuclear relaxation times on the concentration of HPMC in the system. This chapter also discusses

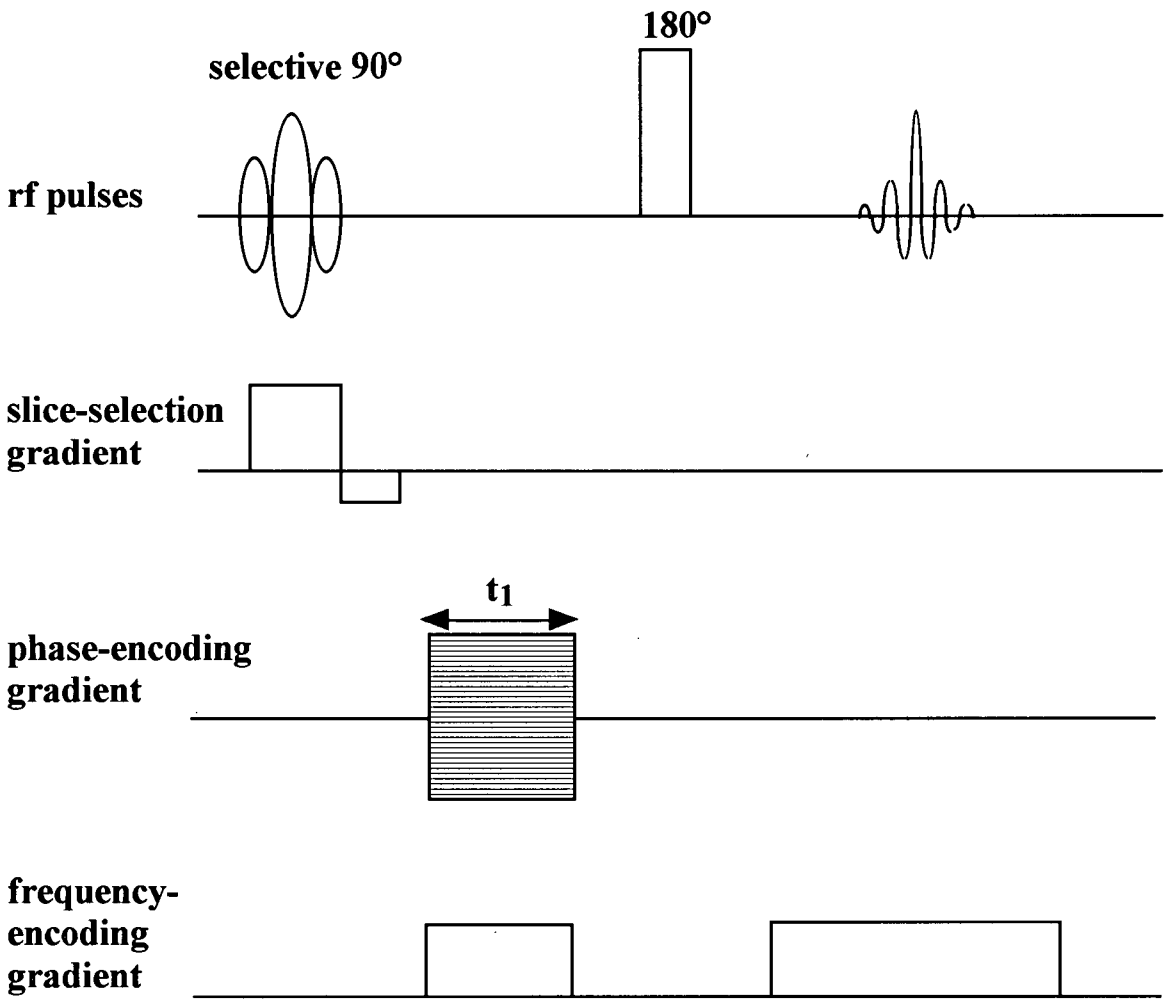

Figure 1.14: The pulse sequence for the two-dimensional spin-warp imaging experiment.

the mobility changes in the HPMC as a function of its concentration in the mixtures.

Chapters 3 and 4 develop the NMR imaging protocol required to obtain quantitative species distributions within a swelling polymer tablet. A simple geometrical arrangement for the swelling tablet is introduced that allows quantitative distributions for the water and polymer to be obtained rapidly. Chapter 3 focusses on the water in the system and tests various factors that may influence the swelling behaviour of the tablet. The method of calculating the polymer concentration from one-dimensional imaging data is presented and the polymer distributions are compared for different systems. Air bubbles in the swollen gel, the most significant factor affecting the polymer distribution results, are discussed separately in Chapter 4 where a method for removing air from the dry tablet is presented.

Chapter 5 contains the results of drug imaging studies performed in a similar manner to Chapters 3 and 4. The model drugs chosen for this study both contained fluorine so that their NMR signal could be observed without interference from the abundant water signal. Fluorine is an ideal nucleus for these imaging studies because of its high sensitivity, second only to water, and the lack of background signal from other species in the system. The distributions of the two drugs are compared to gain an understanding of the factors that affect drug release. The drug images are also used to calculate polymer distributions which are then compared with the distributions obtained from the water images.

Chapter 6 describes preliminary modelling investigations of the quantitative water, polymer and drug distributions obtained in Chapters 4 and 5. The initial modelling calculations assumed that the movement of all three species could be described by Fickian diffusion equations. A segmented tablet model for describing the polymer movement was also investigated. In this second model, the tablet is divided into segments, each of which swell according to the amount of water present, and the sum of the individual swellings results in the overall swelling of the tablet.

The final chapter provides conclusions and suggestions for future work.

Chapter 2

Spectroscopic Investigations of Mixtures Containing HPMC, Model Drugs, and Water

2.1 Introduction

One of the aims of the thesis research was to obtain quantitative concentration distributions for the components of a swelling hydrophilic matrix tablet in order to gain a better understanding of the factors that govern controlled drug release from these systems at the molecular level. To ensure that the NMR imaging experiments provided the desired information, a detailed knowledge of the NMR relaxation times of each component of the matrix was required. In addition, the nature of the hydrophilic matrix was expected to depend on the amount of water present and the degree of tablet swelling. Thus, a study of the effect of different HPMC concentrations on the NMR relaxation parameters, as well as on the diffusivity of the water and the model drugs through the polymer matrix, was also necessary. The water and drug components in the matrix can be measured directly but NMR studies of hydrated HPMC and other polymers in the gel state are hampered by their broad spectral lines and short relaxation times. However, as will be shown, the characteristics of the polymer can be inferred indirectly through the influence of the polymer on other components in the system.

In mixtures of polymer, drug and water, the drug and the water can exist in various states which are defined in terms of their interactions with the polymer. A species in a free

state has no interaction with the polymer and its movement is not hindered by the polymer in any way. When there is a bonding interaction with the polymer, the species is in a bound state which can vary in degree from a minor interaction to complete immobilization. Also, there may be multiple distinct bound states which introduces the possibility of exchange between states. NMR relaxation times depend strongly on the mobility of a species, as discussed in Section 1.2.2, and, therefore, the different states for a species would exhibit different NMR properties. Self-diffusion coefficients would also be affected by the nature of different states because the overall translational motion of a species would decrease as a result of the residency time in the less-mobile bound states.

When there are free and bound states for a particular species, the rate of exchange between the different states has a significant effect on the resulting T_2 properties of the system. If the rate of exchange is fast with respect to the rate of relaxation of the species in the NMR experiment then the measured T_2 parameter is an average of the values for the different states weighted by the fraction of time the species resides in each state as shown in Equation 2.1 where p_i is the fraction residing in the ith state [70]. When the rate of exchange is slow compared to the relaxation, then the NMR properties of the separate states are not averaged and the value of the parameter for each state is apparent in the experimental results. The latter system is still straightforward to interpret if there are only a few distinct states. When there are multiple states with a range of different relaxation rates, the analysis of the multiexponential decay behavior becomes more complex and requires non-linear least-squares calculations.

$$\frac{1}{T_{2,obs}} = \sum_i \frac{p_i}{T_{2,i}} \tag{2.1}$$

2.2 Experimental

2.2.1 Preparation of Mixtures

The structures for the materials used in this thesis—HPMC [71], trifluprom azine-

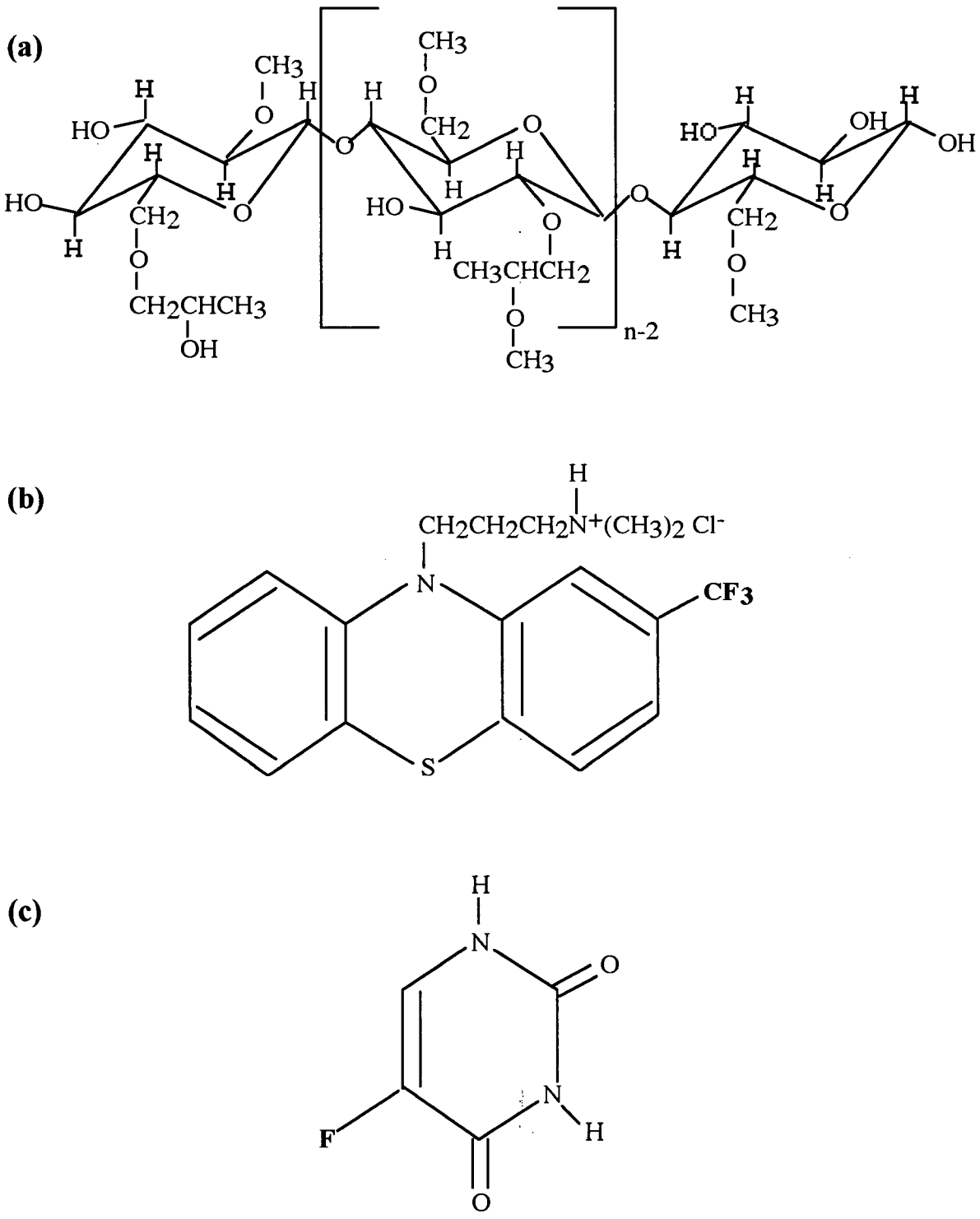

Figure 2.1: Structures of the materials used in this thesis, (a) hydroxypropylmethylcellulose (HPMC), (b) triflupromazine-HCl, and (c) 5-fluorouracil.

HCl [72] and 5-fluorouracil [72]— are shown in Figure 2.1. Hydroxypropylmethylcellulose (HPMC 2208, Methocel K4M Premium) was obtained from Dow Chemical Co. as a free-flowing white powder. The molecular weight for HPMC was 90000 g mol^{-1}, the methyl substitution was 19-24% and the hydroxypropyl substitution was 7-12% [73]. The moisture content of the powder was determined by TGA to be 5.4%. The moisture content remained constant so the powder was used as-supplied. Trifluprom azine-HCl (F.W. = 388.9 g mol^{-1}) was purchased from Aldrich Chemical company. The compound, commonly used as a tranquilizer in veterinary practice [72], was chosen because of its water solubility and because it contained a CF_3 moiety. The second model drug, 5-fluorouracil (F.W. = 130.1 g mol^{-1}), was obtained from Sigma. This drug is used as a chemotherapy agent [72]. It was chosen because of its smaller size compared to trifluprom azine-HCl and because it is uncharged.

Each mixture was prepared by weighing the appropriate amounts of HPMC, drug and distilled water into a vial. The total weight of the mixtures varied from one to two grams and representative weight ranges for each component, with an error of ± 0.00005 grams, are 0.01000 to 0.06000 grams for the model drug materials, 0 to 0.60000 grams for the polymer and >0.40000 grams for the water. Although the materials were weighed to five decimal places, the calculated concentrations were quoted with less precision due to the possibility of material loss during mixing. The components in each vial were mixed, the vial was capped, sealed with parafilm and stored in a refrigerator to allow the mixture to equilibrate. The vials were mixed a second time after several days of equilibration. The concentrations of polymer and drug in these mixtures are expressed as weight percent (w/w% or just %) which is the ratio of the weight of the specified component to the total weight of the mixture.

2.2.2 NMR Measurements

The relaxation times for the water (^1H) and drug (^{19}F) components in the HPMC mixtures were measured using a Bruker MSL400 (9.4 T) spectrometer with a Bruker micro-imaging probe incorporating a 15 mm vertical coil tuned to either ^1H or ^{19}F. The NMR measurements were performed on the mixtures in the same vials in which they were prepared.

The temperature, as determined by a variable-temperature unit, was 22 ± 1 °C. The T_1 relaxation times in the mixtures were determined by the inversion recovery sequence (180-τ-90-acquire) [59]. The signal intensity (S) variation with respect to the τ value was fit to Equation 2.2, where a and b are constants, using nonlinear least-squares fitting in the Mathematica program [74]. The T_2 times were determined using the spin-echo sequence (90-τ-180-τ-acquire) [62]. The signal intensity (S) variation with respect to 2τ or the time-to-echo (T_E) was plotted using Equation 2.3 and the value of T_2 was extracted from the slope of the straight line. The nonlinearity of the plot of Equation 2.3 for some ^{19}F measurements suggested that there were multiple T_2 species in mixtures of high HPMC concentration. In these cases, Equation 2.4 was used in Mathematica to fit the data to produce two T_2 values with the relative ratios of each species determinable from the constants c and d.

$$S = a + b \exp \frac{-\tau}{T_1} \tag{2.2}$$

$$ln(S) = \frac{-1}{T_2} T_E + constant \tag{2.3}$$

$$S = c \exp \frac{-T_E}{T_{2,1}} + d \exp \frac{-T_E}{T_{2,2}} \tag{2.4}$$

T_2 relaxation times measured using the spin-echo method can be affected by diffusion of the nuclear species through regions of magnetic field inhomogeneity [61, 62, 75, 63]. In a plot of Equation 2.3, diffusion causes an additional decrease in ln(S), above that of T_2 dephasing, leading to a downwards turn from the expected linear behavior with the greatest effect seen at the largest values of T_E. For mixtures where the plot of Equation 2.3 exhibited this effect, the T_E values for the T_2 measurement were restricted to the values used in the imaging experiments thus ensuring that the calibration conditions reflected those of imaging experiments discussed in later chapters.

The self-diffusion coefficients (D) of the water and drug components of the mixtures were measured by the Pulsed-Gradient-Spin-Echo (PGSE) method using the z-gradient of

a Doty Scientific micro-imaging probe. The diffusion coefficient of water in 10mM $CuSO_4$ solution, 2.35 x 10^{-5} cm^2 s^{-1}, was used to calibrate the z-gradient for the diffusion measurements up to the maximum gradient strength of 60 G/cm. The self-diffusion coefficients were calculated from the slopes of the plots of $\ln(A_G)$ versus the gradient strength squared (G^2) as shown in Equation 2.5 where γ is the gyromagnetic ratio of the nucleus and δ and Δ variable time parameters in the PGSE experiment. The δ and Δ times in the sequence were varied for some samples resulting in self-diffusion coefficients which were consistent with the values presented in this thesis.

$$ln(A_G) = -\gamma^2\delta^2(\Delta - \frac{\delta}{3})DG^2 + ln(A_0) \quad (2.5)$$

$$D = -\frac{slope}{\gamma^2\delta^2(\Delta - \frac{\delta}{3})}$$

Cross-relaxation or z-spectroscopy experiments were performed for selected mixtures of HPMC and water. In these experiments, a weak off-resonance preparation pulse, with an excitation width of 500 Hz, was applied for 5 s before the spectrum of water was observed. As the offset of the preparation pulse was varied, the intensity of the water signal decreased from a maximum value at offsets far from the resonance frequency of water, to a minimum value at zero offset. The z-spectra for the mixtures were prepared by plotting the normalized signal intensity versus the offset of the preparation pulse [66]. The width-at-half-height for each z-spectrum was taken as the difference between the two offset frequencies that decreased the water signal intensity to 50% of the maximum.

2.3 Results and Discussion

2.3.1 ^{1}H T_1 and T_2 Relaxation Times for Water in the Mixtures

The ^{1}H spin-lattice and spin-spin relaxation times, T_1 and T_2, respectively, were measured for the water resonance in equilibrated HPMC mixtures. Only one relaxation time was observed for each mixture, even at concentrations as high as 60% HPMC, indicating that there is rapid exchange between free water and polymer-bound water. The single relaxation

Table 2.1: Measured ^1H T_1 and T_2 relaxation parameters for the water component in mixtures of HPMC and water.

HPMC[a] / w/w%	T_1^b / s	T_2^c / ms
0	2.74	1247
2.34	2.31	472
4.71	2.20	224
7.05	2.18	186
9.44	1.82	145
14.3	1.67	67.4
18.7	1.48	45.5
23.6	1.28	30.6
28.5	1.11	25.6
38.3	0.890	15.1
47.8	0.777	8.83
56.6	0.663	6.52

[a] Corrected for 5.4% moisture content

[b] Measured by the Inversion-Recovery method, error ± 5%

[c] Measured by the Spin-Echo method, error ± 5%

time also suggests that the ^1H signal from mobile polymer protons in the mixtures is low. The T_2 relaxation times for protons in a solid polymer are typically several orders of magnitude shorter than the values for water. In the HPMC mixtures, however, the polymer chains are hydrated and the increased mobility of the hydroxyl groups may lead to T_2 values that are comparable to those of water. At 60% HPMC, using 90000 g mol^{-1} as the molecular weight, 200 g mol^{-1} as the molecular weight of each glucose unit, and three hydroxyl groups per glucose unit, the signal intensity for water would be about 5 times larger than the intensity for the hydroxyl. At 40% HPMC, the water signal is about 11 times greater than the hydroxyl signal. These calculations assume that all of the hydroxyl signal would be detectable and they do not take the ~20% methyl substitution of the hydroxyl proton into account. In section 3.3.1, imaging experiments performed with D_2O confirm that the ^1H signal from the polymer is an insignificant component of the observed ^1H signal.

The relaxation times of the water component in the HPMC mixtures are dependent on the mobility of the water within the polymer matrix and are expected to decrease with

increasing polymer concentration. The relaxation times given in Table 2.1 show that both T_1 and T_2 decreased as the weight percent of HPMC increased, reflecting the decrease in the tumbling frequency of water due to the increase in the number of hydrogen bonding interactions to the polymer chain hydroxyls. Calculations discussed in Chapter 3 required a calibration equation relating the T_2 relaxation parameter and the HPMC concentration. Equations 2.6 and 2.7 were generated from non-linear least-squares fitting to the relaxation data using the Mathematica program. The phenomenological equations describe the dependence of the relaxation times on HPMC concentrations as shown in Figure 2.2.

$$[HPMC] = 136.7\ e^{-1.274\ T_{1,H}} - 3.395 \tag{2.6}$$

$$[HPMC] = 54.86\ e^{-0.07119\ T_{2,H}} + 21.52\ e^{-0.006028\ T_{2,H}} \tag{2.7}$$

2.3.2 ^{19}F T_1 and T_2 Relaxation Times for the Trifluprom azine-HCl and 5-Fluorouracil in the mixtures

The model drugs chosen for this study both contained fluorine, an ideal nucleus for NMR studies, second only to protons in sensitivity. Detection of fluorine rather than protons allows for the observation of the model drugs independently without interference from the abundant water signal.

The dependence of the relaxation times on the HPMC concentration and on the drug concentration was investigated for each model drug. The concentration ranges chosen for the drugs in these mixtures were based on the 5% drug composition of the HPMC tablets used in the NMR imaging experiments of Chapter 5. As water penetrates the tablet and the tablet swells, the drug concentration drops from the maximum 5%. The concentrations of 3%, 1% and 0.5% were chosen to represent high, medium and low drug concentrations, respectively. Also, there is an expected correlation between drug and HPMC concentrations with the higher drug concentrations found in the more polymer-concentrated regions of the swollen tablet. Thus, the chosen concentrations for the prepared mixtures are not required

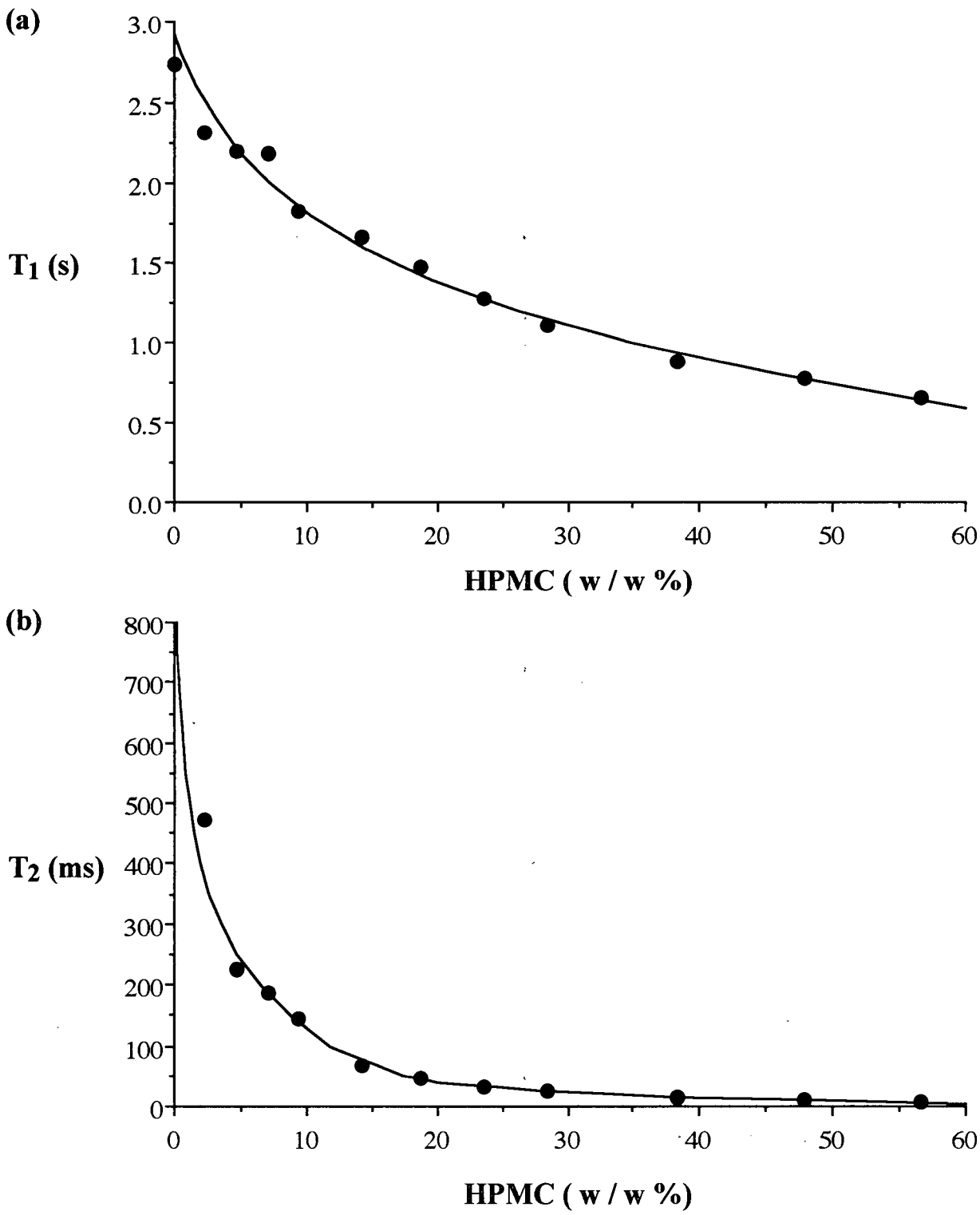

Figure 2.2: Variation of ^{1}H relaxation times of the water resonance in HPMC mixtures at equilibrium (a) T_1 values and (b) T_2 values. The filled circles are the experimental points and the lines are the curves calculated using Equations 2.6 and 2.7, respectively.

Table 2.2: Measured ^{19}F T_1 and T_2 relaxation parameters for the triflupromazine-HCl component of mixtures of HPMC, triflupromazine-HCl and water.

Drug / w/w%	HPMC[a] / w/w%	T_1^b / s	T_2^c / ms
0.50	0	1.19	682
0.50	2.14	1.11	274
0.50	4.76	0.998	120
0.50	9.56	0.874	92.6
0.50	13.6	0.803	63.3
0.50	20.2	0.748	43.0
1.0	0	1.12	600
1.0	2.53	1.03	276
1.0	4.48	0.981	147
1.0	15.2	0.833	64
1.0	19.9	0.771	49.1
1.0	24.2	0.730	35.9
1.0	30.8	0.700	23.4 (54%)[d], 8.0 (46%)
1.0	39.2	0.673	9.1 (63%), 2.0 (37%)
1.0	46.3	0.623	5.5 (50%), 1.02 (50%)
1.0	60.0	—	5.9 (21%), 0.75 (79%)
3.0	0	0.884	206
3.0	2.49	0.867	162
3.0	5.23	0.838	111
2.9	10.2	0.803	75.7
3.0	16.0	0.776	57.9
3.0	21.4	0.760	45.2
3.0	29.7	0.674	25.1 (54%), 9.2 (46%)
3.0	40.3	0.690	12.8 (51%), 1.77 (49%)
3.0	46.2	0.671	5.0 (58%), 1.18 (42%)
3.0	58.4	—	2.41 (28%), 0.74 (72%)

[a] Corrected for 5.4% moisture content

[b] Measured by the Inversion-Recovery method, error ± 5%

[c] Measured by the Spin-Echo method, error ± 5%

[d] Percentage of the species with the preceding T_2 value

to cover all the possible combinations of drug and HPMC concentration.

Trifluprom azine-HCl was the first model drug studied. The measured ^{19}F relaxation times for it in the HPMC mixtures are given in Table 2.2 and displayed in Figure 2.3. The relaxation times decreased with increasing HPMC concentration as expected. The relaxation times also exhibited a dependence on the trifluprom azine-HCl concentration at low HPMC concentrations. The polymer influence on the relaxation times became the dominant effect at concentrations above 10% as little difference was observed between the relaxation times of mixtures of varying drug composition.

Unlike the water measurements, two T_2 relaxation species were observed for trifluprom azine-HCl at polymer concentrations 30% and above. The observation of the distinct species suggests that the bonding interactions between trifluprom azine-HCl and the polymer lead to an exchange rate between states slower than the T_2 relaxation rate corresponding to each state. The relative abundance of the short T_2 species indicates that there will be some signal lost from trifluprom azine-HCl in the imaging experiments, even at the shortest T_E times. The imaging experiments of the drug will require an external signal calibration to correct for the loss of signal in high HPMC regions in order to obtain concentration distributions that are quantitative throughout the swollen tablet. The T_2 values of the trifluprom azine-HCl were used to obtain an average relationship between the relaxation time of the ^{19}F and the HPMC concentration. The resulting Equation 2.8 was obtained by non-linear least-squares fitting of a subset of the data in Table 2.2. The relaxation times of the 3% mixtures below $\approx$20% HPMC were not used in the fit because these concentration combinations are unlikely to be present in the swollen tablet. In the mixtures where two distinct T_2 species were present, the relative amounts of each species and the range of T_E values for the imaging experiments of Chapter 5 were used to determine effective T_2 values. For all but two of the mixtures, the apparent T_2 values were the same as those in Table 2.2. For the specific conditions of ^{19}F imaging experiments of this thesis, the calculated apparent T_2 values for the 30.8% and 39.2% mixtures were 13.9 ms and 8.87 ms respectively. These latter values were used to determined Equation 2.8, the calibration

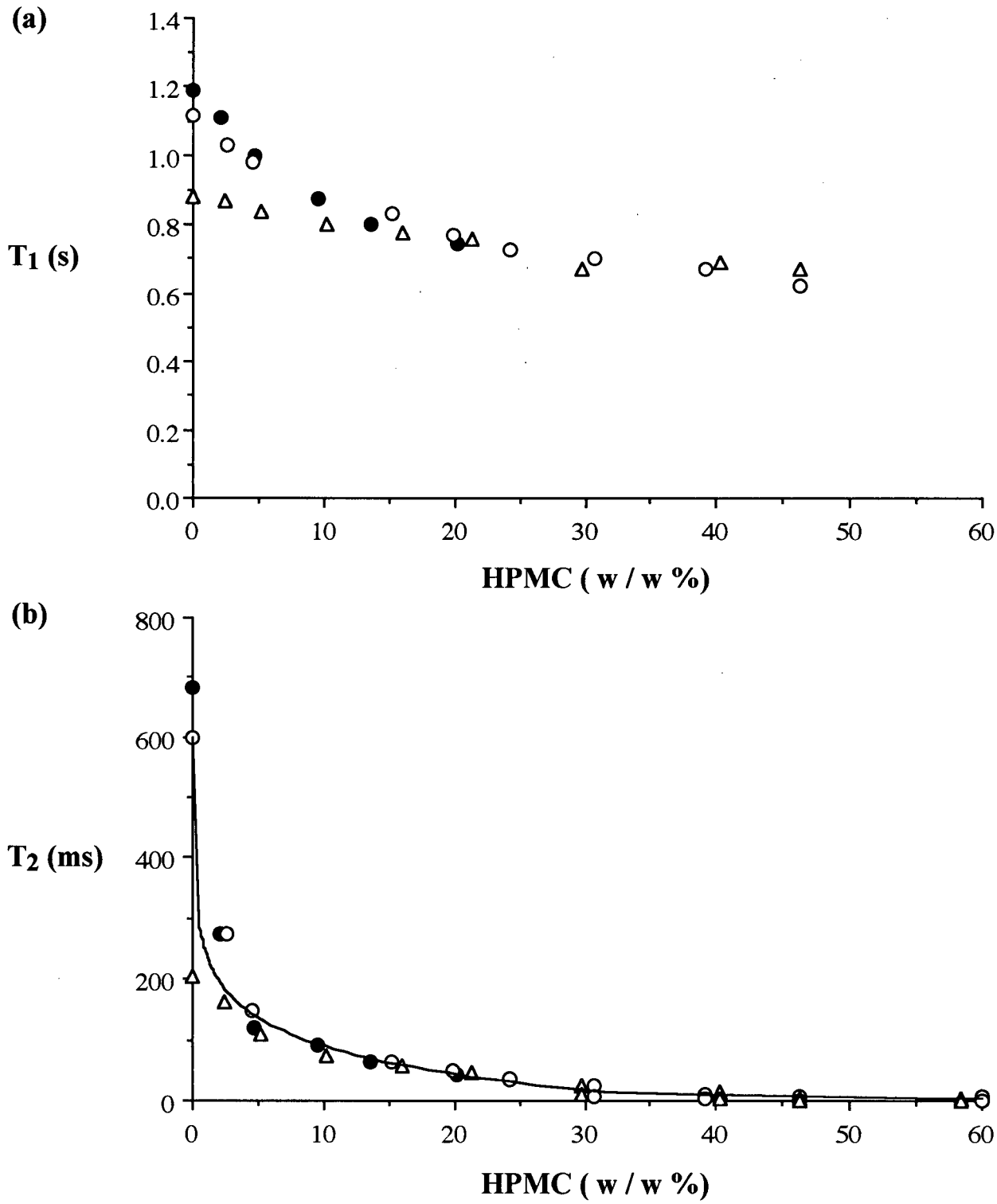

Figure 2.3: Variation of ^{19}F relaxation times of the trifluprom azine-HCl component in HPMC mixtures at equilibrium (a) T_1 values and (b) T_2 values. The concentrations of the drug are 0.5% (filled circles), 1% (open circles), and 3% (open triangles). The line in (b) is the curve calculated from Equation 2.8.

equation relating T_2 values calculated from the ^{19}F imaging experiments of Chapter 5 to HPMC concentration.

$$[HPMC] = 38.18\ e^{-0.01489\ T_{2,triflu}} + 87.09\ e^{-0.2869\ T_{2,triflu}} \qquad (2.8)$$

Table 2.3: Measured ^{19}F T_1 and T_2 relaxation parameters for the 5-fluorouracil component of mixtures of HPMC, 5-fluorouracil, and water.

Drug / w/w%	HPMC[a] / w/w%	T_1^b / s	T_2^c / ms
0.50	0	3.64	390
0.54	10.6	2.26	200
0.50	20.4	1.51	93.2
1.0	0.909	3.33	306
1.0	9.93	2.26	205
1.1	18.0	1.61	130
1.0	30.0	1.06	25.4
3.0	19.9	1.43	74.3
3.0	31.5	1.01	20.2
3.0	39.7	0.822	7.1
2.9	46.7	0.734	≈9-30 (≈13%)[d], ≈2.9 (≈87%)

[a] Corrected for 5.4% moisture content
[b] Measured by the Inversion-Recovery method, error ± 5%
[c] Measured by the Spin-Echo method, error ± 5%
[d] Percentage of the species with the preceding T_2 value

The data given in Table 2.3 show the combinations of HPMC and 5-fluorouracil concentrations that were prepared in the study of the relaxations times of the second model drug. The trends in relaxation times, clearly shown in Figure 2.4, are similar to those of trifluprom azine-HCl. Both the T_1 and T_2 relaxation times decrease with increasing HPMC concentration. There is a slight indication in the plots that the relaxation times are dependent on the 5-fluorouracil concentration as well. In contrast to the trifluprom azine-HCl results, single T_2 relaxation species were observed for 5-fluorouracil up until 50%. The results of the double-exponential fits to the intensity data for this concentration yielded a small percentage of a variable, oddly-large, T_2 species, in combination with a species

of a more reasonable T_2 value. The relaxation times for 5-fluorouracil suggest that the signal obtained for this drug in the imaging experiments will be essentially quantitative in all regions of the swollen tablet and will not need to be corrected as extensively as in the triflupromazine-HCl experiments. The data of Table 2.3 were fit to Equation 2.9 using non-linear least-squares fitting.

$$[HPMC] = 20.72\ e^{-0.1017\ T_{2,5flu}} + 47.92\ e^{-0.002902\ T_{2,5flu}} - 16.61 \quad (2.9)$$

2.3.3 Self-diffusion Coefficients for Water, Triflupromazine-HCl and 5-Fluorouracil in the Mixtures

The diffusion behaviors of the water and drug within the swollen gel are major factors in the rate of drug release from a hydrophilic matrix tablet. The rate of gel formation depends strongly on how rapidly water can move into dry and concentrated polymer regions. Once the gel is formed, the drug can escape the tablet either by the erosion of the gel or by diffusion through the gel.

Table 2.4: Measured self-diffusion coefficients for the water component of mixtures of HPMC and water.

HPMC[a] / w/w%	D[b] / 10^{-5} cm^2 s^{-1}
0	2.17
4.71	1.95
9.44	1.83
18.7	1.4
28.5	0.96
38.3	0.51

[a] Corrected for 5.4% moisture
[b] PGSE method, error ±0.05

The measured self-diffusion coefficients for water, given in Table 2.4, decrease smoothly as the HPMC concentration is increased, dropping to approximately one quarter of the diffusion value for distilled water. The diffusion coefficients for the model drugs,

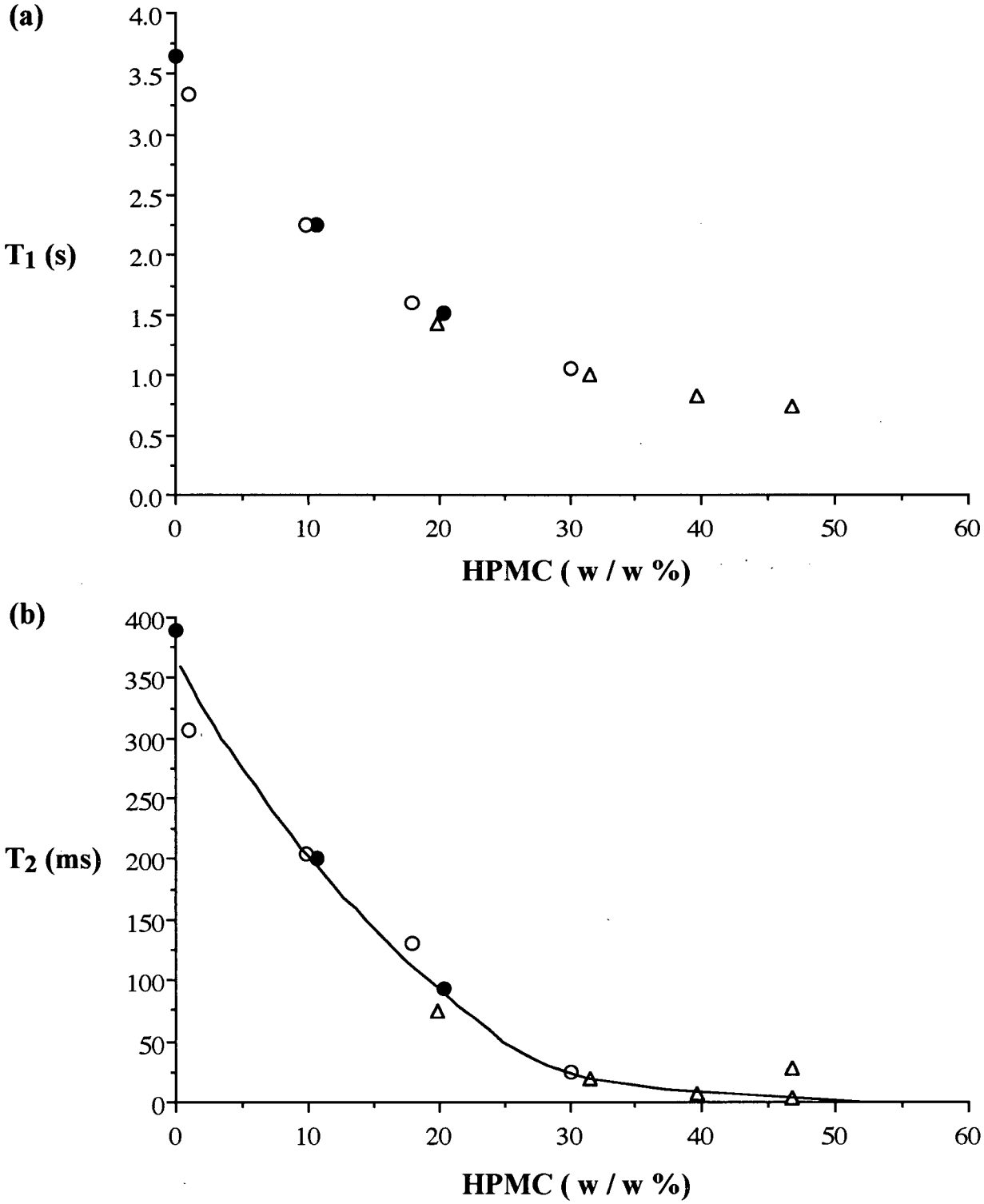

Figure 2.4: Variation of ^{19}F relaxation times of the 5-fluorouracil component in HPMC mixtures at equilibrium (a) T_1 values and (b) T_2 values. The concentrations of the drug are 0.5% (filled circles), 1% (open circles), and 3% (open triangles). The line in (b) is the curve calculated from Equation 2.9.

Table 2.5: Measured self-diffusion coefficients for the trifluprom azine-HCl (^{19}F) component of mixtures of HPMC, trifluprom azine-HCl and water.

Drug / w/w%	HPMC[a] / w/w%	D[b] / 10^{-6} cm^2 s^{-1}
0.50	0	4.53
1.0	0	3.67
1.0	4.61	1.81
1.0	9.66	1.02
1.0	19.3	0.36
3.0	0	1.94
3.0	4.11	1.31
3.0	9.64	0.94
3.0	19.3	0.60

[a] Corrected for 5.4% moisture

[b] PGSE method, error ±0.05

Table 2.6: Measured self-diffusion coefficients for the 5-fluorouracil (^{19}F) component of mixtures of HPMC, 5-fluorouracil and water.

Drug / w/w%	HPMC[a] / w/w%	D[b] / 10^{-5} cm^2 s^{-1}
0.50	0	1.01
0.54	10.6	0.86
0.50	20.4	0.28
1.0	0.909	0.92
1.0	9.93	0.86
1.1	18.0	0.32
1.0	30.0	0.34
1.1	37.5	0.17
3.0	31.5	0.27
3.0	39.7	0.15

[a] Corrected for 5.4% moisture

[b] PGSE method, error ±0.05

Tables 2.5 and 2.6, indicate that 5-fluorouracil self-diffuses about twice as quickly as triflupromazine-HCl in solutions containing only 0.5% drug. As the HPMC concentration increased, the diffusion coefficients of both drugs decreased but not at the same rate. The diffusion of triflupromazine-HCl appears to be more strongly affected by the increasing polymer concentration.

The self-diffusion coefficients for all three species are shown in Figure 2.5. The diffusion coefficients measured for the water and model drugs in the mixtures should reflect the values for the same species in regions of the tablet with similar composition. A comparison of the measured diffusion coefficients to the apparent diffusion parameters determined from the modeling calculations of Chapter 6 will be of great interest.

2.3.4 Mobility Changes in the Polymer as Determined by NMR Spectroscopy

In the simplest description of a swollen polymer-water system, the water can be considered to exist in one free and one bound state. The fact that only one relaxation component is observed for the water nuclei indicates that these states are in rapid equilibrium. The free water has a longer T_2 value than the bound water and the resulting average in the fast-exchange limit is a combination of the two T_2 values as shown by Equation 2.1, yielding Equation 2.10. A plot of the inverse of the observed T_2 as a function of the fraction of bound water should yield a straight line with an intercept of $1/\ T_{2,free}$, in this case the inverse of the T_2 of distilled water.

$$\frac{1}{T_{2,obs}} = \frac{p_{free}}{T_{2,free}} + \frac{p_{bound}}{T_{2,bound}} = \frac{1}{T_{2,free}} + p_{bound}\left(\frac{1}{T_{2,bound}} - \frac{1}{T_{2,free}}\right) \qquad (2.10)$$

For the various HPMC mixtures, the fraction of bound water is unknown but should be related to the concentration of the polymer. Figure 2.6 shows the plot of $1/T_{2,obs}$ versus HPMC weight percent. The data in Figure 2.6 appear to separate into three distinct linear regions. The data from 0% to 10% HPMC fall on one line, the data from 10% to 30% fall

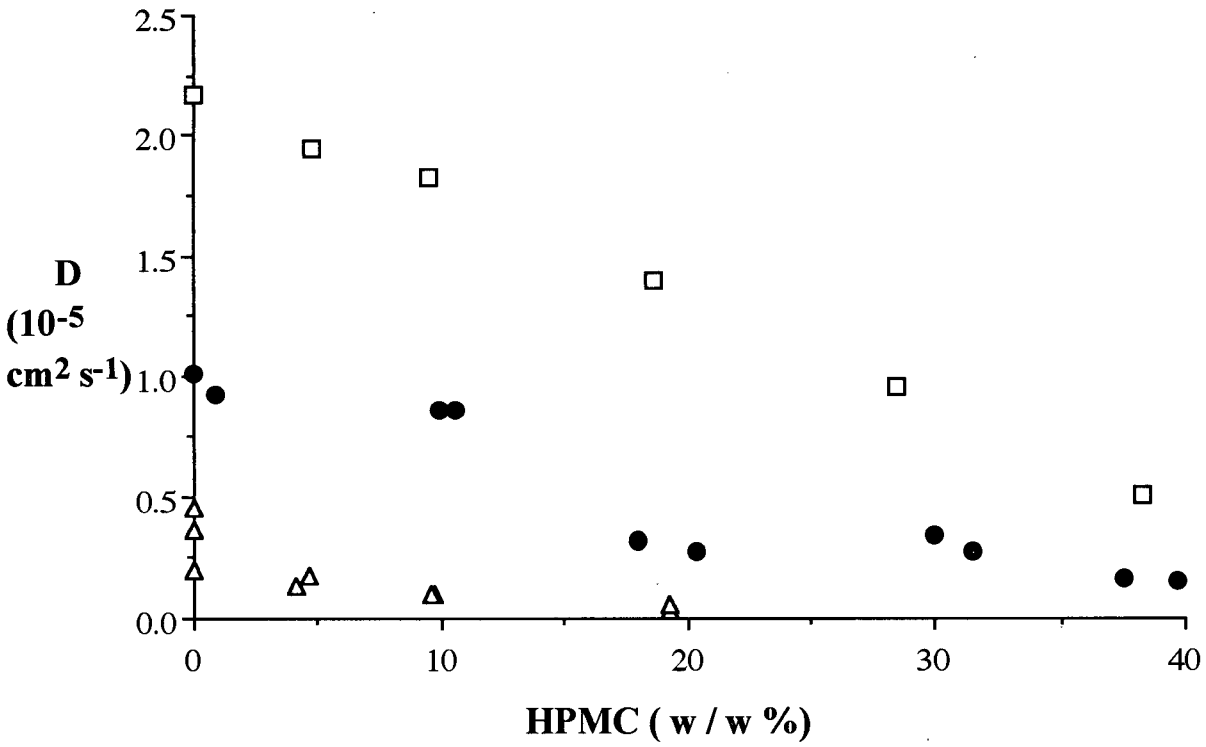

Figure 2.5: Self-diffusion coefficients of water (open squares), trifluprom azine-HCl (filled circles), and 5-fluorouracil (open triangles) in selected HPMC mixtures. No distinction has been made between mixtures of varying drug concentration.

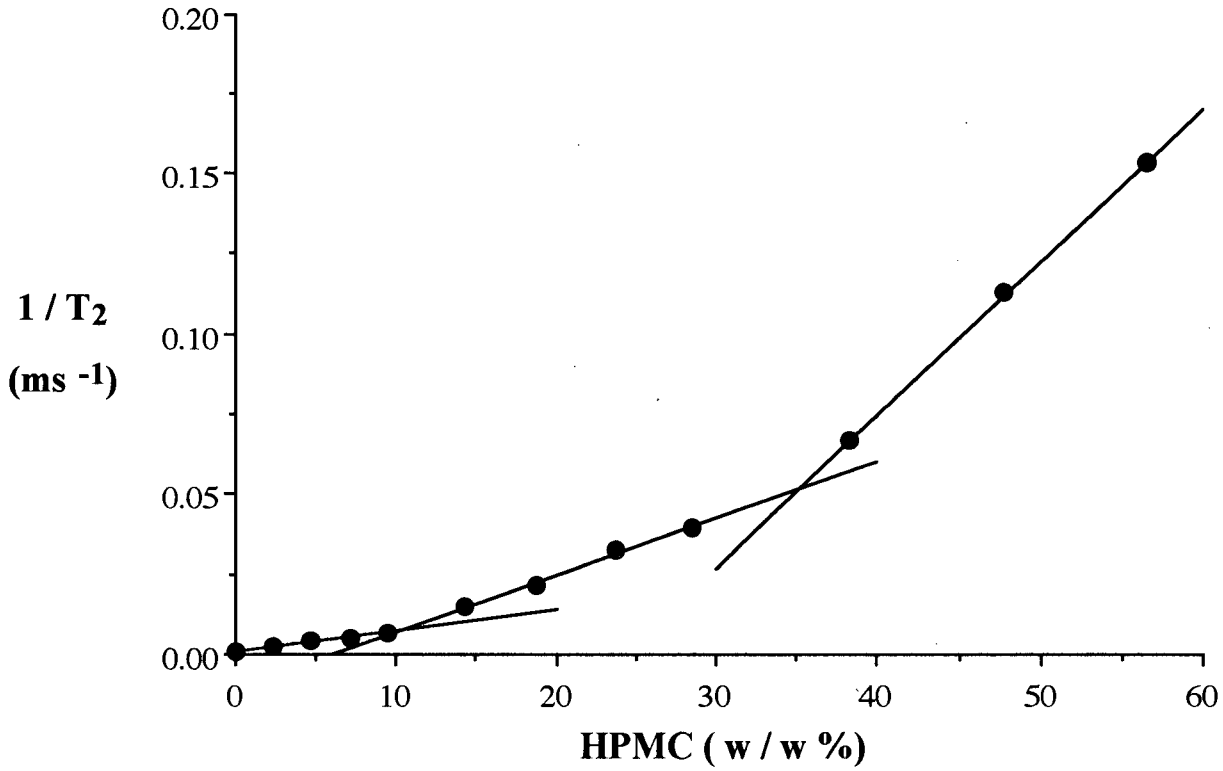

Figure 2.6: The inverse of the T_2 of the water component in HPMC mixtures as a function of HPMC weight percent indicating discontinuities at ≈12% and ≈35% HPMC.

on a second line, and the values from 40% to 60% appear to fall on a third line. The slope for each line is $h\{1/T_{2,bound} - 1/T_{2,free}\}$ where the fraction of bound water is the product of the constant h and the weight percent HPMC. The intercept for the 0-10% line yields $1/T_{2,free}$ as expected according to Equation 2.10, but the intercepts for the second and third lines are far removed from that value.

There are two possible explanations for the discontinuities that occur at approximately 12% HPMC and 35% HPMC [76]. The hydration of the polymer may have changed, thus altering the bound water fraction and the coefficient h in the slope. Another explanation is that the T_2 of the bound water has changed. Since the T_2 of the bound water depends on the mobility of the polymer to which it is bound, a substantial change in the mobility of the polymer chains in the polymer-water mixture would cause a significant change in the $T_{2,bound}$. The first discontinuity in Figure 2.6 appears in the same, semi-dilute concentration region where the mixture would first be classified as a gel rather than as a viscous solution. The polymer chains in the gel state would be expected to be more restricted than in solution but more mobile than in the solid polymer. Thus, the first discontinuity is probably due to a substantial decrease in chain mobility when the polymer becomes concentrated enough to form the physical entanglements required for the gel state. The second discontinuity occurs in the concentration region where the mixtures lose their transparency and resemble wetted powders rather than gels. The discontinuity at higher HPMC concentration may be due to dehydration below the water concentration necessary for optimum water-mediated, interchain H-bond cross-linking. When the H-bonding interaction occurs directly between the polymer chains, rotational motion would become greatly restricted.

In order to check this interpretation of the data of Figure 2.6, the mobility of the polymer component in the polymer-water mixtures was probed with the technique of cross-relaxation or z-spectroscopy. This experiment requires water to be in the presence of a polymer which provides so-called solid-like protons to interact with the bound water component. An off-resonance pulse, applied to saturate the resonances of the solid-like

component. An off-resonance pulse, applied to saturate the resonances of the solid-like protons in the system, indirectly affects the magnetization of the water because, during the length of the pulse, cross-relaxation through dipolar coupling occurs between the protons of the bound water and those of the polymer. When the spectrum of the water is acquired after the off-resonance pulse, the intensity of the signal will decrease relative to the intensity in the absence of the preparation pulse, reflecting the amount of cross-relaxation that has occurred. The z-spectrum is the plot of the normalized signal intensity, M/M_0, versus the offset of the presaturation pulse. Figure 2.7 shows the z-spectra for some of the HPMC mixtures. In general, these z-spectra provide direct evidence that substantial interaction occurs between the water and the polymer protons. Only water nuclei in close proximity to the polymer, *i.e.* bound water, can participate in cross-relaxation with the polymer protons because the magnitude of the dipolar coupling interaction is inversely proportional to the internuclear distance cubed. Exchange between the hydroxyls of the HPMC and the hydroxyls of the water would be an additional mechanism for magnetization transfer between the water and the polymer. The z-spectrum of distilled water is included to show the result of the same experiment on a sample where the possibility for cross-relaxation is absent and indicates that direct saturation from the off-resonance pulse is minimal for moderate offsets.

An important feature of these plots is that the width-at-half-height, $\Delta_{1/2}$, of the z-spectrum is related to the width of the spectral line for the solid-like protons, even where, as in the present case, the proton spectrum of the solid component is not observed directly. The broad lines of solids are due to the presence of dipolar couplings that are not averaged to zero by motion. Thus, the less mobile the polymer chains, the broader the line for the polymer protons and the broader the corresponding z-spectrum for the water in the polymer. Table 2.7 shows that the widths of the z-spectra increase with increasing polymer concentration. The width-at-half-height for the 20% mixture was almost five times that for the 10% mixture. No other doubling in polymer concentration resulted in such an increase in the width of the z-spectrum; widths doubled for all other comparisons. These results

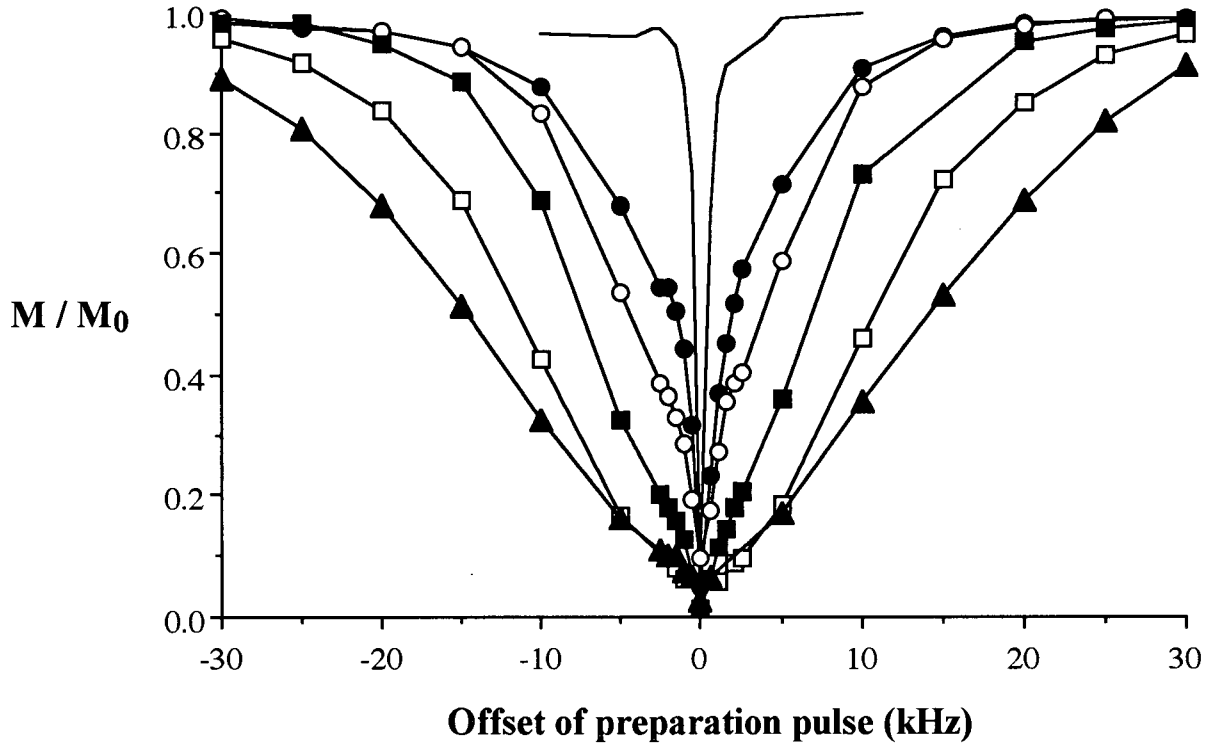

Figure 2.7: ^{1}H NMR Z-spectra for selected HPMC mixtures from observations of the ^{1}H signal of H_2O. The mixtures shown are water (line), 9.4% (filled circles), 14.2% (open circles), 18.7% (filled squares), 38.3% (open squares) and 56.6% (filled triangles). A preparation pulse with an excitation width of 500 Hz was applied at different offset frequencies for five seconds prior to the acquisition on the water signal. (Only the range of offsets of -30 kHz to +30 kHz is shown.)

Table 2.7: Width-at-half-height values for z-spectra of HPMC mixtures.

HPMC[a] / w/w%	$\Delta_{1/2}$ / kHz	Relative $\Delta^b_{1/2}$
4.71	1.42	1
9.44	3.18	2.24
14.3	7.45	5.25
18.7	14.3	10.1
28.5	18.5	13.0
38.3	22.0	15.5
56.6	28.8	20.3

[a] Corrected for 5.4% moisture content

[b] Relative to the $\Delta_{1/2}$ of the 4.71% mixture

suggest that there is a significant change in the mobility of the polymer when the polymer concentration passes between 10% and 20%. Thus, the results of the z-spectroscopy support the interpretation that the discontinuity at ~12% in Figure 2.6 is the result of a change in the polymer mobility. Since there was not a correspondingly large change in the z-spectrum around 35% HPMC, the second discontinuity in Figure 2.6 was interpreted as a change in the hydration characteristics of the polymer.

2.4 Summary

The dependences of the relaxation times for the water and the model drugs on HPMC concentration were determined. These values are assumed to be representative of the polymer environment in the swollen tablet in regions of similar composition. The calibration of the water T_2 values and HPMC concentration will be used in Chapter 3 to calculate HPMC concentrations from T_2 values measured from the ^{1}H NMR imaging experiments. Similar phenomenological equations relating the T_2 relaxation times of the fluorinated drugs to the polymer concentration were also determined. The use of these equations in the ^{19}F imaging experiments of Chapter 5 will allow for alternate calculations of the polymer distribution which can be compared with the one obtained from the imaging studies of water.

The mobility changes of the polymer were studied by relaxation time measurements

and z-spectroscopy. Both experiments suggested that the mobility of the polymer decreases substantially when the HPMC concentration passes between 10% and 20%. The formation of a gel state in this concentration region is believed to be the cause of the mobility change. The position of the gel-solution transition point in the swollen tablet, an important factor in the drug release process, can now be monitored. . .

Chapter 3

One-dimensional ^{1}H NMR Imaging Investigations of Water and Polymer in Swelling HPMC Tablets

3.1 Introduction

The swelling of hydrophilic polymers such as HPMC depends on a number of different processes such as water penetration, polymer hydration and the subsequent increases in polymer chain mobility. Traditionally, the swelling behavior of tablets prepared from HPMC and similar polymers has been studied by examining bulk changes in the tablet by direct physical measurement or with optical microscopy and photography as described in Section 1.1.4. Changes in tablet dimensions and the water penetration front into the tablet have been used to draw conclusions regarding the nature of the water and polymer transport processes. An in-depth understanding of these swelling systems, however, requires an exact knowledge of the water and polymer concentrations as functions of position and swelling time. Such concentration distributions are necessary to develop and test models for the swelling behavior of the polymer. NMR imaging is an ideal technique for studying these systems because it can provide spatially-resolved concentrations for individual chemical species and can monitor changes in their concentrations within a single sample during the entire swelling process in a non-invasive and non-destructive manner.

Some previous investigators have used NMR imaging to probe the penetration of water into hydrophilic polymer tablets [46, 47, 48, 49]. In these studies, tablets were

placed in water to swell and, at various intervals, the water was carefully removed and two-dimensional, slice-selective images of the water within the tablet were acquired. The images showed water penetration into the tablet core and overall dimensional increases of the tablet due to the swelling. These studies, however, yielded only a qualitative description of the swelling process because the images were not acquired with experimental parameters that guaranteed quantitative signal intensities. Thus, the signals in the images could not be directly related to the concentrations of water in the system. Also, these studies were limited to the water in the tablet; the polymer concentration distributions in the swelling tablet were not investigated directly although the overall swelling behavior of the tablet was discussed in terms of the changes in the apparent tablet 'dimensions' that were visible in the images.

The acquisition of quantitative concentration distributions in reasonably short times, and at frequent intervals, during the course of the experiment is an essential requirement for the detailed study of swelling polymer tablets. Two-dimensional imaging techniques generally do not meet this criterion. The total experimental time to acquire one quantitative two-dimensional image of water is of the order of hours rather than of minutes due to the relatively long T_1 relaxation time of water. The unrestricted swelling of a tablet is also a very complex system to analyse because the processes of water diffusion and polymer expansion occur in three dimensions. These two experimental considerations necessitate an alternate system for the imaging studies from those presented in the literature. In the present work, a flat-faced, disk-shaped polymer tablet was placed in a tube such that only one of its faces was exposed to water. The diffusion and expansion processes in this system occur along one dimension only, the long axis of the tube. Because of the cylindrical symmetry, the concentration distributions of the water and polymer can be determined by using a single gradient along the axis of the tube to produce one-dimensional images. The major advantages of the latter imaging technique compared to two-dimensional imaging are the greatly decreased experimental time required to obtain quantitative images and the simplicity of the subsequent analysis.

3.2 Experimental

3.2.1 Preparation of HPMC Tablets

Tablets were prepared by direct compression of the as-supplied HPMC powder using a rotary tablet press modified to detect compressional forces. The HPMC powder was weighed on a top-loading balance and then transferred to the die of a Beta Manesty rotary tablet press. The thickness of the tablet and the peak force of compression were controlled by an adjustable screw that varied the position of the upper compression wheel of the press and thus the position of the upper punch during compression. Each tablet was weighed after compression and its dimensions recorded. Different types of tablet were prepared by varying the amount of HPMC and the force of compression. The properties of each tablet type are summarized in Table 3.1.

Table 3.1: Definition of HPMC tablet types and summaries of their characteristics

Type	HPMC[a] (mg)	Compressional Force (MPa)	Diameter[b] (mm ± 0.01)	Thickness[b] (mm ± 0.01)
1	162 ± 1	62± 3	12.75	1.33
2	323 ± 3	60 ± 1	12.75	2.66
3	323	103	12.75	2.46

[a] corrected for 5.4% w/w in as-supplied material water content

[b] as measured with digital calipers

3.2.2 Experimental Setup for Swelling Investigations

The swelling experiments were carried out with the tablet and water in a 15 mm o.d. (12.8 mm i.d.) NMR tube held vertical in the rf coil. Figure 3.1 shows the two variations of the experimental setup used in these studies. The upward-swelling arrangement, Figure 3.1(a), was used for the majority of the experiments. In this experimental variation, the HPMC tablet was placed on a support at the end of the tube with only one face exposed to water. The bottom face and the edges of the tablet were sealed with a small amount of fluorinated grease to prevent leakage of water between the tablet and the tube wall. The second variation of the setup, depicted in Figure 3.1(b), was used to obtain data for

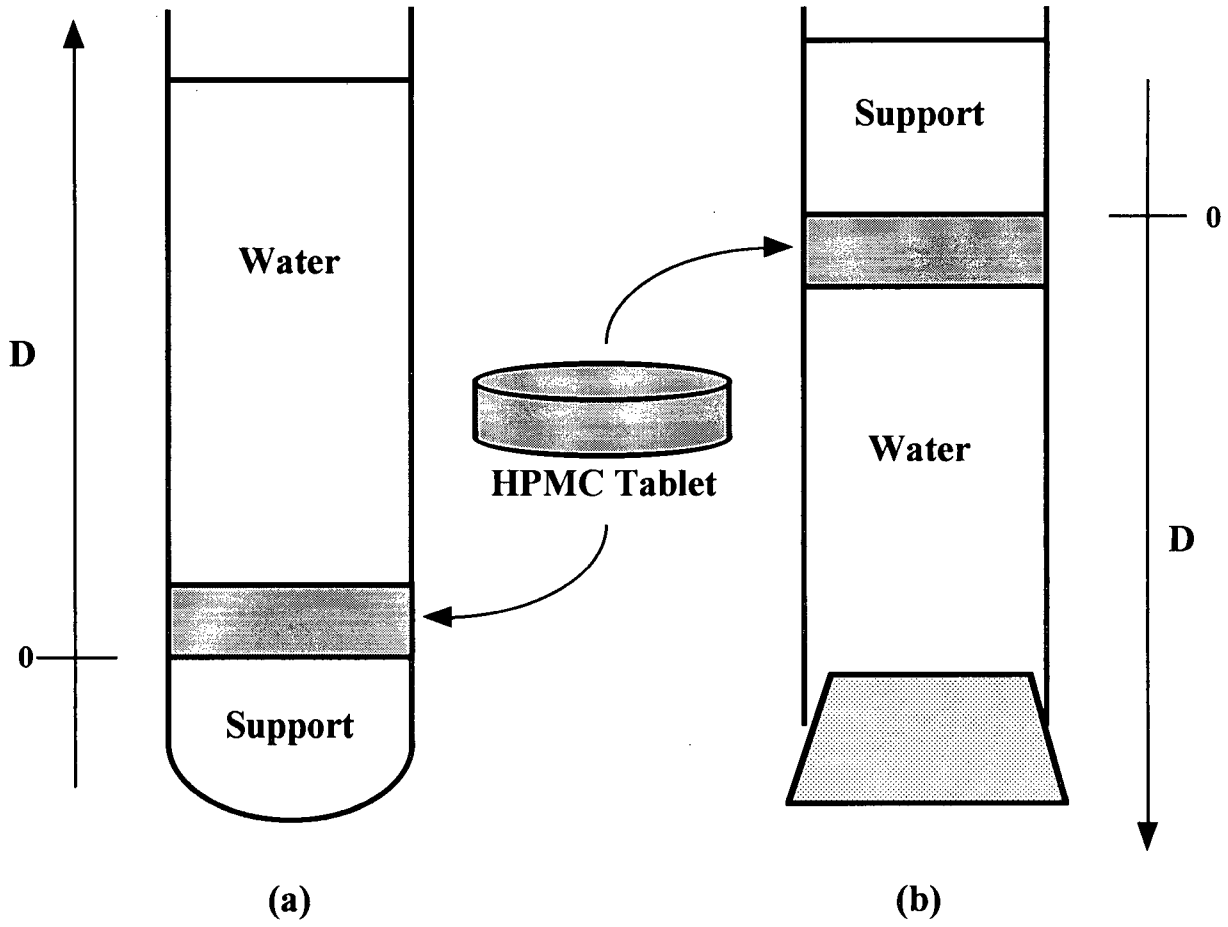

Figure 3.1: Tablet arrangement for swelling (a) upwards and (b) downwards. The arrows indicate the direction of increasing distance as measured from the back face of the tablet resting against the solid support.

downward-swelling to test for possible effects due to gravity. In this system, the top face of the tablet was held against the support and the bottom face was exposed to water. The top face and edges of the tablet were sealed with grease which, in addition to preventing water penetration along the tablet edges, adhered the tablet to the support.

The preparation of the tablet for imaging of upwards-swelling was straightforward. First, the glass support was placed in the NMR tube. Then, Fluorolube GR-90, a fluorocarbon grease manufactured by Fisher Scientific, was applied between the edges of the glass support and the wall of the tube using a long home-made 'syringe' composed of a piece of tubing and a plastic rod. The tablet was then added to the tube and carefully pressed into the grease. A marker, consisting of a glass bulb at the end of a thin rod, was positioned in the tube and the distance between the centre of the bulb and the bottom face of the tablet was measured. This distance, typically 1 cm, provided an additional reference for the calibration of the distance scale in the swelling experiments as will be discussed in Section 3.2.3. The preparation for the downwards-swelling was similar except that the position marker was not used.

The swelling of the HPMC tablet was initiated by the addition of water to an initially dry tube. When the upward-swelling of the tablet was investigated, 5 mL of distilled water were added to the NMR tube to ensure that a large enough excess of water was present to have a semi-infinite expansion of the polymer tablet. For the downward-swelling variation, only 2 mL of water were used because of imaging constraints. A larger volume of water would require that the tablet be placed higher in the tube which could result in the tablet residing at the edge of the coil and therefore outside the reliable image field of view. Because of the limited volume of water, this setup was only used with Type 1 tablets which contained the least amount of HPMC and would be least affected by a limited source of water. For this system, the glass support, grease, tablet, and water were added while the tube was inverted with respect to the arrangement in Figure 3.1(b). A greased rubber septum was used to stopper the open end of the tube. When the septum was put in place, it was punctured with a needle to allow pressure equilibration and escape

of air bubbles that would rest against the tablet when the tube was inverted and distort the NMR images.

3.2.3 One-dimensional Imaging

The one-dimensional imaging experiments were performed on a Bruker MSL400 (9.4T) spectrometer with a Bruker microimaging probe incorporating a 15 mm vertical coil tuned to 400.12 MHz, the ^{1}H resonance frequency. The NMR tube containing the tablet was suspended in the centre of this coil for the entire duration of the swelling experiment. The z-gradient of the Bruker microimaging probe was along the same direction as the main magnetic field and the long axis of the NMR tube. A tube containing a 10 mM $CuSO_4$ solution was used to determine the 180° and 90° pulse times and to adjust the shimming to ensure a homogenous magnetic field.

One-dimensional ^{1}H images were obtained for this system using the spin-echo pulse sequence given in Figure 3.2. All images were acquired with quadrature phase cycling which requires that the number of scans be a multiple of 4. The relationship between the concentration of proton spins, ρ, and the signal obtained with the imaging experiment, $S(T_E)$, was given previously in Equation 1.15. Table 3.2 gives the typical parameters used in the experiments presented in this chapter. The experimental time per image was about 3 minutes and the ten images with T_E variation were obtained in about 30 minutes. The data sets were acquired at 3 hour intervals during an approximately 37 hour swelling experiment. The repetition delay (T_R) of 20 s was more than five times the maximum T_1 value for water in the system, guaranteeing no signal loss in the images due to T_1 effects. The time-to-echo (T_E) in the spin-echo sequence was varied from 2 ms to 128 ms, in the order 2 ms, 4 ms, 16 ms, 32 ms, 96 ms, 128 ms, 64 ms, 24 ms, 8 ms, and 3 ms, by adjusting the variable delay (VD). This T_E variation made possible the measurement of the T_2 relaxation times at each position in the image. The signal intensities in the shortest T_E image (2 ms) were essentially quantitative but could be improved for any signal loss due to T_2 decay by using the T_2 distribution and Equation 3.1 which is a rearrangement of Equation 1.8. All of the water signal should be visible in the corrected images. However, the imaging experiment

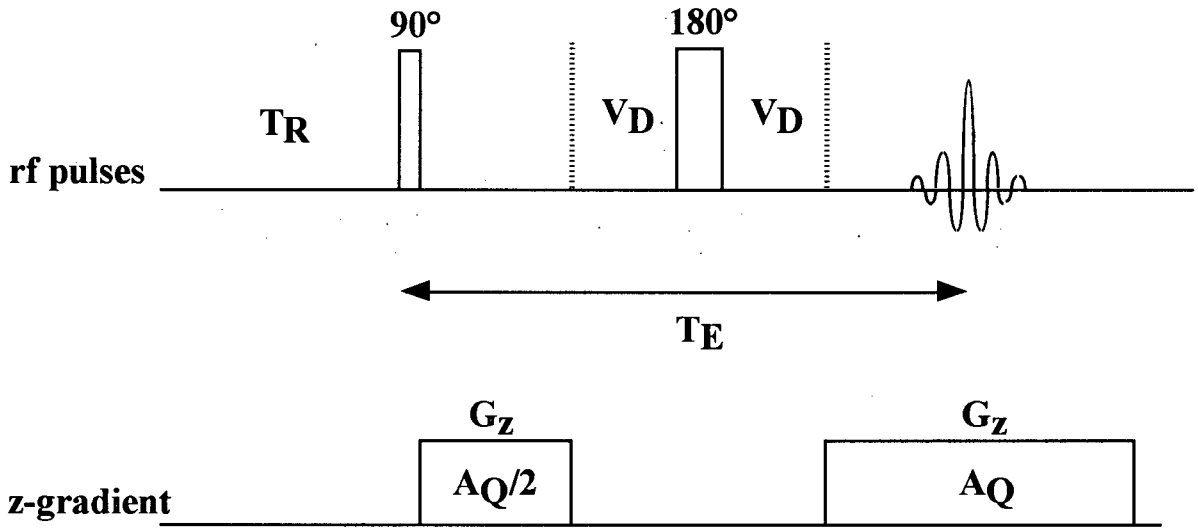

Figure 3.2: Pulse sequence used to acquire the one-dimensional projections. The variable experimental parameters are defined as follows: T_R is the delay between successive experiments, 90° and 180° labels are rf pulses, G_z is the strength of the z-gradient, A_Q is the acquisition time, V_D is a variable delay and T_E is the time-to-echo.

Table 3.2: Typical values for parameters used in the spin-echo pulse sequence for acquiring the one-dimensional images.

Parameter	Value
90° radiofrequency pulse (μs)	18–19
180° radiofrequency pulse (μs)	36–38
Spectral Width, S_W (Hz)	83333.33
Number of points acquired, T_D (Words[a])	128
Number of points in FT, S_I (Words)	256
Acquisition Time, A_Q (μs)	768
Z-gradient, G_z (G/cm)	9.8 ± 0.2
Repetition delay, T_R (s)	20
Number of Scans	8
Time-to-echo, T_E (ms)	variable

[a] On the Bruker MSL Aspect3000 computer, one Word equals 24 bits

used in this chapter detects only mobile water. Thus, any tightly bound, immobilized water could be invisible in these measurements due to its anticipated extremely short T_2 value.

$$M_0 = M_{x,y}\, e^{\frac{T_E}{T_2}} \tag{3.1}$$

3.2.4 Processing of Image Data

Each one-dimensional image was initially obtained in the form of an echo where the NMR signal was encoded in intensity as a function of time. Fourier transformation and magnitude calculation were performed on the Aspect 3000 computer of the MSL400 spectrometer to convert each image into a map of signal intensity as a function of frequency. One image in the data set for a particular swelling experiment was chosen as an absolute intensity reference and the intensities of the rest of the images in the data set were scaled with respect to its intensity. For further processing, the image files were transferred to a Macintosh Centris 650 computer via Bruker NMRLink software. The files were converted to IBM format and then Bruker WIN-NMR was used to export an ASCII file, an example of which is given in Appendix A.1, that contained imaging parameters such as the number of data points, the start and end frequency values, the frequency increment, and the list of NMR signal intensities. In later experiments, a converter program, written in Java and run on a Macintosh LC475 computer, was used to extract the same parameters from Fourier transformed one-dimensional image files. The second converter program, listed in Appendix A.2, increased the speed of image processing as it could convert image files in batches whereas with WIN-NMR, the files had to be processed individually. The frequency scale was calculated using a computer program that read in the files, calculated the frequency list using the start frequency and the frequency increment and then wrote new image files in the form of (frequency, intensity) data pairs. This program is listed in Appendix A.3.

In a typical experiment, the frequency scale extended from -41666.66 Hz to + 41666.66 Hz. The image of the water in the tablet was not always in the same position in this frequency range because the position of the sample with respect to the coil

was rarely duplicated exactly. The interpretation and comparison of data from separate experiments was made easier by relating the intensity of water to the more meaningful scale of distance. In order to convert the frequency scale into a distance scale, two terms needed to be defined. The first was the position of the origin, the reference position from which all distances would be measured. In the swelling tablet system, the logical choice for the origin was the position of the tablet face that rests against the glass support in the tube. Next, increasing distance was defined as the direction away from the support towards the bulk water as indicated in Figure 3.1. This definition allowed for easy comparison of data sets regardless of whether the tablet was swelling upwards or downwards. Distance in the image was related to frequency by Equation 3.2 where D_i is the distance, in cm, from the origin for the ith point, f_i is the frequency of the ith point, f_0 is the frequency of the origin, γ_H is the gyromagnetic ratio of ^{1}H in Hz/G, and G_z is the gradient strength in G/cm. With this equation, the images were converted from a frequency scale into a distance scale. There was a $\pm$750 Hz error in determining the position of the origin from the images which corresponds to an error of about $\pm$0.02 cm in each distance value. Because of the nature of the calculation, the error was systematic and the entire distance scale would be shifted either to slightly larger distances or to slightly smaller ones. An additional reference for the distances was the position of a marker which appeared as a dip in the image intensity around 1 cm. The distance to this marker was known and was used to verify the distance scale.

$$D_i = \frac{f_i - f_0}{\gamma_H \, G_z} \tag{3.2}$$

Each intensity value in the one-dimensional image represented the average NMR signal from a specific volume element in the sample whose size was determined by the resolution of the imaging experiment and the diameter of the NMR tube that contains the tablet. For the experiments presented in this chapter, the resolution was 0.016 cm and the cross-sectional area for the NMR tube was 1.287 cm^2. Therefore, each data point in

the water image was the NMR signal from water in a volume of 0.020 cm^3. The intensity values in the images, as they were originally obtained, were arbitrary and varied between experiments. In NMR spectroscopy, the signal from an internal or external reference of known concentration is often used to calibrate the signal of a species whose concentration is unknown. The same procedure can be used in NMR imaging. In the one-dimensional images of water, care was taken to ensure that both water in the tablet region and water in the bulk region were visible. The concentration of water in the bulk is known and can be used to calibrate the intensities in all regions of the tablet. The images presented in Section 3.3.1 are shown with the intensities of water in the tablet regions normalized by the bulk water concentration. In the imaging experiment performed with D_2O, the ^1H signal from the swollen polymer tablet was referenced in a similar manner to the intensity of water signal from a 5 mm o.d. (4.2 mm i.d.) tube. Using the square of ratio of the inner diameters ($12.8^2/4.2^2$), which is the same as the ratio of the cross-sectional areas of the large and small tube, the intensity of ^1H signal from the small tube is 9.3 times less than from the large tube when the resolution is the same. Thus, the intensity of the ^1H signal from the tablet swollen in D_2O can be directly related to the signal intensity obtained in the imaging experiments with distilled water.

Several further calculations were performed with the image data files. The first was the calculation of the T_2 distribution in the swelling polymer from the ten files that composed the 2 ms to 128 ms T_E variation at each data collection interval. The T_2 value was determined by taking the inverse of the slope of the plot of Ln(signal intensity) versus T_E, the same procedure used to calculate the T_2 values for the calibration equation in Chapter 2. A computer program, listed in Appendix A.4, was written to perform the least-squares calculation on the signal intensity data in the T_E variation files to determine the slope and hence the T_2 value for each point in the image. The program read in the image files and the corresponding T_E values for each of the ten files of the T_E-variation dataset and combined the data into an array in order of increasing T_E. The calculation procedure was to determine the slope and the error in the slope for subsets of the data, starting from

the four shortest T_E files and then adding one file at a time to the calculation up to the maximum number of ten files. Thus for each distance, seven separate slopes were computed using 4, 5, 6, 7, 8, 9, and 10 data pairs, respectively. The calculation that resulted in the lowest relative error in the slope was chosen as the best result and its slope was used to compute T_2. The slope calculated from all 10 data pairs was chosen as the default result when its relative error was no more than 50% greater than the lowest relative error.

This method of calculating the T_2 distribution was chosen because of the range of T_2 values in the swollen polymer and the range of T_E values used to characterize them. The measurements of the T_2 values in mixtures of HPMC and water presented in Section 2.3.1 showed that the T_2 of the water component can vary between about 10 ms and 1000 ms. For species whose T_2 values are greater than 50 ms, there is still visible signal in the image acquired with the longest T_E of 128 ms. However, in the regions of the swollen tablet where T_2 is shorter than 50 ms, the NMR signal from these regions essentially disappears in the long T_E images, resulting in one or more data points where the signal intensity is zero. If these zero points are included in the least-squares calculation, the slope is heavily skewed towards them and the error in the slope increases substantially. Thus, by starting with the short T_E data points and using the relative error in the slope as the criterion for how many data points should be used in the final calculation, the T_2 values can be determined from the appropriate subset of data. With this method, the majority of T_2 values in the system were calculated using the default number of 10 data pairs and only those in the most concentrated polymer regions with the much shorter T_2 values were determined from fewer data pairs.

The resulting T_2 distributions were needed in two additional calculations. They were used to correct the signal intensities of the 2 ms projections for any signal loss due to T_2. They were also converted into HPMC weight distributions through Equation 2.7 which describes the relationship between the T_2 of water and the HPMC concentration in HPMC-water mixtures. The Pascal programs that performed these functions are listed in Appendices A.5 and A.6, respectively. The HPMC weight percent distributions were also

processed further to convert the units of the distribution into grams per centimetre cubed. The conversion was performed by multiplying each weight fraction value by 0.0201 cm^3, the result of Equation 3.3 where ρ is the density, assumed to be 1, A is the cross-sectional area of the NMR tube, γ is the gyromagnetic ratio and and S_W, T_D, and G_z are experimental parameters listed in Table 3.2.

$$Factor = \rho\ A\ \frac{S_W}{\gamma\ G_z\ T_D} \tag{3.3}$$

3.3 Results and Discussion

3.3.1 Water Penetration into HPMC Tablets

The penetration of water into the HPMC tablet began immediately upon its addition to the dry tablet and continued for the duration of the swelling experiment. Figure 3.3 shows a one-dimensional image of the water distribution taken with the shortest possible T_E of 2 ms at a swelling time of 4 hours. The tablet in this system was of the Type 1 variety with an original thickness of 0.133 cm, as indicated in the figure by the dashed vertical line. Both the penetration of water into the tablet and the expansion of the HPMC are visible in this image. The increased ^1H NMR signal in the tablet region clearly shows that water has moved a fair distance into the tablet from the original water-tablet interface. The displacement effect of the polymer expansion is apparent as a decrease of water signal away from the initial tablet position in what was originally a bulk water region. Water appears not to have penetrated the tablet completely at this swelling time as there is a region of the tablet that exhibits no ^1H signal.

The signal intensity of Figure 3.3 is assumed to arise solely from the water protons. However, the protons of the swollen polymer may contribute to the overall signal. To test the extent of this contribution, a ^1H imaging experiment was performed on a tablet swelling in D_2O rather than H_2O. The ^1H signal in this system could arise from mobile functionalities on the polymer chain such as hydroxyl and methyl groups and also from HDO which would be the result of exchange between the polymer hydroxyls and D_2O. Figure 3.4 shows that

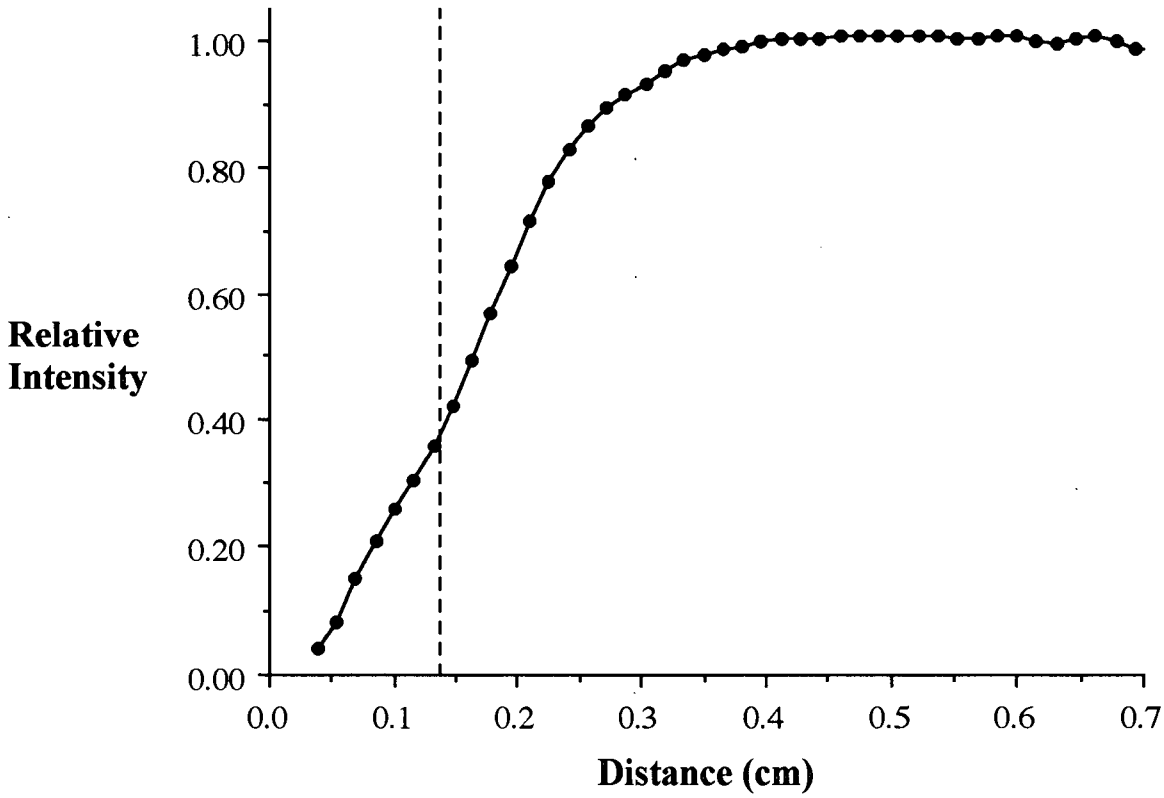

Figure 3.3: An example of a one-dimensional image showing normalized water penetration into an HPMC tablet and the resulting tablet swelling at a time of 4 hours. The original water-tablet interface is indicated by the dashed vertical line at 0.133 cm.

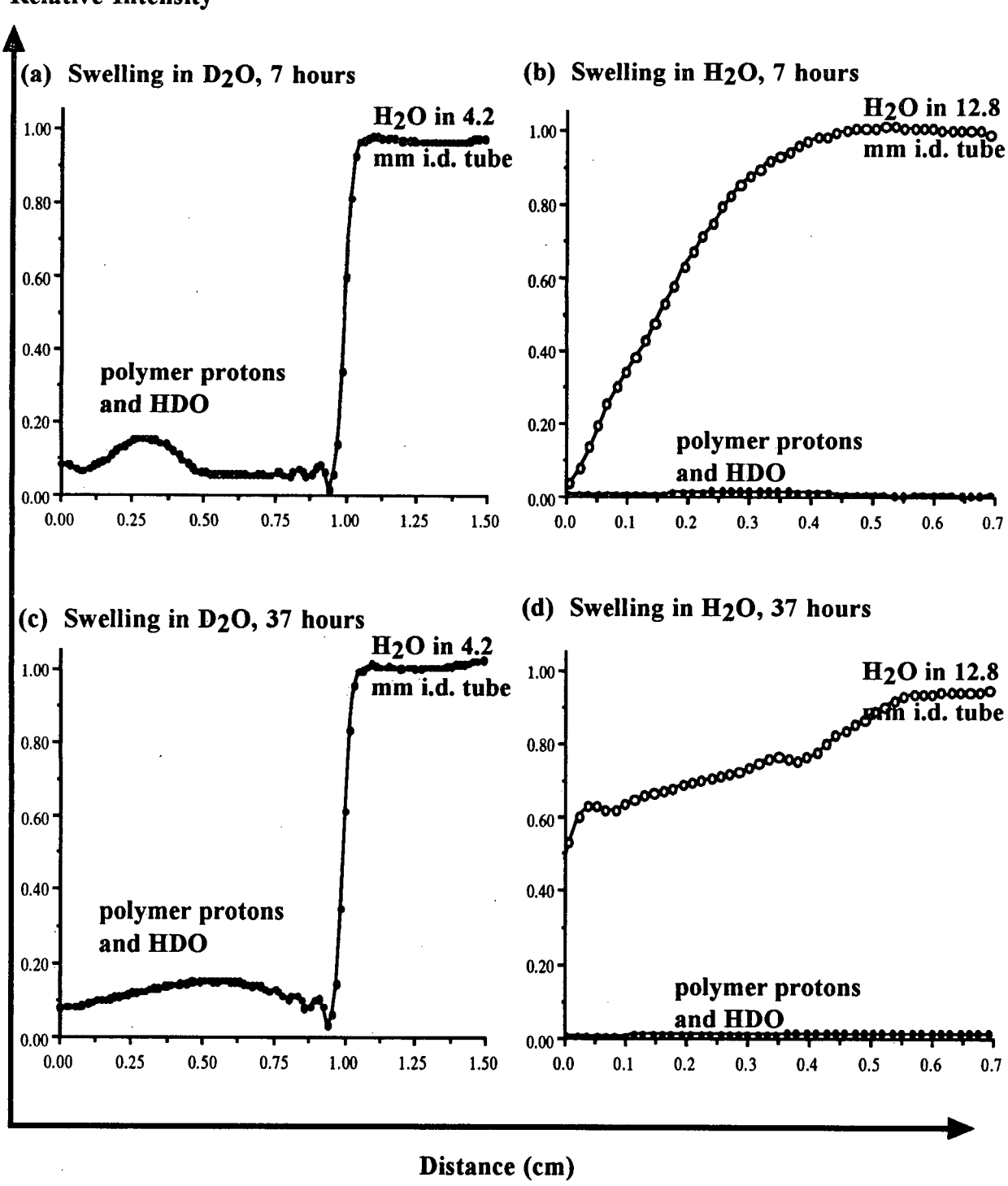

Figure 3.4: ^{1}H images obtained from a tablet swelling in D_2O, (a) 7 hours (c) 37 hours. The axes labels for the four plots are the same and are defined by the arrows. The image intensities in (a) and (c) are relative to the maximum signal intensity from the 4.2 mm i.d. tube, seen as a signal plateau above 1 cm. In (b) and (d), the proton signals from the D_2O experiment are renormalized to the signal intensity from a 12.8 mm i.d.
tube and overlapped with images from a swelling experiment using H_2O. The distance scale in (b) and (d) is expanded to focus on the region containing the swollen polymer tablet.

the measured proton signal from this system is quite low. At the swelling time of 7 hours, the tablet has been penetrated completely by water and the majority of proton exchange between the polymer and the D_2O has occurred. The appearance of ^1H signal in regions away from the polymer tablet at such an early swelling time suggested that diffusion or repeated chemical exchange had spread HDO throughout the system. The signal intensities from the swelling experiment in D_2O are originally referenced to the signal intensity in a 4.2 mm i.d. tube containing water. To compare the signal intensities from the swelling experiment in D_2O to those of the swelling experiments in H_2O, the signal from the D_2O experiment must be referenced to the same intensity as in the H_2O experiments, the water signal in a 12.8 i.d. tube. Therefore, the signal in Figure 3.4(a) and (c) is divided by 0.107, the ratio of the squares of the diameters of the two reference tubes, $(4.2)^2/(12.8)^2$. The contribution of the polymer protons to the overall proton signal, clearly seen in Figure 3.4(b) and (d), is negligible under the conditions of these imaging experiments.

The quantitative reliability of the NMR signal in images such as Figure 3.3 depends on the degree of signal dephasing due to T_2 relaxation that occurs during the imaging T_E of 2 ms. The T_2 values of the ^1H of water were presented in Section 2.3.1 and shown to depend strongly on the concentration of HPMC in an HPMC-water mixture. Therefore, the loss of signal from different regions of the swollen tablet should vary with the amount of polymer that is present. The images acquired with a T_E of 2 ms can be made quantitative by correcting for the T_2-dephasing with Equation 3.1.

To correct all regions of the image, the T_2 relaxation time distribution was determined by varying the T_E parameter in the spin-echo pulse sequence as described in Section 3.2.3. The effect of T_E on ^1H signal intensity is seen in Figure 3.5(a). As T_E is increased, the water signal from the more concentrated polymer regions decreases more rapidly than that from the less concentrated polymer regions. The T_2 value for each distance point can be calculated from the slope of a linear least-squares fitting of Ln(signal intensity) as a function of T_E. Figure 3.5(b) shows the resulting T_2 distribution which can be used to correct the signals in the 2 ms projection. Significant differences between the

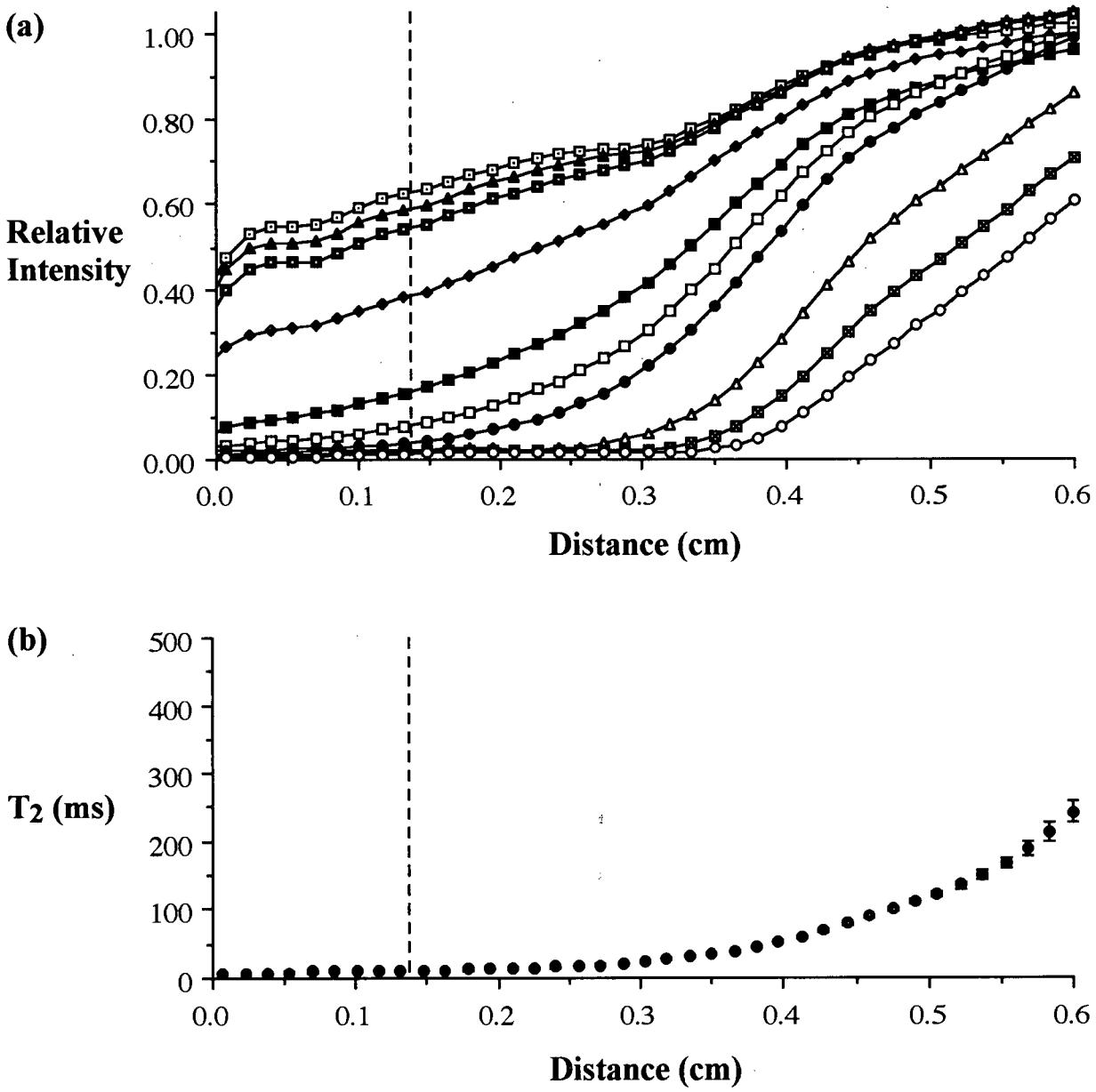

Figure 3.5: The variation of the signal intensity in the water images as a function of the T_E (a) and the corresponding T_2 values (b) calculated from the data in (a) after 25 hours of swelling. The dashed vertical line indicates the initial position of the water-tablet interface at 0.133 cm. The T_E values are 2 ms (dotted open squares), 3 ms (filled triangles), 4 ms (dotted filled squares), 8 ms (filled diamonds), 16 ms (filled squares), 24 ms (open squares), 32 ms (filled circles), 64 ms (open triangles), 96 ms (open crossed squares) and 128 ms (open circles).

measured and corrected water images are clearly visible in Figure 3.6 which shows various stages of water penetration into the 0.133 cm thick tablet. The shapes of the corrected distributions match the measured ones except at the swelling time of 1 hour. For that time, there appears to be no adjustment in signal intensity for the water that has penetrated most deeply into the tablet. When the water concentration is relatively low and the T_2 relaxation parameter is relatively short compared to other regions of the system, the error in the signal intensity makes the determination of a T_2 value extremely difficult. Thus, because certain intensity values in the distribution are not corrected, the distribution apparently changes shape. The signal intensities in the corrected images are quantitatively reliable and are directly proportional to water concentrations in all regions of the system.

The water penetration behaviors of several variations of HPMC tablets were studied to determine which factors were important. The effects of three factors were tested: the direction of swelling with respect to gravity, the thickness of the tablet, and the peak compressional force in the tablet preparation. When the results from tablets of different thickness were compared, the distances for the thinner tablet were adjusted by a constant shift to larger values to allow the initial water-tablet interfaces of the two tablet systems to coincide.

The imaging data from experiments performed with the tablet swelling upward and those performed with the tablet swelling downward were compared to test the effect of the force on gravity on the mechanical stability of the gel. The force of gravity would cause viscous polymer solutions, about 10% HPMC and below, to flow. In the system where the tablet is allowed to swell downward, the flow of polymer in solution may result in a different water distribution than for a system that swells in the upwards direction. Figure 3.7 shows the similarity of the water distributions for the two systems indicating that gravity has no discernible influence on the swelling tablet in this system. The elimination of all air bubbles from the downward-swelling system was problematic and the effect of such an air bubble is visible in Figure 3.7.

The next variation of the swelling experiment was a comparison of similarly prepared

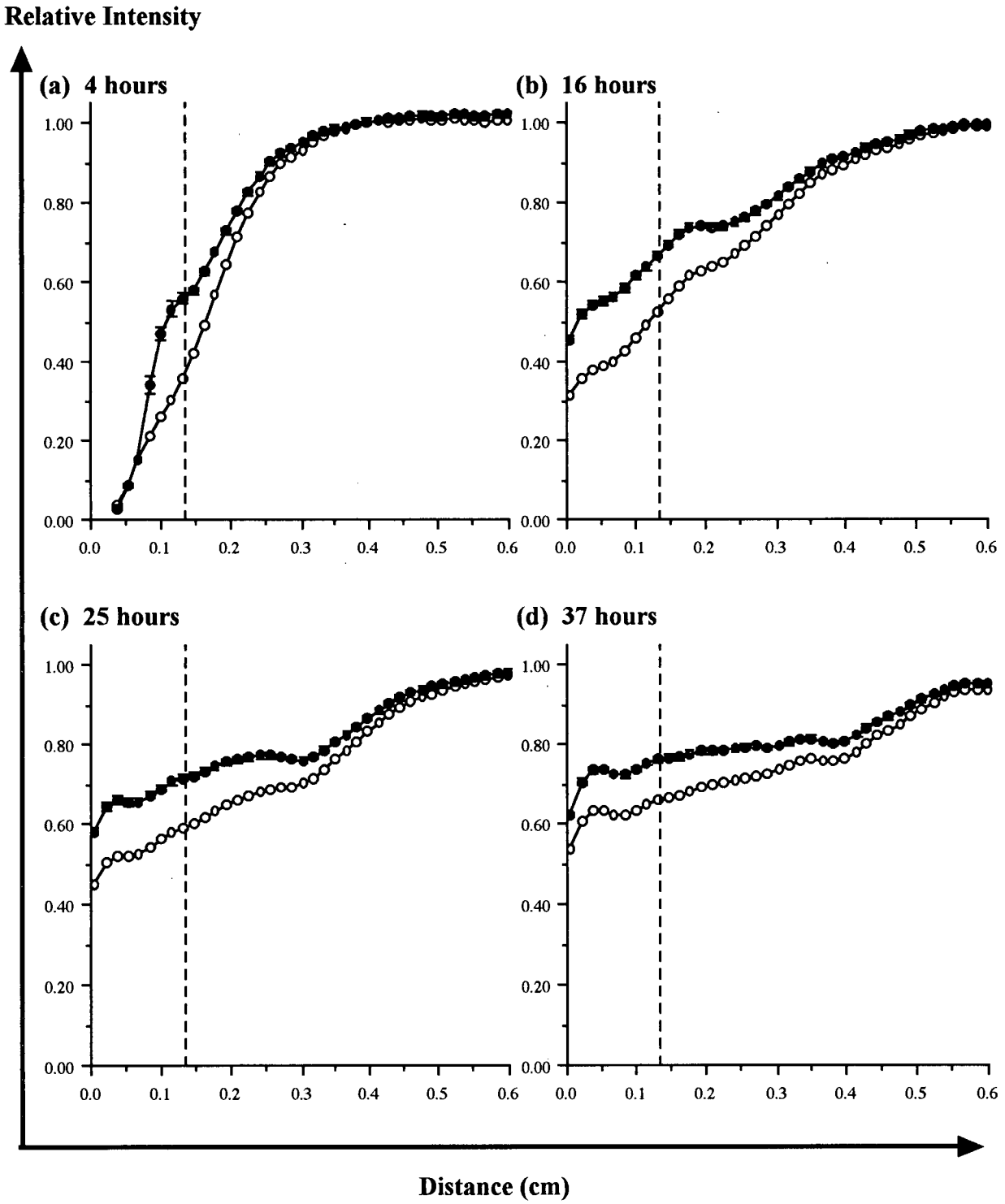

Figure 3.6: Water images showing both the 2 ms image (open circles) and the T_2-corrected distributions (filled circles) at different swelling times, (a) 4 hours, (b) 16 hours, (c) 25 hours, (d) 37 hours. The axes labels for the four plots are the same and are defined by the arrows. The intensities in the images are relative to the bulk water intensity.

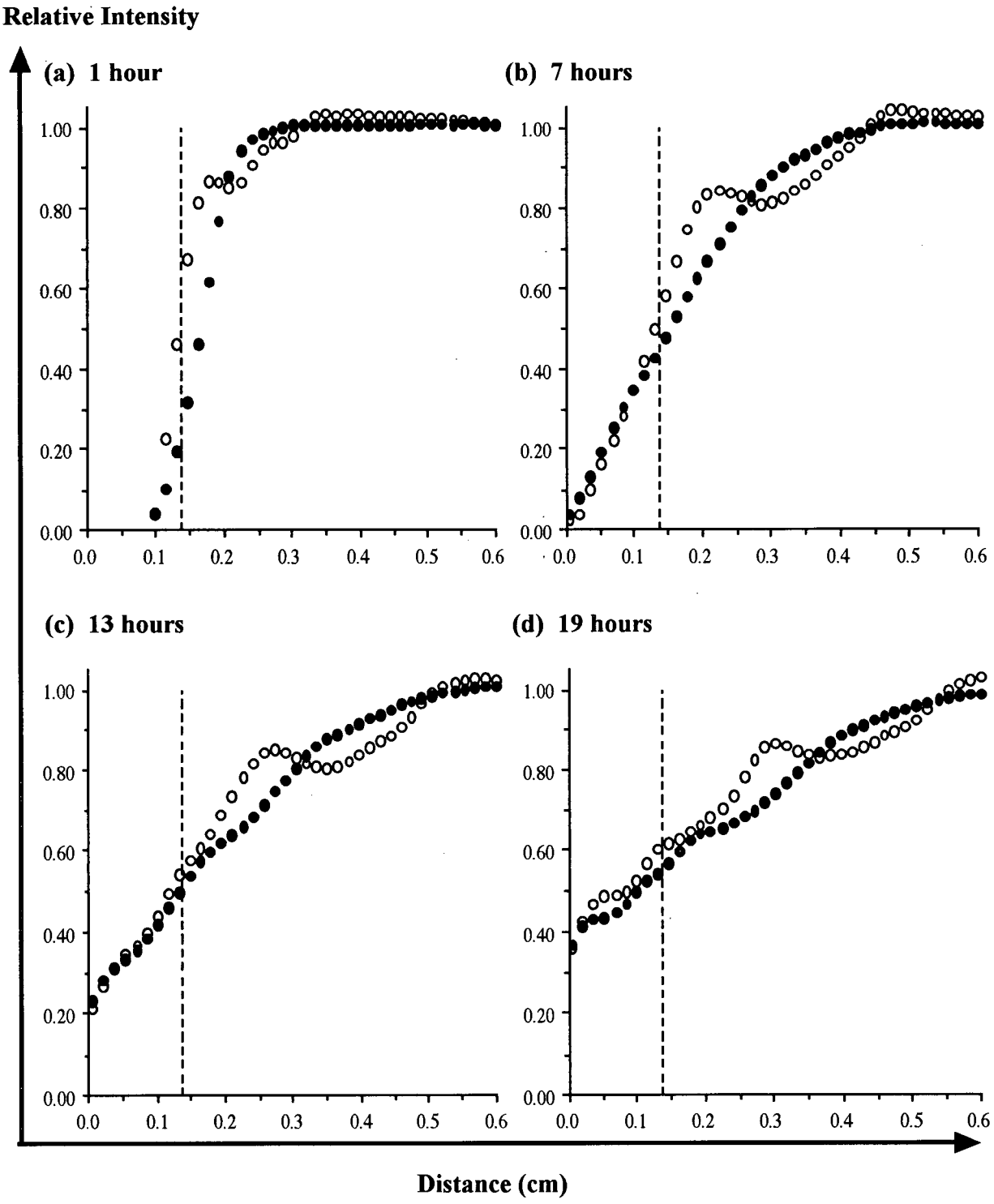

Figure 3.7: Water distributions from upwards (filled circles) and downwards (open circles) swelling experiments, 2 ms images taken at swelling times of (a) 1 hour, (b) 7 hours, (c) 13 hours, and (d) 19 hours. The axes labels for the four plots are the same and are defined by the arrows. The intensities in the images are relative to the bulk water intensity. The marked deviation from a smooth curve visible in the downwards swelling data is the result of an air bubble.

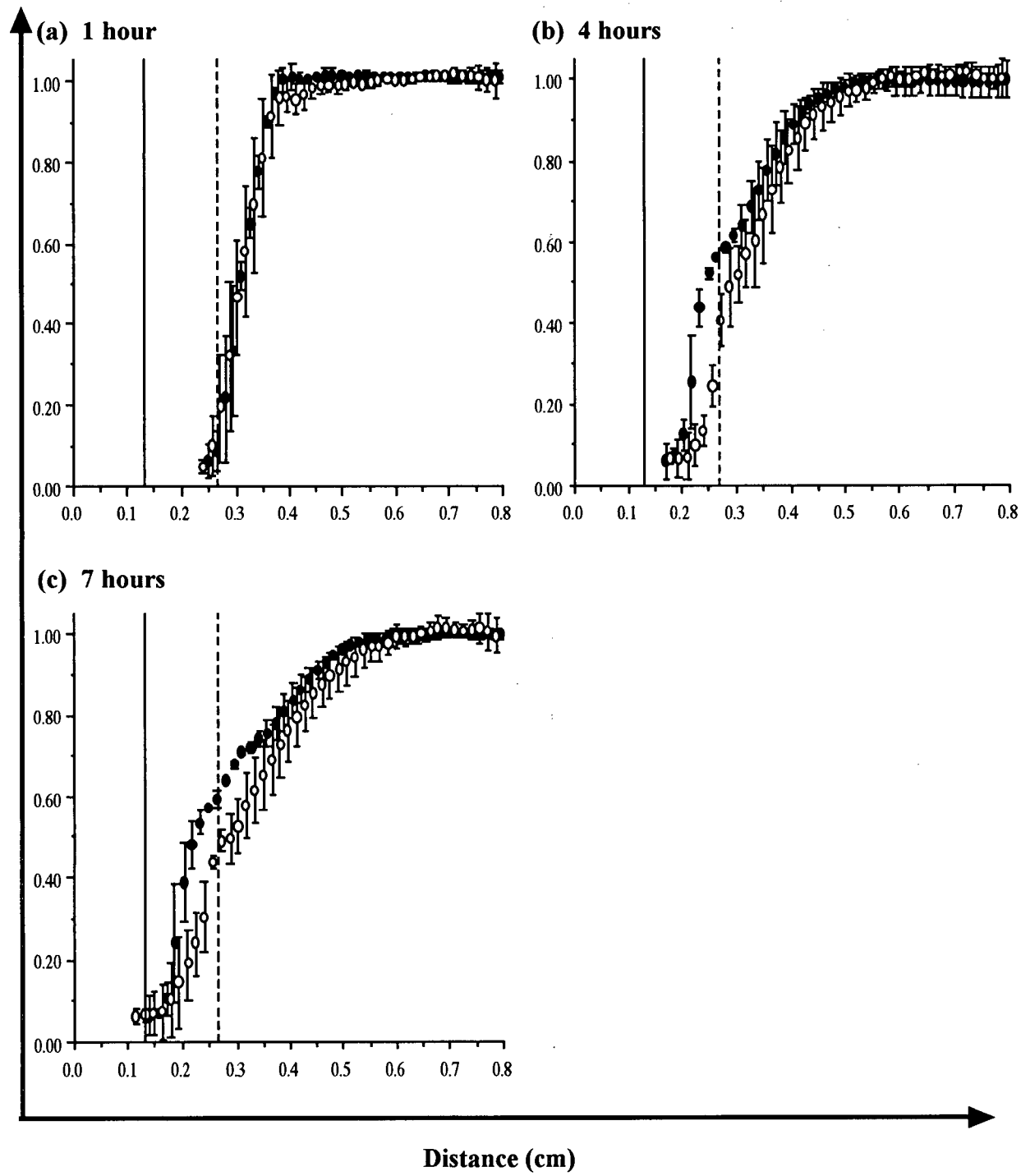

Figure 3.8: Corrected average water distributions for the Type 1 tablet (filled circles, n=2) and the Type 2 tablet (open circles, n=3) at swelling times of (a) 1 hour, (b) 4 hours and (c) 7 hours. The axes labels for the four plots are the same and are defined by the arrows. The intensities in the images are relative to the bulk water intensity. The distance values for the Type 1 tablet data have been shifted by +0.133 cm, the difference in thickness between the two tablets. The dashed vertical line at 0.266 cm indicates the initial water-tablet interface for the Type 2 tablet and the solid vertical line at 0.133 cm marks the zero position for the Type 1 tablet.

tablets with different thicknesses. Type 2 tablets contained twice the amount of HPMC and, when compressed with the same peak force, were twice as thick as Type 1 tablets. The upwards swelling experiment was performed for both of these tablets. After 1 hour, the water images for the two tablets were identical as seen in Figure 3.8. At 4 hours, the distributions are quite similar, although the middle section of the two distributions appears to deviate slightly. After 7 hours of swelling, the two tablet systems are no longer directly comparable because water has penetrated the thinner tablet completely but has only penetrated half-way into the thicker tablet. Because the water distributions for both tablet types at 1, 4 and 7 hours have similar shapes, the deviations between the two systems may be the result of the error in setting the zero position which is $\approx$0.02 cm for each experiment. The similarity between the water distributions at early times suggests that the thin tablet can be regarded as the outer layer of the thick tablet.

The final comparison was between Type 2 and Type 3 tablets, both of similar weight and thickness but prepared with different peak compressional forces. These tablets showed the same water penetration behavior for most of the swelling experiment as shown in Figure 3.9. At a swelling time of approximately 30 hours, the slightly thinner Type 3 tablet was completely penetrated by water whereas the Type 1 tablet was completely penetrated a few hours later. The distributions at 37 hours in Figure 3.9 appear to deviate because of this difference in complete penetration times. Materials such as HPMC compress easily but often expand slightly once the force of compression is removed. Tablets prepared with different compressional forces may expand by varying degrees to the same 'equilibrium' state which could explain how the tablet thicknesses remain very similar under different compressional forces and why the water penetration behaviors are similar.

In order to compare the imaging results from all the experimental variations, the water penetration distance (WPD) was defined. This parameter is the furthest distance that water has penetrated into the tablet as detected in the NMR image and is measured from the original water-tablet interface position. The magnitude of the WPD thus ranges from 0 when no water has penetrated the tablet to the initial tablet thickness when water

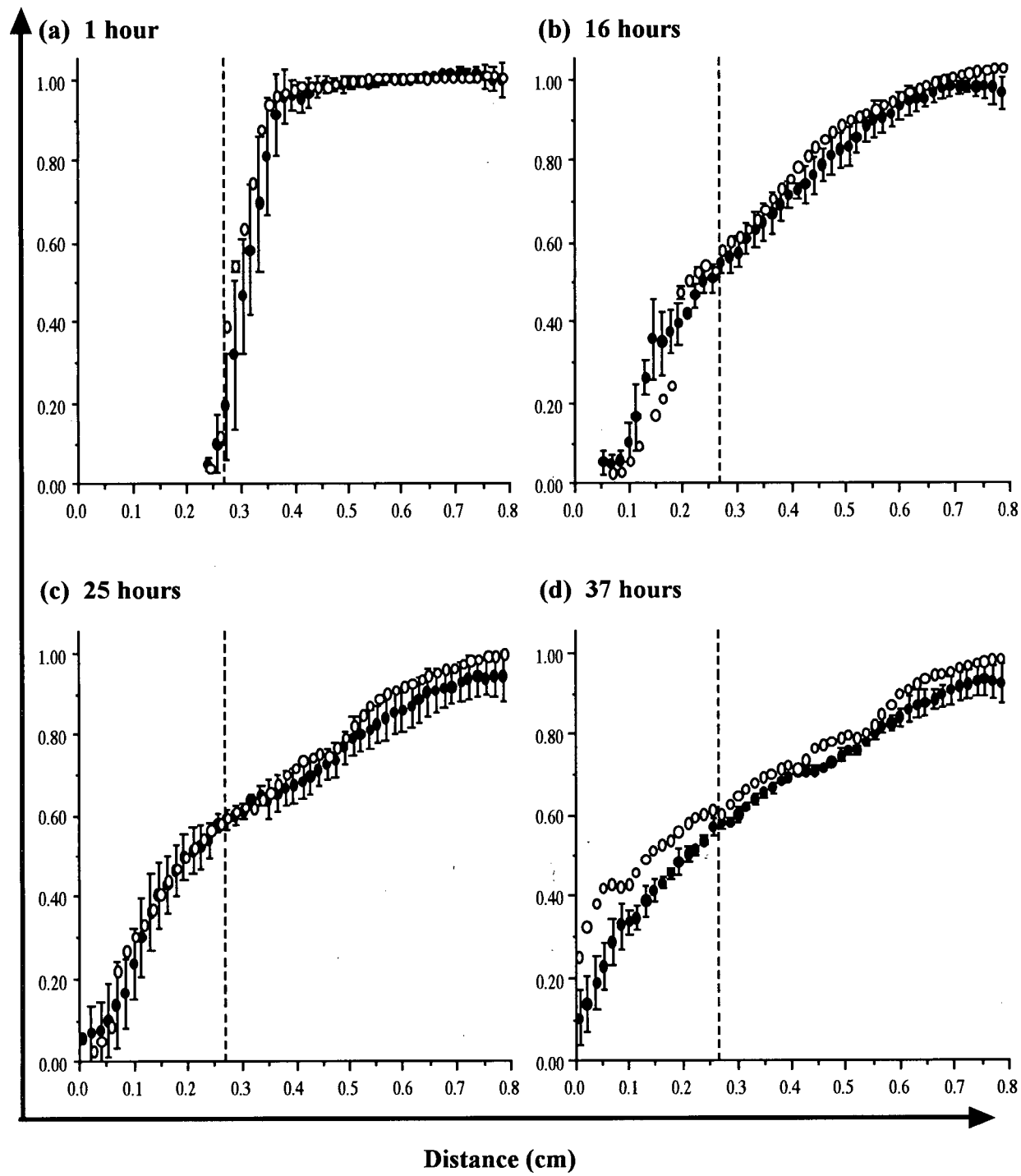

Figure 3.9: Corrected average water distributions for the Type 2 tablet (filled circles, n=3) and the Type 3 tablet (open circles, n=1) at swelling times of (a) 1 hour, (b) 16 hours, (c) 25 hours, and (d) 37 hours. The axes labels for the four plots are the same and are defined by the arrows. The intensities in the images are relative to the bulk water intensity. The distance values for the Type 3 tablet data have been shifted by +0.02 cm, the difference in thickness between the two tablets. The dashed vertical line at 0.266 cm indicates the initial water-tablet interface for the Type 2 tablet.

has penetrated to the far side of the tablet. Table 3.3 lists the average penetration distance for each experimental variation for different times in the swelling experiment. There was a small variability in the swelling times for repetitions of the same experiment which is quoted as a standard deviation of the time. The error in the water penetration distance is within the error of setting the zero position from the imaging experiments. The linearity of a plot of the water penetration distance as a function of the square root of time is the standard proof for a Fickian water penetration process [13]. However, the test gives no details regarding the specific mechanism of the water penetration. Figure 3.10 shows that all the data points from Table 3.3 fall on the same straight line suggesting that the water penetration process into HPMC tablets is Fickian regardless of the direction of swelling, tablet thickness and compression force. The negative intercept of the straight line fit may indicate that the water penetration visible in the one-dimensional images is slightly behind the true penetration front of the water into the polymer, the initial water molecules being immobilized by strong bonding to the polymer.

Table 3.3: Summary of average water penetration distances (WPD) for each tablet type and experimental variation.

Tablet	**Time (min)**	**St. Dev.**[a]	**WPD (cm)**	**St. Dev.**
Type 1, upwards (n=2)	40	9	0.03	0.01
	220	11	0.09	0.01
	399	11	0.12	0.02
	570	—	0.13	—
Type 1, downwards (n=2)	44	4	0.03	0.01
	224	4	0.07	0.02
	404	4	0.12	0.02
Type 2 (n=3)	36	3	0.03	0.01
	218	5	0.07	0.02
	578	6	0.15	0.02
	938	7	0.20	0.01
	1297	6	0.22	0.02
	1656	7	0.25	0.02
Type 3 (n=1)	38	—	0.02	—
	218	—	0.07	—
	399	—	0.12	—
	579	—	0.14	—
	759	—	0.16	—
	940	—	0.18	—
	1119	—	0.21	—
	1299	—	0.22	—

[a] Measure of the variability of the swelling time between repetitions of the same experiment.

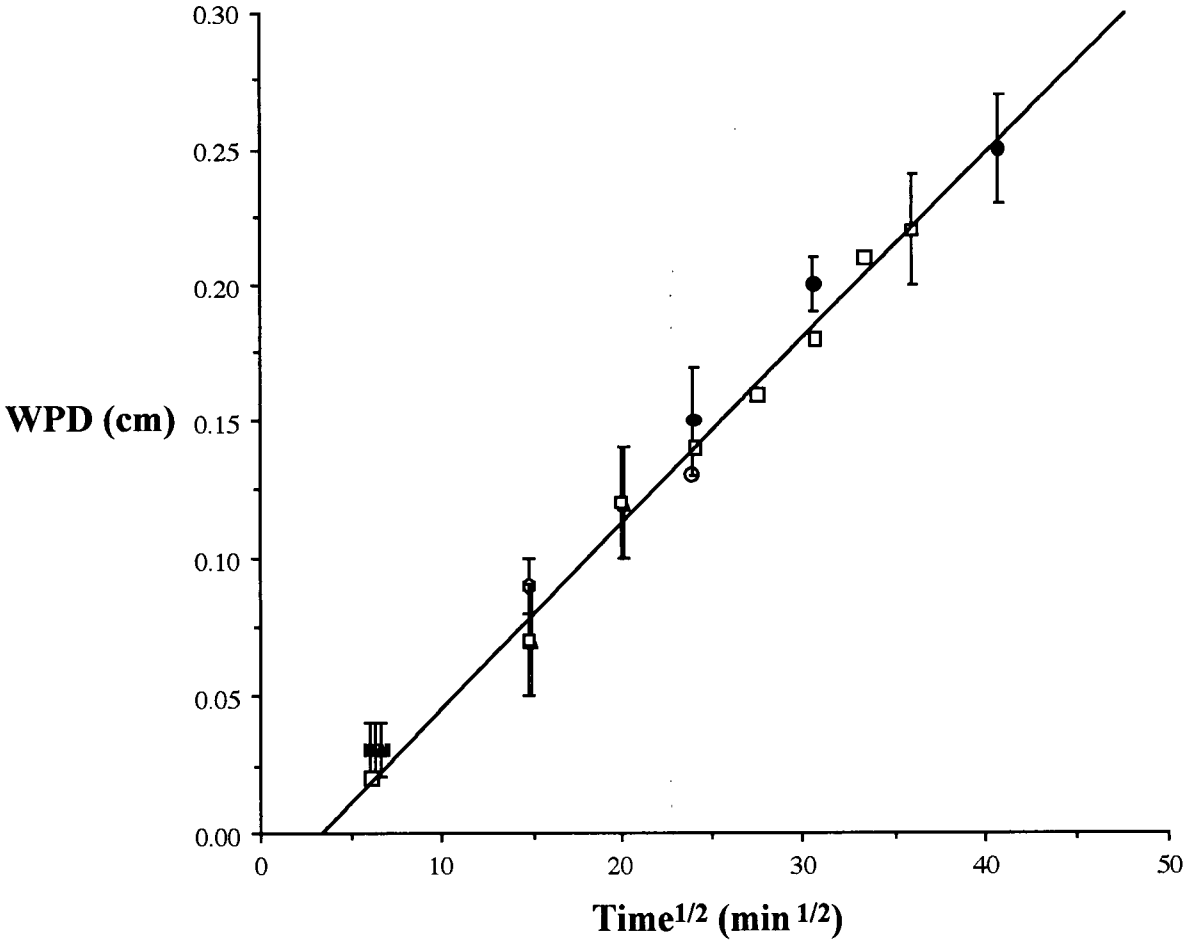

Figure 3.10: The water penetration distance (WPD) as a function of the square root of time for Type 1 upwards swelling (open circles), Type 1 downwards swelling (filled triangles), Type 2 (filled circles) and Type 3 (open squares) tablets. The standard deviations in the WPD are comparable to the error in setting the zero position for each experiment. The deviations in the experimental time are too small to be evident in the plot. The least-squares straight line fit, r^2 of 0.994, gives a slope of 0.006794 cm $min^{1/2}$ and an intercept of -0.0236 cm.

3.3.2 Distribution of HPMC in the Swelling Tablet

As discussed previously, direct NMR imaging of the HPMC in the swelling tablet could not be performed with the imaging techniques of this thesis. Instead, the HPMC distribution was calculated from the water images acquired during the course of the swelling. As discussed previously, the polymer has a significant influence on the T_2 relaxation time of the water component in mixtures of HPMC and water, an effect which was evident in the variation of the signal intensity of the water images with variation of T_E in the spin-echo pulse sequence. This signal variation was used to calculate T_2 distributions as shown in Figure 3.5. In Section 2.3.1, a calibration relating the T_2 relaxation time of water with the weight percent of HPMC was developed from mixtures containing varying ratios of HPMC and water. With the assumption that the relaxation times of water in the swollen tablet are the same as those in the mixtures with equivalent concentrations, this calibration (Equation 2.7) can be used to convert the T_2 distributions determined from the imaging data into HPMC weight percent distributions. This method can be used to calculate HPMC distributions at any time during the swelling of the polymer tablet.

The average HPMC distributions for a 0.133 cm tablet are shown in Figure 3.11. In these distributions, HPMC concentrations above 40% are considered to be only semi-quantitative because of the very limited dependence of T_2 on the weight percent HPMC between 40% and 60% HPMC. Because the HPMC distribution is calculated from the water images, HPMC concentrations can only be obtained where there is sufficient water present to allow for the experimental determination of a T_2 value. Thus, the calculated HPMC points do not extend as far into the original tablet position as the water unless the entire tablet has been sufficiently wetted. After 37 hours of swelling, the tablet has expanded to four times its original thickness with a concentration gradient from approximately 40% HPMC in its most concentrated region down to zero.

Polymer distributions for the different experimental variations were also calculated to determine whether there were any significant differences in the HPMC concentration gradients. The imaging results from the three variations—direction of swelling with respect

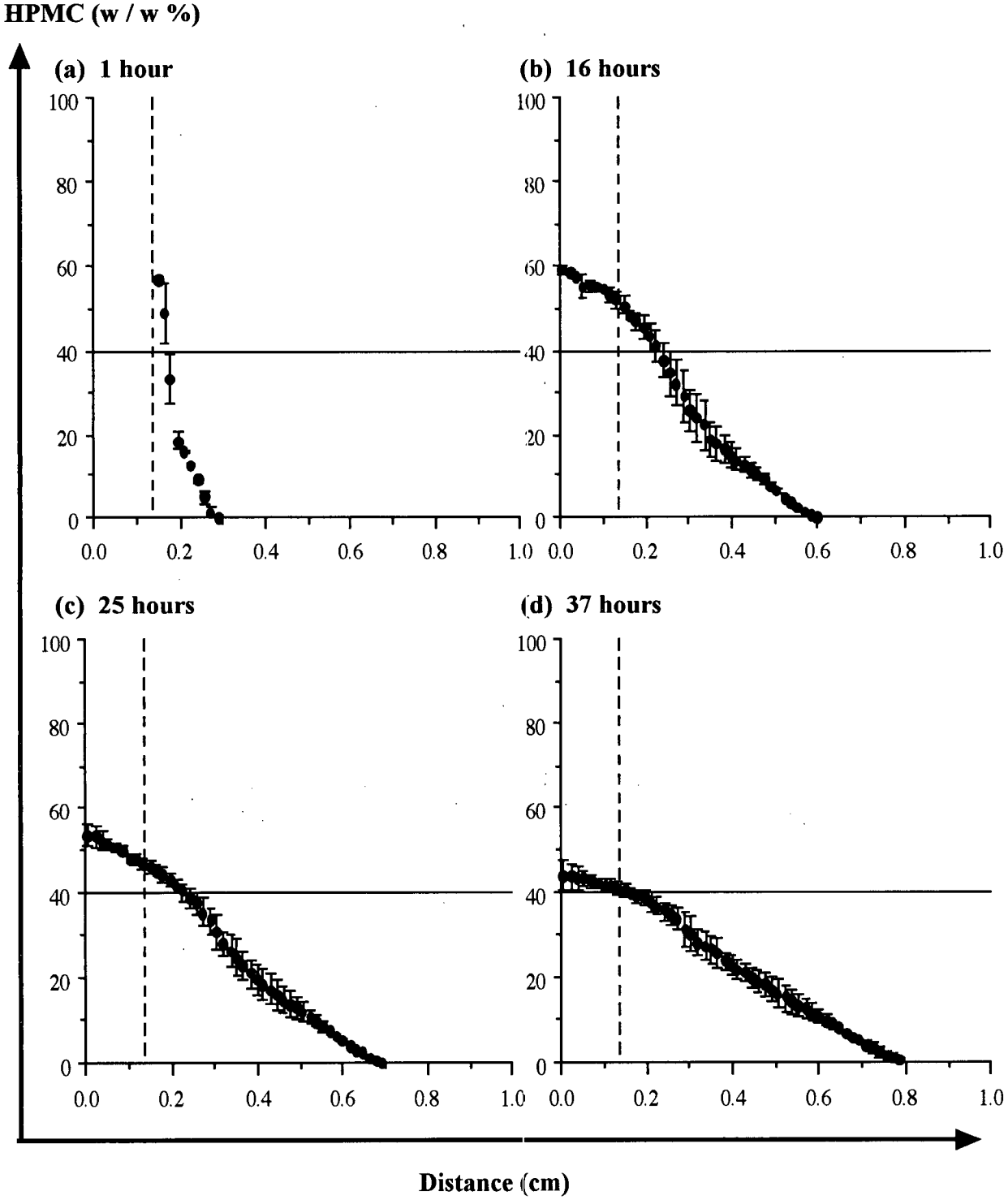

Figure 3.11: Average HPMC weight percent curves obtained from corresponding T_2 curves calculated from one-dimensional images take at different T_E as in Figure 3.5, at median swelling times of (a) 1 hour, (b) 16 hours, (c) 25 hours, and (d) 37 hours. The axes labels for the four plots are the same and are defined by the arrows. The error bars represent standard deviations and the dashed vertical lines indicate the position of the initial water-tablet interface. The solid horizontal lines in the figure mark the upper limit for quantitative reliability of the HPMC weight percent.

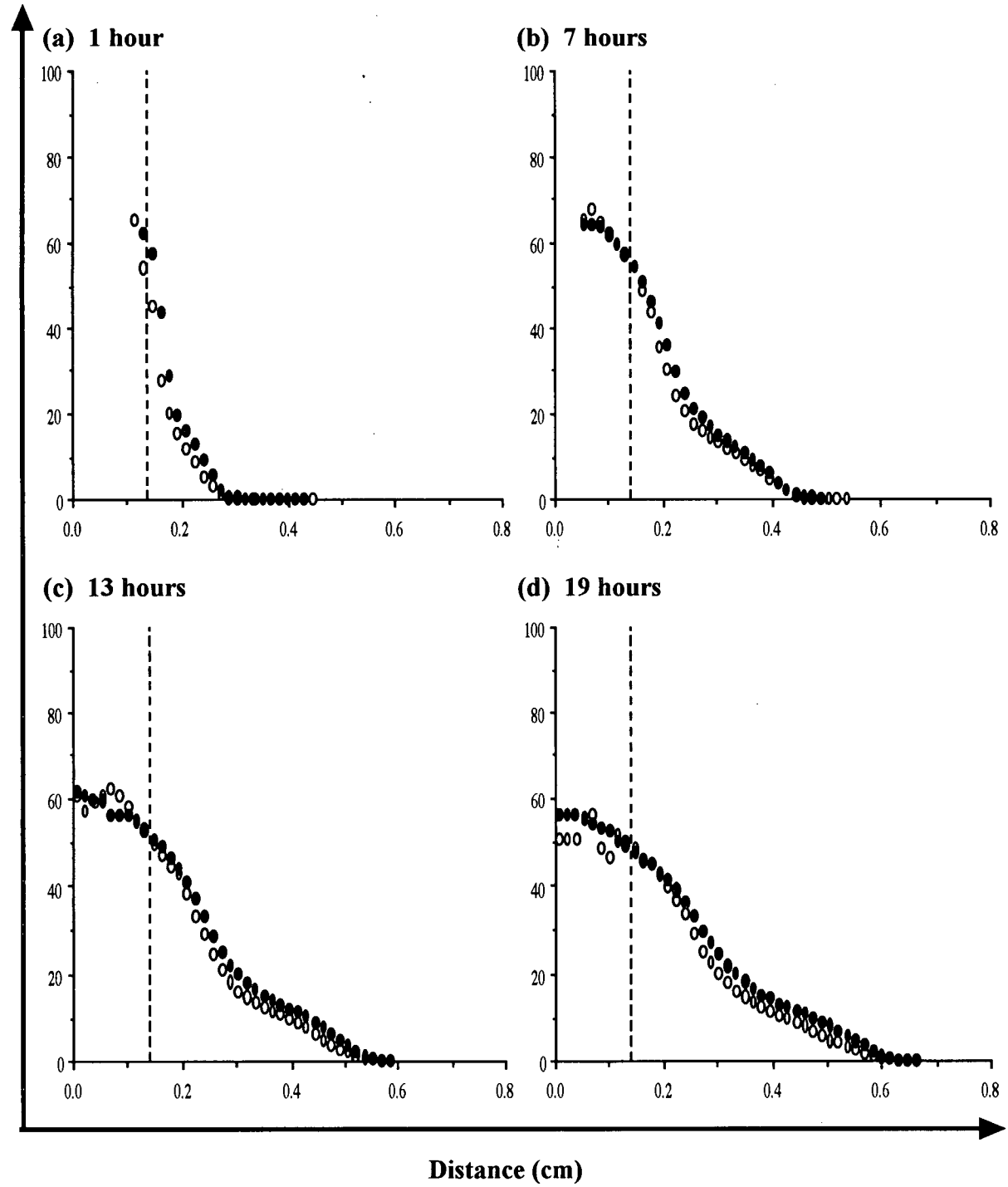

Figure 3.12: HPMC weight percent distributions from upwards (filled circles) and downwards (open circles) swelling experiments, 2 ms images taken at swelling times of (a) 1 hour, (b) 7 hours, (c) 13 hours, and (d) 19 hours. The axes labels for the four plots are the same and are defined by the arrows. The dashed vertical line at 0.133 cm indicates the initial position of the water-tablet interface.

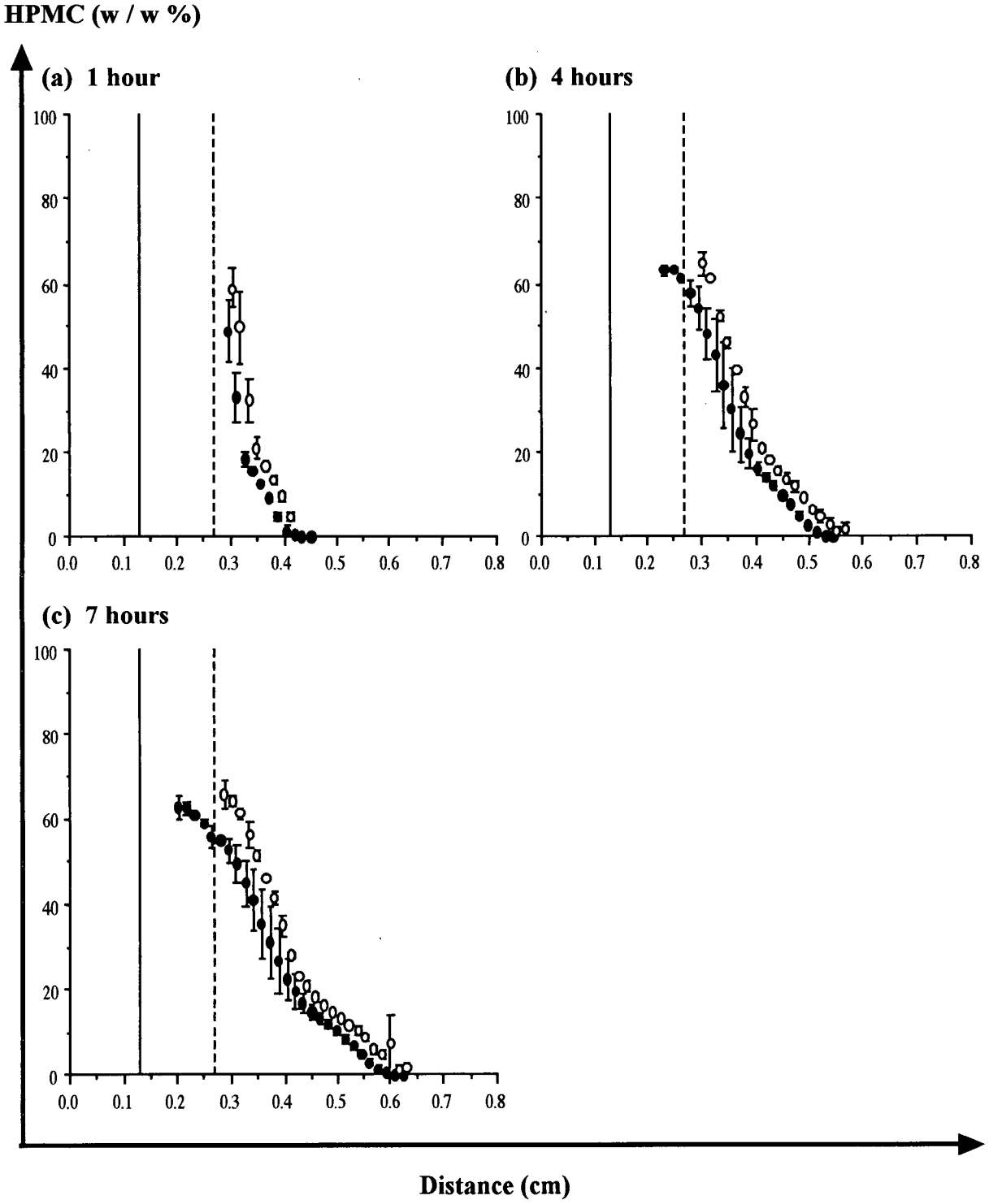

Figure 3.13: Average HPMC weight percent distributions for the Type 1 tablet (filled circles, n=2) and the Type 2 tablet (open circles, n=3) at swelling times of (a) 1 hour, (b) 4 hours and (c) 7 hours. The axes labels for the four plots are the same and are defined by the arrows. The distance values for the Type 1 tablet data have been shifted by +0.133 cm, the difference in thickness between the two tablets. The dashed vertical line at 0.266 cm indicates the initial water-tablet interface for the Type 2 tablet and the solid vertical line at 0.133 cm marks the zero position for the Type 1 tablet.

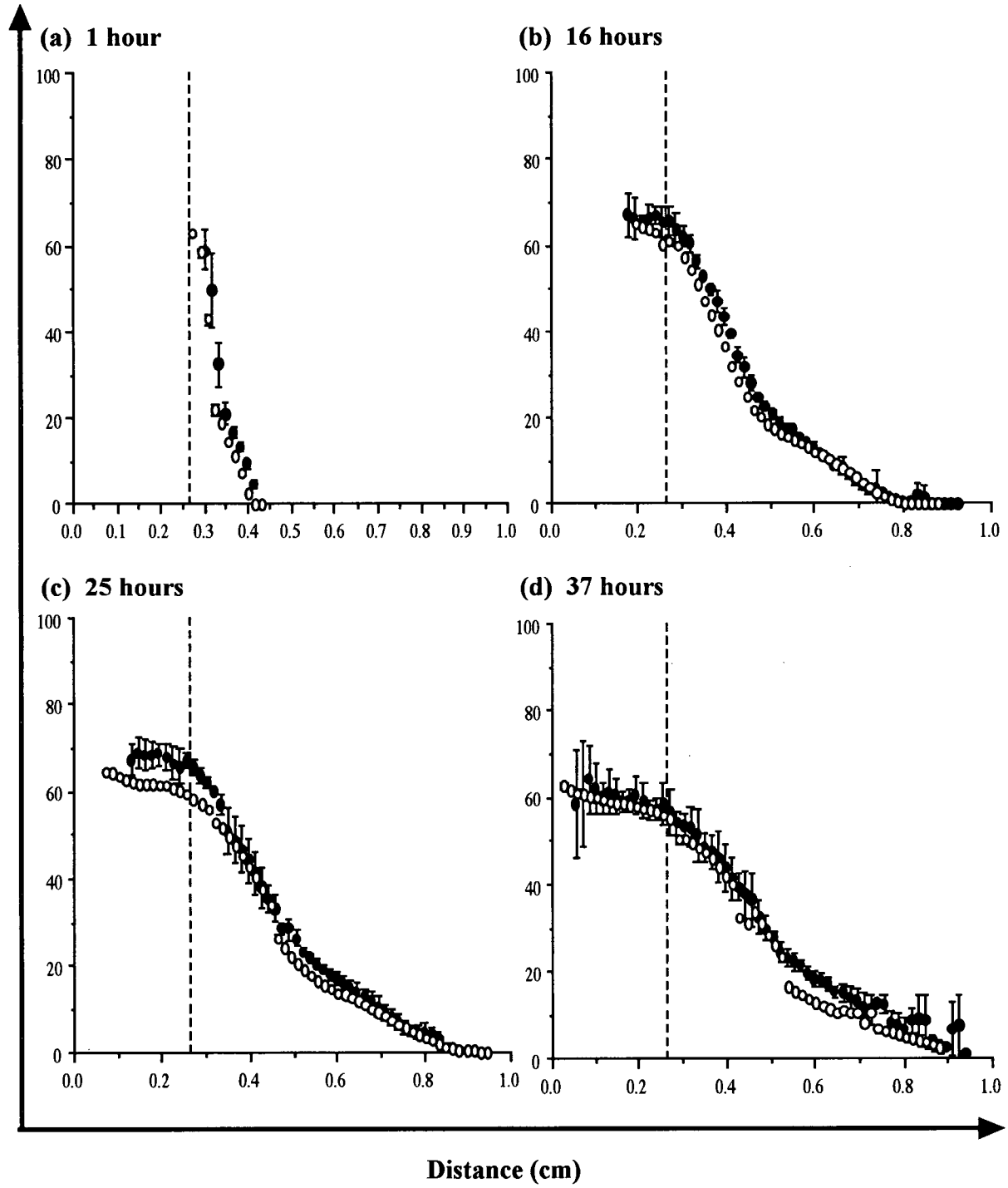

Figure 3.14: Corrected average HPMC weight percent distributions for the Type 2 tablet (filled circles, n=3) and the Type 3 tablet (open circles, n=1) at swelling times of (a) 1 hour, (b) 16 hours, (c) 25 hours, and (d) 37 hours. The axes labels for the four plots are the same and are defined by the arrows. The distance values for the Type 3 tablet data have been shifted by +0.02 cm, the difference in thickness between the two tablets. The dashed vertical line at 0.266 cm indicates the initial water-tablet interface for the Type 2 tablet.

to gravity, tablet thickness, and peak compressional force during tablet preparation— were converted into HPMC weight percent distributions and compared.

Figure 3.12 presents the comparison of the calculated HPMC distributions for swelling-upwards and swelling-downwards variations of the imaging experiment. These distributions appear very similar at all swelling times suggesting that the gravity-induced flow of HPMC solutions has little effect on the resulting HPMC distribution. The presence of the air bubble in the swelling-downwards experiment seems to have only a small influence on the calculated T_2 values and the resulting HPMC weight percent distributions as there is only a slight lowering of the HPMC% in the vicinity of the air bubble. Figure 3.13 shows a similar comparison of the behaviors of the similarly prepared Type 1 and Type 2 tablets (thicknesses of 0.133 cm and 0.266 cm respectively). The calculated HPMC distributions have similar shapes at the three swelling times shown in the figure but appear to be offset from each other. As the offset is within the combined error of setting the zero position for the two imaging experiments, the calculated HPMC distribution is assumed not to depend on tablet thickness. Figure 3.14 shows that the HPMC distributions for tablets prepared with different compressional forces are also similar suggesting that the polymer distribution is not affected by the compression force used in the tablet preparation.

3.3.3 Total Weight of HPMC from Calculated Polymer Distributions

The ultimate goal of the imaging investigations of HPMC tablets was to parameterize the expansion of the tablet in terms of polymer concentration as functions of both time and distance in order to test various possible models for the swelling process. Each data point in the HPMC weight percent distributions of Section 3.3.2 represents the amount of polymer in a certain region, a disk of volume 0.0201 cm^3. If the volume and density are known, the weight percent profiles are easily converted into concentration units such as g cm^{-3} which describe the amount of polymer at each location.

When the tablet is fully hydrated, a complete HPMC distribution in g cm^{-3} units can be calculated. The sum of the polymer weights over each volume region provides

Table 3.4: Average total weights of HPMC calculated from the one-dimensional imaging studies of a Type 1 tablet. The percent deviations are calculated from the known weight of 166 mg HPMC in the tablet.

Time (hrs)	Total HPMC[a] (mg)	Error (mg)	% dev[b]
19	220	18	33
25	239	18	44
31	241	20	45
37	240	21	45

[a] The assumed density was 1 g cm^{-3}

[b] % dev =100 % × (HPMC - 166) / 166

an experimental measure of the total amount of polymer in the system which should be comparable, within experimental error, to the known weight of the HPMC in the tablet. When this total weight calculation was performed for the HPMC distributions calculated from the Type 1 tablet, the apparent amount of polymer, given in Table 3.4 was found to be up to 45% larger than the known weight of HPMC in the tablet. This over-estimation of weight occurred even when all the calculated weight percents in the polymer distribution were below 40% and therefore considered reliable. This discrepancy, discussed in greater detail in Chapter 4, was found to be caused by the presence of air bubbles in the swollen gel which occupy a fraction of the volume assumed to be composed only of HPMC and water.

3.3.4 Possible Effects of Water Diffusion on the Imaging Results

The pulse sequence for the one-dimensional imaging experiments is very similar to the pulse sequence presented in Section 1.2.3 which was used to measure the self-diffusion coefficient of the water. This raises the concern that the images of water may be affected by the diffusion that occurs during the time the gradients are applied. Fast diffusion of water causes the apparent T_2 value measured from an imaging experiment to be less than the true T_2 value and the difference between the measured and true T_2 values becomes greater as the spatial resolution in the images increases [77]. Using Equation 3.4 with a resolution, Δx, of 0.016 cm and a diffusion coefficient of 2.35×10^{-5} $cm^2 s^{-1}$ (the value for free water),

the measured value for the true T_2 of 500 ms would be 371 ms when T_E is 2 ms and 341 ms when T_E is 128 ms. Although this ~32% decrease in the apparent T_2 is significant for free water, the effect of diffusion on the T_2 values measured for the swollen polymer tablet is much less significant because the deviation decreases substantially as the true T_2 value decreases and as the diffusion coefficient decreases. For the HPMC-water mixtures between 5% and 10%, the T_2 values are approximately 200 ms and above 10% HPMC, the T_2 values drop below 100 ms. The decrease in the apparent T_2 value drops to ~16% and ~9%, respectively for these two limits and may be even lower because the diffusion coefficient decreases with increasing HPMC weight percent (cf. Section 2.3.3).

$$\frac{1}{T_{2,obs}} = \frac{1}{T_{2,true}} + \frac{D\pi^2}{\Delta x^2}\left\{\frac{T_E - \frac{2}{3}A_Q}{T_E}\right\} \tag{3.4}$$

The T_2 values determined from the imaging experiments are used in two separate calculations which could be influenced by the diffusion attenuation of the measured T_2 relaxation time. The first calculation is the correction of signal intensity using Equation 3.1. Replacing the true T_2 values in this equation with the diffusion attenuated values leads to an average increase of 0.2% in the exponential term of Equation 3.1. Therefore, the effect of diffusion on the T_2 values has no effect on the correction of the signal intensity. The second calculation involves the conversion of T_2 values to HPMC weight percent using the calibration of Equation 2.7. When the apparent T_2 values are used instead of the true values, the calculated HPMC weight percent is about 1% higher. For example, if the true T_2 is 100 ms, then the apparent T_2 of 91 ms produces a HPMC weight percent of 12.4% instead of 11.8%. This converts into a percent deviation of +5.5%. For true T_2 values of 200 ms and 500 ms, the HPMC concentrations are 7.8% compared to 6.5% and 2.8% compared to 1.1%. These are 'worst case' estimates based on the fast diffusion in pure water; the deviations in the swollen HPMC tablet will be lower because the diffusion of water through the polymer gel is slower than in pure water. The error that the diffusion attenuation of the T_2 value introduces into the HPMC weight percent distribution is small

and falls within the error caused by other factors. The distributions in this chapter were not corrected for the diffusion effect because there is another much larger factor that causes discrepancies in the HPMC weight percent, namely the presence of air bubbles.

3.4 Summary

The one-dimensional imaging studies performed on the HPMC tablet permitted the rapid determination of both the water and polymer distributions at various times during the swelling process. The repetition of the experiment under various conditions showed that the results were reproducible and did not depend strongly on such factors as swelling direction with respect to gravity, the thickness of the tablet, or the compression force used during tablet preparation. The penetration of water into the HPMC tablet appeared to be the same regardless of the experimental variation and exhibited a linear relationship with the square root of time, indicating Fickian diffusion. The polymer distributions obtained in this chapter over-estimate the amount of polymer present. This discrepancy has been traced to the presence of numerous small air bubbles in the swollen gel which occupy volume assumed to be filled by polymer and water only.

Chapter 4

Detection of Air Spaces in the Swollen HPMC Tablet

4.1 Introduction

Tablets are generally prepared by the compression of granules obtained from either a wet or dry granulation method or by direct compression of an untreated powder mixture [78]. During the compression, air between the particles can be trapped within the tablet. The porosity of a tablet depends on factors such as the size of the particles, the force of compression and the speed of compression [79]. When the tablet preparation conditions result in a large volume of air trapped within the tablet, the resulting internal pressure can cause the tablet to rupture in an occurrence termed 'capping' [80].

During the swelling of a hydrophilic matrix tablet, the movement of the polymer reduces the pressure exerted on the trapped air resulting in the formation of air bubbles. These bubbles will occupy space which might otherwise be filled by the swollen polymer and may result in a different apparent increase in the tablet size than that due to polymer swelling alone. Analysis methods that require knowledge of the volume occupied by the swollen gel will be strongly influenced by the presence of these bubbles. Such an effect was observed in Section 3.3.3 where estimates of the total polymer weight in the swollen tablet exceeded the known polymer weight by up to 45%.

There are two basic approaches to eliminating the effect of the air bubbles: measuring and correcting for the volume occupied by the air or removing the air from the tablet prior to the imaging experiment. This chapter describes the second approach in which an

HPMC tablet is treated under vacuum to remove air from the pores of the tablet.

4.2 Experimental

4.2.1 Vacuum Treatment to Remove Air from the Tablet

Type 1 tablets were prepared from the as-supplied HPMC powder and placed in an NMR tube as described in Sections 3.2.1 and 3.2.2, respectively. Prior to each imaging study, the tablet was treated with vacuum to remove any air which might be trapped in the pores of the tablet. The tube containing the tablet was placed inside a long Schlenk tube, as shown in Figure 4.1, and kept under a vacuum of approximately 12 mm Hg for 5 minutes. Glass rods were required to prevent the tablet from rising up in the tube during the vacuum treatment which tended to cause water leakage between the tablet and tube wall. After the treatment, water was allowed to enter the system to break the vacuum and prevent the reincorporation of air into the tablet. The water drawn into the tube was replaced by 5 mL of fresh water to make the remainder of the swelling experiment of the vacuum-treated tablet as similar as possible to that of the untreated tablet.

4.2.2 One- and Two-dimensional Imaging

The two-dimensional images of the water distribution were acquired with the slice-selective spin warp sequence shown in Figure 1.14. Two variations of the imaging experiment were performed for both the untreated and the vacuum-treated tablets. In one version of the experiment, the two dimensional water signal intensity was acquired from a slice parallel to the long axis of the tube. The second version recorded the two dimensional signal intensity in a plane orthogonal to the long axis of the tube. The tablet systems for the two-dimensional imaging experiment were prepared with a solution containing 10 mM $CuSO_4$, rather than distilled water, to shorten the T_1 relaxation time of the water protons and thus shorten the time required to obtain semi-quantitative two-dimensional images of the swelling tablets. Table 4.1 gives the parameters for each of the two-dimensional imaging variations.

The one-dimensional imaging studies of the vacuum-treated tablet were performed

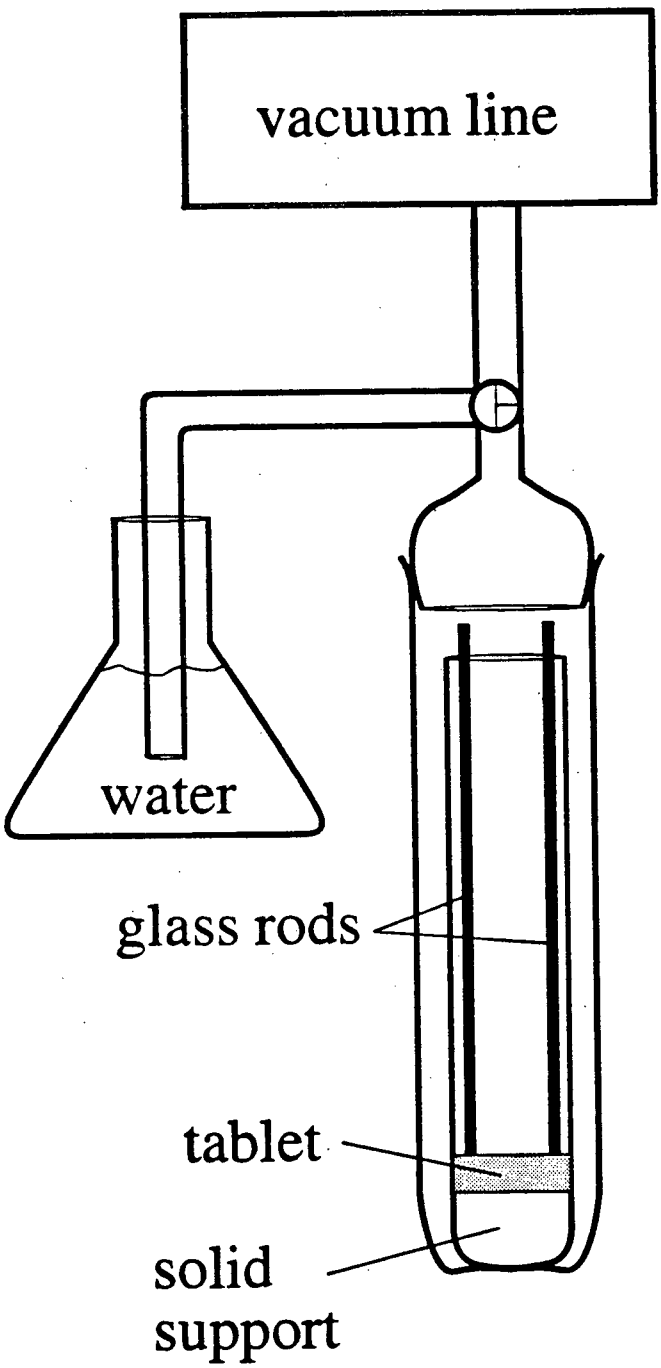

Figure 4.1: A schematic representation of the experimental set-up for vacuum-treating the HPMC tablets. Glass rods are used to hold down the tablet in the NMR tube which is then placed in a long Schlenk tube and connected by a three-way valve to a vaccum line and a source of water. The tablet is subjected to a vacuum of 12 mm Hg for 5 minutes and then water is drawn into the Schlenk tube to break the vacuum. Before the tablet is placed in the magnet for imaging, the glass rods are removed and the water drawn in by the vacuum is replaced by fresh water.

Table 4.1: Typical parameters used in the spin warp imaging sequence to acquire the two-dimensional images of swelling HPMC tablets. The Version 1 values are for the longitudinal images and the Version 2 values are for the cross-sectional images.

Parameter		**Version 1**	**Version 2**
Selective 90° pulse	Shape	sinc2	sinc2
	Duration (ms)	2	2
Slice-selection gradient	Direction	y	z
	Strength (G/cm)	7.3	16
	Duration (ms)	2.8	2.2
Phase-encoding gradient	Direction	x	y
	Strength (G/cm)	-9.9 to +9.9	-28.8 to +28.8
	Duration (μs)	660	600
	Increments	256	256
Frequency-encoding gradient	Direction	z	x
	Strength (G/cm)	8.1	16.9
	Duration[a] (μs)	660	600
Spectral Width, S_W (kHz)		50	125
Number of points in frequency domain, T_D (Words)		256	256
Number of points in the FT, S_I (Words)		512	512
Time-to-echo, T_E (ms)		2.5	2.5
Repetition delay, T_R (s)		0.5	1
Number of repeats		16	32
Time to acquire image (min)		34	136
Slice thickness (μm)		650	300
In-plane resolution (μm)		60	70

[a] The frequency encoding gradient remains on longer during the acquisition of the echo in the second half of the spin warp sequence.

in the same manner as for the untreated tablet in Chapter 3. Processing of the imaging data for the vacuum-treated tablet was the same as that described in Section 3.2.4. The additional processing of the data to correct for the effects of diffusion during the gradient pulses of the imaging experiment was performed in an iterative manner. Equation 4.1, determined from a Mathematica fit to water diffusivity the data in Section 2.3.3, was used to interpolate the diffusion coefficient for HPMC weight percents, [HPMC], in between those of the prepared mixtures. The diffusion coefficient of 0.51×10^{-5} cm^2 s^{-1} was used as the minimum value for HPMC concentrations above 40%. The initial T_2 values were converted into HPMC weight percents which were then used to determine the initial diffusion coefficients for the correction. The diffusion-corrected T_2 values were calculated using Equation 4.2 which is a rearrangement of Equation 3.4 where the $(T_E - 2/3A_Q)/T_E$ term is assumed to be unity in order to determine the maximum effect of diffusion. The new T_2 values are converted into a second set of HPMC weight percent values which in turn are used to determine the second set of diffusion coefficients. The calculation with Equation 4.2 was repeated with the new set of diffusion coefficients to obtain a third set of HPMC weight percents. Further iterations were not required as the second and third sets of weight percents were identical to the 2nd decimal place.

$$D_H = 2.164 - 0.03785[HPMC] - 0.0001423[HPMC]^2 \qquad (4.1)$$

$$\frac{1}{T_{2,true}} = \frac{1}{T_{2,obs}} - \frac{D\,\pi^2}{0.016^2} \qquad (4.2)$$

4.3 Results and Discussion

4.3.1 Two-dimensional Images of Untreated and Vacuum-Treated Tablets

The two-dimensional imaging experiments were performed to determine the extent of air present throughout the tablet and to monitor the changes in the air distribution in the

tablet as it swells. Two-dimensional imaging experiments with the vacuum-treated tablet were performed to determine how successfully the vacuum technique removed the air from the pores within the tablet.

The series of longitudinal images for both tablet systems are shown in Figure 4.2. In these grey-scale images, the light regions indicate the presence of water and the dark or black regions indicate a low concentration or the complete absence of water. The air bubbles in the untreated tablet are visible as dark blobs surrounded by water. They appeared as early as 4 hours after the beginning of tablet swelling and formed continuously as the water penetration and swelling continued. At later times, the swollen tablet has quadrupled its original thickness and essentially fills the two-dimensional image in Figure 4.2(h). At these later times, there appeared to be a fairly even distribution of bubbles throughout the gel. In contrast, the images from the vacuum-treated system are almost completely free of air bubbles indicating that the vacuum technique removed the air from the tablet pores. The true air bubble volume cannot be determined from the images of Figures 4.2 and 4.3 because the changes in magnetic susceptibility across the air-water interface cause the air bubbles to appear larger than their actual size. Although, these images are only of one longitudinal slice through the sample, the air bubble distributions visible in them can be assumed to be representative of the distribution throughout the swollen tablet.

The cross-sectional image through the middle of the untreated tablet in Figure 4.3 confirms that air bubbles occupy an extensive volume in the swollen tablet. The image of the vacuum-treated tablet shows only a few small air bubbles indicating that the majority of air in the tablet pores was removed in the exposure to vacuum. This effect is also somewhat visible in the longitudinal images of the untreated tablet. Water leakage between the tablet and the tube wall does not appear to be the cause of this effect as the water penetration front into both the untreated and vacuum-treated tablets, as seen in Figure 4.2, remained straight throughout the experiment. The air trapped in the outer regions of a newly compressed tablet can equilibrate to atmospheric pressure more easily than air trapped deep within the tablet and perhaps the lower air pressure results in fewer bubbles in these

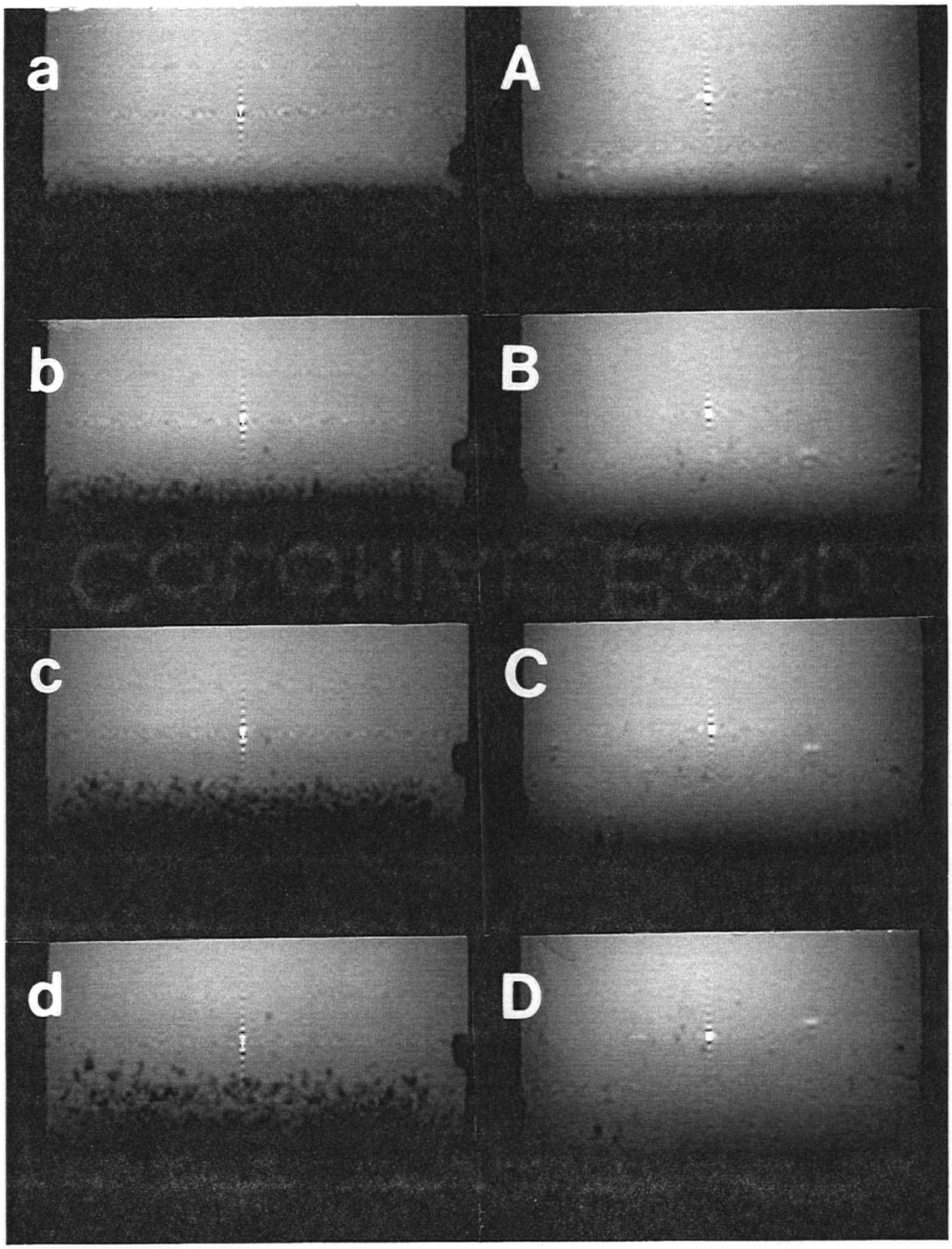

Figure 4.2: Longitudinal images of the water distribution in an untreated tablet ((a) through (h)) and a vacuum-treated tablet ((A) through (H)) taken at approximately the same position in the two swelling tablet systems. The images show the bottom portion of the NMR tube. The times for the eight sets of images are (a, A) 1 hour, (b, B) 4 hours, (c, C) 7 hours, (d, D) 13 hours, (e, E) 19 hours, (f, F) 25 hours, (g, G) 31 hours, and (h, H) 37 hours. The relationship between distance in the image and distance in the tablet is 1:0.22. The parameters for the imaging experiment are indicated in Table 4.1. (The figure is continued on the next page.)

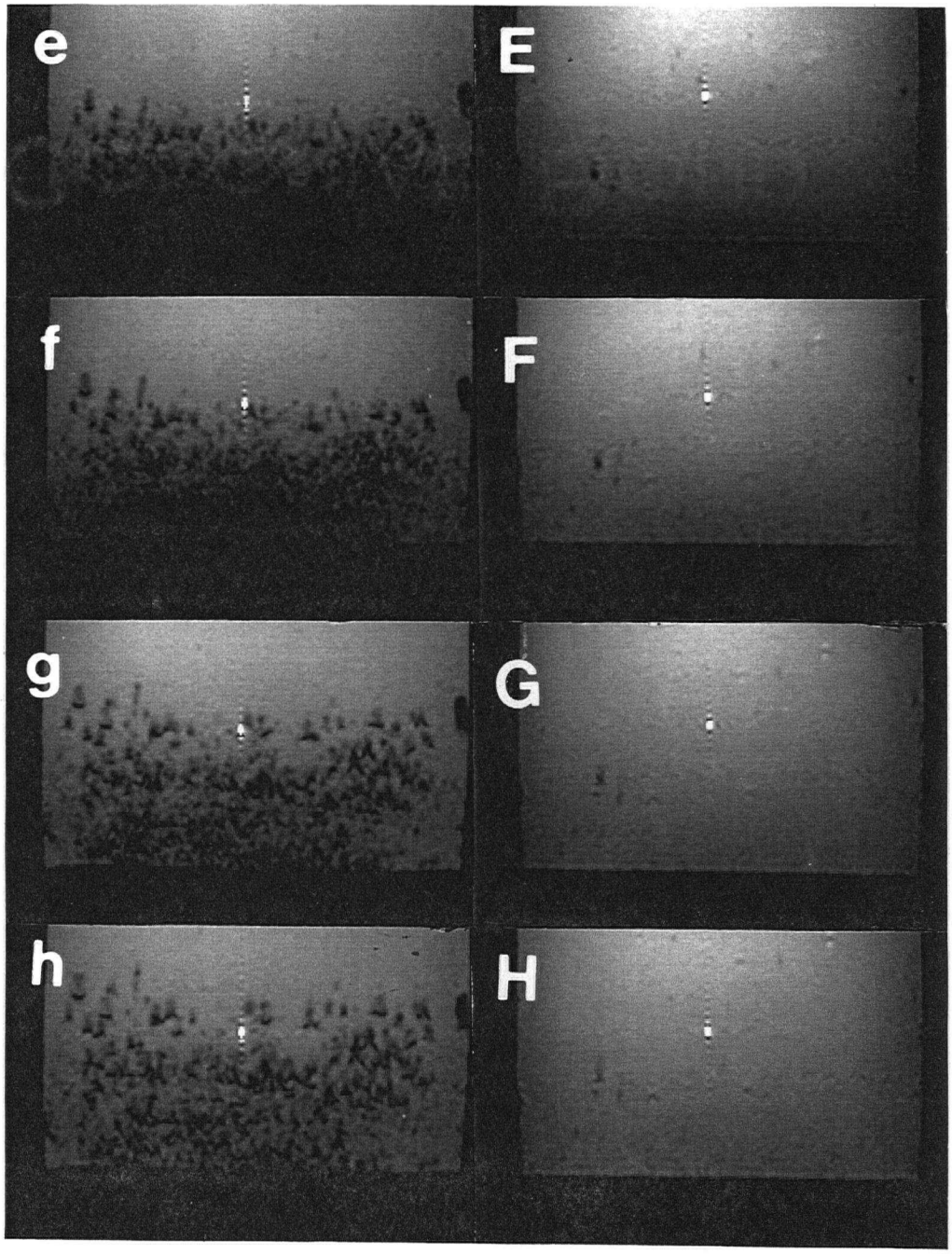

Figure 4.2 continued: images (e) to (h) and (E) to (H).

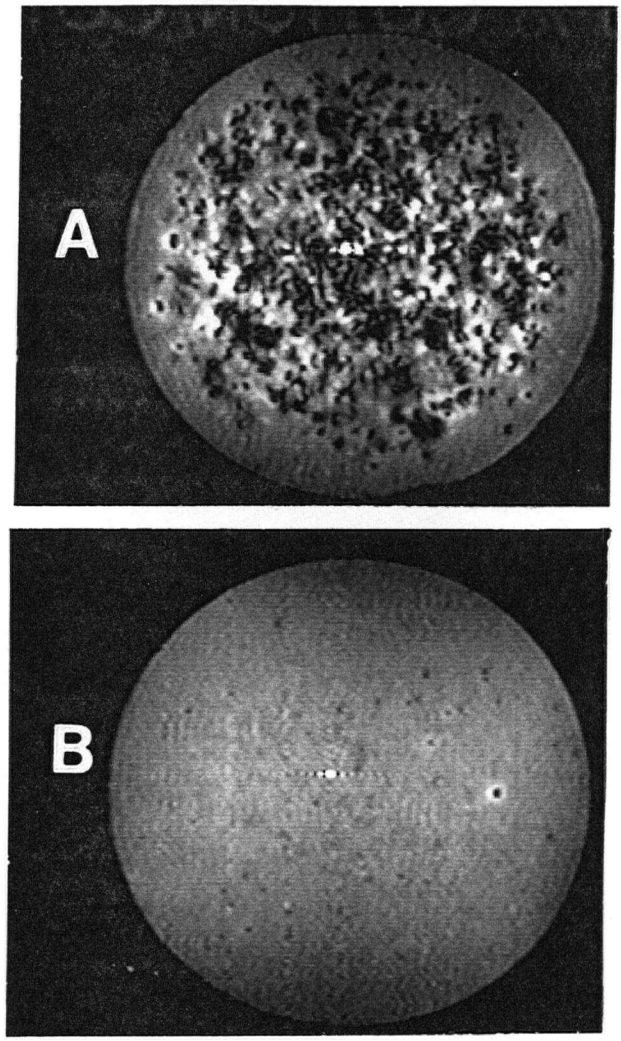

Figure 4.3: Cross-sectional images of the water distribution in an untreated tablet (A) and a vacuum-treated tablet (B) taken at approximately the same position in the middle of the swollen tablet at a swelling time of 43 hours. The relationship between distance in the image and distance in the tablet is 1:0.20. The parameters for the imaging experiment are indicated in Table 4.1.

regions of the swollen tablet.

4.3.2 Total Weight of Polymer in Untreated and Vacuum-Treated Tablets

A comparison between the known weight of polymer in the system and the total polymer weight calculated from a polymer distribution determined experimentally is a very direct and incisive test of the accuracy of the experimentally determined polymer distribution. The imaging studies of Chapter 3 produced distributions whose total polymer content deviated greatly from the known tablet weight (cf. Table 3.4). A similar comparison was made with the data from the vacuum-treated samples to determine if the air bubbles present in the swollen gel were the cause of the total weight deviation.

Table 4.2 shows the results of the total weight calculation for two separate imaging experiments with vacuum-treated tablets, before and after correcting the measured T_2 values for diffusion effects. The total weight calculation was not performed for distributions earlier than 19 hours because the water either had not penetrated regions of the tablet or had penetrated such that its concentration level was not high enough to calculate HPMC weight percents. The differences between the original polymer distributions and the diffusion-corrected distributions was on average only 5 mg or about 3% of the known tablet weight. The average error of each of the calculated polymer weights is about 14 mg which includes errors from the weight percent calculation and parameters used in determining the volume of each segment such as the cross-sectional area of the tube and the gradient strength.

The two vacuum trials produced polymer weights that were much closer to the actual weight of HPMC in the tablet than those determined from the untreated system which indicated that the removal of air affects the total polymer weight calculation. However, the total weights from both vacuum trials were greater than the actual weight of the tablet suggesting either that the vacuum-treatment does not remove all the air from the pores of the tablets or that the imaging method for determining HPMC concentration suffers from a small systematic error towards higher HPMC concentration.

Table 4.2: Total weights of HPMC calculated from one-dimensional imaging experiments at various times during the swelling of vacuum-treated tablets. The original results are those computed from distributions calculated as in Chapter 3. The corrected results have been adjusted for any diffusion effects.

Time (hrs)	Trial 1				Trial 2			
	Original		Corrected		Original		Corrected	
	HPMC[a]	% dev[b]	HPMC	% dev	HPMC	% dev	HPMC	% dev
19	179	8	175	5	184	11	180	8
25	188	13	183	10	189	14	186	12
31	190	14	185	11	192	16	188	13
37	188	13	182	10	193	16	188	13

[a] **HPMC** is the total weight of polymer in milligrams with an average error of ±14 mg.

[b] Percent deviation from the known polymer weight of 166 mg, 100% × (**HPMC**−166)/166 .

4.3.3 Water Distributions in the Vacuum-Treated Tablets

The water distributions for the vacuum treated tablets were determined using the ^{1}H imaging procedure previously described in Chapter 3. They are displayed in Figure 4.4 in comparison with the water distributions from the untreated tablet systems. The distributions are quite similar at all swelling times, although it appears as if the amount of water in the concentrated region of the swollen tablet is consistently larger in the vacuum-treated system than in the untreated system suggesting that more water penetrates the tablet in the absence of trapped air. The differences in water concentration are generally small, however, and may be within the combined errors of the two experiments.

There was a concern that the vacuum treatment of the tablet would result in water drawn deep into the tablet to replace the air in the pores of the tablet. However, the extent of water penetration into the tablet for the vacuum-treated system is the same as for the untreated system and the water penetration distance (WPD) data from the vacuum-treated system would also fall on the straight line of the plot of WPD as a function of the square-root of time, presented in Figure 3.10. Thus, the vacuum-treatment did not change the Fickian nature of the water penetration process.

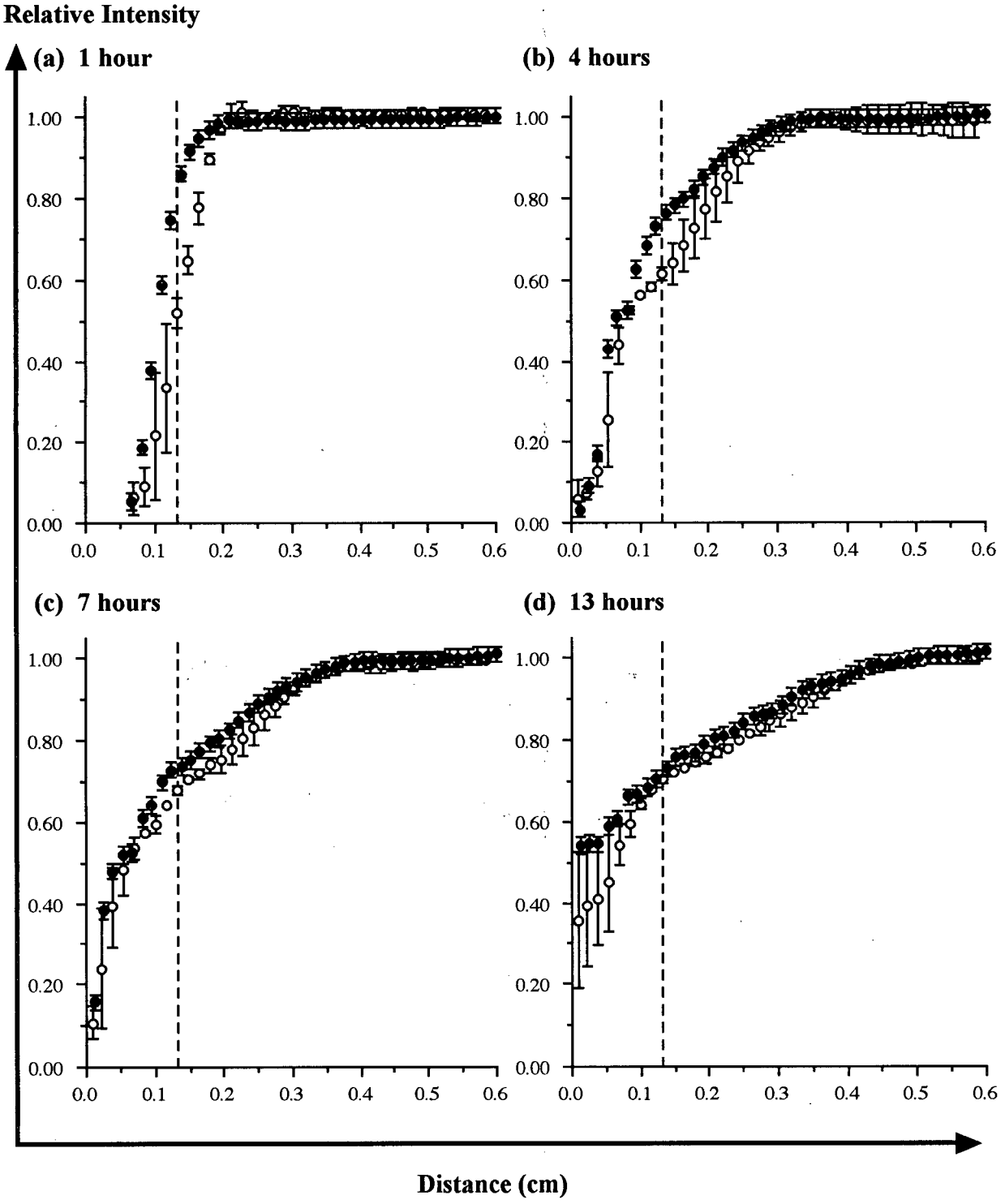

Figure 4.4: Water distributions of the untreated (open circles, n=2) and vacuum-treated (filled circles, Trial 2) tablets at swelling times of (a) 1 hour, (b) 4 hours, (c) 7 hours, (d) 13 hours, (e) 19 hours, (f) 25 hours, (g) 31 hours and (h) 37 hours. The error bars for the untreated tablet system indicate the standard deviations determined from the averaging while the error bars for the vacuum-treated tablet are fixed at ± 0.02. The axes in the eight plots are the same and are defined by the arrows. The intensities in the distributions are relative to the intensity of the bulk water. The dashed vertical line in the figure indicates the initial position of the water-tablet interface. (The figure is continued on the next page)

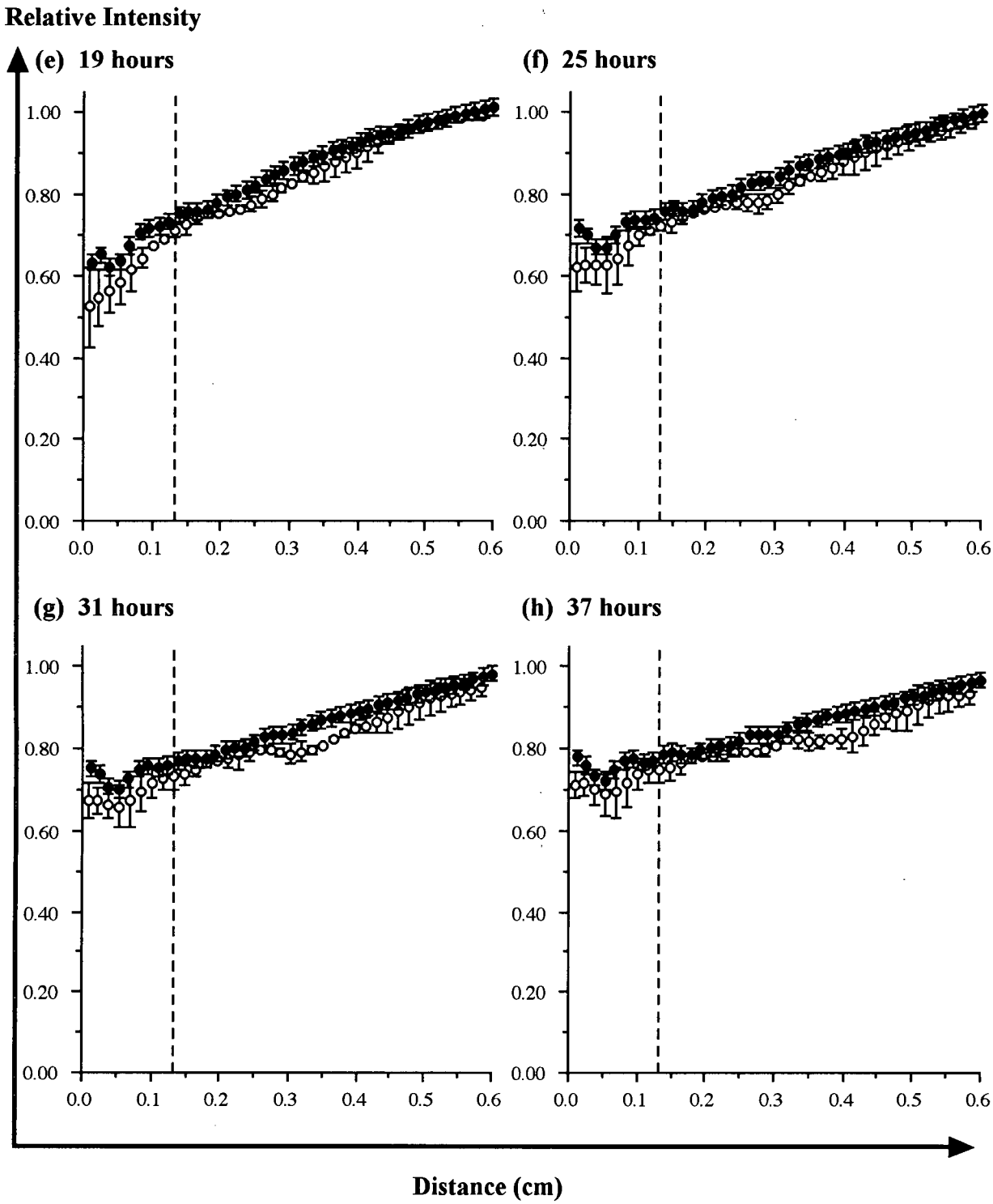

Figure 4.4 continued: plots (e) to (h).

4.3.4 HPMC Distributions in the Vacuum-Treated Tablets

As was apparent in Table 4.2, the correction for the diffusion of water during the imaging experiment was very small. Figure 4.5 shows the difference between the HPMC distributions calculated from the measured T_2 values and those calculated from the diffusion-corrected T_2 values. The HPMC weight percent scale is expanded to allow the differences between the two distributions to be seen clearly. The result of the diffusion correction is a slight lowering of HPMC weight percents in the dilute region of the swollen tablet. The water in this region has larger T_2 values and faster diffusion than the more concentrated regions that show little or no change after the correction for water diffusion is applied.

The diffusion corrected HPMC distributions are shown again in Figure 4.6 compared with the polymer distributions from the untreated tablet system. At all swelling times, the HPMC weight percents calculated from the imaging experiments of the vacuum-treated system are less than those from the untreated system in most regions of the swollen tablet. The most significant differences between the two distributions occurs in the concentrated polymer regions where there are numerous air bubbles present. In the less concentrated regions, the two distributions are very similar because the air has either escaped the gel or dissolved in the more abundant water. The extent of tablet swelling was the same in both tablet systems which was not the expected result. The presence of the air bubbles in the untreated tablet was expected to cause a larger apparent tablet swelling than that due to the polymer alone.

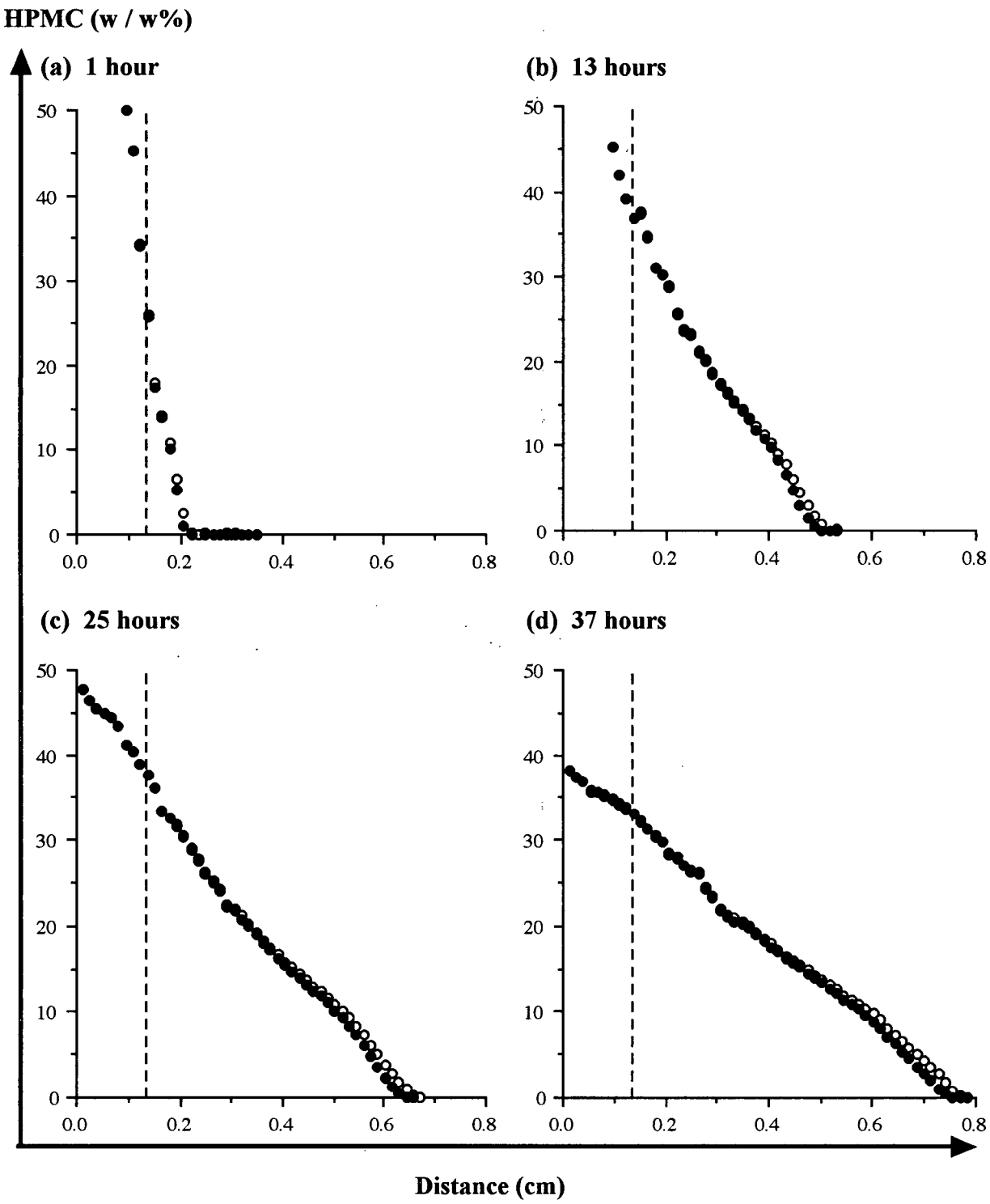

Figure 4.5: HPMC weight percent distributions of the Trial 2 vacuum-treated tablet as calculated (open circles) and diffusion-corrected (filled circles) at swelling times of (a) 1 hour, (b) 13 hours, (c) 25 hours, and (d) 37 hours. The axes in the plots are the same and are defined by the arrows. The dashed vertical line in the figure indicates the initial position of the water-tablet interface.

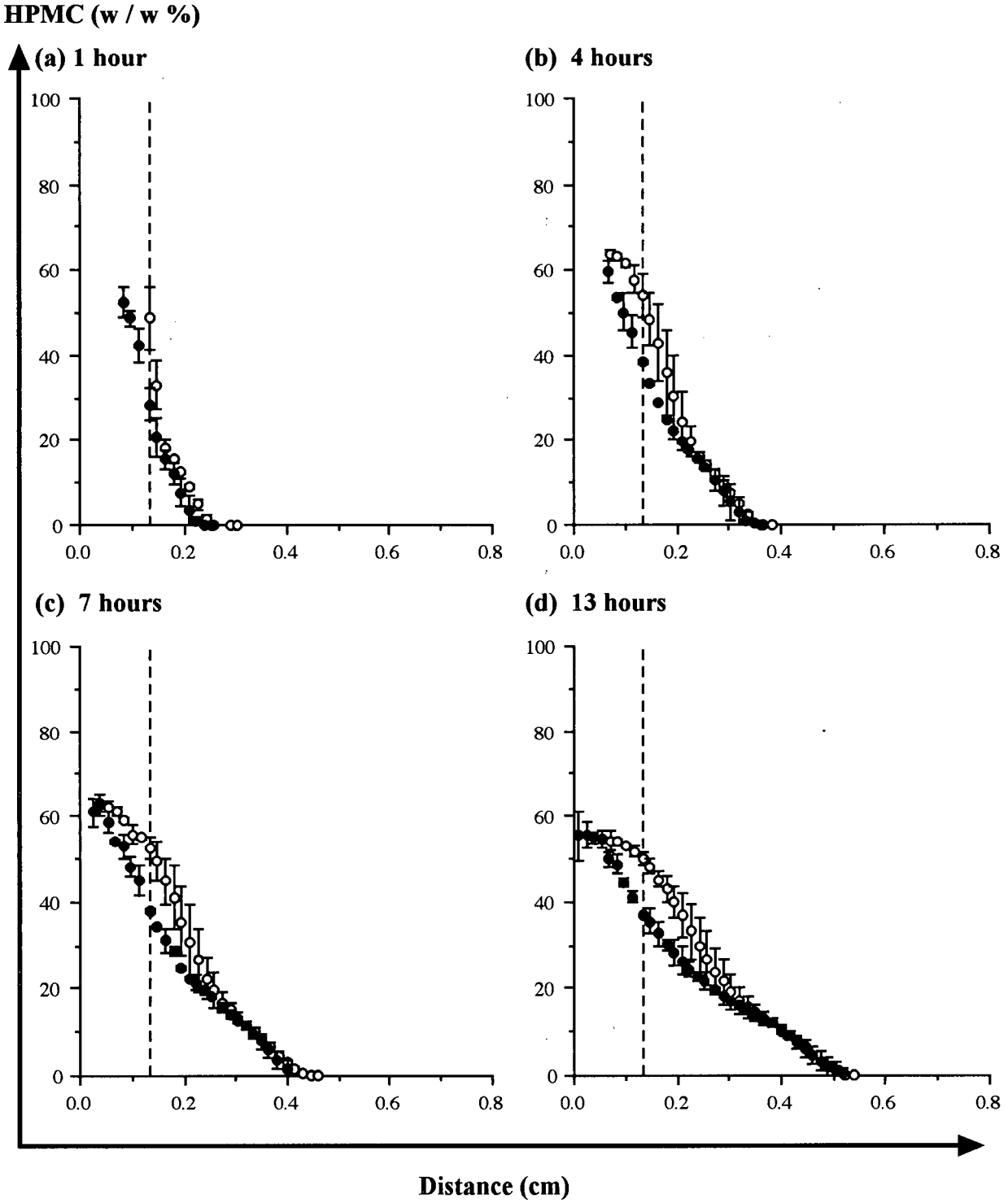

Figure 4.6: Average HPMC weight percent distributions of the untreated (open circles, n=2) and vacuum-treated (filled circles, n=2) tablets at swelling times of (a) 1 hour, (b) 4 hours, (c) 7 hours, (d) 13 hours, (e) 19 hours, (f) 25 hours, (g) 31 hours and (h) 37 hours. The error bars for both tablet systems are the standard deviations from the averaging. The axes in the plots are the same and are defined by the arrows. The dashed vertical line in the figure indicates the initial position of the water-tablet interface. (The figure is continued on the next page)

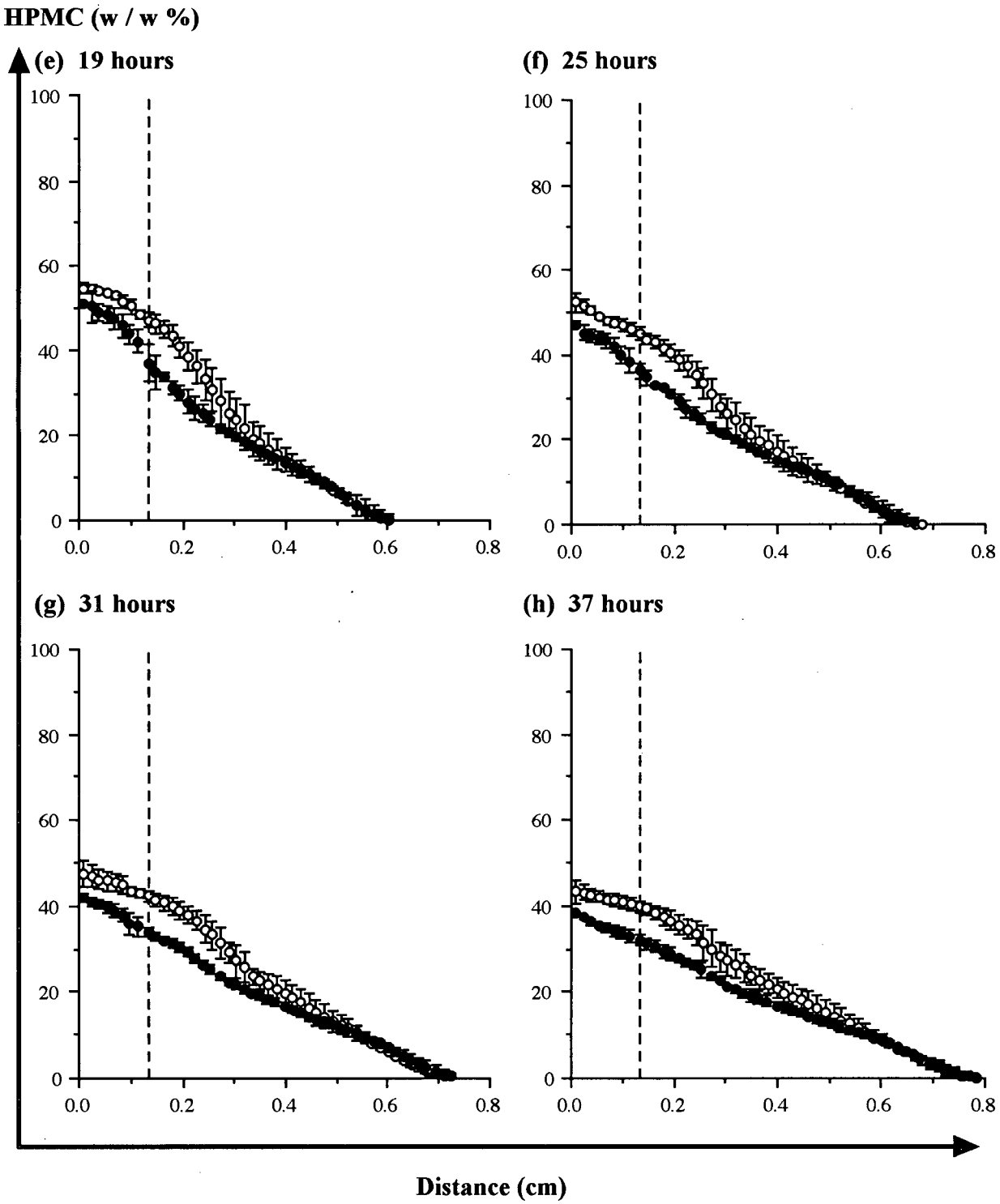

Figure 4.6 continued: plots (e) to (h).

4.4 Summary

The vacuum-treatment of HPMC tablets prior to the imaging experiment was shown to remove the air bubbles and decrease the calculated total polymer weight from the experimental HPMC weight percent distributions. The vacuum-treatment was shown to vary in efficiency and the total polymer weight was used as a criterion for determining the accuracy of the HPMC distributions from an imaging experiment. The water and polymer distributions obtained from the vacuum-treated tablet are now suitable for comparison with theoretical models.

Chapter 5

One-Dimensional ^{19}F NMR Imaging Investigations of Model Drugs in Swelling HPMC Tablets

5.1 Introduction

Drug release from swelling-controlled delivery systems has been studied primarily by the USP dissolution methods where the tablet is suspended in a media bath, or flow-cell, and the amount of drug released into solution is measured as a function of time [21]. The relationship between the fraction of drug released and time is used to determine whether the drug release process follows Fickian or non-Fickian kinetics which is related to the water penetration process as discussed in Section 1.1.3. Dissolution tests, however, can not probe the drug present within the swollen tablet and do not provide information on the relative importance of the two mechanisms of drug release from swelling-controlled devices, namely diffusion through the swollen polymer or, in cases of slow diffusion, the release of drug at the edges of the tablet through erosion.

In Chapter 3, a simple geometry was presented to study the swelling of an HPMC tablet and NMR imaging of ^{1}H was used to determine the distributions of water and polymer as the tablet swelled. In a similar experiment, using a tablet that contains a model drug, NMR imaging of a nucleus specific to the drug, in this case ^{19}F, permits the independent monitoring of the drug distribution within the polymer tablet as it swells. The relationship between the distributions of the drug and polymer makes it possible to

distinguish between drugs that are released only by erosion of the tablet and those that are also released by diffusion through the polymer gel. The mechanism of release in any specific case will depend on the properties of the drug and tablet system.

5.2 Experimental

5.2.1 Preparation of Tablets Containing Fluorinated Drug

The tablets for the ^{19}F imaging experiments were similar to the Type 1 tablets of Section 3.2.1. The tablets were compressed from mixtures of HPMC and drug containing 5.30% and 5.25% by weight of trifluprom azine-HCl and 5-fluorouracil, respectively. The tablet parameters, given in Table 5.1, indicate that the two tablets are essentially identical. The tablets contained approximately the same concentration of fluorine because the larger molecular weight for trifluprom azine-HCl compared to 5-fluorouracil is compensated by the larger number of ^{19}F atoms in the former drug.

Table 5.1: Parameters for the HPMC tablets containing the fluorinated model drugs.

Drug in Tablet	Weight[a] (mg±0.01)	Thickness (mm±0.01)	Drug (mg±0.01)	^{19}F (10^{-5}) (moles±0.04)
trifluprom azine-HCl	174	1.30	9.22	7.11
5-fluorouracil	176	1.31	9.24	7.10

[a]The weight of the HPMC component, once corrected for moisture content, was 156 mg for the trifluprom azine-HCl tablet and 158 mg for the 5-fluorouracil tablet.

5.2.2 One-dimensional Imaging

The one-dimensional imaging studies of the drug-containing tablets were performed in a similar manner to those of Chapter 3 with the additional vacuum-treatment step described in Chapter 4. There were a few significant differences for the ^{19}F version of the imaging experiments. The rf coil was tuned to 376.45 MHz, the frequency of ^{19}F in a 9.4 T magnet. The spectral width was increased to 100 kHz to include more of the region outside the tablet, and thus, the resolution increased to 0.020 cm. The number of scans for the experiment was increased because of the lower concentration, and hence lower signal, of the fluorinated

drugs compared to water. Because of the increased number of scans, the T_E range for the variable-T_E series was shortened to a maximum value of 64 ms, acquired in the order 2 ms, 4 ms, 16 ms, 32 ms, 64 ms, 24 ms, 8 ms, and 3 ms, to decrease the time required to obtain the set of images. Also, a calibration step to quantify the ^{19}F signal was added to the previously described imaging procedure.

5.2.3 Calibration of Fluorine Signal

The signal in the ^{19}F images of the fluorinated drugs was obtained on an arbitrary scale that varied from experiment to experiment. To obtain concentration information, the signal from the drugs in the tablet was referenced to the signal from another fluorinated compound of known concentration. 3-Fluoro-4-nitrotoluene (F.W. 155.13 g mol^{-1}) was obtained from Aldrich Chemical Co. and was chosen because its resonance frequency was well removed from the frequencies of trifluprom azine-HCl and 5-fluorouracil and its signal did not appear in the ^{19}F images of the swollen tablet. The T_1 and T_2 relaxation times for the ^{19}F in 3-fluoro-4-nitrotoluene in $CDCl_3$ were approximately 3 s and 350 ms, respectively, so a spin-echo spectrum acquired with a T_R of 15 s and a T_E of 2 ms would be quantitative. A small amount of this compound, 10.7 mg, was weighed into a 5 mm o.d. NMR tube and dissolved in $CDCl_3$. The 5 mm tube was then suspended in the larger tube containing the tablet. The calibration for the drugs was performed by acquiring spectra and images as listed in Table 5.2. The procedure for the tablets with 5-fluorouracil was adjusted slightly because the T_1 of the drug in dilute solutions is about 4 s. If the T_R in the T_E-variation series was chosen to avoid any T_1 dephasing, then the 8 images would take 3-4 hours to acquire which was deemed to be too long. An alternate procedure, where the 2 ms image was acquired with a T_R of 20 s and then the T_E variation was performed with a shorter T_R, allowed for the quantitative determination of the 5-fluorouracil concentrations and also a measurement of the T_2 distribution. To ensure complete detection of the signal intensity from a particular species, the offset of the excitation pulse was adjusted for each experiment in the sequence such that the species of interest was on resonance.

The signal intensity of a spin-echo spectrum of the drug was quantified in relation

Table 5.2: Sequence of experiments for calibration of ^{19}F signal at various times during the swelling of the drug-containing tablet. The parameters for each experiment, as well as the time for acquisition, are indicated.

Trifluprom azine-HCl:	1. Spin-echo spectrum of 3-fluoro-4-nitrotoluene T_E = 2 ms, T_R = 15 s, 80 scans, 20 minutes 2. Spin-echo spectrum of trifluprom azine-HCl T_E = 2 ms, T_R = 7 s, 80 scans, 9.5 minutes 3. 8 variable-T_E one-dimensional images T_E = 2–64 ms, T_R = 7 s, 80 scans, 75 minutes
5-Fluorouracil:	1. Spin-echo spectrum of 3-fluoro-4-nitrotoluene T_E = 2 ms, T_R = 15 s, 64 scans, 16 minutes 2. Spin-echo spectrum of 5-fluorouracil T_E = 2 ms, T_R = 20 s, 64 scans, 22 minutes 3. Quantitative image of 5-fluorouracil T_E = 2 ms, T_R = 20 s, 64 scans, 22 minutes 4. 8 variable-T_E one-dimensional images T_E = 2–64 ms, T_R = 10 s, 64 scans, 86 minutes

to the signal intensity of the spin-echo spectrum of 3-fluoro-nitrotoluene taken under the same experimental conditions. The signal in the spin-echo spectrum of the drug was then assumed to be the same as the total signal in the one-dimensional image with a T_E of 2 ms as any signal loss due to T_2 dephasing would affect both experiments equally. The calibration for the trifluprom azine-HCl required 20 minutes to obtain the spin-echo spectrum and the 2 ms image. The same procedure for the 5-fluorouracil required about 45 minutes. The calibration equations, relating the arbitrary intensity scale of the images to concentrations of drug, were obtained by plotting the concentrations of ^{19}F determined from the internal reference as a function of the total signal in the images at various times during the swelling of the tablet. Such plots for trifluprom azine-HCl and 5-fluorouracil, using data from swelling times of 7 hours to 37 hours, are shown in Figure 5.1. The least-squares fits to these data sets resulted in Equations 5.1 and 5.3, with an r^2 of 0.997 in both cases. The y-intercept is the offset from the zero concentration at zero time and was assumed to be spread evenly over all the points in the distribution. When the value of the y-intercept was divided equally between the number of relevant data points in each ^{19}F distribution, 101 for trifluprom azine-HCl and 96 for 5-fluorouracil, the new calibrations, Equations 5.2 and 5.4, respectively, could be used to convert the signal intensities in the T_2-corrected images of the drugs to moles ^{19}F. As each point in the ^{19}F images represents the signal from a volume of 0.0256 cm^3, a distribution of ^{19}F in units of molarity can be calculated. When the number of ^{19}F nuclei per molecule is taken into account, the distribution can also be expressed in molarity of the drug.

$$Total\ moles\ ^{19}F = 5.0244 \times 10^{-13}(Total\ Signal_{triflu}) - 1.0673 \times 10^{-5} \quad (5.1)$$

$$moles\ ^{19}F = 5.0244 \times 10^{-13}(Signal_{triflu}) - 1.0567 \times 10^{-7} \quad (5.2)$$

$$Total\ moles\ ^{19}F = 2.6119 \times 10^{-13}(Total\ Signal_{5flu}) + 5.7204 \times 10^{-6} \quad (5.3)$$

$$moles\ ^{19}F = 2.6119 \times 10^{-13}(Signal_{5flu}) + 5.9587 \times 10^{-8} \quad (5.4)$$

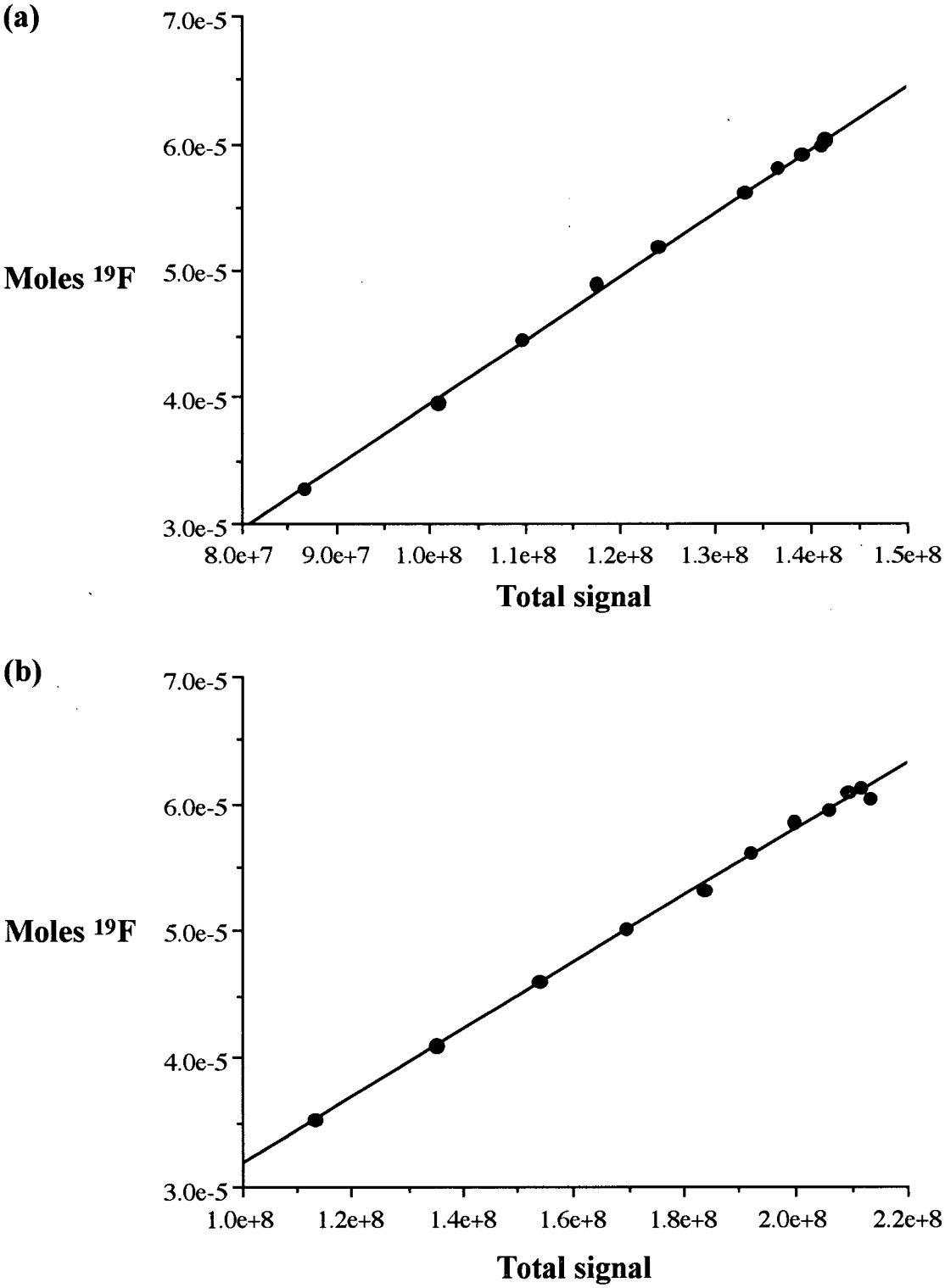

Figure 5.1: Calibration plots relating ^{19}F concentration determined from the internal reference to the total signal in the 2 ms image acquired at the same times during the swelling of an HPMC tablet containing drug, (a) trifluprom azine-HCl and (b) 5-fluorouracil. The line in each plot is the result of a least-squares fit to the data, (a) Equation 5.1 and (b) Equation 5.3.

5.3 Results and Discussion

5.3.1 Distributions of Trifluprom azine-HCl and 5-Fluorouracil in the Swelling Tablet

The one-dimensional imaging studies of drug-containing HPMC tablets were used to determine the distributions of the model drugs in the swollen tablet. The HPMC tablets, prepared with either trifluprom azine-HCl or 5-fluorouracil, contained essentially the same weights of the drug and, coincidentally, the same moles of ^{19}F. Thus, the comparison between the trifluprom azine-HCl and 5-fluorouracil distributions in the two systems, Figure 5.2, is presented in concentration of ^{19}F rather than drug so that the comparison between the imaging results for the two drugs will be clearer. (The 5-fluorouracil concentration distribution will be identical to its ^{19}F distribution because the drug molecule has one ^{19}F group whereas the trifluprom azine-HCl concentration distribution would be 1/3 of its ^{19}F distribution because the drug molecule has three ^{19}F from a CF_3 group.)

Table 5.3: The total detectable moles ^{19}F in the T_2 corrected one-dimensional images of HPMC tablets containing trifluprom azine-HCl and 5-fluorouracil.

	moles ^{19}F ($\pm$ 0.05$\times 10^{-5}$)			
Time (hours)	**Trifluprom azine-HCl**	**%** [a]	**5-fluorouracil**	**%** [a]
1	2.20	31	2.06	29
4	3.46	49	1.67	24
7	4.18	59	3.86	54
13	5.29	75	5.08	72
19	5.81	82	5.77	81
25	6.18	87	6.12	86
31	6.42	90	6.30	89
37	6.52	92	6.35	89

[a] Percentage ratio of detected versus known moles of ^{19}F in tablet

The total detectable amount of each drug as a function of swelling time is given in Table 5.3. In both these systems, the detectable ^{19}F in the images increased slowly with swelling time. At early times, a large portion of the drug within the tablet was immobile and invisible to the imaging technique. As water penetrated further and further into the tablet, the drug was dissolved and its high resolution NMR signal grew. However, the

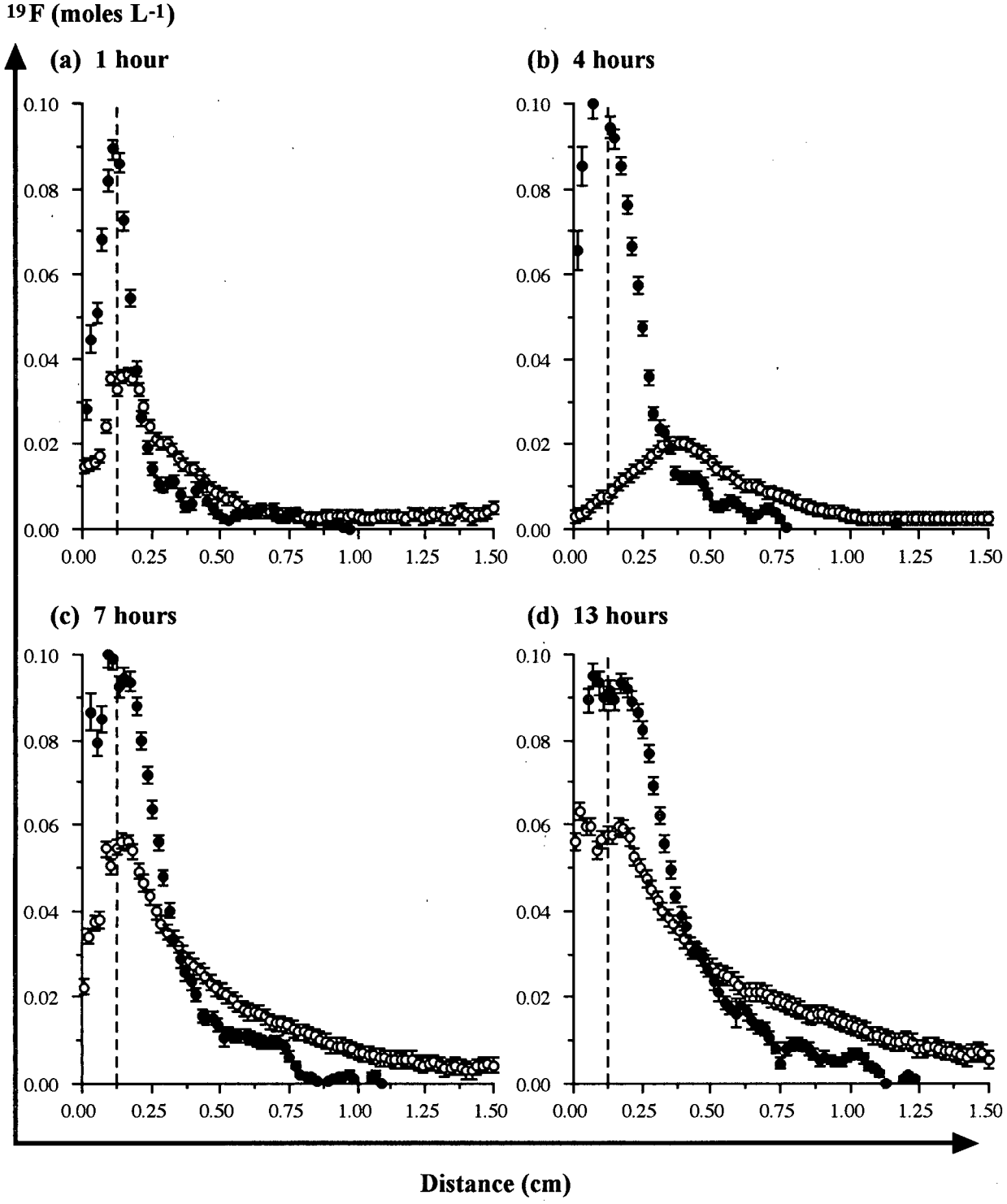

Figure 5.2: Molar distributions of ^{19}F in swollen HPMC tablets containing trifluprom azine-HCl (filled circles) and 5-fluorouracil (open circles). The swelling times in the figure are (a) 1 hour, (b) 4 hours, (c) 7 hours, (d) 13 hours, (e) 19 hours, (f) 25 hours, (g) 31 hours, and (h) 37 hours. The axes are the same in all 8 plots and are defined by the arrows. The dashed vertical line at 0.130 cm indicates the initial position of the water-tablet interface. (The figure is continued on the next page.)

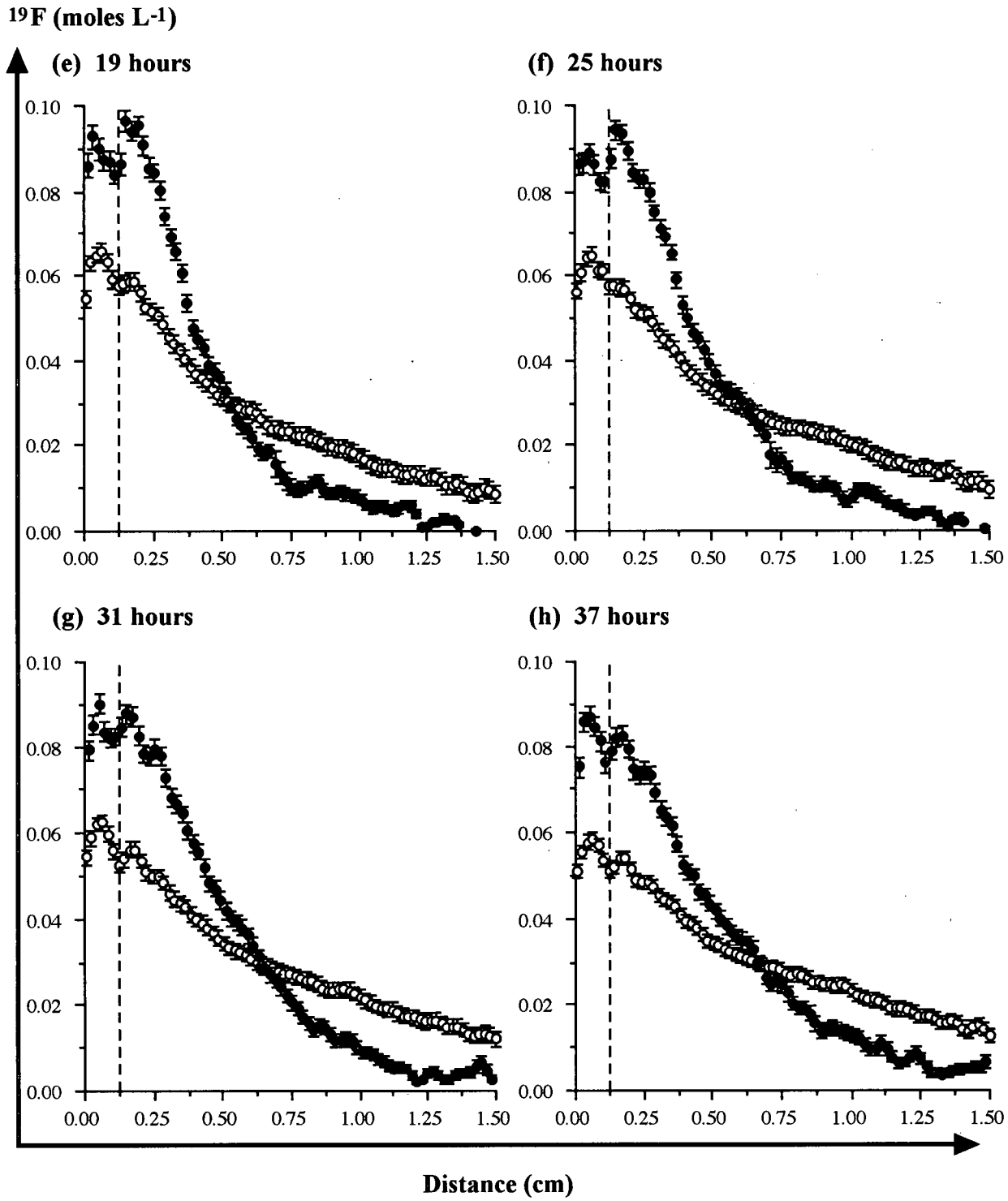

Figure 5.2 continued: plots (e) through (h).

known concentration of $(7.11 \pm 0.04) \times 10^{-5}$ moles ^{19}F within both tablets was not reached for either system. Even at the longest swelling times, only about 90% of the total ^{19}F signal was detectable. In the trifluprom azine-HCl distributions, it is believed that the short T_2 species that are present in HPMC concentrations above $\approx$30% cause such a large signal loss in the 2 ms image that the T_2 values calculated for regions of the polymer above $\approx$30% do not adequately correct for these species. In the 5-fluorouracil system, diffusion of the 5-fluorouracil outside the region of the coil, and hence out of the imaging field of view, is the most likely explanation for the missing 10% of signal at 37 hours. At earlier times, the presence of white flecks in the swollen gel suggested that the 5-fluorouracil was not completely dissolved which would account for the lack of high-resolution NMR signal.

Figure 5.2 clearly shows that the 5-fluorouracil was able to diffuse more freely than the trifluprom azine-HCl. A proportion of the 5-fluorouracil appeared to have diffused out of the field of view of the imaging experiments as early as 13 hours. The differences in these distributions will be discussed further in Section 5.3.3.

5.3.2 HPMC Concentration Distributions Calculated from Images of the Model Drugs

The T_2 distributions calculated from the variable-T_E images of the model drugs in the swollen HPMC tablet can be used to calculate HPMC distributions in the same manner as described in Chapter 3. The calibration relationships between the T_2 values of the model drugs and HPMC weight percent were generated in Chapter 2, resulting in Equations 2.8 and 2.9 for trifluprom azine-HCl and 5-fluorouracil, respectively. The T_2 values determined from the imaging experiments of the drugs were not corrected for diffusion-effects because the diffusion coefficients of the drugs are much lower than those of water. The correction for the drugs would therefore be much smaller than that for water which was shown, in Section 4.3.4, to be minimal.

One example of the variation of the ^{19}F signal intensity of trifluprom azine-HCl as a function of T_E is shown in Figure 5.3 where the signal intensity decreased as the T_E increased. The most significant signal changes occurred in the concentrated regions of

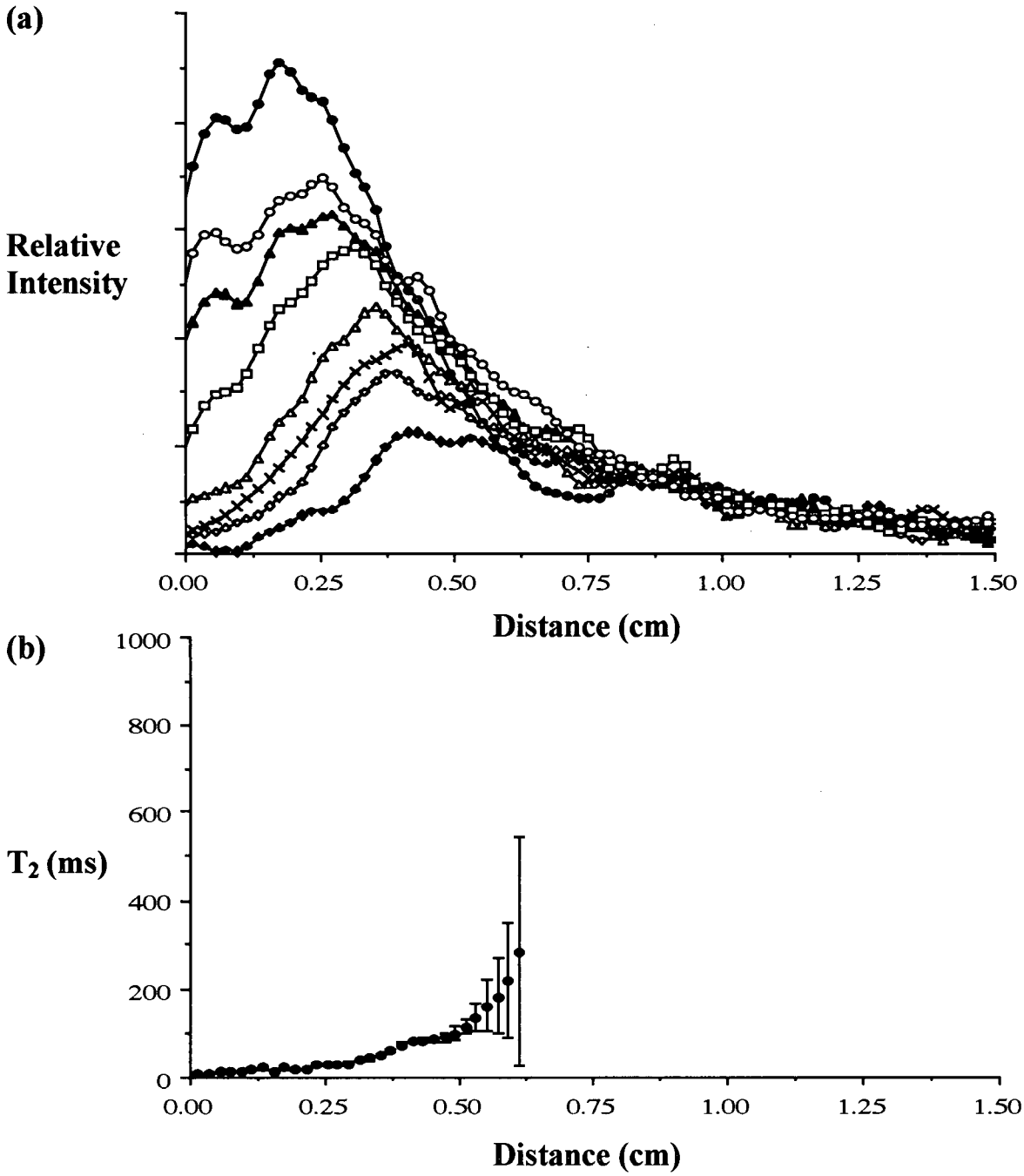

Figure 5.3: The variation of the signal intensity in the trifluprom azine-HCl images as a function of T_E (a) and the corresponding T_2 values (b) calculated from the data in (a) after 19 hours of swelling. The T_E values are 2 ms (filled circles), 3 ms (open circles), 4 ms (filled triangles), 8 ms (open squares), 16 ms (open triangles), 24 ms (crosses), 32 ms (open diamonds) and 64 ms (filled diamonds).

the tablet. At distances above ≈0.6 cm, there was very little change in intensity with increasing T_E. The accurate determination of T_2 values above 200 ms is therefore difficult with a maximum T_E of only 64 ms. The calculated T_2 distribution is considered to be approximate due to the 75 minutes of experimental time required to obtain the complete set of images for the calculation.

Figure 5.4 shows an example of the ^{19}F signal variation of 5-fluorouracil as a function of T_E. These images are affected by T_1 relaxation because the T_R of 10 s does not allow drug in dilute polymer regions to relax completely between successive repetitions of the pulse sequence. However, the degree of T_1 dephasing should remain constant in the set of images acquired at each time interval, not affecting the calculation of T_2 values from the intensity changes. The calculated T_2 distribution, the average over 86 minutes of experimental time, appears reasonable. However, the range of T_2 values extends far beyond the maximum T_2 value of about 400 ms determined from the 0.5 w/w %, or 0.038 M, solution of 5-fluorouracil in distilled water. The T_2 relaxation time for a 0.1%, or 0.0077 M, mixture was measured to determine if the high T_2 values correspond to 5-fluorouracil in concentrations lower than those previously measured. The T_2 values for the 0.1% mixture were 497 ms when the T_R was 30 s and 449 when the T_R was 10 s, as in the imaging experiments. Although the T_2 value does rise as the 5-fluorouracil concentration decreases, the measured value for the mixture does not reach the 700 ms value determined in the imaging experiments in a similar concentration region. Also, the loss of signal due to the shortened T_R appears to lower the measured T_2 value rather than raise it. Thus, the anomalously high T_2 values must be the result of the diffusion of 5-fluorouracil during the acquisition of the variable-T_E dataset. The movement of the 5-fluorouracil during the 86 minutes of the experiment causes a slight increase in the signal intensity in dilute regions of the polymer. The increase in intensity is quite significant because the relatively large T_2 values in these regions result in only a slight loss of signal even at the maximum T_E of 64 ms. Thus, the resulting apparent T_2 value is larger than the true T_2 value because the signal intensity appears to decreases less rapidly with increasing T_E.

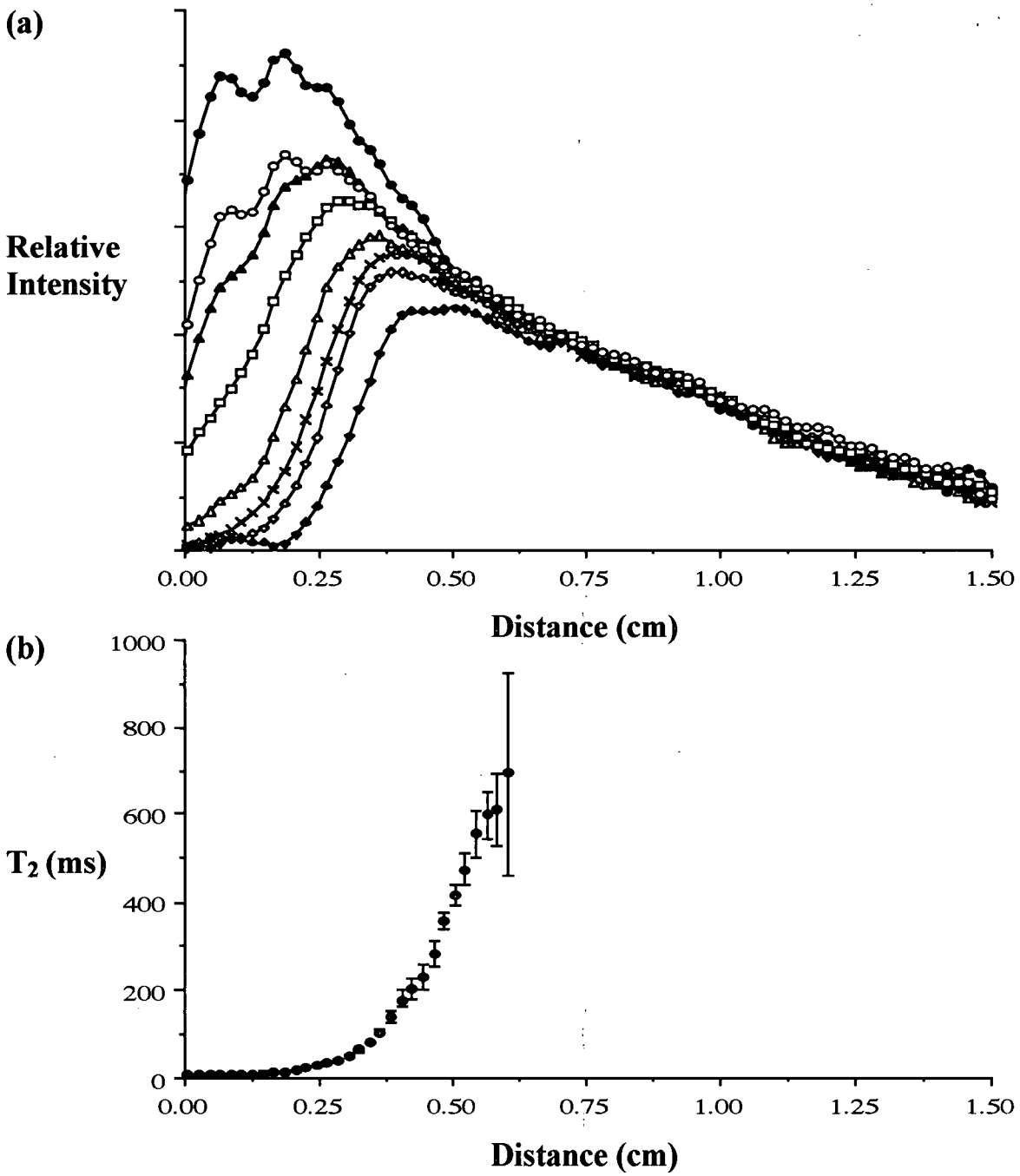

Figure 5.4: The variation of the signal intensity in the 5-fluorouracil images as a function of T_E (a) and the corresponding T_2 values (b) calculated from the data in (a) after 19 hours of swelling. The T_E values are 2 ms (filled circles), 3 ms (open circles), 4 ms (filled triangles), 8 ms (open squares), 16 ms (open triangles), 24 ms (crosses), 32 ms (open diamonds) and 64 ms (filled diamonds).

The HPMC distributions calculated from the T_2 distributions determined from the water and triflupromazine-HCl imaging experiments are shown in Figure 5.5. The HPMC distributions from the 5-fluorouracil data were similar to those obtained from the water and triflupromazine-HCl data but showed marked deviations in regions of lower HPMC concentration due to the erroneously large T_2 values obtained in these regions as discussed previously. The two sets of distributions in Figure 5.5 are fairly similar and indicate the same degree of polymer swelling at all eight measurement intervals. The total weights calculated from the triflupromazine-HCl distributions are given in Table 5.4 and agree quite well with the known weight of HPMC in the tablet.

Table 5.4: The total weight of HPMC calculated from the HPMC distributions obtained from the ^{19}F imaging experiments of HPMC tablets containing triflupromazine-HCl.

Time (hours)	**HPMC (±20 mg)**	**% dev**[a]
19	162	3.8
25	166	6.4
31	164	5.1
37	173	10.9

[a] Percent deviation, $100\% \times (\mathbf{HPMC} - 156)/156$

The differences between the procedures for the ^1H and ^{19}F imaging experiments suggest that the HPMC concentrations in the distributions obtained from the water imaging experiments are more reliable than those from the drug experiments. The lower signal intensity in the drug imaging experiments doubles the experimental time necessary to obtain the dataset for calculating the HPMC weight percents from 30 minutes for the water experiments to 75 and 86 minutes, for triflupromazine-HCl and 5-fluorouracil respectively, and results in more variability in the calculated HPMC values. The range of T_E values used in the drug and water experiments is another criterion favouring the HPMC distributions from the water experiments. The number of T_E values for the drug experiments was 8 compared to the 10 used in the water experiments and the maximum value of T_E was only 64 ms for the drug experiments compared to 128 ms for the water experiments. The changes were made to reduce the time to acquire the data necessary to calculate the HPMC

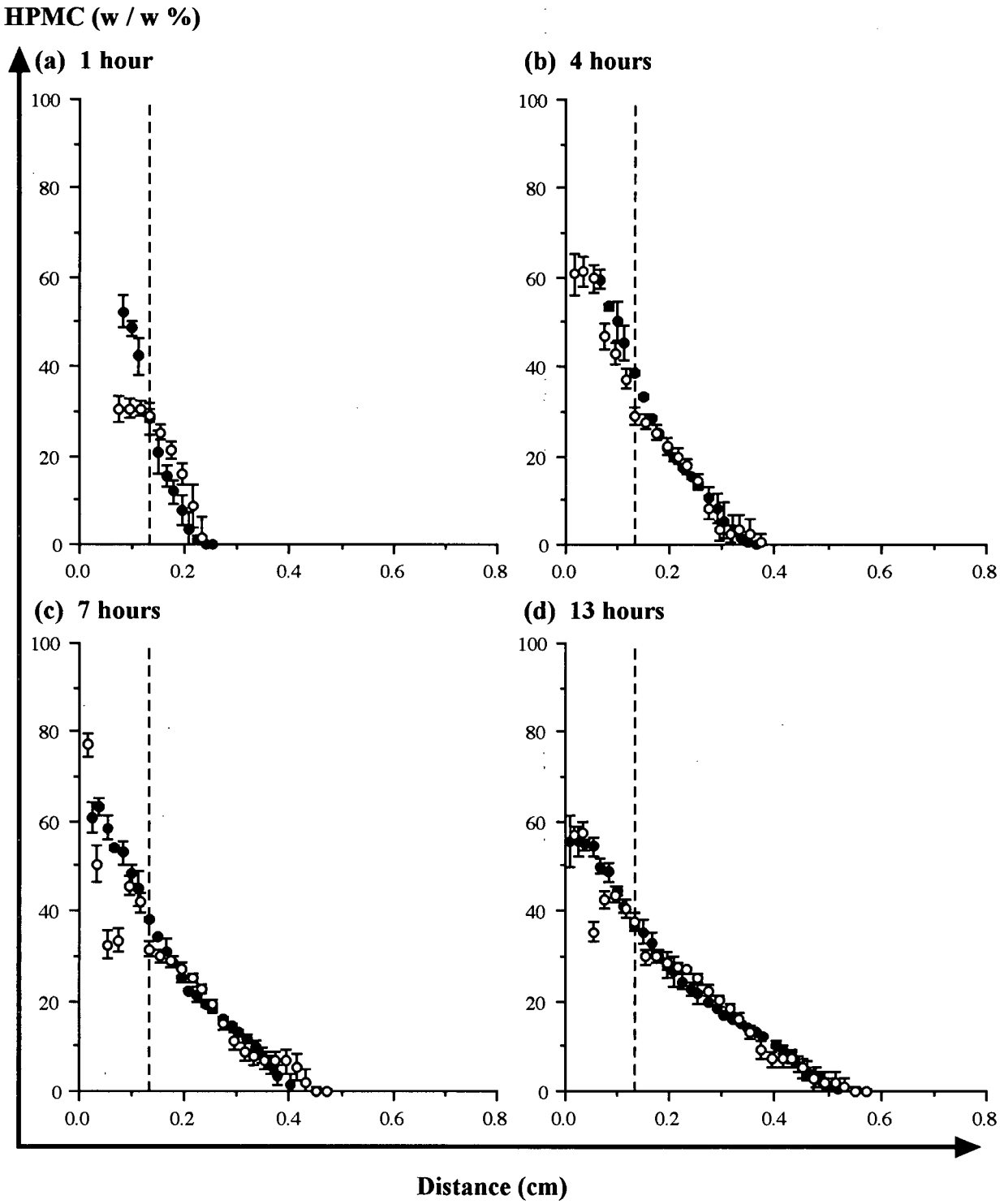

Figure 5.5: HPMC distributions calculated from the water images (filled circles), and trifluprom azine-HCl images (open circles). The swelling times in the figure are (a) 1 hour, (b) 4 hours, (c) 7 hours, (d) 13 hours, (e) 19 hours, (f) 25 hours, (g) 31 hours, and (h) 37 hours. The axes are the same in all 8 plots and are defined by the arrows. The vertical dashed line indicates the original position of the water tablet interface. (The figure is continued on the next page.)

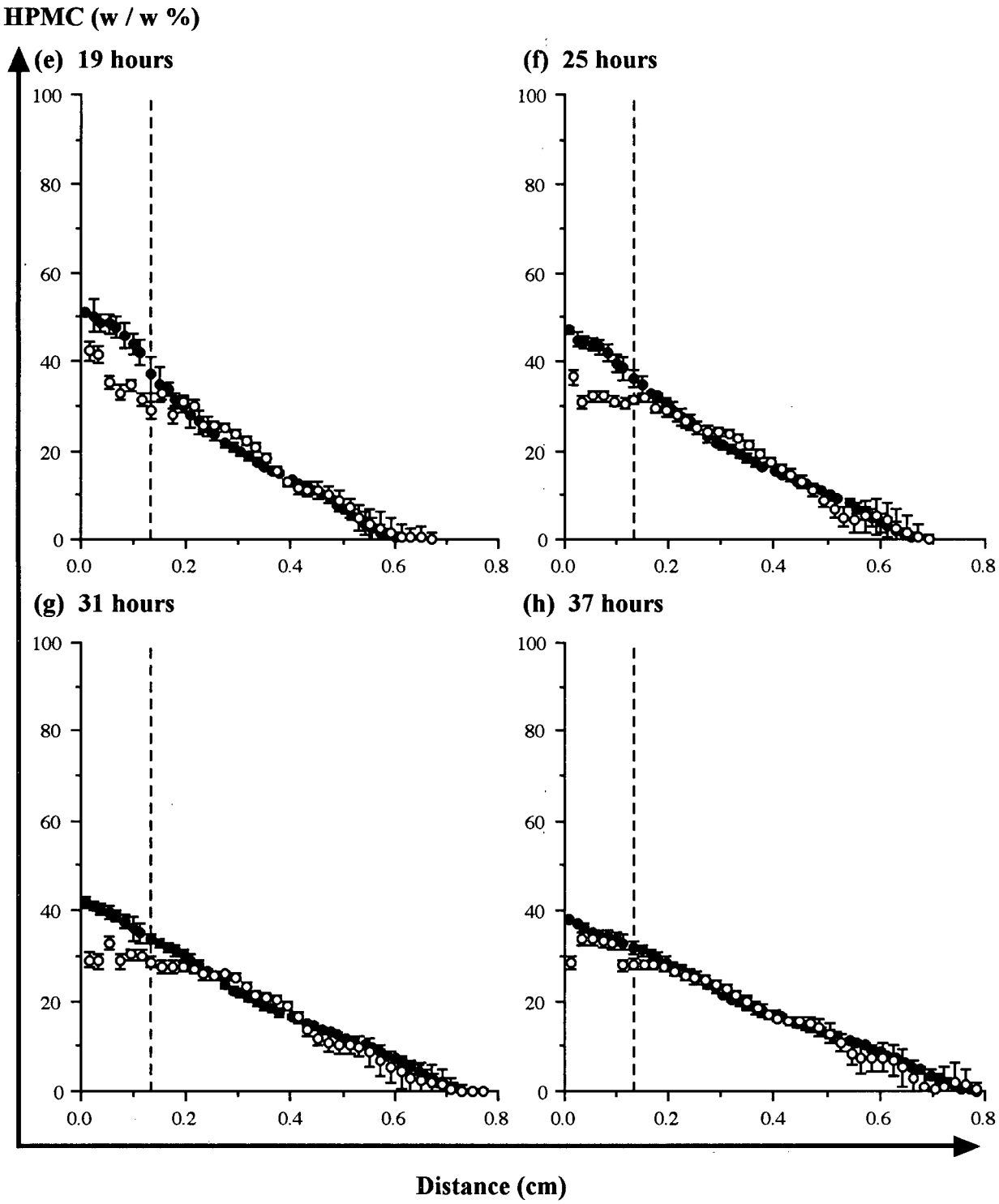

Figure 5.5 continued: plots (e) through (h).

weight percents. The reduction in the T_E range, however, may have reduced the accuracy of the resulting HPMC values, especially in regions with lower HPMC concentration. Thus, even though the distributions from the imaging experiments performed on water contain about 5% more polymer than those obtained from the imaging experiments performed on the drug, the former are deemed to be the most accurate distributions which describe the swelling-controlled drug release system. In general, polymer distributions obtained from water-based data will always be the most accurate because of the greater signal-to-noise in the experiments and the shorter experimental times required to obtain the T_2 datasets.

5.3.3 Discussion of Drug Release Mechanism

The mechanism of drug release from hydrophilic matrix tablets can be deduced from a comparison of the drug and polymer distributions. The HPMC distributions obtained from the water imaging data of Chapter 4 were considered to be the most accurate of the three sets of data and were used for the comparison.

When the distributions of trifluprom azine-HCl and HPMC are overlapped, as in Figure 5.6, one can clearly see that the majority of the drug is still contained within the polymer tablet. In each of the plots of this figure, the HPMC concentrations are given by the scale on the left and the ^{19}F molarities of the drug are given by the scale on the right. The relative amounts of the drug and polymer in the dry tablet was about 4.56×10^{-4} moles ^{19}F per gram. The parallel slopes for the trifluprom azine-HCl and HPMC distributions suggested that the ratio of trifluprom azine-HCl to HPMC concentration remained fairly constant and in fact, the calculated ratios in this region were within 20% of the original ratio. The similarity between the drug and polymer distributions suggested that the majority of the drug movement is the result of the swelling of the polymer. Drug release only occurred when the polymer concentration dropped below about 10% HPMC. At this point the HPMC is no longer in the gel form and is slowly dissolving in solution, resulting in the erosion of the tablet. Thus, the dominant mechanism for trifluprom azine-HCl release appears to be tablet erosion. The diffusion coefficients measured for trifluprom azine-HCl in the HPMC concentrations of this eroding region range from 2×10^{-6} to 4×10^{-6} $cm^2\ s^{-1}$.

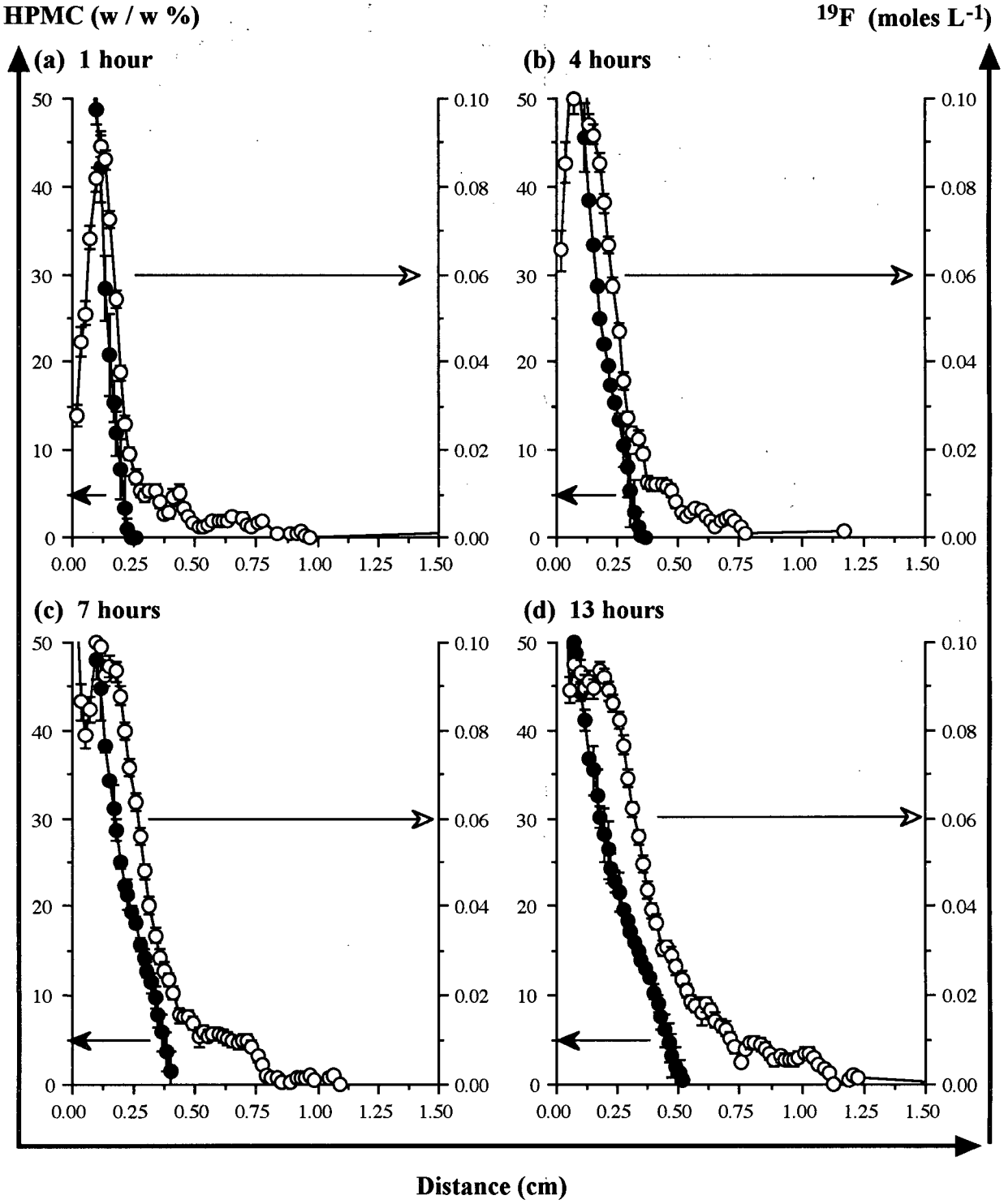

Figure 5.6: Molar ^{19}F distributions of triflupromazine-HCl (open circles) overlapped with HPMC distributions (filled circles) calculated from the water images. The swelling times in the figure are (a) 1 hour, (b) 4 hours, (c) 7 hours, (d) 13 hours, (e) 19 hours, (f) 25 hours, (g) 31 hours, and (h) 37 hours. The axes are the same in all 8 plots and are defined by the large arrows. The position of the 5% HPMC concentration region is indicated by the filled arrow. (The figure is continued on the next page.)

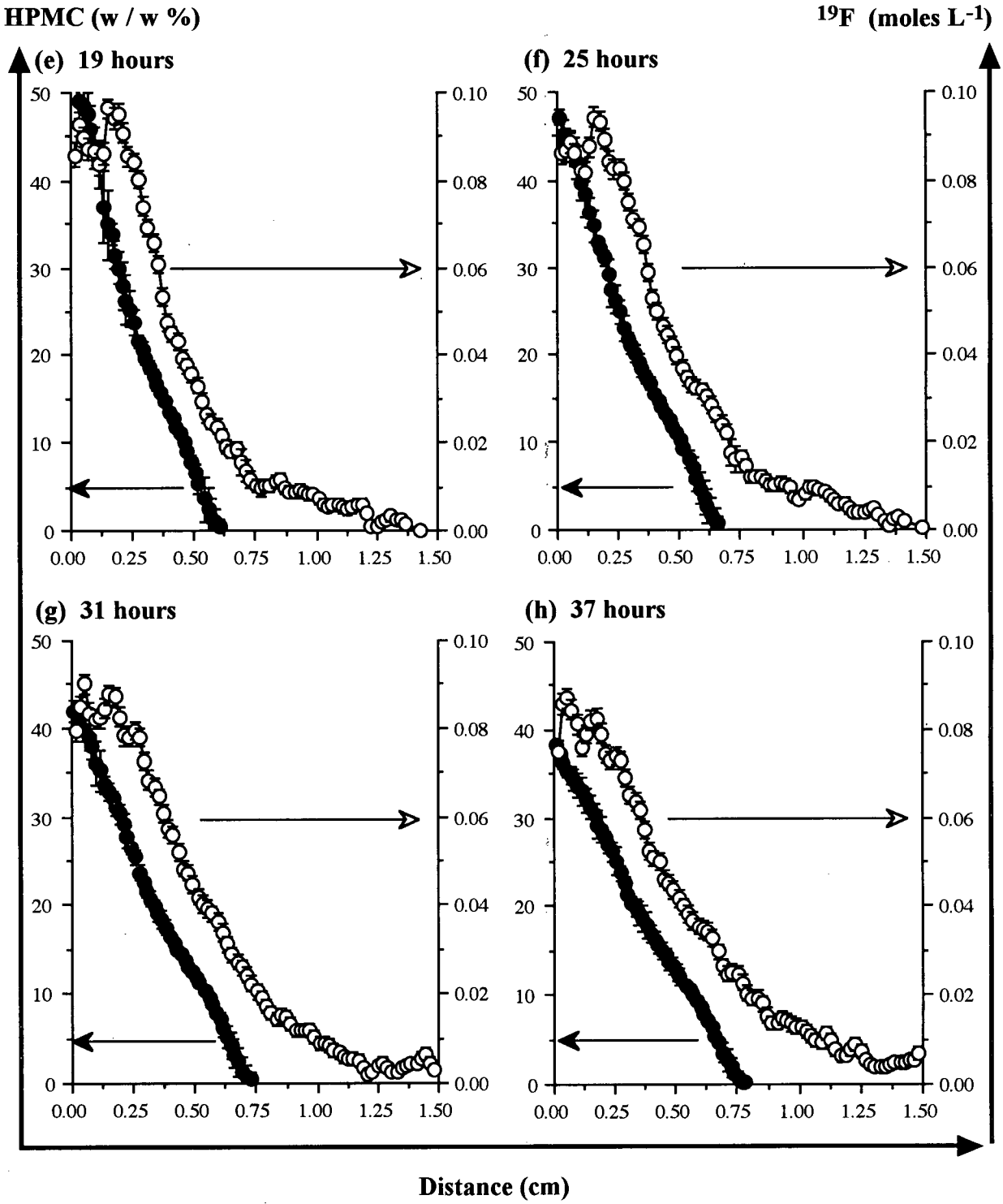

Figure 5.6 continued: plots (e) through (h).

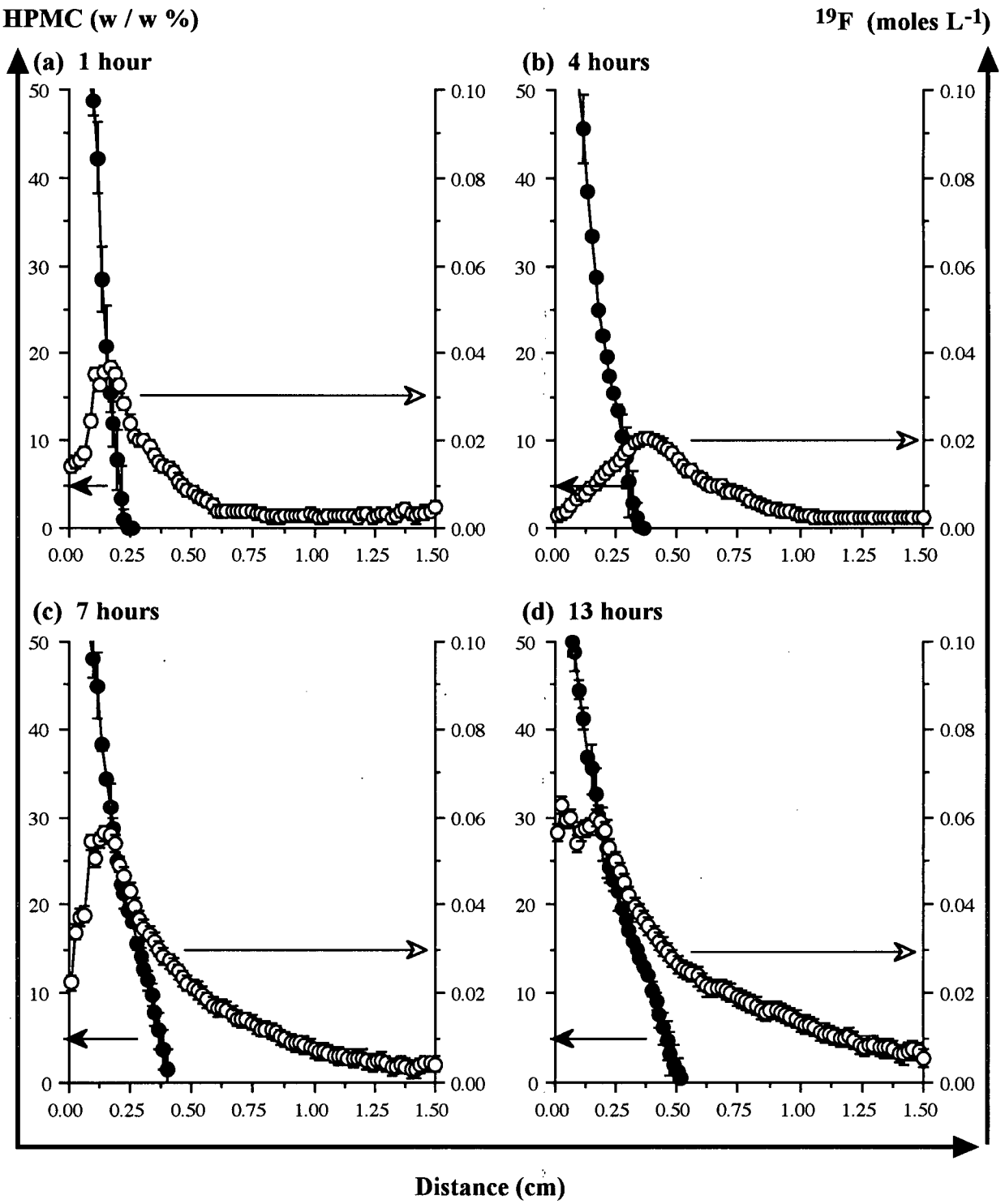

Figure 5.7: Molar ^{19}F distributions of 5-fluorouracil (open circles) overlapped with HPMC distributions (filled circles) calculated from the water images. The swelling times in the figure are (a) 1 hour, (b) 4 hours, (c) 7 hours, (d) 13 hours, (e) 19 hours, (f) 25 hours, (g) 31 hours, and (h) 37 hours. The axes are the same in all 8 plots and are defined by the large arrows. The position of the 5% HPMC concentration region is indicated by the filled arrow. (The figure is continued on the next page.)

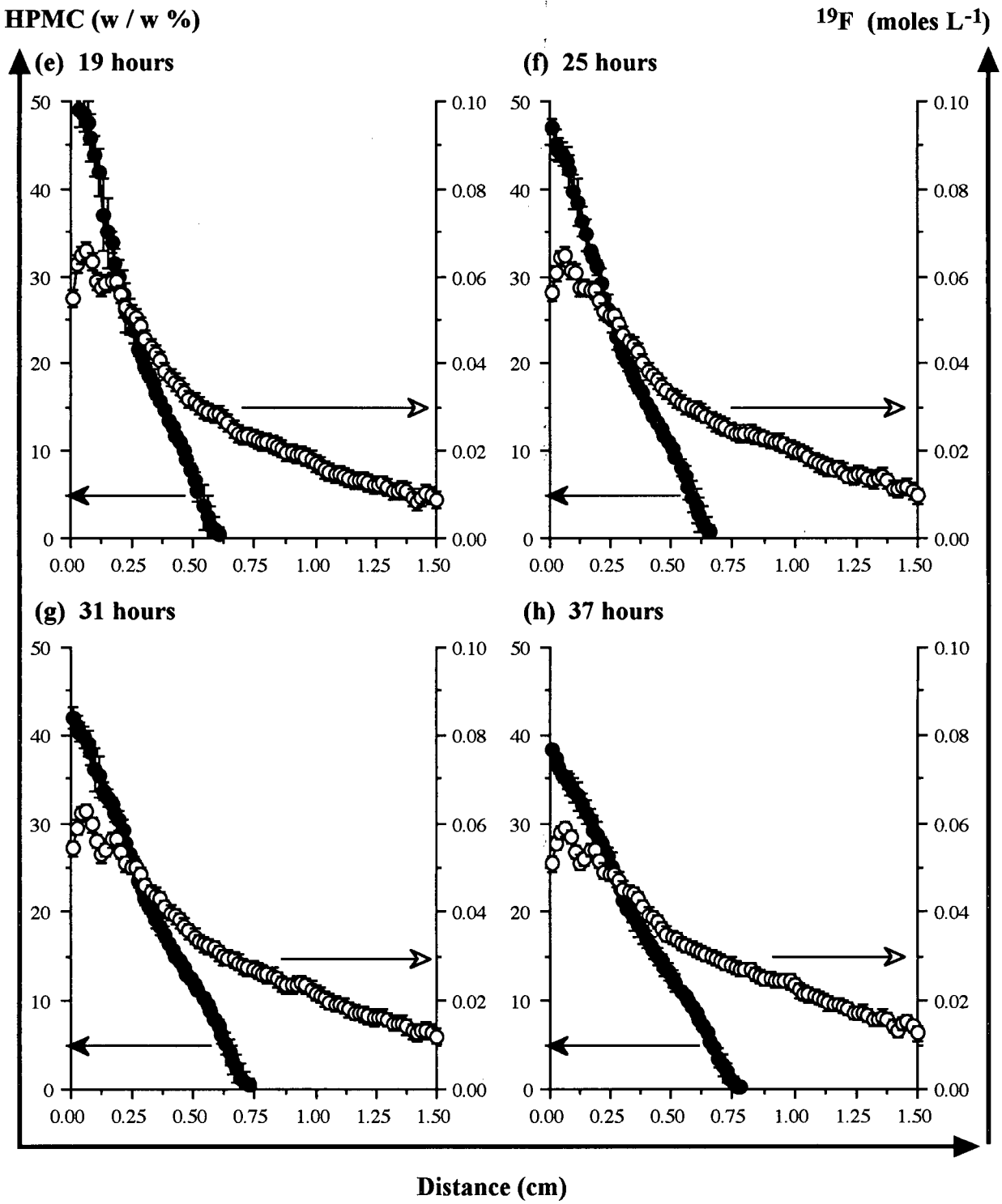

Figure 5.7 continued: plots (e) through (h).

Table 5.5: Distances of various concentration regions in the HPMC concentration distributions calculated from the imaging experiments of Chapter 4.

Time (hours)	Distance (±0.01 cm)		
	≈0% HPMC	5% HPMC	10% HPMC
0	0.13[a]	—	—
1	0.25	0.20	0.19
4	0.36	0.31	0.28
7	0.40	0.37	0.33
13	0.52	0.46	0.40
19	0.60	0.52	0.46
25	0.66	0.58	0.51
31	0.73	0.63	0.54
37	0.79	0.67	0.57

[a] Only the 0% region should coincide with the tablet thickness at zero time.

Similar comparisons for 5-fluorouracil in Figure 5.7 suggest that the drug is diffusing freely from the tablet from the start of the swelling. The maximum of the exponentially-shaped concentration gradient appears to coincide with a polymer concentration of ≈30% at all swelling times. The measured diffusion coefficient of 5-fluorouracil in 30% HPMC was 3.4×10^{-6} cm^2 s^{-1} for the 1% drug mixture and 2.7×10^{-6} cm^2 s^{-1} for the 3% drug mixture. This is the same diffusion coefficient range observed for trifluprom azine-HCl in 0% to 10% HPMC, suggesting that a diffusion coefficient of about 3×10^{-6} cm^2 s^{-1} is required to escape the swelling tablet and that the rate of the swelling must be comparable to, or less than, that value.

An estimate of the rate of tablet expansion can be obtained by tracking the position of the tablet thickness as a function of swelling time. The edge of the tablet can be defined by a particular HPMC concentrations from the HPMC distributions. Three different concentration regions were considered as representing the 'edge of the tablet': ≈0% HPMC would be the tablet edge measured by bulk methods, 10% HPMC was discussed in Section 2.3.4 as the transition concentration for gel formation, and 5% HPMC was chosen as an intermediate concentration between the two extremes. The distances of the ≈0%, 5% and 10% concentration regions as a function of time are presented in Table 5.5. These distances exhibited linear relationships with the square root of time, as shown in Figure 5.8,

resulting in different slopes for each concentration region. In order to compare the swelling of the tablet with the diffusion coefficients of the drugs, apparent rate constants for tablet expansion were determined by squaring the slopes, resulting in 3.16×10^{-6} cm^2 s^{-1} for 0% region, 2.34×10^{-6} cm^2 s^{-1} for the 5% region and 1.59×10^{-6} cm^2 s^{-1} for the 10% region. As will be shown in Chapter 6, these apparent expansion rates are not the same as the apparent diffusion coefficient determined for the polymer but are a simple measure of the movement of the tablet front. It was suggested previously that drug would not be released from the HPMC tablet until the diffusion coefficient of the drug was approximately 3×10^{-6} cm^2 s^{-1}. The apparent expansion rates of the tablet edge are within the same range as the diffusion coefficient required for drug release suggesting that the relationship between the diffusion coefficients of the drug in a polymer and the apparent expansion rate of the polymer, as determined by plots such as Figure 5.8, could be used in other systems to determine drug release behavior. The average of the three apparent rate constants for tablet expansion is $(2.4\pm0.8)\times10^{-6}$ cm^2 s^{-1}.

Table 5.6: Drug inside and outside the HPMC tablets as determined from the ^{19}F imaging experiments. The edge of the swelling tablet, defined as 5% HPMC, is determined from the HPMC distributions obtained from the ^{1}H imaging experiments of Chapter 4.

Time (hours)	Swelling Tablet edge (cm)	moles ^{19}F ($\pm$ 0.05$\times10^{-5}$)			
		Trifluprom azine-HCl		5-fluorouracil	
		Inside	Outside	Inside	Outside
1	0.20	1.57[a]	0.63[a]	0.75[a]	1.30[a]
4	0.31	2.92[a]	0.53[a]	0.46[a]	1.21[a]
7	0.37	3.46	0.72	2.13	1.73
13	0.46	4.34	0.94	2.95	2.13
19	0.52	4.72	1.09	3.42	2.35
25	0.58	5.02	1.17	3.68	2.44
31	0.63	5.18	1.24	3.81	2.49
37	0.67	5.14	1.39	3.87	2.48 (3.24)[b]

[a] The deviations at early times are the result of the higher relative noise level, especially at larger distances.

[b] Amount released if the 10% missing from the maximum amount of ^{19}F is assumed to be outside of the imaging field of view

The signal in the ^{19}F images of the drugs can be divided into two regions, drug

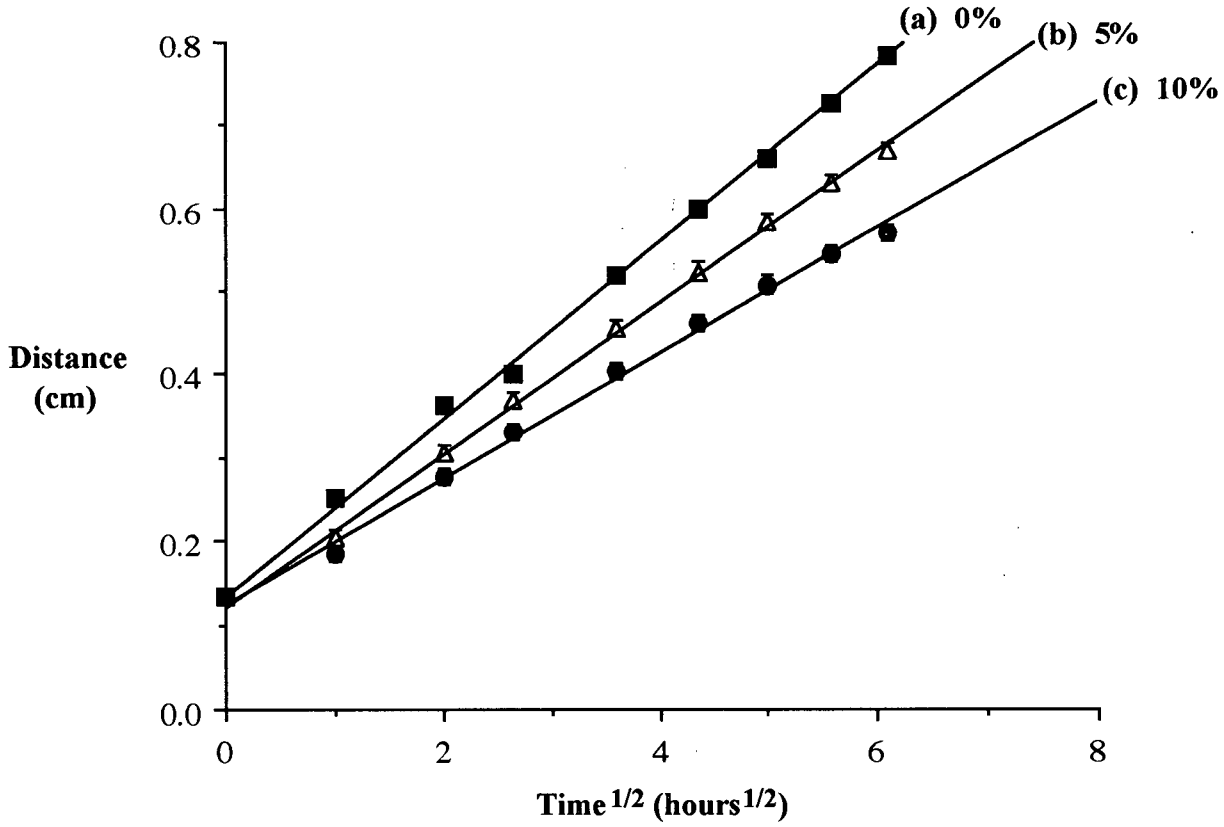

Figure 5.8: The distance of various regions in the swelling HPMC tablet as a function of the square root of the swelling time. The three sets of data are (a) ≈0% (filled squares) and least squares fit line to the data with slope 0.1066 cm $h^{1/2}$, intercept 0.134 cm and r^2 0.999 (b) 5% (open triangles) and least squares fit line to the data with slope 0.09170 cm $h^{1/2}$, intercept 0.121 cm and r^2 0.999 and (c) 10% (filled circles) and least squares fit line to the data with slope 0.07570 cm $h^{1/2}$, intercept 0.124 cm and r^2 0.995.

inside the tablet and drug outside the tablet. The latter represents the drug released from the device at each swelling time. The intermediate 5% HPMC region was chosen as the dividing line between the inside and outside of the tablet. The concentrations of drug in the two regions of the system are given in Table 5.6. The amount of drug released from the trifluprom azine-HCl tablets increased slowly with time. The amount of 5-fluorouracil released became difficult to determine at longer swelling times because some of the drug had diffused out of the imaging field of view. At 37 hours, it was assumed that the missing 10% of the total ^{19}F signal was the result of this diffusion and should count as drug released from the tablet. For both of the drugs, the fraction of drug released was a linear function of the square-root of time indicating that drug release from the swelling HPMC tablet was Fickian. The ratio of the square of the slopes indicates that the rate of 5-fluorouracil release from these HPMC tablets was about five times faster than the rate of trifluprom azine-HCl release.

5.4 Summary

NMR imaging of the ^{19}F in the model drugs was used to monitor the drug distributions within the swelling tablets. The HPMC distributions calculated from variable-T_E experiments of both drugs agreed reasonably well with the HPMC distributions calculated from the water experiments. A comparison of the distributions of drug and polymer showed that the majority of trifluprom azine-HCl remained within the swollen tablet even at later swelling times. In contrast, the 5-fluorouracil diffused within the tablet system at early times and more of this drug was released. The condition for drug release from the tablet requires that the diffusion coefficient of the drug be greater than the expansion rate of the tablet, estimated to be $(2.4\pm0.8)\times10^{-6}$ cm^2 s^{-1}. For trifluprom azine-HCl, this condition was only met at the edge of the swelling tablet where low HPMC concentrations resulted in tablet erosion. The diffusion coefficient of 5-fluorouracil in 30% HPMC was large enough to satisfy the condition for drug release and this drug escaped the tablet through diffusion at this HPMC concentration. The fraction of drug released for both drugs was linear with

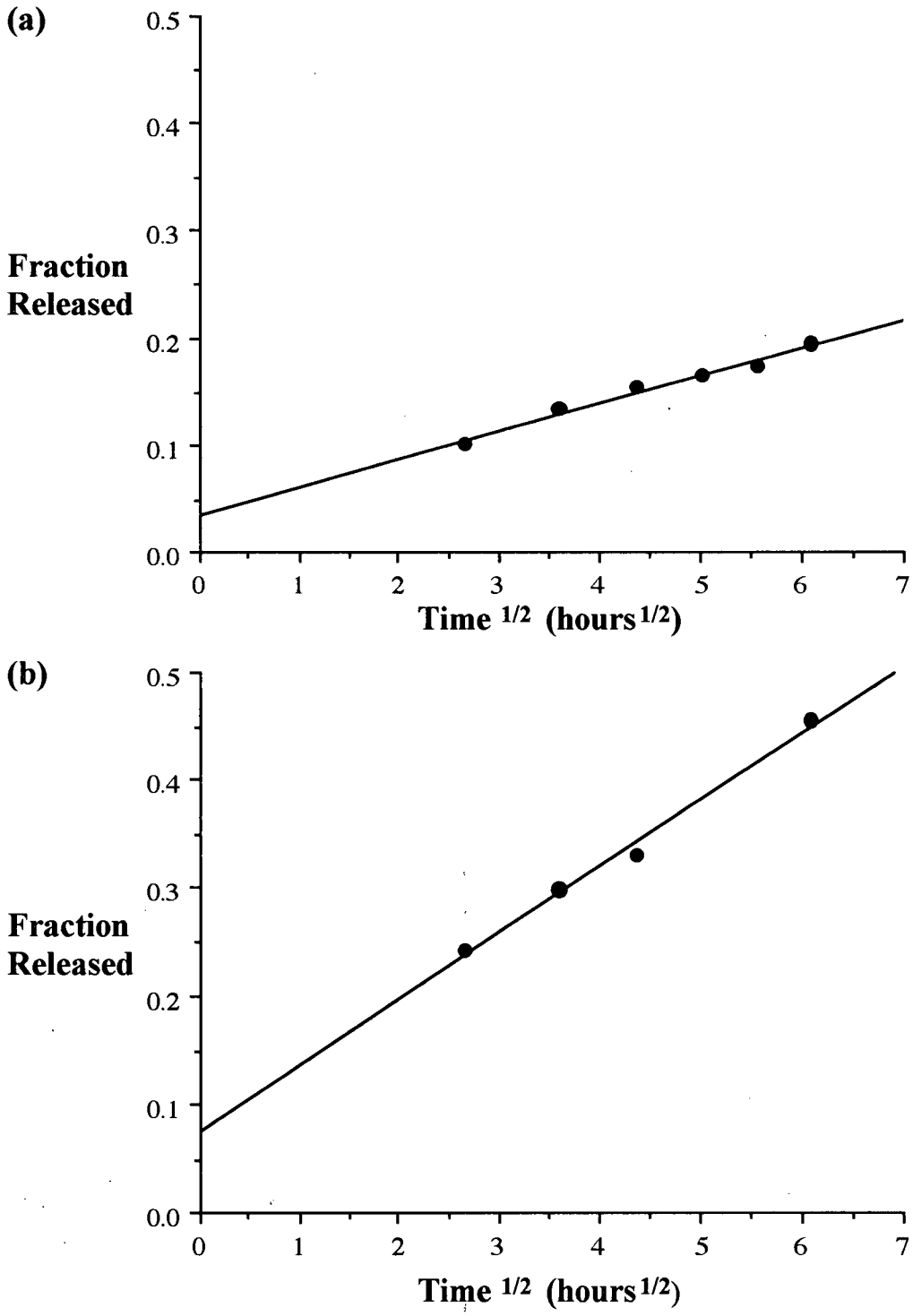

Figure 5.9: Fraction of drug released as a function of the square-root of the swelling time. The two plots are (a) fraction trifluprom azine-HCl released and least squares fit line to the data with slope 0.02573 $h^{1/2}$, intercept 0.03644 and r^2 0.983 and (b) fraction 5-fluorouracil released and least squares fit line to the data with slope 0.06152 $h^{1/2}$, intercept 0.07555 and r^2 0.990.

the square-root of time indicating that the drug release was Fickian.

Chapter 6

Evaluation of Theoretical Models of Transport Processes in Swelling HPMC Tablets

6.1 Introduction

Previous theoretical treatments of swelling-controlled drug delivery systems have been based on changes in bulk properties of the system such as changes in thickness [19, 20], weight of absorbed water [81] or fraction of remaining drug in the matrix [82]. Some theoretical work has been presented to model the concentration distributions of water and drug in the gel layer of a swelling hydrophilic matrix tablet using a pseudo-steady state one-dimensional single-face diffusion method [27]. The limited work on modelling the concentration distributions of water, drug and polymer in all regions of a swelling controlled drug delivery system has resulted from the lack of a complete set of these concentration data prior to the NMR imaging study presented in this thesis. Although the previous theoretical treatments are not directly applicable to the concentration data obtained from the NMR imaging, the general approaches of the authors are useful in developing a simple model to fit the concentration changes that are seen as the HPMC tablet swells.

The geometry chosen for the tablet swelling experiments of Chapters 3–5 restricted the movement of the components of the tablet to one dimension, that perpendicular to the face of the tablet. This slab geometry is the simplest case for modelling the transport of water, polymer and drug. In the initial stage of the calculations, the components of

the hydrophilic matrix tablet were assumed to diffuse via a Fickian diffusion mechanism resulting in effective diffusion parameters. Further investigations examined a segmented tablet model to describe the polymer distribution. In this model, the overall tablet swelling is regarded as the sum of the swelling of individual segments of the original dry tablet.

6.2 Theory

6.2.1 Fickian Diffusion

A brief description of Fickian diffusion theory for one-dimensional diffusion is presented here. More extensive descriptions of the theory and treatments of other geometries are available in the literature [83].

Fick's 1st and 2nd laws for diffusion based on random molecular motions are given in Equations 6.1 and 6.2, respectively, where J is the flux, C is the concentration of the diffusing species, x is the position, t is the time and D is the constant diffusion coefficient. The solutions to Fick's 2nd law depend on the initial conditions for the diffusing substance. Examples of different diffusing systems are shown in Figure 6.1.

$$J = -D\frac{\partial C}{\partial x} \tag{6.1}$$

$$\frac{\partial C}{\partial t} = D\,\frac{\partial^2 C}{\partial x^2} \tag{6.2}$$

Equation 6.3 is the resulting solution to Fick's 2nd law when the diffusing substance originates from a plane sheet at x=0 as in Figure 6.1(a). When the initial region is extended to infinite dimension and the species diffuses into an adjacent region also of infinite dimension, as in Figure 6.1(b), then the combination of Gaussian diffusion from all the positions in the extended region results in Equation 6.4 where the error-function complement (erfc) and the error function (erf) are defined by Equations 6.5 and 6.6, respectively.

$$C = \frac{C_0}{\sqrt{4\pi Dt}}\, e^{-\frac{x^2}{4Dt}} \tag{6.3}$$

$$C(x,t) = \frac{C_0}{2}\ erfc\ \frac{x}{\sqrt{4Dt}} \tag{6.4}$$

$$erfc\ z = 1 - erf\ z \tag{6.5}$$

$$erf\ z = \frac{2}{\sqrt{\pi}} \int_0^z e^{-\frac{y^2}{4Dt}}\ dy \tag{6.6}$$

When the species diffuse from or into a region of limited size, -h < x < h, as shown in Figure 6.1(c) and (d), then Equations 6.7 and 6.8, respectively, can be used to determine the concentration distribution of the species. These equations are symmetrical about zero and can also be used to describe the system where $0 \leq x < h$.

$$C(x,t) = \frac{C_0}{2}\ \{erf\ \frac{h-x}{\sqrt{4Dt}} + erf\ \frac{h+x}{\sqrt{4Dt}}\} \tag{6.7}$$

$$C(x,t) = \frac{C_0}{2}\ \{erfc\ \frac{h-x}{\sqrt{4Dt}} + erfc\ \frac{h+x}{\sqrt{4Dt}}\} \tag{6.8}$$

The given solutions to Fick's 2nd law under the initial conditions shown in Figure 6.1 all require that certain regions extend to infinite dimensions. In practice, this requirement is met by a semi-infinite system where the diffusing species does not reach the external boundaries.

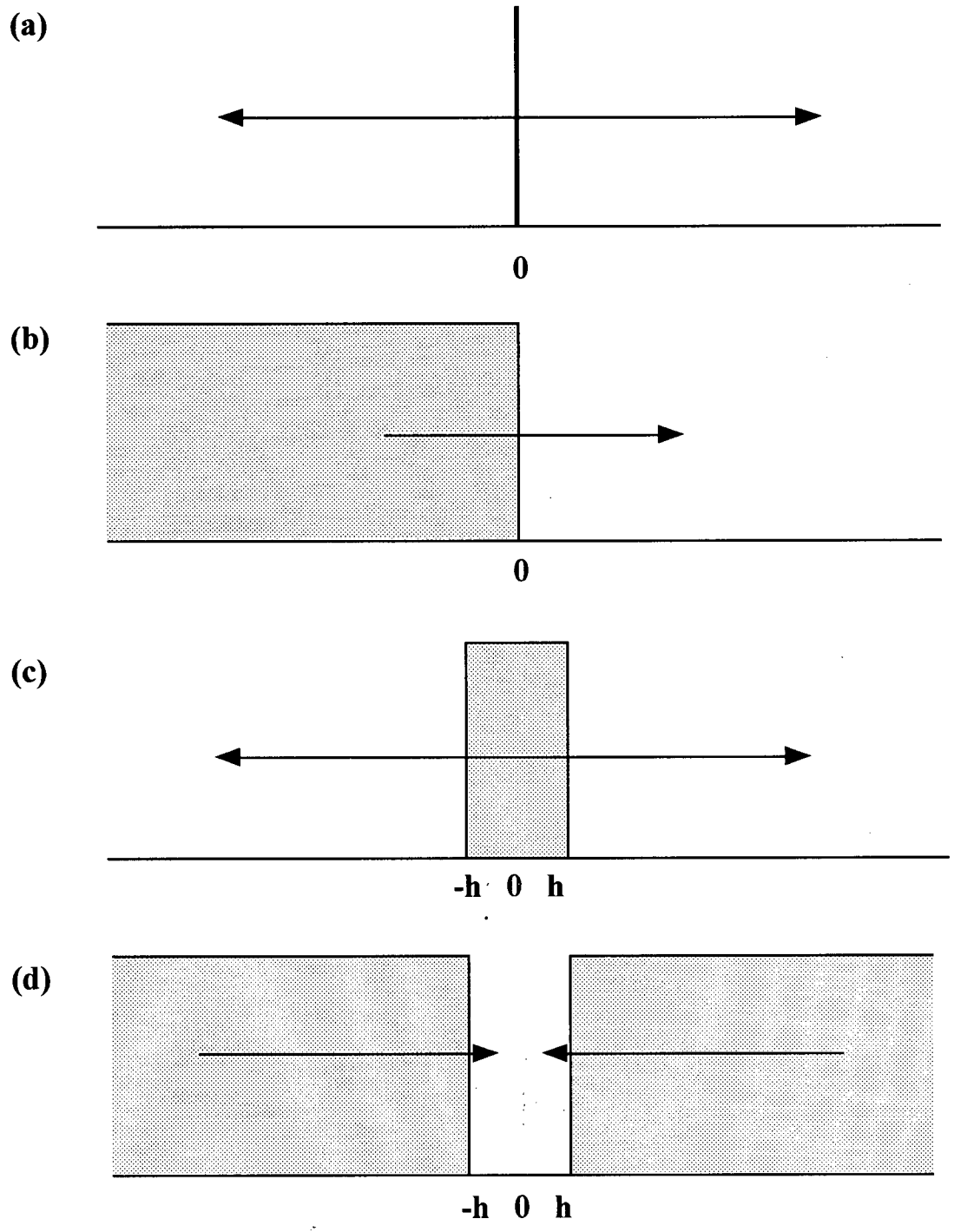

Figure 6.1: Initial conditions for one-dimensional Fickian diffusion, (a) from a plane sheet, (b) from one infinite region to another, (c) from a limited region, -h < x < h, into an infinite region and (d) from an infinite region into a limited region, -h < x < h. The arrows indicate the direction of diffusion in each case.

6.2.2 Segmented Tablet Model

The segmented tablet model was presented in the literature as a method of fitting the change in thickness of a swelling tablet [19]. The model can be extended to also predict the polymer concentration distribution in the swollen tablet.

In the model, a dry polymer tablet, of thickness h, is divided into segments of equal size, dx_0, as shown in Figure 6.2(a). The swelling of the tablet at each time is the result of the combination of two processes, the hypothetical Fickian water penetration into the dry segments and subsequent segment swelling resulting in Figure 6.2(b). Each segment swells in relation to the amount of water present given by Equation 6.9 which ensures that the water concentration at the water-tablet interface for the dry tablet is C_0, the initial water concentration in the surrounding medium. The amount of swelling of each segment is given by Equation 6.10. (The factor, given as $dx_0/(1 - \alpha C_w)$ in the literature, was modified for the calculations presented here for reasons that are discussed in Section 6.4.2.) The overall swelling of the tablet is the combination of the individual swellings as indicated by Equation 6.11. The integration of Equation 6.11 is not straight forward and requires short and long time approximations [19]. The discrete method of calculation, where a sum replaces the integral, is more practical for the calculations of this thesis.

$$C_w = C_0 - \frac{4C_0}{\pi} \sum_{n=0}^{\infty} \frac{(-1)^n}{(2n+1)} \cos\frac{(2n+1)\pi x}{2h} \, e^{-\frac{(2n+1)^2\pi^2 Dt}{4h^2}} \tag{6.9}$$

$$dx' = dx_0 \, \frac{\alpha}{1 - C_w} \tag{6.10}$$

$$\Delta x = x' - x_0 = \int_0^h (dx' - dx_0) = \int_0^h dx_0 \, (\frac{\alpha}{1 - C_w} - 1) \tag{6.11}$$

The generation of a polymer concentration distribution requires the calculation of distances and polymer concentrations for the swollen segments. The new distance for a particular swollen segment is given by the sum of the thickness increases in each of the previous segments as in Equation 6.12. Each segment also contains an amount of

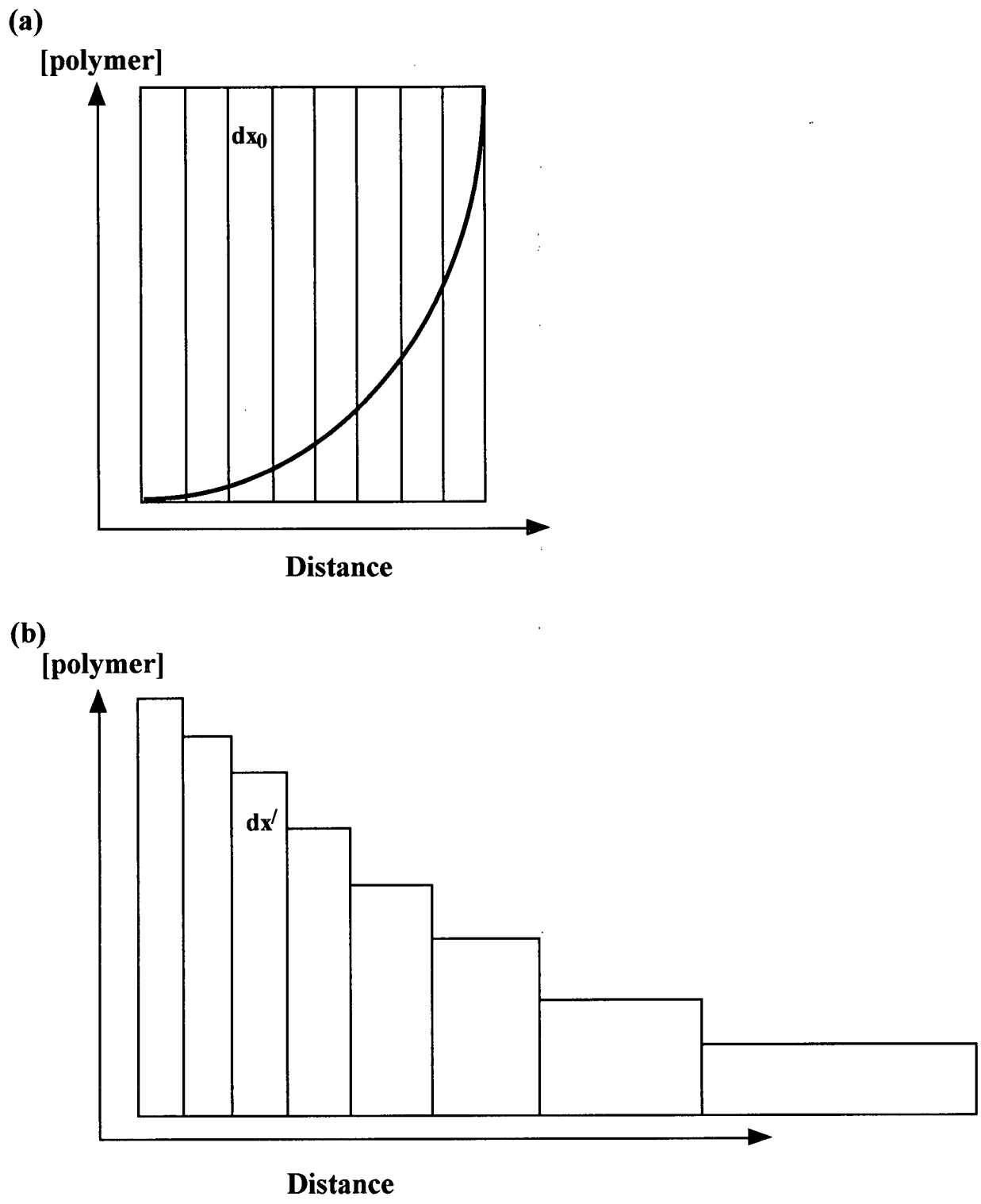

Figure 6.2: Description of the segmented tablet model. The dry tablet in (a) is divided into segments each of thickness dx_0 and the water concentration distribution (solid line) is calculated based on the original tablet thickness, the time and a hypothetical diffusion coefficient for the water ingress into a non-swelling tablet. Each segment of tablet is then swelled based on the amount of water present, resulting in a new thickness and position. As each segment contains a fixed amount of polymer, the concentration of polymer decreases inversely with the increase in volume.

polymer given by the initial volume of the segment. As a segment swells, the amount of polymer remains constant but the concentration of polymer decreases because the volume of the segment increases. The new concentration for the swollen segment is given by Equation 6.13.

$$x_i' = x_i + \sum_0^i dx_0 \, (\frac{\alpha}{1 - C_w} - 1) \tag{6.12}$$

$$C_p(x_i', t) = C_{0,p} \, \frac{dx_0}{dx_i'} = C_{0,p} \, \frac{(1 - C_w)}{\alpha} \tag{6.13}$$

6.3 Notes on the Calculations

The concentration distributions from the vacuum-treated systems of Chapters 4 and 5 were used for comparison with the theoretical distributions. The theoretical distributions based on Fickian diffusion were calculated with the program listed in Appendix B.2. In this program, the time, t, and thickness, h, were fixed and the diffusion coefficient, D, was incremented through a series of values. The χ^2 values, the sum of the squares of the differences between the measured and theoretical concentrations for each position in the measured concentration distribution, were used as goodness-of-fit parameters and minimized to provide the best-fit results. The overall best-fit was determined by minimizing the sum of the χ^2 values for the individual fits at various swelling times. Table 6.1 provides specific details regarding the fitting calculations for each species in the swelling tablet.

Table 6.1: Equations and initial parameters used in the Fickian fitting calculations.

Species	Eq.	C_0	h (cm)	Times (hrs)	Focus[a]
water	6.8	1	0.105	1,4,7,13,19,25,31,37	0.1—0.6 cm
HPMC	6.7	97%[b]	0.133	1,4,7,13,19,25,31,37	all
trifluprom azine-HCl	6.7	0.42 M	0.133	19,25,31,37	'steep' slope
5-fluorouracil	6.7	0.42 M	0.133	19,25,31,37	all

[a] The specific region of the measured distribution used in the χ^2 calculation.

[b] Polymer concentration expressed in w/w% to be consistent with previously presented data.

The C_0 value for each species was determined by the initial concentration in the dry tablet and the requirement that each theoretical distribution conserve the total amount of the species. The water intensities have been presented relative to the bulk water concentration, hence the C_0 value of 1. For the polymer, the C_0 value of 97 w/w% was chosen to ensure that each theoretical concentration curve contained the known weight of 166 mg of HPMC. The ratio of 166 mg HPMC to the volume of the tablet, 1.287 $cm^2 \times$ 0.133 cm or 171 cm^3, is the same as the C_0 value suggesting that the density of the tablet is 1 g cm^{-3}. Each of the drug-containing tablets had 7.11×10^{-5} moles of ^{19}F in the same volume of tablet, resulting in an initial ^{19}F concentration of 0.42 M.

The values for h in the equations was the dry tablet thickness for all the species apart from water. In the initial calculations for water with h=0.133 cm, it became apparent that there was more water present in the tablet than could be accounted for by theory. The water distribution after 1 hour suggested that the vacuum-treatment had pulled water into the outermost layers of the tablet. The water-tablet interface for the water calculation was moved into the polymer to 0.105 cm, the position with 50% HPMC concentration in the measured 1 hour distribution. This extra water penetration at early times results in a small increase in the mobility of the polymer and drug in this region of the tablet. The variable mobilities of the polymer and drug species during water penetration and polymer swelling are already assumed to be averaged in the Fickian model, thus, the additional mobilities at early times are accounted for by the apparent Fickian diffusion parameter.

Various times were used in the calculation of the theoretical concentration distributions. Only the later times were used for the drug calculations because the measured distributions at early times do not show all of the drug contained in the system. The χ^2 comparisons for the water and trifluprom azine-HCl distributions were restricted to certain regions of the measured distributions to prevent other regions from distorting the resulting theoretical distribution. The distances from 0–0.1 cm in the water distributions were not used in the χ^2 calculation because, at early times, the visible signal may not have represented the amount of water in that region of the tablet. For the trifluprom azine-

HCl distributions, the region of interest was the 'steep' slope that mirrored the polymer distribution and the calculations were focussed to fit this region best.

The segmented tablet calculations were performed using the program listed in Appendix B.3. In the calculations, the tablet was divided into 133 segments of width 0.001 cm. The C_0 values were 1 for the water and 97% for the polymer. In this program, theoretical water distributions were calculated using Equation 6.9 with fixed time and thickness, 0.133 cm, and variable diffusion coefficients. The water distributions were then used to calculate the new thickness, distance and polymer concentration for each segment based on Equations 6.12 and 6.13 where α was variable. The minimum sum of the χ^2 values for each time was used to determine the overall best-fit.

6.4 Results and Discussion

6.4.1 Fickian Diffusion Calculations

A swelling hydrophilic matrix tablet is a complex system where the transport of the water, polymer and drug components are related. In this system, the polymer and drug have limited mobility in the tablet until the water concentration reaches some critical level. Also, the water and drug mobilities depend strongly on the polymer concentration. The attempt to model this system based on a simple Fickian diffusion model disregards the complexity of the system in the hopes that an average, effective diffusion parameter can adequately describe the time-dependent concentration distributions for each species.

The results of fitting the water distributions to Equation 6.8 are presented in Table 6.2. The water penetration into the tablet at the earliest time of one hour suggested that the vacuum-treatment drew water into the outer layers of the tablet. The comparison between theoretical distributions calculated with the original tablet thickness of 0.133 cm and the region thickness of 0.105 cm suggested by the 1 hour image indicated that the latter were better fits to the measured water distributions. The best-fit diffusion coefficient to each individual time increased at longer swelling times reflecting the increasing mobility of the water in the swollen polymer tablet.

Table 6.2: The results of one-dimensional Fickian fitting to the water distributions in the swelling tablet. The theoretical water distributions were calculated using Equation 6.8 with h=0.105 cm.

Time (hrs)	**D ($\pm$ 0.05$\times10^{-7}$)[a] ($cm^2\ s^{-1}$)**	χ^2
1	1.30	0.003376
4	2.00	0.06568
7	2.85	0.07084
13	3.50	0.03891
19	3.90	0.02346
25	4.00	0.008998
31	4.00	0.004917
37	4.05	0.003108
overall	3.35	0.2875[b]

[a] The given error in the apparent diffusion coefficient results in a change in the last quoted digit of the χ^2 value

[b] Minimum sum of χ^2 values from the individual fits

The theoretical distributions calculated with the overall best-fit diffusion coefficient of 3.35×10^{-7} $cm^2\ s^{-1}$ are presented in Figure 6.3 in comparison with the measured water distributions from Chapter 4. The average diffusion coefficient produces greater water penetration into the tablet at early swelling times and less at later times when compared to the measured distributions. The average theoretical distributions, however, are fairly good approximations of the water distribution at all times.

The diffusion parameters obtained from the one-dimensional diffusion model are of a lower order of magnitude than the measured self-diffusion coefficients for water given in Table 2.4. The lowest self-diffusion coefficient measured was 5.1×10^{-6} $cm^2\ s^{-1}$ for water in 40% HPMC. Measurements for water diffusion in higher concentrations of HPMC were not performed due to experimental limitations. The maximum gradient strength available for the PGSE experiment was not sufficient to measure the decreased diffusion coefficients without using long gradient pulses. The resulting T_E values in the experiment were too long to observe signal in the concentrated HPMC mixtures whose T_2 values were of the order of 10 ms. The results of the Fickian fitting suggest that the diffusion of water in regions of HPMC concentration much greater than 40% is an order of magnitude lower

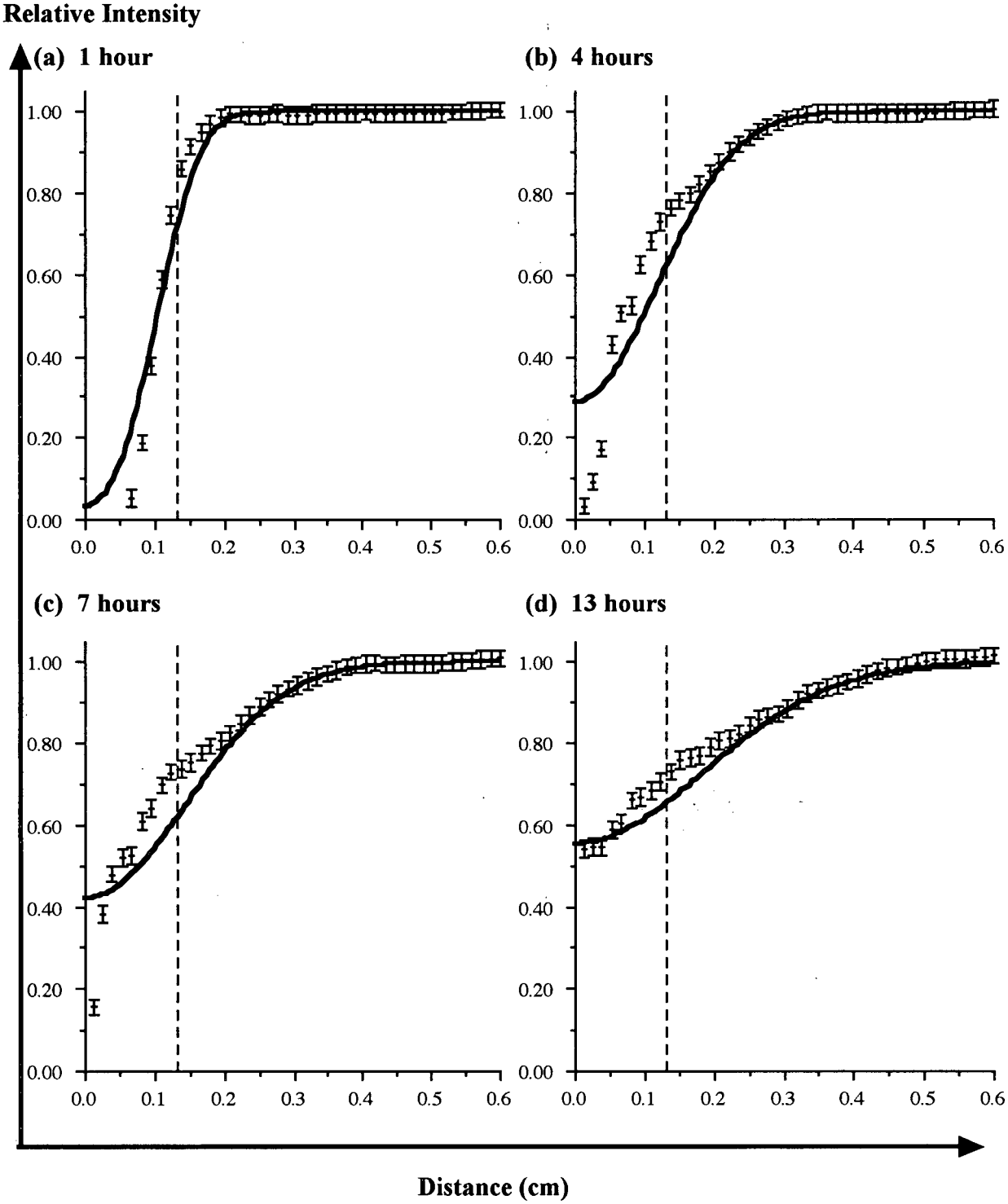

Figure 6.3: Comparison of water distributions from the vacuum-treated tablet (dots, Trial 2) and the theoretical distributions assuming one-dimensional Fickian diffusion (solid line) calculated using Equation 6.8 with the tablet thickness of 0.105 cm and an apparent diffusion coefficient of 3.35×10^{-7} cm^2 s^{-1} at swelling times of (a) 1 hour, (b) 4 hours, (c) 7 hours, (d) 13 hours, (e) 19 hours, (f) 25 hours, (g) 31 hours and (h) 37 hours. The axes in the eight plots are the same and are defined by the arrows. The intensity in the images are related to the intensity of the bulk water. (The figure is continued on the next page)

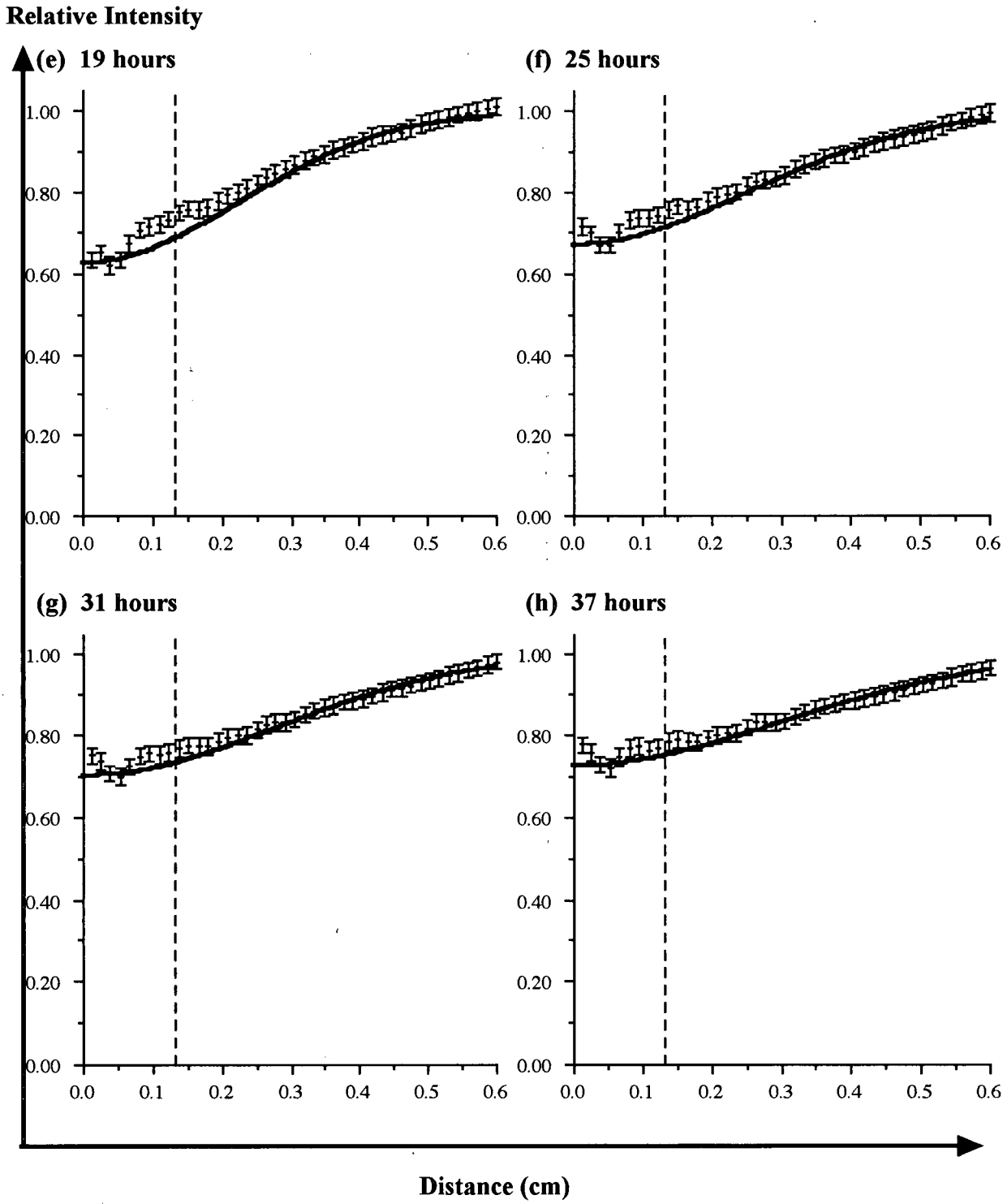

Figure 6.3 continued: plots (e) to (h).

Table 6.3: The results of one-dimensional Fickian fitting to the HPMC distributions in the swelling tablet. The theoretical polymer distributions were calculated using Equation 6.7 with h=0.133 cm.

Time (hrs)	**D ($\pm$ 0.05$\times10^{-7}$)[a] ($cm^2\ s^{-1}$)**	χ^2
1	4.95	2055.9
4	4.60	448.3
7	4.20	269.9
13	3.40	285.8
19	3.10	388.4
25	3.05	476.7
31	3.15	472.5
37	3.20	399.1
overall	3.40	5268.5[b]

[a] The given error in the apparent diffusion coefficient results in a change in the last quoted digit of the χ^2 value

[b] Sum of χ^2 values from the individual fits

than the measured value for 40% HPMC. The diffusion parameter result from the fitting for the 1 hour time interval, 1.30×10^{-7} $cm^2\ s^{-1}$, approximates the diffusion coefficient of water into $\approx$100% HPMC.

The results of the fitting of the HPMC distributions by Equation 6.7 are given in Table 6.3. The additional water penetration into the outermost layers of the HPMC tablet caused by the vacuum-treatment would result in a increased mobility for the polymer in this region at early times. The range of polymer mobilities throughout the tablet are assumed to be averaged by fitting to Fickian diffusion theory and this average would also include the effect of increased mobility for the polymer at early times. The theoretical distributions calculated with the effective diffusion parameter of 3.40×10^{-7} $cm^2\ s^{-1}$ show reasonable agreement with the HPMC distributions at various swelling times as shown in Figure 6.4. Some of the deviations between the theoretical and measured polymer distributions at longer swelling times may be related to the slight overestimation in the measured polymer distributions which contain 5-10% more polymer than the known weight of 166 mg HPMC in the dry tablet. When the same parameters are used, Equations 6.7 and 6.8 are complements of each other and their sum would result in C_0. The similarity

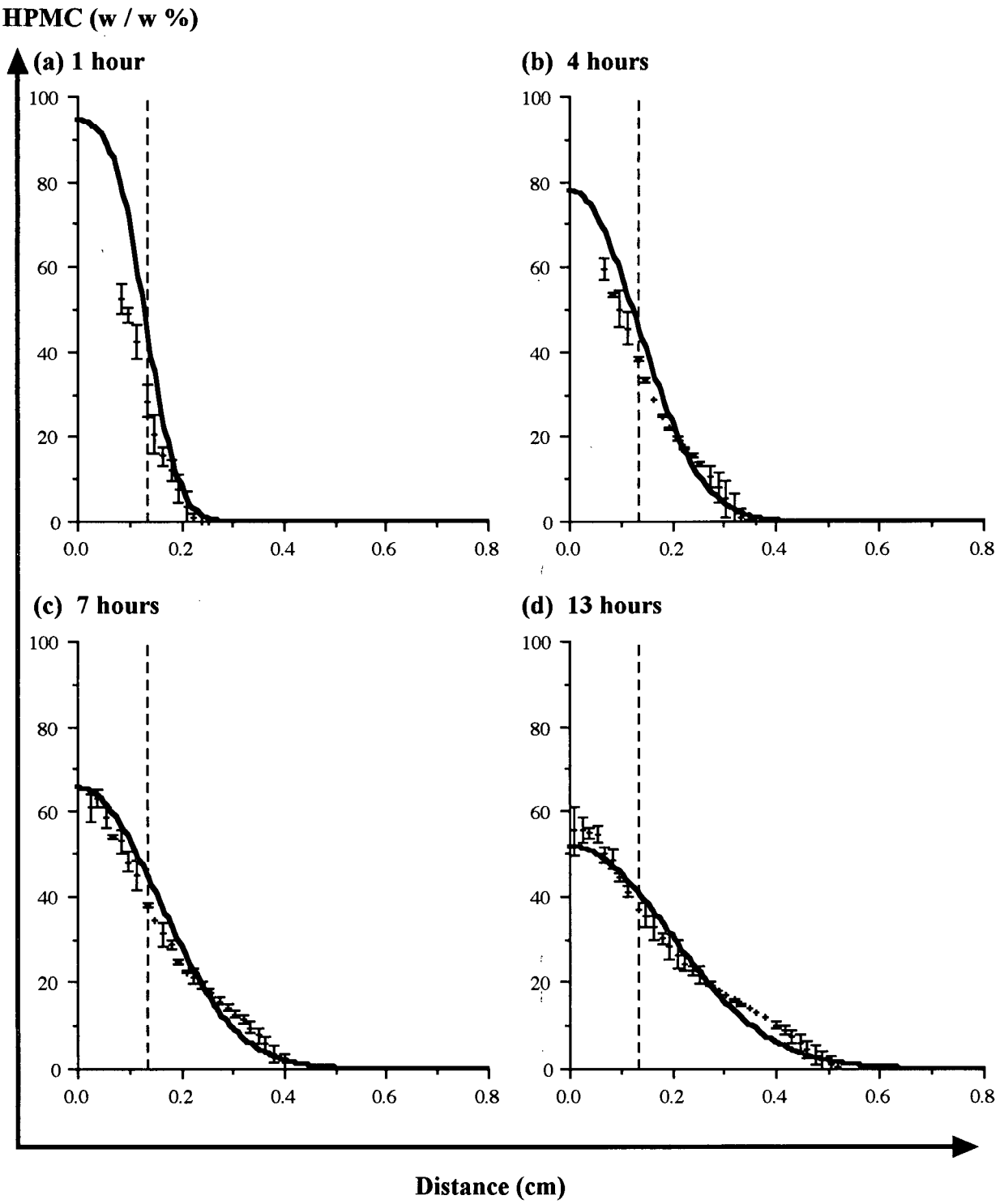

Figure 6.4: Comparison of average HPMC distributions from the vacuum-treated tablet (dots) and the theoretical distributions assuming one-dimensional Fickian diffusion (solid line) calculated using Equation 6.7 with the tablet thickness of 0.133 cm and an apparent diffusion coefficient of 3.40×10^{-7} cm^2 s^{-1} at swelling times of (a) 1 hour, (b) 4 hours, (c) 7 hours, (d) 13 hours, (e) 19 hours, (f) 25 hours, (g) 31 hours and (h) 37 hours. The axes in the eight plots are the same and are defined by the arrows. (The figure is continued on the next page)

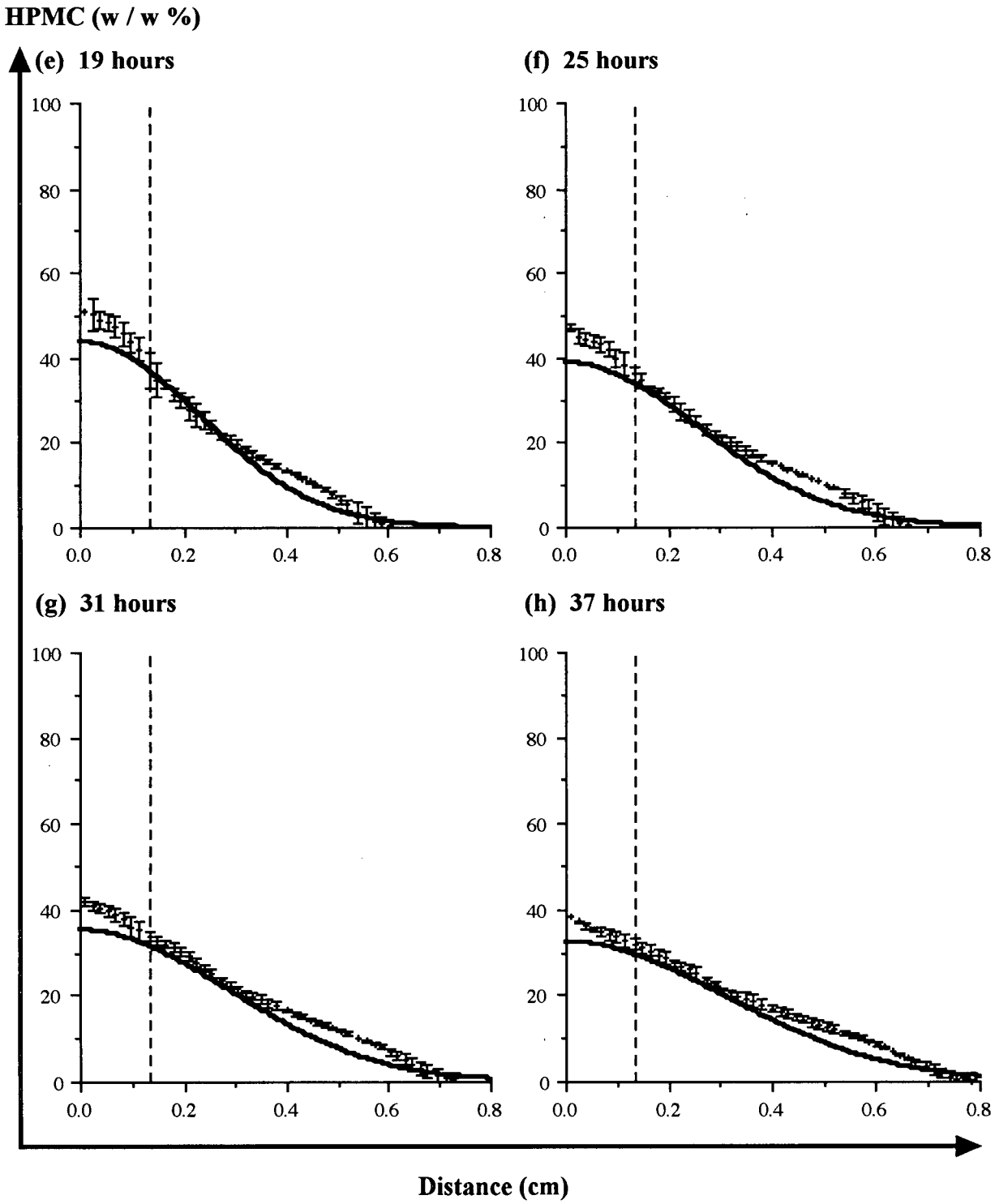

Figure 6.4 continued: plots (e) to (h).

Table 6.4: The results of one-dimensional Fickian fitting to the triflupromazine-HCl distributions in the swelling tablet. The theoretical drug distributions were calculated using Equation 6.7 with h=0.133 cm.

Time (hrs)	**D ($\pm$ 0.05$\times 10^{-7}$)[a] ($cm^2\ s^{-1}$)**	χ^2
19	7.20	0.004102
25	8.60	0.002810
31	9.05	0.001653
37	9.90	0.002252
overall	8.80	0.01120 [b]

[a] The given error in the apparent diffusion coefficient results in a change in the last quoted digit of the χ^2 value

[b] Sum of χ^2 values from the individual fits

between the overall effective diffusion parameters for polymer and water suggests that the polymer and water distributions, when presented in the same units, are complements of each other.

The drug distributions were difficult to fit at early times because not all the drug was visible in the ^{19}F images. Thus, theoretical drug distributions were only calculated for the longer swelling times and the overall best-fit to the entire dataset was also determined from these calculations. The average diffusion coefficient determined from the later times was then used to calculate theoretical drug distributions for the early times. The goodness-of-fit test was focussed on the 'steep' slope of the triflupromazine-HCl distribution, the region between about 0.25 and 0.75 cm. The results of the fitting calculations are presented in Table 6.4. The overall best-fit theoretical concentration distribution matches the triflupromazine-HCl concentration quite well at the later times as shown in Figure 6.5. At early swelling times, the slopes of the measured and theoretical distributions are essentially parallel but other comments about the quality of the fit cannot be made. The total percents of detectable moles of ^{19}F from the images, as given by Table 5.3, were 92% at 37 hours, 82% at 19 hours, but only 31% at 1 hour. Thus, the deviations visible between the theoretical and measured triflupromazine-HCl distributions may be due, in part, to the lower total drug present in the measured drug distributions.

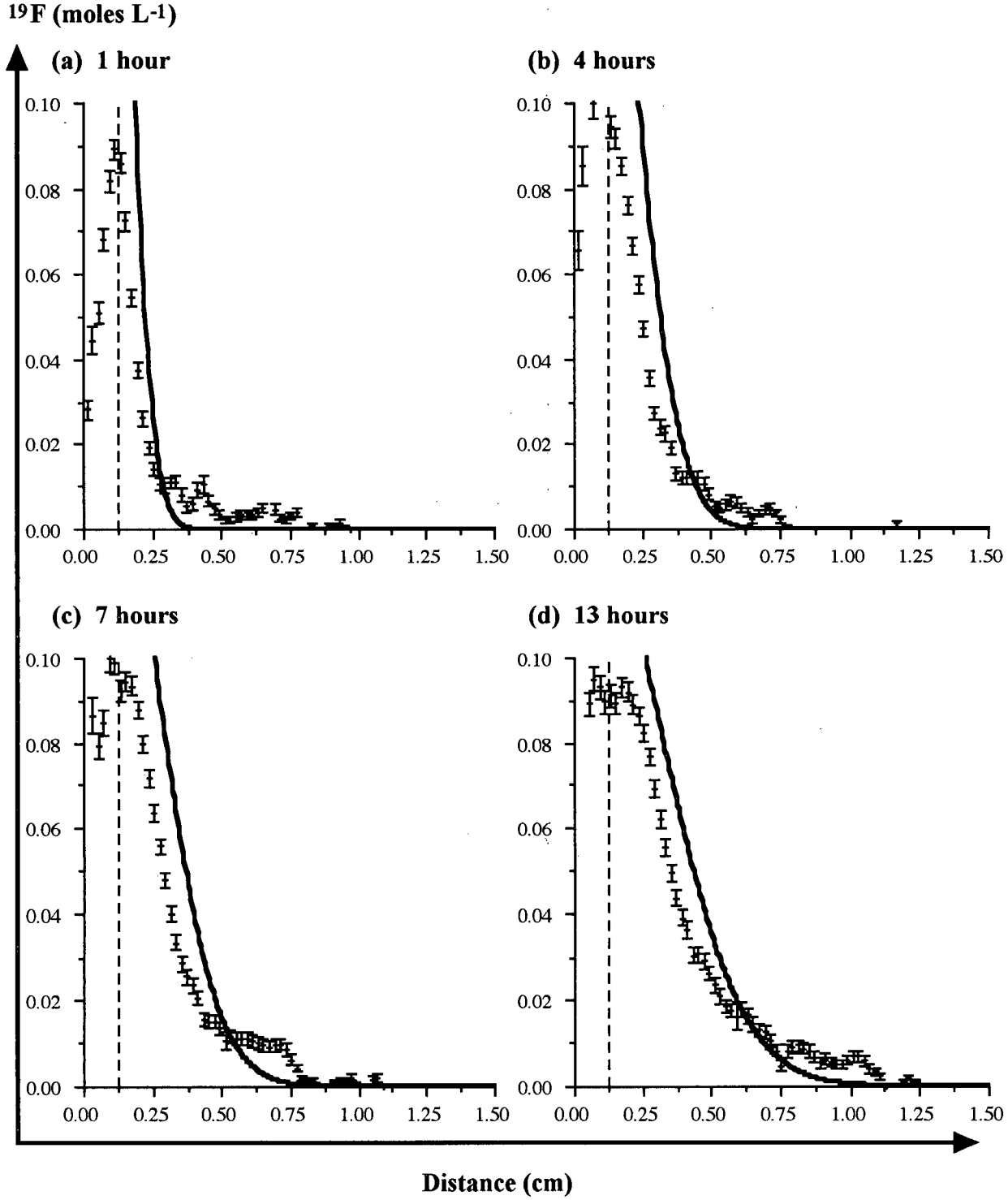

Figure 6.5: Comparison of the trifluprom azine-HCl distributions from the vacuum-treated tablet (dots) and the theoretical distributions assuming one-dimensional Fickian diffusion (solid line) calculated using Equation 6.7 with the tablet thickness of 0.133 cm and an apparent diffusion coefficient of 8.80×10^{-7} cm^2 s^{-1} at swelling times of (a) 1 hour, (b) 4 hours, (c) 7 hours, (d) 13 hours, (e) 19 hours, (f) 25 hours, (g) 31 hours and (h) 37 hours. The axes in the eight plots are the same and are defined by the arrows. (The figure is continued on the next page)

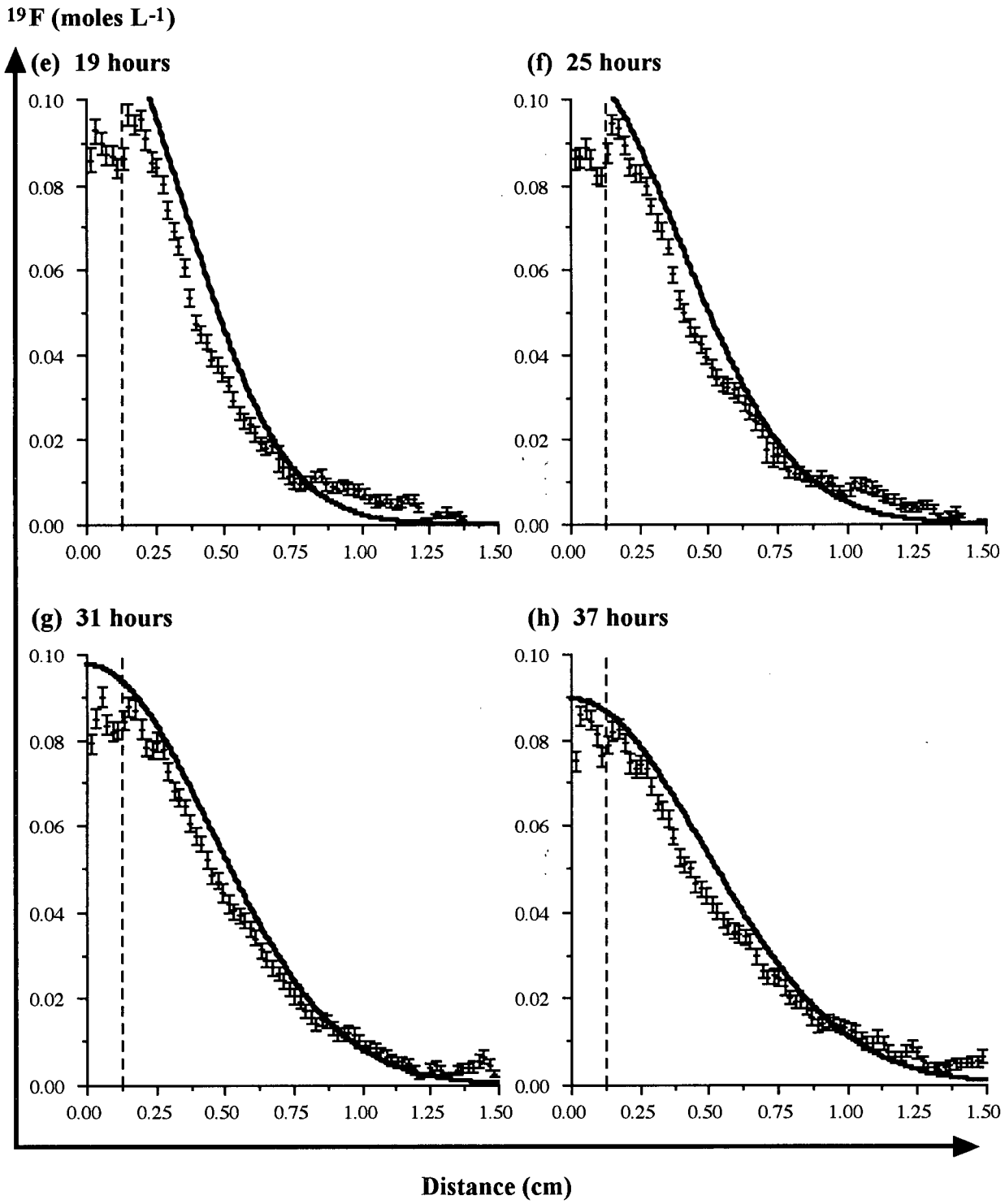

Figure 6.5 continued: plots (e) to (h).

Table 6.5: The results of one-dimensional Fickian fitting to the 5-fluorouracil distributions in the swelling tablet. The theoretical drug distributions were calculated using Equation 6.7 with h=0.133 cm.

Time (hrs)	**D ($\pm$ 0.05$\times10^{-6}$)[a] ($cm^2\ s^{-1}$)**	χ^2
19	4.75	0.005811
25	3.75	0.003878
31	3.25	0.002509
37	3.00	0.001753
overall	3.65	0.0154337[b]

[a] The given error in the apparent diffusion coefficient results in a change in the last quoted digit of the χ^2 value

[b] Sum of χ^2 values from the individual fits

The effective diffusion coefficient of 8.80×10^{-7} $cm^2\ s^{-1}$ from the Fickian diffusion calculations is within the range of measured self-diffusion coefficients determined for triflupromazine-HCl and presented in Table 2.5. The diffusion coefficients for the drug in 10% HPMC was 10.2×10^{-7} and 9.4×10^{-7} $cm^2\ s^{-1}$ for 1% and 3% drug, respectively. In 20% HPMC, the values dropped to 3.6×10^{-7} and 6.0×10^{-7} $cm^2\ s^{-1}$ for 1% and 3% respectively.

The previous Fickian fitting calculations for the polymer and triflupromazine-HCl showed reasonably good agreement with the measured distributions. The lack of mobility for each species in the dry portions of the tablet at early times does not affect the overall shape of the distribution because the diffusion or movement rate for the two species in the wetted portions of the tablet was still relatively slow. This is not the case for the drug 5-fluorouracil which diffused freely and rapidly almost immediately after water had penetrated the tablet. The best-fit results for Fickian fitting to the 5-fluorouracil distributions at the longer swelling times are given in Table 6.5 and the theoretical concentration distributions for these times are plotted in Figure 6.6. The agreement between the theoretical and measured distributions for this drug is not very good. The shape of the measured distributions reflects the portion of 5-fluorouracil that was not diffusing from the initiation of tablet swelling. The 5-fluorouracil diffusion was fast enough that the freely diffusing drug

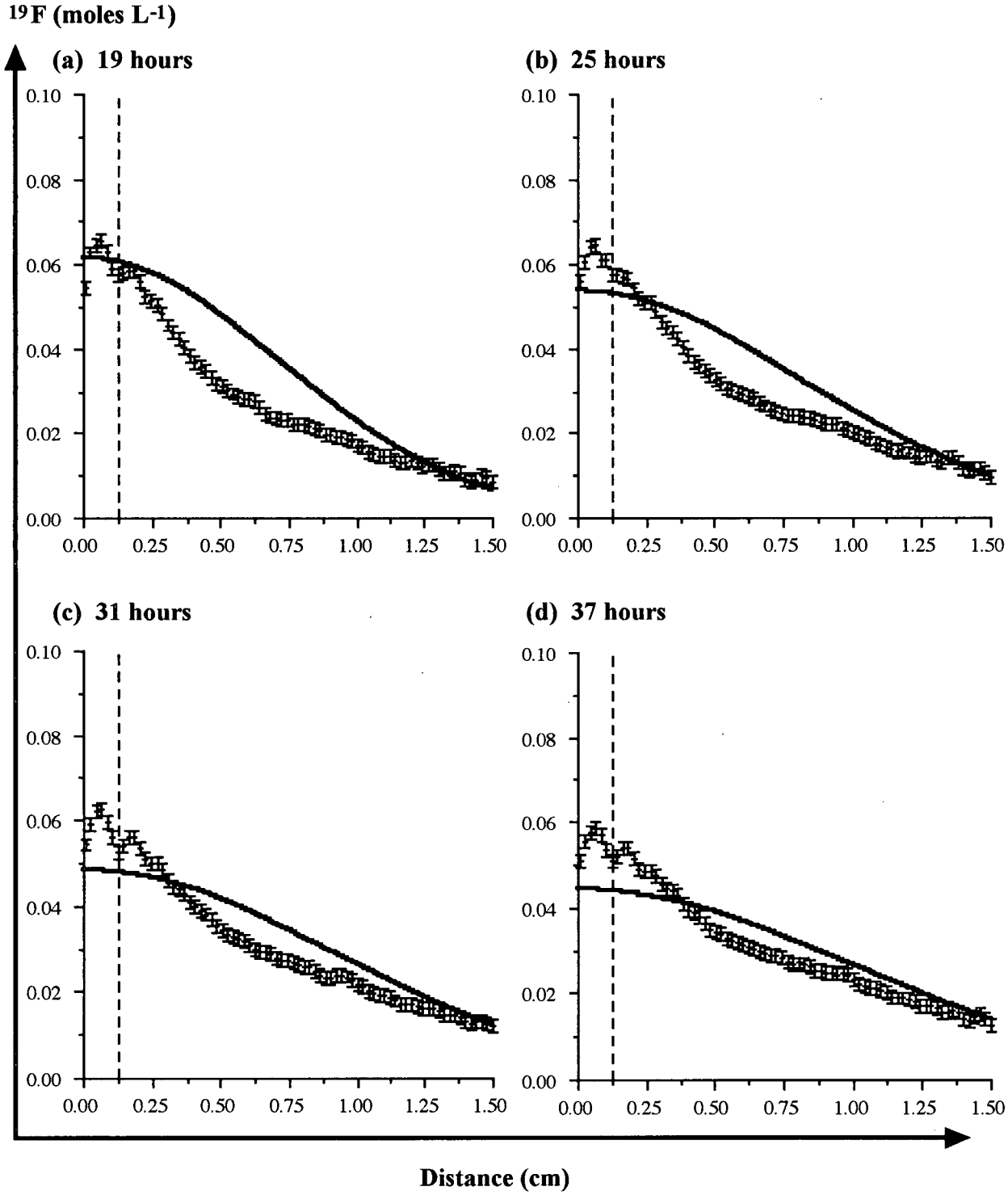

Figure 6.6: Comparison of the 5-fluorouracil distributions from the vacuum-treated tablet (dots) and the theoretical distributions assuming one-dimensional Fickian diffusion (solid line) calculated using Equation 6.7 with the tablet thickness of 0.133 cm and an apparent diffusion coefficient of 3.65×10^{-6} cm^2 s^{-1} at swelling times of (a) 19 hours, (b) 25 hours, (c) 31 hours and (d) 37 hours. The axes in the four plots are the same and are defined by the arrows.

was able to separate itself rapidly from the less mobile drug in the tablet. Although the theoretical distributions for 5-fluorouracil do not exactly match the shapes of the measured ones, they do indicate how far the drug has extended from the tablet. Consistent with this, the overall best-fit diffusion parameter from the Fickian modelling, 3.65×10^{-6} cm^2 s^{-1}, is approximately the same diffusion coefficient measured for the drug in 30% HPMC (Table 2.6) and in the same range as that required for drug release from from the swelling tablet as discussed in Section 5.3.3.

The effective diffusion parameter for 5-fluorouracil is about four times larger than that for trifluprom azine-HCl suggesting that the former drug would be released from the tablet about four times faster than the latter. In reasonable agreement, the plots of fraction of drug released as a function of the square-root of time in Section 5.3.3 indicated that 5-fluorouracil was released about five times faster than trifluprom azine-HCl.

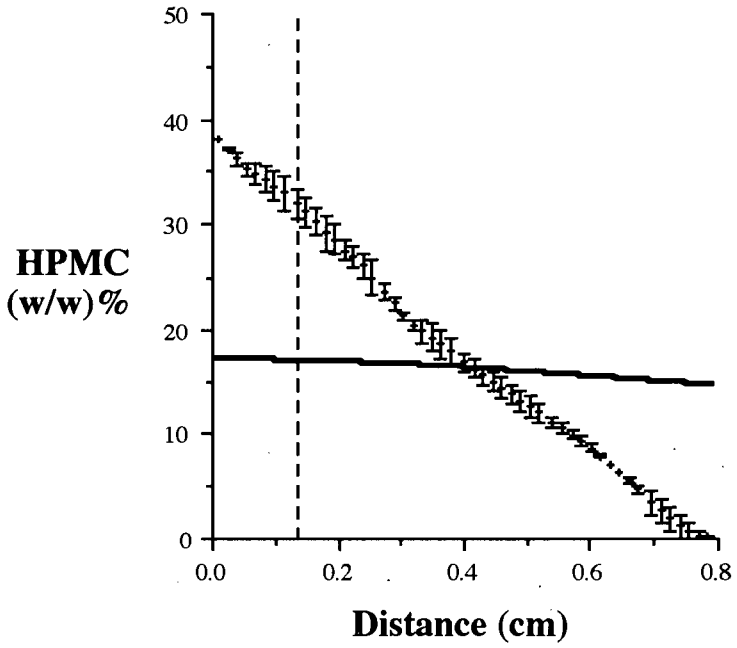

Figure 6.7: Example of the theoretical HPMC distribution (solid line) obtained using $1/(1\text{-}\alpha C_w)$ as the segment swelling factor compared with the measured HPMC distribution (dots) at 37 hours. The theoretical distribution was calculated with a diffusion coefficient of 2×10^{-7} cm^2 s^{-1} and α of 0.85.

6.4.2 Segmented Tablet Calculations

The original form of the segment swelling model contained the swelling factor $1/(1\text{-}\alpha C_w)$ rather than the factor given in Equation 6.10. The goal of the model, as originally presented in the literature [19], was to fit the changes in thickness of an axially-swelling tablet. As is evident in Figure 6.7, the theoretical distribution calculated using this factor in the segmented tablet model can be used to effectively match the thickness of the tablet. However, the polymer concentrations in the theoretical distribution do not even closely resemble the actual polymer distribution in the swollen tablet. No value of the diffusion coefficient or α would result in a better match to the measured concentrations.

When the factor was rearranged to the one presented in Equation 6.10, the concentration distributions in the swollen polymer were more closely matched by the theoretical distributions. The diffusion coefficient and the α factor were freely varied in the fitting calculation and the overall best-fit was provided by a water diffusion coefficient of 9.0×10^{-8}

$cm^2\ s^{-1}$ and α equal to 1. The diffusion coefficient for the water is lower than the value determined from the Fickian diffusion calculations because the former is for a hypothetical situation where the water is diffusing into a tablet that does not swell. The χ^2 value for the best-fit result to the segmented tablet model was 12667.3, about 2.5 times greater than the minimum χ^2 value from the Fickian fitting to the same distributions, suggesting that the theoretical distributions from the segmented tablet model fit the measured data poorly. The comparison of the theoretical polymer distributions calculated from the segmented tablet model and the measured HPMC distributions show clearly that the segment-swelling calculation, Equations 6.12 and 6.13, predicts substantially more swelling at longer times than the measured polymer distribution. The fits at early times more closely match the measured polymer distributions.

The segmented tablet model provides a more physically meaningful description of the tablet swelling process than Fickian diffusion theory, as the former considers the importance of water penetration in the movement of the polymer. The differences in the theoretical results at different times suggest that the degree of segment swelling may be related to water concentration in a complex manner. NMR spectroscopy experiments in Section 2.3.4 suggested that the mobility of HPMC fell into three distinct regions depending on the HPMC concentration and hence, the water concentration. The swelling of an HPMC segment may be related to the mobility of the contained polymer which would be determined by the amount of water present. Further experiments will be necessary to determine the exact nature of the relationship between the swelling of a polymer segment and an equilibrium concentration of water.

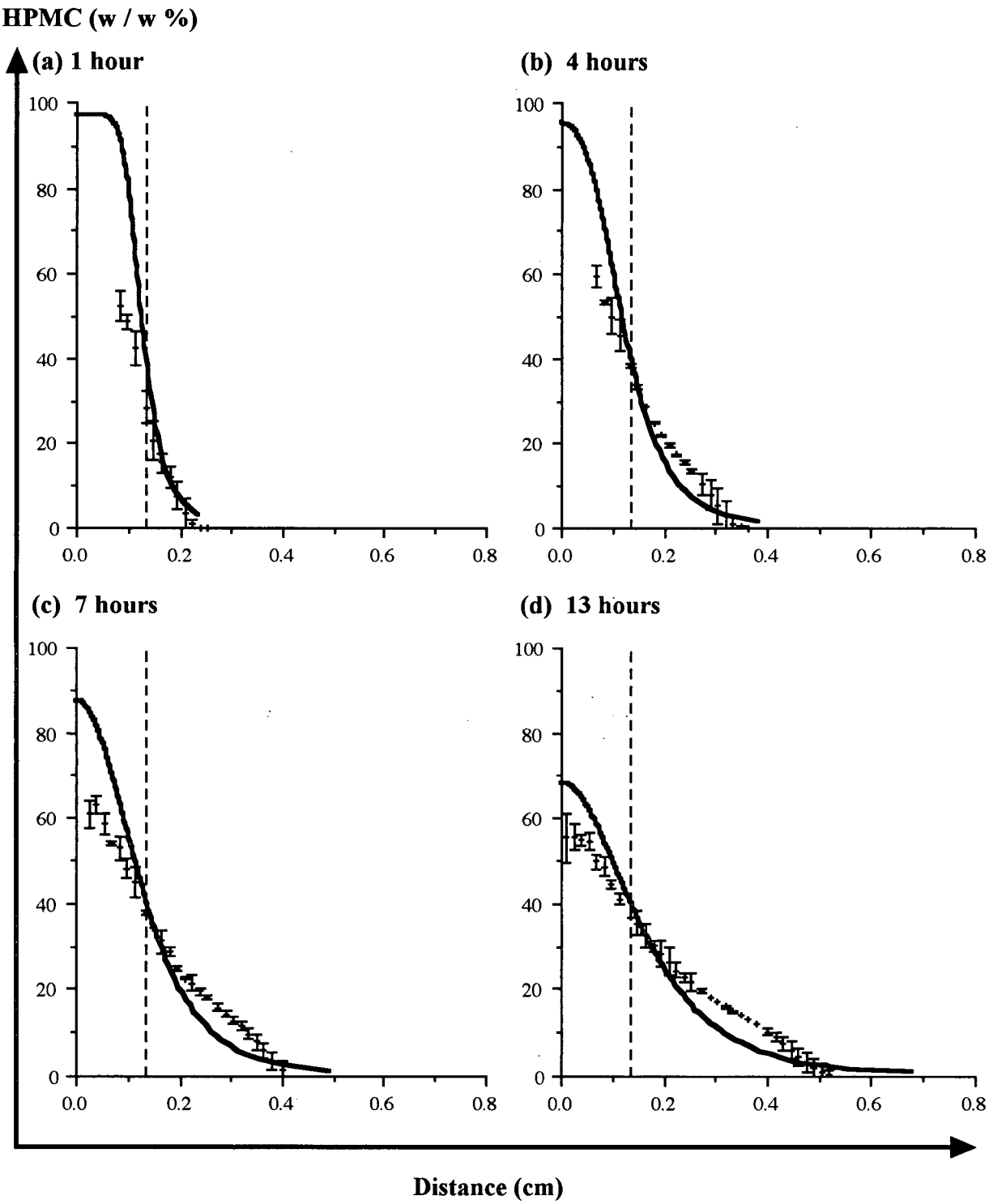

Figure 6.8: Average HPMC distributions of the vacuum-treated tablet (dots) and the theoretical distribution (solid line) calculated using the segmented tablet model, Equations 6.12 and 6.13 with the tablet thickness of 0.133 cm and a water diffusion coefficient of 9.0×10^{-8} cm^2 s^{-1} and α of 1, at swelling times of (a) 1 hour, (b) 4 hours, (c) 7 hours, (d) 13 hours, (e) 19 hours, (f) 25 hours, (g) 31 hours and (h) 37 hours. The axes in the eight plots are the same and are defined by the arrows. (The figure is continued on the next page)

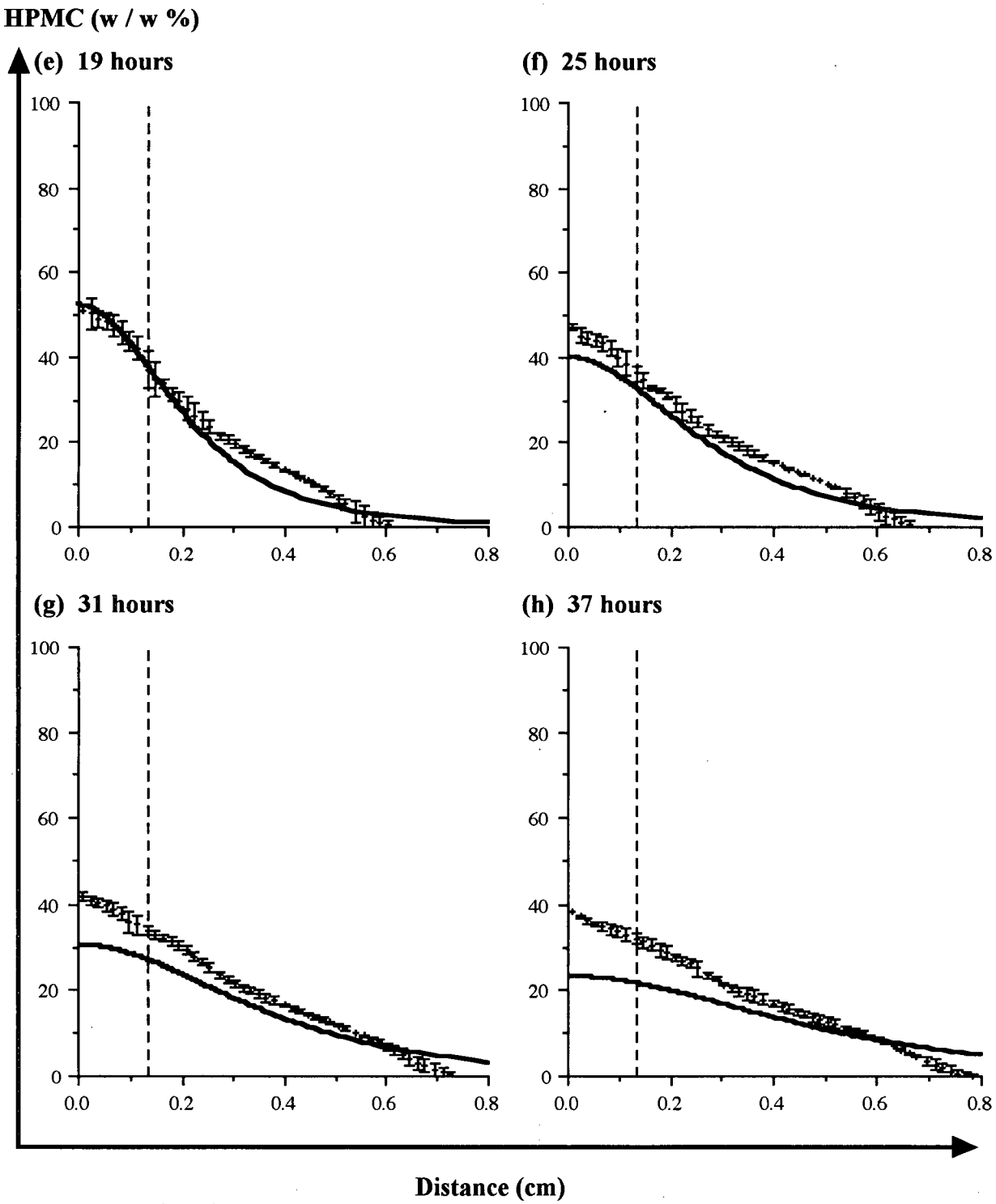

Figure 6.8 continued: plots (e) to (h).

6.5 Summary

The modeling calculations for the water, polymer and drug distributions based on one-dimensional Fickian diffusion provided reasonable approximations to the measured concentration distributions for each species. The average effective diffusion parameter for the water was much lower than the lowest measured self-diffusion coefficient for water in 40% polymer suggesting that the diffusion of water continues to decrease in concentrations of polymer greater than 40%. The effective diffusion parameters for the drugs were comparable to their measured self-diffusion coefficients in mixtures of HPMC.

The segmented tablet model reproduced the polymer distributions in the swollen HPMC tablet at early times reasonably well but predicted greater swelling at later times than was measured experimentally. The calculations with this model suggested that the swelling of a segment of the tablet was related to the concentration of water in a more complex manner than originally proposed, in agreement with earlier NMR spectroscopic results, presented in Chapter 2, that indicated that the mobility of HPMC in an HPMC-water mixture was dependent on the amount of water present.

Chapter 7

Conclusions and Suggestions for Future Work

7.1 Conclusions

The work presented in this thesis has demonstrated that NMR spectroscopy and NMR imaging are invaluable techniques in the study of swelling-controlled drug delivery systems.

The dependence of parameters such as T_1, T_2 and diffusivity of the water and drug species on the polymer concentration were determined in Chapter 2 with NMR spectroscopy. These parameters provided insight into the mobility changes of the water, drug and polymer components in the swelling tablet. The changes in polymer mobility observed in the z-spectroscopic study also indicated the polymer concentration range required to obtain a gel rather than a viscous solution. The drug release behavior from the swelling tablet could be directly related to the measured diffusion coefficients of the drugs in various HPMC concentrations.

The one-dimensional NMR imaging protocol developed in Chapters 3 and 4 made possible the determination of quantitative concentration distributions for the water, polymer and model drugs (Chapter 5) at many time intervals during the swelling process. These distributions provided a complete description of the processes of water penetration, tablet swelling and drug release. The drug release behavior was found to depend on the relative rate of drug diffusion compared to the rate of expansion of the device. The drug release was faster, as in the case of the drug 5-fluorouracil, when the drug diffusion in concentrated polymer regions was comparable to or larger than the apparent tablet expansion

rate obtained from plots of thickness as a function of the square-root of time. With slow drug diffusion, as in the case of the drug trifluprómazine-HCl, the drug does not escape the tablet until very low HPMC concentrations where the tablet begins to erode.

The preliminary modeling calculations for the water, polymer and drug distributions were based on one-dimensional Fickian diffusion which provided reasonable approximations to the concentration distributions for each species. A segmented tablet model was also tested to predict the polymer distributions in the swollen HPMC tablet. Initial calculations with this model suggested that the swelling of a segment of the tablet was related to the concentration of water in a much more complex manner than the model originally assumed.

7.2 Suggestions for Future Work

The work in this thesis focussed on the axial swelling of HPMC tablets *in vitro* at room temperature. The study of this specific case of a swelling-controlled drug delivery system yielded conclusions regarding drug release behavior and preliminary theoretical models to describe the polymer distribution.

The vacuum-treatment of the HPMC tablets prior to the imaging experiments removed compressed air from the tablet which made possible the quantitative determination of the polymer concentration distributions. However, the vacuum-treatment appeared to cause increased water penetration into the outermost layers of the tablet. It was noted in Chapter 4 that air present in the tablet at atmospheric pressure did not result in air bubbles in the swollen tablet. A modification of the vacuum-treatment, where air is permitted to re-enter the tablet at atmospheric pressure may minimize both the effects of air bubbles in the swollen gel and the increased water penetration.

Further experiments on tablet swelling, where the degree of swelling with a controlled concentration of water is determined, will provide a better understanding of how tablet swelling is related to water concentration. This information is necessary to improve the fitting of the polymer distribution based on the segmented tablet model.

To determine the generality of the conclusions of this thesis, the focus of study

must be broadened to include systems where the swelling of the tablet is less restricted. Ultimately, the unrestricted swelling of the system in three dimensions will determine the quality of theoretical models based on axial swelling. The NMR imaging studies of these complex systems will pose experimental difficulties as they will require the use of two- or three-dimensional NMR imaging techniques rather than the one-dimensional technique that was successfully applied in this thesis. The problems of quantitation and acquisition time for the additional dimensions in the imaging experiment would require changes to the methodology presented in this thesis.

The *in vivo* behavior of these systems may be better understood by performing the imaging experiments at physiological temperature, 37°C for humans, and using physiological media such as simulated gastric fluid. Ultimately, MRI of the tablet as it passed through the digestive tract of a person would provide direct information on the behavior of swelling-controlled drug delivery systems *in vivo*. Such experiments could be efficiently carried out using T_2-selective imaging with the data from this thesis.

Bibliography

[1] V. V. Ranade and M. A. Hollinger. *Oral Drug Delivery.* CRC Press, Boca Raton, FL, USA, 1996. Chapter 5.

[2] A. Zaffaroni. Controlled-delivery therapy is here. *CHEMTECH*, **Dec**:756–761, 1976.

[3] D. L. Sackett and J. C. Snow. The Magnitude of Compliance and Noncompliance. In R. B. Haynes, D. W. Taylor, and D. L. Sackett, editors, *Compliance in Health Care*, pages 11–22. Johns Hopkins University, Baltimore, MD, USA, 1979.

[4] M. Powers Cramer and S. R. Saks. Translating Safety, Efficacy and Compliance into Economic Value For Controlled Release Dosage Forms. *PharmacoEconomics*, **5**:482–504, 1994.

[5] R. W. Baker. *Controlled Release of Biologically Active Agents.* John Wiley & Sons, New York, NY, USA, 1987. Chapters 1, 3, 4 and 5.

[6] V. H. Lee and J. R. Robinson. Methods to Achieve Sustained Drug Delivery—The Physical Approach: Oral and Parenteral Dosage Forms. In J. R. Robinson, editor, *Sustained and Controlled Release Drug Delivery Systems*, pages 123–209. Marcel Dekker, Inc., New York, NY, USA, 1978.

[7] B. E. Ballard. An Overview of Prolonged Action Drug Dosage Forms. In J. R. Robinson, editor, *Sustained and Controlled Release Drug Delivery Systems*, pages 1–69. Marcel Dekker, Inc., New York, NY, USA, 1978.

[8] R. Langer. New Methods of Drug Delivery. *Science*, **249**:1527–1532, 1990.

[9] P. Sinko and J. Kohn. Polymeric Drug Delivery Systems. In M. A. El-Nokaly, D. M. Piatt, and B. A. Charpentier, editors, *Polymeric Delivery Systems: Properties and Applications*, pages 18–41. American Chemical Society, Washington, DC, USA, 1993. ACS Series 520.

[10] I. C. Jacobs and N. S. Mason. Polymer Delivery Systems Concepts. In M. A. El-Nokaly, D. M. Piatt, and B. A. Charpentier, editors, *Polymeric Delivery Systems: Properties*

and Applications, pages 1–17. American Chemical Society, Washington, DC, USA, 1993. ACS Series 520.

[11] J. Heller. The Use of Polymers in the Construction of Controlled-Release Devices. In R. S. Rapaka, editor, *Membranes and Barriers: Targetted Drug Delivery*, pages 107–131. National Institutes of Health, 1995. NIDA Research Monograph 154.

[12] P. Colombo. Swelling-Controlled Release in Hydrogel Matrices for Oral Route. *Adv. Drug Delivery Rev.*, **11**:37–57, 1993.

[13] S. H. Gehrke, D. Biren, and J. J. Hopkins. Evidence for Fickian Water Transport in Initially Glassy Poly(2-Hydroxyethyl Methacrylate). *J. Biomater. Sci. Polymer Edn.*, **6**(4):375–390, 1994.

[14] H. B. Hopfenberg. Anomalous Transport of Penetrants in Polymeric Membranes. In J. E. Flinn, editor, *Membrane Science and Technology: Industrial, Biological and Waste Treatment Processes*, pages 16–32. Plenum Press, New York, NY, USA, 1970.

[15] D. A. Alderman. A Review of Cellulose Ethers in Hydrophilic Matrices for Oral Controlled-Release Dosage Forms. *Int. J. Pharm. Technol. Prod. Manuf.*, **5**(3):1–9, 1984.

[16] A. Ya. Polishchuk, L. A. Zimina, R. Yu. Kosenko, A. L. Iordanskii, and G. E. Zaikov. Diffusion-Activation Laws for Drug Release from Polymer Matrices. *Polym. Degrad. Stab.*, **31**:247–254, 1991.

[17] P. I. Lee. Dimensional Changes during Drug Release from a Glassy Hydrogel Matrix. *Polym. Commun.*, **24**:45–47, 1983.

[18] P. Colombo, U. Conte, A. Gazzaniga, L. Maggi, M. E. Sangalli, N. A. Peppas, and A. La Manna. Drug Release Modulation by Physical Restriction of Matrix Swelling. *Int. J. Pharm.*, **63**:43–48, 1990.

[19] T. Koizumi, S. P. Panomsuk, T. Hatanaka, and K. Katayama. Kinetics of Swelling of Compressed Cellulose Matrices: A Mathematical Model. *Pharm. Res.*, **13**:329–333, 1996.

[20] L. S. C. Wan, P. W. S. Heng, and L. F. Wong. Matrix Swelling: A Simple Model Describing Extent of Swelling of HPMC Matrices. *Int. J. Pharm.*, **116**:159–168, 1995.

[21] US Pharmacopeial Convention, Inc., Rockville, MD, USA. *The US Pharmacopeia*, 1995. Dissolution <711>.

[22] P. I. Lee and C.-J. Kim. Probing the Mechanisms of Drug Release from Hydrogels. *J. Controlled Release*, **16**:229–236, 1991.

[23] N. A. Peppas and P. Colombo. Analysis of Drug Release Behavior from Swellable Polymer Carriers using the Dimensionality Index. *J. Controlled Release*, **45**:35–40, 1997.

[24] A. Thu Pham and P. I. Lee. Probing the Mechanisms of Drug Release from Hydroxypropylmethylcellulose Matrices. *Pharm. Res.*, **11**:1379–1384, 1994.

[25] V. Vigoreaux and E. S. Ghaly. Fickian and Relaxational Contribution Quantification of Drug Release in a Swellable Hydrophilic Polymer Matrix. *Drug Dev. Ind. Pharm.*, **20**(16):2519–2526, 1994.

[26] N. A. Peppas. Analysis of Fickian and Non-Fickian Drug Release from Polymers. *Pharm. Acta. Helv.*, **60**(4):110–111, 1985.

[27] N. A. Peppas, R. Gurny, E. Doelker, and P. Buri. Modelling of Drug Diffusion Through Swellable Polymeric Systems. *J. Membr. Sci.*, **7**:241–253, 1980.

[28] I. Colombo, M. Grassi, R. Lapasin, and S. Pricl. Determination of the Drug Diffusion Coefficient in Swollen Hydrogel Polymeric Matrices by means of the Inverse Sectioning Method. *J. Controlled Release*, **47**:305–314, 1997.

[29] U. Conte, L. Maggi, P. Colombo, and A. La Manna. Multi-layered Hydrophilic Matrices as Constant Release Devices (Geomatrix^{TM} Systems). *J. Controlled Release*, **26**:39–47, 1993.

[30] S. K. Baveja, K. V. Ranga Rao, J. Arora, and S. Dhir. A Novel Method to Measure the Swelling Front in Swelling Controlled- Release Systems. *Indian J. of Pharm. Sci.*, **53**(4):156–158, 1991.

[31] P. Gao and R. H. Meury. Swelling of Hydroxypropyl Methylcellulose Matrix Tablets. 1. Characterization of Swelling Using a Novel Optical Imaging Method. *J. Pharm. Sci.*, **85**(7):725–731, 1996.

[32] L. S. Cutts, S. Hibberd, J. Adler, and C. D. Melia. Characterising Drug Release Processes within Controlled Release Dosage Forms using the Confocal Laser Scanning Microscope. *J. Controlled Release*, **42**:115–124, 1996.

[33] C. D. Melia, P. Marshal, P. Stark, S. Cunningham, A. Kinahan, and J. Devane. Investigation *in vitro* Drug Release Mechanisms Inside Dosage forms: Monitoring Liquid Ingress in HPMC Hydrophilic Matrices Using Confocal Microscopy. In D. Young, J. G.

Devane, and J. Butler, editors, I*n vivo-in vitro Correlations.Advances in Experimental Medicine and Biology.*, volume 423, page 129. Plenum Press, New York, NY, USA, 1997.

[34] P. C. Lauterbur. Image Formation by Induced Local Interactions: Examples Employing Nuclear Magnetic Resonance. *Nature*, **242**:190–191, 1973.

[35] P. Mansfield and P. K. Grannell. NMR 'Diffraction' in Solids? *J. Phys. C: Solid State Phys.*, **6**:L422–L426, 1973.

[36] W. P. Rothwell, D. R. Holecek, and J. A. Kershaw. NMR Imaging: Study of Fluid Absorption by Polymer Composites. *J. Polym. Sci., Polym. Lett. Ed.*, **22**:241–247, 1984.

[37] W. P. Rothwell, P. N. Tutunjian, and H. J. Vinegar. NMR Imaging: Nonmedical Applications. In B. L. Shapiro, editor, *New directions in Chemical Analysis*, pages 366–395. Texas A&M University, Texas, USA, 1985.

[38] S. Blackband and P. Mansfield. Diffusion in Liquid-Solid Systems by NMR Imaging. *J. Phys. C: Solid State Phys.*, **19**:L49–L52, 1986.

[39] L. A. Weisenberger and J. L. Koenig. NMR Imaging of Diffusion Processes in Polymers: Measurement of the Spatial Dependence of Solvent Mobility in Partially Swollen PMMA Rods. *Macromolecules*, **23**:2445–2453, 1990.

[40] C. A. Fyfe, L. H. Randall, and N. E. Burlinson. Water Penetration in Nylon 6,6: Absorption, Desorption, and Exchange Studies by NMR Microscopy. *J. Polym. Sci., Part A: Polym. Chem.*, **31**:159–168, 1993.

[41] T. A. Carpenter, L. D. Hall, and P. G. Hogan. Magnetic Resonance Imaging of the Delivery of a Paramagnetic Contrast Agent by an Osmotic Pump. *Drug Des. Delivery*, **3**(3):263–266, 1988.

[42] M. Shapiro, M. A. Jarema, and S. Gravina. Magnetic Resonance Imaging of an Oral Gastrointestinal- Therapeutic System (GITS) Tablet. *J. Controlled Release*, **38**:123–127, 1996.

[43] G. Nebgen, D. Gross, V. Lehmann, and F. Müller. ^{1}H-NMR Microscopy of Tablets. *J. Pharm. Sci.*, **84**:282–291, 1995.

[44] B. J. Fahie, A. Nangia, S. K. Chopra, C. A. Fyfe, H. Grondey, and A. Blazek. Use of NMR Imaging in the Optimization of a Compression Coated Regulated Release System. *J. Controlled Release*, **51**:179–184, 1998.

[45] N. Black, T. Vienneau, and Y. Pan. NMR Microimaging, A Useful Tool to Study the Dissolution of Solids. Book of Abstracts, 4th International Conference on Magnetic Resonance Microscopy and Macroscopy, Albuquerque, NM, USA, Sept. 21-25, 1997, page 32.

[46] R. W. Bowtell, J. C. Sharp, A. Peters, P. Mansfield, A. R. Rajabi-Siahboomi, M. C. Davies, and C. D. Melia. NMR Microscopy of Hydrating Hydrophilic Matrix Pharmaceutical Tablets. *Magn. Reson. Imaging*, **12**(2):361–364, 1994.

[47] A. R. Rajabi-Siahboomi, R. W. Bowtell, P. Mansfield, A. Henderson, M. C. Davies, and C. D. Melia. Structure and Behavior in Hydrophilic Matrix Sustained Release Dosage Forms: 2. NMR-Imaging Studies of Dimensional Changes in the Gel Layer and Core of HPMC Tablets Undergoing Hydration. *J. Controlled Release*, **31**:121–128, 1994.

[48] A. R. Rajabi-Siahboomi, R. W. Bowtell, P. Mansfield, M. C. Davies, and C. D. Melia. Structure and Behavior in Hydrophilic Matrix Sustained Release Dosage Forms: 4. Studies of Water Mobility and Diffusion Coefficients in the Gel Layer of HPMC Tablets Using NMR Imaging. *Pharm. Res.*, **13**(3):376–380, 1996.

[49] M. Ashraf, V. L. Iuorno, D. Coffin-Beach, C. A. Evans, and L. L. Augsburger. A Novel Nuclear Magnetic Resonance (NMR) Imaging Method for Measuring the Water Front Penetration Rate in Hydrophilic Polymer Matrix Capsule Plugs and Its Role in Drug Release. *Pharm. Res.*, **11**(5):733–737, 1994.

[50] R. Dinarvand, B. Wood, and A. D'Emanuele. Measurement of the Diffusion of 2,2,2-Trifluoroacetamide within Thermoresponsive Hydrogels Using NMR Imaging. *Pharm. Res.*, **12**(9):1376–1379, 1995.

[51] C. A. Fyfe and A. I. Blazek. Investigations of Hydrogel Formation from Hydroxypropylmethylcellulose (HPMC) by NMR Spectroscopy and NMR Imaging Techniques. *Macromolecules*, **30**(20):6230–6237, 1997.

[52] C. A. Fyfe and A. I. Blazek. Complications in Investigations of the Swelling of Hydrogel Matrices from the Presence of Trapped Gas. *J. Controlled Release*, **52**:221–225, 1998.

[53] E. M. Purcell, H. C. Torrey, and R. V. Pound. Resonance Absorption by Nuclear Magnetic Moments in a Solid. *Phys. Rev.*, **69**:37–38, 1946.

[54] F. Bloch, W. W. Hansen, and M. Packard. Nuclear Induction. *Phys. Rev.*, **69**:127, 1946.

[55] R. K. Harris. *Nuclear Magnetic Resonance Spectroscopy: A Physicochemical View.* Longman Scientific & Technical, Essex, UK, 1987.

[56] C. Dybowski and R. L. Licter. *NMR Spectroscopy Techniques*, volume 5. Marcel Dekker, Inc., New York, NY, USA, 1987.

[57] A. Abragam. *Principles of Nuclear Magnetism.* Clarendon Press, Oxford, UK, 1983.

[58] R. Freeman. *A Handbook of Nuclear Magnetic Resonance.* Longman Scientific & Technical, Essex, UK, 1983.

[59] R. L. Vold, J. S. Waugh, M. P. Klein, and D. E. Phelps. Measurement of Spin Relaxation in Complex Systems. *J. Chem. Phys.*, **48**:3831–3832, 1968.

[60] N. Bloembergen, E. M. Purcell, and R. V. Pound. Relaxation Effects in Nuclear Magnetic Resonance Absorption. *Phys. Rev.*, **73**:679–712, 1948.

[61] E. L. Hahn. Spin echoes. *Phys. Rev.*, **80**(4):580–594, 1950.

[62] H. Y. Carr and E. M. Purcell. Effect of Diffusion on Free Precession in Nuclear Magnetic Resonance Experiments. *Phys. Rev.*, **94**(3):630–638, 1954.

[63] P. Stilbs. Fourier Transform Pulsed-Gradient Spin-Echo Studies of Molecular Diffusion. *Prog. Nucl. Magn. Reson. Spectrosc.*, **19**:1–45, 1987.

[64] E. O. Stejskal and J. E. Tanner. Spin Diffusion Measurements: Spin Echoes in the Presence of a Time- Dependent Field Gradient. *J. Chem. Phys.*, **42**:288–292, 1965.

[65] J. Y. Wu, R. G. Bryant, and T. M. Eads. Detection of Solidlike Components in Starch Using Cross-Relaxation and Fourier Transform Wide-Line ^{1}H NMR Methods. *J. Agric. Food Chem.*, **40**:449–455, 1992.

[66] J. Grad and R. G. Bryant. Nuclear Magnetic Cross-Relaxation Spectroscopy. *J. Magn. Reson.*, **90**:1–8, 1990.

[67] A. Kumar, D. Welti, and R. R. Ernst. NMR Fourier Zeugmatography. *J. Magn. Reson.*, **18**:69–83, 1975.

[68] R. R. Ernst. Methodology of Magnetic Resonance Imaging. *Q. Rev. Biophys.*, **19**(3/4):183–220, 1987.

[69] W.A. Edelstein, J.M.S. Hutchinson, G. Johnson, and T. Redpath. Spin Warp NMR Imaging and Applications to Human Whole-body Imaging. *Phys. Med. Biol.*, **25**:751–756, 1980.

[70] J. R. Zimmerman and W. E. Brittin. Nuclear Magnetic Resonance Studies in Multiple Phase Systems: Lifetime of a Water Molecule in an Adsorbing Phase on Silica Gel. *J. Phys. Chem.*, **61**:1328–1333, 1957.

[71] The Dow Chemical Company. *METHOCEL Cellulose Ethers Technical Handbook.* Form No. 192-1062-791-JB.

[72] S. Budavari, editor. *The Merck Index.* Merck & Co., Inc., Whitehouse Station, NJ, USA, 1996.

[73] The Dow Chemical Company. *Formulating for Controlled Release with METHOCEL Premium cellulose ethers.* Form No. 198-1029-1089 AMS.

[74] Wolfram Research. *Guide to Standard Mathematica Packages*, 1992. Technical Report Version 2.1.

[75] S. Meiboom and D. Gill. Modified Spin-Echo Method for Measuring Nuclear Relaxation Times. *Rev. Sci. Instrum.*, **29**(8):688–691, 1958.

[76] W. Derbyshire. The Dynamics of Water in Heterogeneous Systems with Emphasis on Subzero Temperatures. In F. Franks, editor, *Water: A Comprehensive Treatise*, volume 7, chapter 4. Plenum Press, New York, NY, USA, 1982.

[77] M. Brandl and A. Haase. Molecular Diffusion in NMR Microscopy. *J. Magn. Reson., Ser. B*, **103**:162–167, 1994.

[78] H. A. Lieberman, L. Lachman, and J. B. Schwartz, editors. *Pharmaceutical Dosage Forms: Tablets*, volume 1. Marcel Dekker, Inc., New York, NY, USA, 1989.

[79] E. Shotton, J. J. Deer, and D. Ganderton. The Instrumentation of a Rotary Tablet Machine. *J. Pharm. Pharmacol.*, **15**(Suppl.), 1963.

[80] F. J. Bandelin. Compressed Tablets by Wet Granulation. In H. A. Lieberman, L. Lachman, and J. B. Schwartz, editors, *Pharmaceutical Dosage Forms: Tablets*, volume 1, pages 131–193. Marcel Dekker, Inc., New York, NY, USA, 1989.

[81] H. Schott. Kinetics of Swelling of Polymers and their Gels. *J. Pharm. Sci.*, **81**:467–470, 1990.

[82] M. Singh, J. A. Lumpkin, and J. Rosenblatt. Mathematical Modeling of Drug Release from Hydrogel Matrices via a Diffusion Coupled with Desorption Mechanism. *J. Controlled Release*, **32**:17–25, 1994.

[83] J. Crank. *The Mathematics of Diffusion.* Oxford University Press, London, UK, 1956.

[84] H. S. Carslaw and J. C. Jaeger. *Conduction of Heat In Solids.* Clarendon Press, Oxford, UK, 1959. Appendix II.

Appendix A

Processing of Image Data

A.1 ASCII output from WIN-NMR

The following listing is an example of the ASCII output from the WIN-NMR program which was later reproduced by the Java converter program. The frequency information is given by a start frequency, an end frequency and a frequency interval. The intensity for each frequency is then listed, in arbitrary units, in a column after the header information. To preserve space in this section, the intensities are listed from left to right rather than as one long column.

```
Data file: /MacintoshHD/bhjan21/BHJAN21.001
Starting Point: 0
Ending Point: 127
Point Count: 128
Read Data
SF01: 400.12 Hz
Sweep Width: 83333.3 Hz
Hz/Pt: 651.042
First Point: 39666.7 Hz
Last Point: -43666.7 Hz
First Point: 99.1394 PPM
Last Point: -109.137 PPM
484576   485286   486762   488940   492641   497245   500295   501473
503597   508666   515326   522450   530249   538270   545824   554803
566866   579258   588402   596853   610046   627312   643166   657261
674128   693682   710637   723804   736885   751418   766600   785483
810688   835670   851818   863811   881104   895966   887655   845999
755778   546937   151772   659636   1523293  2266984  2678130  2784588
2787366  2850616  2980960  3077309  3088798  3062632  3059069  3072138
3063307  3034434  3018335  3019557  3011146  2989495  2982559  2997201
2999792  2969777  2932773  2918207  2916614  2904164  2883866  2872988
2868824  2856918  2839863  2830495  2825906  2813718  2796714  2787526
2784881  2777351  2765665  2760037  2759387  2754016  2745389  2743128
2744913  2739457  2727660  2721218  2721315  2718006  2710643  2709328
2715010  2717425  2714806  2716650  2724149  2726752  2721761  2717534
2711643  2686006  2632814  2567302  2504828  2442167  2373221  2308210
2263164  2239889  2227888  2219094  2211218  2202104  2190571  2181377
2181059  2188252  2193558  2190366  2182260  2178785  2184815  2195383
```

A.2 Converter Program for Batch-Processing Files

Below is a listing of the converter program used to batch-process image files. It was written by Dr. Mark Welsh in the Java language and run on a Macintosh LC475 using the Macintosh Java Virtual Machine. The comments, preceded by '//', explain the function of each section.

```
 /**
 * A converter for Almira's MSL binary files.
 **/
import java.io.*;
import java.awt.*;

public class Converter
{
    public static void main()
    {
        // Create our frame
        Frame frame = new Frame();

        // Select a file (actually the directory)
        FileDialog fd = new FileDialog(frame,
                    "Select a file in the directory to be converted",
                     FileDialog.LOAD);
        fd.show();

        // Create a File object for the selected directory
        File dir = new File(fd.getDirectory());
        if (!dir.isDirectory())
        {
            System.out.println("Problem selecting a directory.");
            return;
        }

        // Get a list of all files in this directory
        String fileNames[];
        try
        {
            fileNames = dir.list();
        \
        catch (SecurityException e)
        {
            System.out.println("Problem listing files in directory.");
            return;
        }

        // For each file, perform a conversion
        for (int i = 0; i < fileNames.length; i++)
        {
            convert(fd.getDirectory(), fileNames[i]);
        }
    }
```

```
// Convert a file from MSL binary to an ASCII dump
private static void convert(String directory, String fileName)
{
    byte EOL[] = new byte[2];
    EOL[0] = 0x0D;
    EOL[1] = 0x0A;
    try
    {
        // Create an MSL input stream
        directory += "/";
        AlsBufferedInputStream inFile =
            new AlsBufferedInputStream(
            new FileInputStream(directory + fileName));
        // Create the output file
        PrintStream outFile =
            new PrintStream(
            new FileOutputStream(directory + "X" + fileName));

        // Get the header data
        inFile.skipMSL(43);
        int tdsize = inFile.readMSL();
        inFile.skipMSL(9);
        int spwidthRaw = inFile.readMSL();
        inFile.skipMSL(23);
        int sfreqRaw = inFile.readMSL();
        inFile.skipMSL(103);
        int offsetRaw = inFile.readMSL();
        inFile.skipMSL(74);

        // munge it
        double spwidth = (double)spwidthRaw / 0x40;
        double sfreq = (double)sfreqRaw / 0x4000;
        double offset = (double)offsetRaw / 0x80;

        // and print it out
        outFile.print("Data file: "
            + directory + fileName);
        outFile.write(EOL);
        outFile.print("Starting Point: 0");
        outFile.write(EOL);
        outFile.print("Ending Point: "
            + Integer.toString(tdsize - 1));
        outFile.write(EOL);
        outFile.print("Point Count: "
            + Integer.toString(tdsize));
        outFile.write(EOL);
        outFile.print("Read Data");
        outFile.write(EOL);
        outFile.print("SF01: "
            + Double.toString(sfreq) + " Hz");
        outFile.write(EOL);
        outFile.print("Sweep Width: "
            + Double.toString(spwidth) + " Hz");
        outFile.write(EOL);
        outFile.print("Hz/Pt: "
```

```
                + Double.toString(spwidth/(double)tdsize));
            outFile.write(EOL);
            outFile.print("First Point: "
                + Double.toString(offset + spwidth) + " Hz");
            outFile.write(EOL);
            outFile.print("Last Point: "
                + Double.toString(offset) + " Hz");
            outFile.write(EOL);
            outFile.print("First Point: "
                + Double.toString((offset
                + spwidth) / (double)sfreq) + " PPM");
            outFile.write(EOL);
            outFile.print("Last Point: "
                + Double.toString(offset / (double)sfreq) + " PPM");
            outFile.write(EOL);

            // Print out the real data
            for (int i = 0; i < tdsize; i++)
            {
                outFile.print(Integer.toString(inFile.readMSL()));
                outFile.write(EOL);
                inFile.skipMSL(1);
            }

            // Release resources
            inFile.close();
            outFile.close();
        }
        catch (Exception e)
        {
            System.out.println(e.toString() + ": Problem parsing file");
        }
        finally
        {
            System.out.println(directory + fileName);
        }
    }
}

class AlsBufferedInputStream extends BufferedInputStream
{
    public static final int MSL_WORD = 3;
    public AlsBufferedInputStream(InputStream inStream)
    {
        super(inStream);
    }
    public int skipMSL(int skip) throws IOException
    {
        int toSkip = skip * MSL_WORD;
        if (super.skip(toSkip) != toSkip)
        {
            throw new IOException();
        }
        return toSkip;
    }
    public int readMSL() throws IOException
```

```
    {
        int value = (read() << 0x10) + (read() << 0x08) + read();
        value <<= 8;
        value >>= 8;
        return value;
    }
}
```

A.3 Calculating (Frequency, Intensity) Data Points

The following program reads in the ASCII output of Appendix A.1, extracts the necessary frequency information to calculate the frequency for each point and then writes the (frequency, intensity) data to a new file. It was written and run in Symantec's THINK Pascal version 4.0 on a Macintosh LC475. Comments in the program, bracketed by '(*' and '*)', explain the function of various sections.

```
program READ_WIN_NMR;
    type
        data = array[1..2028] of real;
        Firstpart = array[0..9] of string[1];
        Secondpart = array[0..99] of string[2];

    var
        FirstfileExt, LastfileExt: string[3];
        period: string[1];
        ext1: Firstpart;
        ext2: Secondpart;
        infile, outfile: text;
        Root, Name, NewRoot, NewName: string;
        Datafile, Datatype: string;
        Startpoint, Endpoint, Numpoints: integer;
        Specfreq, Sweepwidth, Res: real;
        Startfreq, Endfreq: real;
        Startppm, Endppm: real;
        i, j, k: integer;
        Intensity: data;
        Frequency: data;

(*****************************************************************)
(*Runs through the characters in the heading of an acquisition  *)
(*parameter in the ASCII file up to the semi-colon character    *)
(*for example, Starting Point:                                  *)
(*****************************************************************)
    procedure ReadToSemicolon;
        var
            x: char;
    begin
        repeat
            Read(infile, x);
```

```
        until Ord(x) = 58;
    end;
(*****************************************************************)
(*Main Program                                                   *)
(*****************************************************************)
begin
(*Introduction to program*)
    ShowText;
    Writeln;
    Writeln('Convert WIN NMR ASCII to data suitable for ');
    Writeln('Kaleidagraph, Excel etc . ');
    Writeln;
    Writeln('This program will ask you to open a WIN NMR ASCII file ');
    Writeln('and to give a name to save the resulting list  ');
    Writeln('of frequency and intensity data pairs.');
    Writeln;
    Writeln('Please note that the MAXIMUM TD for this program is 2K.');
    Writeln;
    Writeln('Hit return to continue . ');
    Readln;
(*The MSL filenames are in the form name.ext where the extension *)
(*is a number from 001 to 999. The following sets up strings for *)
(*file extensions of 000 to 999 so that batch-processing can be*)
(*performed on files that have the same rootname*)
    Period := '.';
    for i := 0 to 9 do
        ext1[i] := Chr(i + 48);
(* Ord('0') = 48, Ord('9') = 57*)

    k := 0;
    for i := 0 to 9 do
        for j := 0 to 9 do
            begin
                ext2[k] := concat(ext1[i], ext1[j]);
                k := k + 1;
            end;

(*Requests file rootnames and extensions*)
    Writeln('Please enter in the Root Name of the files that you');
    Writeln('want to convert.  Do not include the period');
    Writeln;
    Writeln('format:  name of harddrive:folder(:folder etc.):filename');
    Readln(Root);
    Writeln;
    Writeln('Please enter in the first file extension eg 001');
    Readln(FirstfileExt);
    Writeln;
    Writeln('Please enter the last file extension eg 065');
    Writeln('This program can handle file extensions');
    Writeln('from 000 to 999');
    Readln(LastFileExt);
    Writeln('Please enter the root name of the files to save ');
    Writeln('the data as.  The extension for the saved file will');
    Writeln('be the same as that for the file read in');
    Writeln;
    Writeln('format: harddrive:folder:filename');
```

```
    Readln(NewRoot);
(*processing starts*)
(*the following increments the file extension string to the*)
(*value of the first extension entered*)
    k := 0;
    j := 0;
    while concat(ext1[k], ext2[j]) <> FirstFileExt do
        begin
            if j = 99 then
                begin
                    k := k + 1;
                    j := -1;
                end;
            j := j + 1;
        end;
(* need to set j back one to avoid missing the first file*)
    j := j - 1;

(*reads through the files one by one and creates an output file*)
(*of the (frequency,intensity) data points which has a new name*)
(*but the same file extension number as the input file*)
    while concat(ext1[k], ext2[j]) <> LastFileExt do
        begin
            if j = 99 then
                begin
                    k := k + 1;
                    j := -1;
                end;
            j := j + 1;
            Name := concat(Root, Period, ext1[k], ext2[j]);
            Open(infile, Name);
            Readln(infile, Datafile);
            ReadToSemicolon;
            Readln(infile, Startpoint);
            ReadToSemicolon;
            Readln(infile, Endpoint);
            ReadToSemicolon;
            Readln(infile, Numpoints);
            Readln(infile, Datatype);
            ReadToSemicolon;
            Readln(infile, Specfreq);
            ReadToSemicolon;
            Readln(infile, Sweepwidth);
            ReadToSemicolon;
            Readln(infile, Res);
            ReadToSemicolon;
            Readln(infile, Startfreq);
            ReadToSemicolon;
            Readln(infile, Endfreq);
            ReadToSemicolon;
            Readln(infile, Startppm);
            ReadToSemicolon;
            Readln(infile, Endppm);

            i := 0;
            for i := 1 to Numpoints do
```

```
                begin
                    Read(infile, Intensity[i]);

                    if i < Numpoints then
                            Readln(infile);
                end;

(*calculation of the frequency value for each point*)
(*intensity values are listed in order of positive to*)
(*negative frequency*)
            Frequency[1] := Startfreq;
            i := 0;
            for i := 2 to Numpoints do
                Frequency[i] := Frequency[(i - 1)] - Res;

(*outputting to the new file*)
            NewName := concat(NewRoot, Period, ext1[k], ext2[j]);
            Open(outfile, NewName);

            for i := 1 to Numpoints do
                begin
                    write(outfile, Frequency[i] : 10 : 5);
                    write(outfile, '    ');
                    writeln(outfile, Intensity[i] : 10 : 0);
                end;

            Close(infile);
            Close(outfile);
        end;
end.
```

A.4 T_2 Calculation from the Variable-T_E Image Files

This program calculates T_2 and error in T_2 from the dataset of one-dimensional image files acquired at different times to echo. The program was written and run in Symantec's THINK Pascal version 4.0 and run on a Macintosh LC475. The program reads in the output files of Appendix A.3 and calculates the corresponding distance for each frequency and can scale the intensities if desired. The entire dataset is sorted into a array by order of increasing TE. The dataset is then used to calculate the slope of a Ln(intensity) versus TE plot for each frequency point. The program calculates the slopes of subsets of the datafiles, from the four smallest T_E files up to the total number of files. The subset that produces the slope with the lowest relative error is considered the best result for the T_2 calculation unless the relative error of the total number of files is within 50% of the lowest relative error.

```
program filehandling;

    const
        Maxnumfiles = 15;  (*arbitrary number, usually have 10*)
        Maxnumpoints = 256; (*arbitrary, usually have 128*)


    type

        Many1 = array[1..Maxnumfiles] of string;
        Many2 = array[1..Maxnumfiles] of text;
        data = array[1..Maxnumpoints] of real;
        value = array[1..Maxnumfiles] of real;
        built = array[1..Maxnumpoints, 0..Maxnumfiles] of real;


    var
        Response, GoAgain, Check: boolean;
        test: char;
        Name: Many1;
        Infile: Many2;
        Numfiles, Numpoints, i: integer;
        Menu: string[100];
        freq, int: data;
        TE, sortedTE: value;
        Hertzpercm, FreqofZero, temp: real;
        Combined: built;


(*****************************************************************)
(*Reads in the frequency and intensity values from a file        *)
(*****************************************************************)
    procedure Readfile (Numpoints, i: integer; var freq, int: data);
        var
            j: integer;
    begin
        j := 0;
        for j := 1 to Numpoints do
            begin
                Read(infile[i], freq[j]);
                Readln(infile[i], int[j]);
            end;

    end;
(*****************************************************************)
(*Calculates new (distance, intensity) points by using the       *)
(*entered scaling factor, zero position and Hertz per cm factor *)
(*****************************************************************)
    procedure Convert (Numpoints: integer; Hertzpercm,
                    FreqofZero: real; var freq: data);

        var
            j: integer;
            temp1: real;
    begin
```

```
        j := 0;
        temp1 := 0;

        for j := 1 to Numpoints do
            begin
                temp1 := (freq[j] - FreqofZero) / Hertzpercm;
                freq[j] := temp1;
            end;
    end;

(*****************************************************************)
(*Arranges data files into an array in order of increasing TE    *)
(*****************************************************************)
    procedure Buildarray (Numpoints, i, Numfiles: integer;
            TE: value; freq, int: data; var sTE: value;
            var Combined: built);

        var
            j, k: integer;
            lowTE: real;
            rank: integer;

    begin
        j := 0;
        if i = 1 then
            for j := 1 to Numpoints do
                Combined[j, 0] := freq[j];

(*setting ranking of the data based on increasing TE*)
        rank := 1;
        k := 0;
        for k := 1 to Numfiles do
            if TE[i] > TE[k] then
                rank := rank + 1;

        sTE[rank] := TE[i];

(*the ranking determines in which column the intensity data goes*)
        j := 0;
        for j := 1 to Numpoints do
            Combined[j, rank] := int[j];
    end;

(*****************************************************************)
(*This is the main calculation procedure involved in working out*)
(*the T2 value. Temp is the number of files from 4               *)
(* onward that are used to calculate the slope                   *)
(*****************************************************************)
    procedure CalcSlope (temp, j: integer; Combined: built;
            sorTE: value; var slope, denom, int,
            ErrorInSlope, Errorpernumpoints: value);
        var
            n: integer;
            Xsum, Ysum, X2sum, XYsum: real;
            TotDiff2, Diff2: real;
    begin
```

```
(*Least-squares procedure for calculating the slope of a straight*)
(*line. TE is the x variable and ln int is the y variable*)

        n := 0;
        Xsum := 0;
        Ysum := 0;
        X2sum := 0;
        XYsum := 0;
        for n := 1 to temp do
            begin
                Xsum := Xsum + sorTE[n];
                Ysum := Ysum + Combined[j, n];
                X2sum := X2sum + (sorTE[n]) * (sorTE[n]);
                XYsum := XYsum + (sorTE[n]) * (Combined[j, n]);
            end;
        denom[temp] := (X2sum * temp - Xsum * Xsum);

        slope[temp] := (XYsum * temp - Xsum * Ysum) / denom[temp];
        Int[temp] := (X2sum * Ysum - Xsum * XYsum) / denom[temp];

        TotDiff2 := 0;
        n := 0;
        for n := 1 to temp do
            begin
                Diff2 := Sqr((Combined[j, n] - slope[temp]
                    * sorTE[n] - int[temp]));
                TotDiff2 := TotDiff2 + Diff2;
            end;
        ErrorInSlope[temp] := Sqrt((temp * TotDiff2)
            / ((temp - 2) * denom[temp]));
        Errorpernumpoints[temp] := ErrorInSlope[temp] / temp;
    end;

(*****************************************************************)
(*The data set may contain points that would ordinarily be       *)
(*inappropriate to use in the calculation.  To simplify the      *)
(*rejection of points, the following procedure calculates the    *)
(*slope with subsets of 4 files minimum to Numfiles maximum.     *)
(*Since the data has already been sorted based on                *)
(*increasing TE value, calculations with subsets of the data     *)
(*eliminate the problem points at higher TE values for regions   *)
(*of the sample with short T2 values. The best slope is chosen   *)
(*by using the relative error in the slope as the selection      *)
(*criterion.  This best slope is then used to calculate T2       *)
(*****************************************************************)
    procedure T2fromSlope (Numfiles, j: integer; Combined: built;
             sorTE: value; var T2, ErrorInT2: real);

        type
            testcases = array[1..MaxNumfiles] of real;


        var
            k, m: integer;
            slope, denom, int, ErrorInSlope, Errorpernumpoints: value;
            relerr, bestslope, bestErrorInSlope, reltemp: real;
```

```
    begin
(*The minimum number of points that will be used is 4*)
        for k := 4 to Numfiles do
            CalcSlope(k, j, Combined, sorTE, slope, denom, int,
                ErrorInSlope, Errorpernumpoints);

        relerr := 1;
        bestslope := 1;
        bestErrorInSlope := 1;
(*Looking for the subset that gives the lowest relative *)
(*error in the slope*)
        for k := 4 to Numfiles do
            begin
                reltemp := ABS(Errorpernumpoints[k] / slope[k]);
                if reltemp < relerr then
                    begin
                        bestslope := slope[k];
                        bestErrorInSlope := ErrorInslope[k];
                        relerr := reltemp;
                    end;

(*The following lines choose the slope with all the points*)
(*as the default bestslope when the relative error for the entire*)
(*dataset is still close to the best error (i.e. within 50%)*)
                if (k = Numfiles) and (reltemp <= 1.5 * relerr) then
                    begin
                        bestslope := slope[Numfiles];
                        bestErrorInSlope := ErrorInslope[Numfiles];
                        writeln('chose this one for', j);
                    end;
            end;

        T2 := -1 / bestslope;
        ErrorInT2 := Abs(bestErrorInSlope * T2 / bestslope);
    end;

(*****************************************************************)
(*This procedure starts the T2 calculation.  It asks for an      *)
(*outfile name and then calls on other procedures to do the      *)
(*calculation. At the end, it writes the T2 data to the outfile *)
(*****************************************************************)
    procedure CalcT2 (Numpoints, Numfiles: integer;
                stTE: value; var Combined: built);

        var
            j, n: integer;
            temp, temp2: real;
            NewName, SaveT2: string;
            outfile: text;
            T2, ErrorInT2: real;

    begin
        Writeln;
        Writeln('You will be asked to enter in the name of the');
        Writeln('file to save the T2 data. Hit Return to continue.');
```

```
        Readln;
        NewName := Newfilename(SaveT2);
        Open(outfile, NewName);


        for j := 1 to Numpoints do
            begin
                for n := 1 to Numfiles do
                    begin
                        temp := Ln(Combined[j, n]);
                        Combined[j, n] := temp;
                    end;
                T2fromSlope(Numfiles, j, Combined, stTE, T2, ErrorInT2);
                Combined[j, 1] := T2;
                Combined[j, 2] := ErrorInT2;
                for n := 3 to Numfiles do
                    Combined[j, n] := 0;
                Writeln(outfile, Combined[j, 0] : 10 : 5, ' ',
                    Combined[j, 1] : 10 : 5, '  ',
                    Combined[j, 2] : 10 : 5);
            end;
        Close(outfile);
    end;

(*****************************************************************)
(*Main program.  Asks for various parameters and does some       *)
(*checking for responses. Starts the reading in and building    *)
(*of the dataset array and then calls for CalcT2.               *)
(*****************************************************************)
begin
    ShowText;

(*Requests various parameters*)
    Writeln;
    Writeln('Please enter the number of data points');
    Writeln(' (i.e. the TD value from the experiment)');
    Readln(Numpoints);
    Writeln;


    writeln('Please enter in the Hertz/cm conversion factor.');
    Writeln('(Enter 1 for no conversion)');
    Readln(Hertzpercm);
    Writeln;

    Writeln('Enter the zero position in Hz.');
    Writeln('(Enter 0 for no change in the data.)');
    Readln(FreqofZero);
    Writeln;


    Writeln('Hit Return to continue');
    Readln;

(*routine to verify that the entered values are correct*)
    GoAgain := True;
```

```
    while GoAgain = True do
        begin

            Writeln;
            Writeln('Here are the values that you entered');
            Writeln('You may change them if you w ish');
            Writeln;
            Writeln('1  Number of data points = ', Numpoints : 2);
            Writeln('2  Hertz/cm conversion factor = ',
                Hertzpercm : 10 : 5);
            Writeln('3  Frequency of Zero = ', Freqofzero : 10 : 5);
            Writeln;
            Writeln('Are these values correct?');
            repeat
                Writeln('Enter Y for yes and N for no and
                    then Return');
                Readln(test);
            until test in ['y', 'Y', 'N', 'n'];
            while test in ['N', 'n'] do
                begin
                    Writeln;
                    Writeln('Enter the number of the parameter
                        you wish to change');
                    repeat
                        Writeln('Numbers go from 1 to 4.');
                        Readln(i);
                    until i in [1..3];
                    case i of
                        1:
                            begin
                                Writeln('Number of data points = ');
                                Readln(Numpoints);
                            end;
                        2:
                            begin
                                Writeln('Hertz/cm conversion factor = ');
                                Readln(Hertzpercm);
                            end;
                        3:
                            begin
                                Writeln('Frequency of Zero =  ');
                                Readln(Freqofzero);
                            end;

                    end;
                    Writeln;
                    Writeln('All all the values correct?');
                    repeat
                        Writeln('Enter Y for yes and N for no,
                            then Return');
                        Readln(test);
                    until test in ['Y', 'y', 'N', 'n'];
                end;
    (*requests the number of image files in the TE dataset*)
            Writeln;
            Writeln('How many files do you have to analyse?');
```

```
            Writeln('(The maximum is set at ', Maxnumfiles : 2, ')');
            Readln(Numfiles);
            Writeln;

            while Numfiles > Maxnumfiles do
                begin
                    Writeln;
                    Writeln('You cannot exceed the Maximum
                        number of files ( ', Maxnumfiles : 2, ' )!');
                    Writeln;
                    Writeln('Please enter in a new number of files. ');
                    Readln(Numfiles);
                end;

            Writeln;
            Writeln('All your files will be opened now.
                Hit Return to continue.');
            Readln;

(*opens files using the Macintosh 'file open' window*)
            for i := 1 to Numfiles do
                begin
                    Name[i] := Oldfilename(Menu);
                    Open(Infile[i], Name[i]);
                end;
            Writeln;
            Writeln;
            Writeln('The indicated files have been opened.');

(*requests the TE value for each file*)
            Writeln;
            writeln('Please enter the time-to-echo (TE in ms)');
            Writeln('for each of the files as indicated.');
            Writeln;

            i := 0;
            for i := 1 to Numfiles do
                begin
                    Write('Filename: ', Name[i], '    TE(ms) = ');
                    Readln(TE[i]);
                end;
            Writeln;

(*check for correct TE values*)
            Writeln;
            i := 0;
            for i := 1 to Numfiles do
                Writeln(i : 1, ' File: ', Name[i],
                    '   TE(ms) = ', TE[i] : 3 : 2);
            writeln;
            Writeln('Are all the values correct?');
            repeat
                Write('Enter either Y for yes or N for no,
                    then Return ');
                Readln(test);
            until test in ['Y', 'y', 'N', 'n'];
```

```
            case test of
                'Y', 'y':
                    Check := true;
                'N', 'n':
                    Check := false;
            end;

            if Check = false then
                repeat

                    for i := 1 to Numfiles do
                        Writeln(i : 2, ' File: ',
                            Name[i], '   TE(ms) = ', TE[i] : 3 : 2);

                    Writeln;
                    Writeln('Enter the number of the file you wish
                        to change.');
                    repeat
                        Writeln('Numbers go from 1 to ', Numfiles : 2);
                        Readln(i);
                    until i in [1..Numfiles];
                    Writeln('File:', Name[i], '   TE(ms) = ');
                    Readln(TE[i]);
                    Writeln;
                    Writeln('Are all the values correct now?');

                    repeat
                        Writeln('Enter Y for yes and N for no and
                            then Return');
                        Readln(test);
                    until test in ['Y', 'y', 'N', 'n'];
                    case test of
                        'Y', 'y':
                            Check := true;
                        'N', 'n':
                            Check := false;
                    end;
                until Check = true;

(*starts the T2 calculation*)
            writeln;
            writeln('CALCULATING.  PLEASE WAIT.....................');



            for i := 1 to Numfiles do
                begin
                    Readfile(Numpoints, i, freq, int);
                    Convert(Numpoints, Hertzpercm, FreqofZero, freq);
                    Buildarray(Numpoints, i, Numfiles,
                        TE, freq, int, sortedTE, Combined);
                end;

            CalcT2(Numpoints, Numfiles, sortedTE, Combined);
```

```
            for i := 1 to Numfiles do
                Close(Infile[i]);


            Writeln;
            Writeln('Do you want to analyse another set of');
            Writeln('files with the same parameters?');
            Writeln;
            repeat
                Writeln('Enter Y for yes or N for no, then Return');
                Readln(test);
            until test in ['Y', 'y', 'N', 'n'];
            case test of
                'Y', 'y':
                    GoAgain := true;
                'N', 'n':
                    GoAgain := false;
            end;
        end;
end.
```

A.5 Correcting Image Intensity for T_2 Dephasing

The T_2 distribution calculated in Appendix A.4 was used to correct the intensities of the image acquired for dephasing due to T_2 relaxation during the T_E time. The following program, written and run in Symantec's THINK Pascal version 4.0 on a Macintosh LC475, performs the calculation and also allows for scaling of the intensities.

```
program Correct_for_T2;

    var
        infile1, infile2, outfile: text;
        Menu, Name1, Name2, NewName: string;
        i, Numpoints: integer;
        GoAgain: boolean;
        T2, ErrorInT2, TE, position, intensity,
            newintensity, error: real;
        errT2squared, errIntensitysquared, errInt, MaxInt: real;
        x: char;

begin
    GoAgain := true;

(*requests various parameters*)
    Writeln('Enter the number of points');
    Readln(Numpoints);
    Writeln;
    Writeln('What is the TE value in ms?');
    Readln(TE);
    Writeln;
```

```
    Writeln('Enter in the experimental error in the intensity');
    Readln(errInt);
    Writeln('Enter in the maximum intensity');
    Readln(MaxInt);

(*Main calculation procedure that opens the T2 file and the image*)
(*file to be corrected, performs the correction calculation*)
(*and writes the corrected intensities to a new file*)
    repeat
        Writeln('You will be asked to open the T2 file.');

        Name1 := Oldfilename(Menu);

        Writeln('Now open the image file to be corrected');

        Name2 := Oldfilename(Menu);

(*modified filename for output*)
        NewName := Concat(Name2, ' corrected');

        Open(infile1, Name1);
        Open(infile2, Name2);
        Open(outfile, NewName);
        error := 0;
        for i := 1 to Numpoints do
            begin
(*The image file still has position in terms of frequency but*)
(*the T2 file has the calculated distance.  The files are read*)
(*in this order to pass the calculated distances to the*)
(*image file with the corrected intensities*)
                Readln(infile2, position, intensity);
                Readln(infile1, position, T2, ErrorInT2);

(*Scaling to the maximum intensity*)
                intensity := intensity / MaxInt;
                errInt := errInt / MaxInt;

(*the following corrects for signal loss due to T2*)
                newintensity := intensity * Exp(TE / T2);
                errT2squared := (ErrorInT2 * ErrorInT2)
                    * (intensity * TE * Exp(TE / T2) / (T2 * T2))
                    * (intensity * TE * Exp(TE / T2) / (T2 * T2));
                errIntensitysquared := (errInt * errInt)
                    * (Exp(TE / T2)) * (Exp(TE / T2));
                error := Sqrt(errT2squared + errIntensitysquared);
                Writeln(outfile, position : 10 : 5, '    ',
                    newintensity : 5 : 5, ' ', error : 5 : 5);
            end;
        Close(infile1);
        Close(infile2);
        Close(outfile);

        writeln('Would you like to repeat for another file?');
        Readln(x);
        if x in ['n', 'N'] then
            GoAgain := false;
```

```
    until GoAgain = false;
end.
```

A.6 Calculating Polymer Weight Percent Distributions from T_2 Distributions

The following program, written and run in Symantec's THINK Pascal version 4.0 on a Macintosh LC475, requests the coefficients from the non-linear least-squares fit equations that describe the dependence of the relaxation time T_2 on the polymer weight percent. The fit equation is then used to calculate the polymer weight percent distribution for the system at that swelling interval.

```
program Calcpolymerpercent;

    const
        Maxnumfiles = 100;
        Maxnumpoints = 256;
    type
        namestring = array[1..Maxnumfiles] of string[200];
        data = array[1..Maxnumpoints] of real;
    var
        alpha, beta, gamma, delta, epsilon: real;
        Distance, T2, errT2, Poly, errPoly: data;
        Name: namestring;
        Menu: string[200];
        Numfiles, Numpoints, k: integer;

(*****************************************************************)
(*Reads in the coefficients of the non-linear least-squares fit *)
(*equations for the T2 dependence on polymer concentration      *)
(*****************************************************************)
    procedure GetCoefficients (var a, b, c, d, e: real);
    begin
        Writeln('The following equations will be used to calculate the');
        Writeln('polymer concentration and the error
            in the polymer concentration');
        Writeln;
        Writeln('polymer% = a Exp(-b T2) + c Exp(-d T2) + e');
        Writeln;
        Writeln('(err polymer %)^2 = (err T2)^2{- a b Exp(-b T2)
            + (- c d Exp(-d T2))}^2');
        Writeln;
        Writeln('Please enter the in values for a, b, c, d, and e.');
        Write('a=  ');
        Readln(a);
        Write('b=  ');
        Readln(b);
        Write('c=  ');
```

```
        Readln(c);
        Write('d=  ');
        Readln(d);
        Write('e=  ');
        Readln(e);
        Writeln;
    end;

(*****************************************************************)
(*Gets a list of file names to process using the Macintosh 'file*)
(*open' window.                                                 *)
(*****************************************************************)
    procedure Getfilenames (var NName: namestring; MMenu: string;
        var NNumfiles: integer);
        var
            i: integer;
    begin
        Writeln('How many files will be opened?');
        Readln(NNumfiles);
        i := 0;
        for i := 1 to NNumfiles do
            NName[i] := Oldfilename(MMenu);
    end;

(*****************************************************************)
(*Reads in a T2 file                                             *)
(*****************************************************************)
    procedure Readfile (Name: namestring; i: integer;
        Numpoints: integer; var Distance, T2, errT2: data);
        var
            j: integer;
            infile: text;
    begin
        Open(infile, Name[i]);
        for j := 1 to Numpoints do
            begin
                Read(infile, Distance[j]);
                Read(infile, T2[j]);
                Readln(infile, errT2[j]);
            end;
        Close(infile);
    end;

(*****************************************************************)
(*Uses the fit equations to calculate the weight percent and error*)
(*****************************************************************)
    procedure Calculate (TT2, errTT2: data; var PPoly,
        errPPoly: data; a, b, c, d, e: real; Numpoints: integer);
        var
            j: integer;
    begin
        j := 0;
        for j := 1 to Numpoints do
            begin
                PPoly[j] := a * Exp(-b * TT2[j])
                 + c * Exp(-d * TT2[j] + e);
```

```
                errPPoly[j] := errTT2[j] * errTT2[j] *
                    (a * b * Exp(-b * TT2[j])
                    + c * d * Exp(-d * TT2[j]))
                    * (a * b * Exp(-b * TT2[j])
                    + c * d * Exp(-d * TT2[j]));
                errPPoly[j] := Sqrt(errPPoly[j]);
            end;
    end;

(*****************************************************************)
(*Outputs the polymer weight percent results                     *)
(*****************************************************************)
    procedure Writefile (NName: namestring; Numpoints, i: integer;
        DDistance, PPoly, errPPoly: data);
        var
            j: integer;
            outfile: text;
            tempName: string;
    begin
        j := 0;
        tempName := concat(Name[i], ' poly%');
        Open(outfile, tempName);

        for j := 1 to Numpoints do
            Writeln(outfile, DDistance[j] : 5 : 5, '    ',
                PPoly[j] : 5 : 5, ' ', errPPoly[j] : 5 : 5);
        Close(outfile);
    end;

(*Main program that calls the procedures*)
begin

    GetCoefficients(alpha, beta, gamma, delta, epsilon);
    Getfilenames(Name, Menu, Numfiles);
    Writeln;
    Writeln('Enter in the number of points for each file');
    Readln(Numpoints);
    for k := 1 to Numfiles do
        begin
            Readfile(Name, k, Numpoints, Distance, T2, errT2);
            Calculate(T2, errT2, Poly, errPoly, alpha, beta, gamma,
                delta, epsilon, Numpoints);
            Writefile(Name, Numpoints, k, Distance, Poly, errPoly);
        end;
end.
```

Appendix B

Calculating Theoretical Concentration Distributions

B.1 Calculation of Error Function Values

The value of the error function, erf(x), is necessary for computing concentration distributions from Equations 6.7 and 6.8. Tabulated values of the error function are available in the literature [84]. Table B.1 lists the error function values for positive values of x. The error function for negative values of x are the negative of those for positive x, *i.*e. erf(−x) = − erf(x). A procedure was developed to interpolate between the values listed in the table so that the value of the erf(x) could be determined for any x.

The interpolation method used for the calculations of this thesis involved determining coefficients for cubic splines that would define different segments of the data in Table B.1. The points that define the endpoints for each segment are assumed to be two points joined by a cubic equation, resulting in the set of four simultaneous equations, B.1 to B.4, where y_i is the erf(x_i), w_i is the derivative of y_i, and a, b, c, and d are the unknown coefficients of the cubic equation. The coefficients are determined by solving the set of simultaneous equations. The solutions, obtained by matrix inversion in Mathematica, are given in Equation B.5.

$$y_1 = ax_1^3 + bx_1^2 + cx_1 + d \tag{B.1}$$
$$y_2 = ax_2^3 + bx_2^2 + cx_2 + d \tag{B.2}$$
$$w_1 = 3ax_1^2 + 2bx_1 + c \tag{B.3}$$
$$w_2 = 3ax_2^2 + 2bx_2 + c \tag{B.4}$$

Table B.1: The value of the error function.

x	erf(x)
0.00	0
0.50	0.056372
0.10	0.112463
0.15	0.167996
0.20	0.222703
0.25	0.276326
0.30	0.328627
0.35	0.379382
0.40	0.428392
0.45	0.475482
0.50	0.520500
0.55	0.563323
0.60	0.603856
0.65	0.642029
0.70	0.677801
0.75	0.711156
0.80	0.742101
0.85	0.770668
0.90	0.796908
0.95	0.820891
1.00	0.842701
1.10	0.880205
1.20	0.910314
1.30	0.934008
1.40	0.952285
1.50	0.966105
1.60	0.976348
1.70	0.983790
1.80	0.989091
1.90	0.992790
2.00	0.995322
2.10	0.997021
2.20	0.998137
2.30	0.998857
2.40	0.999311
2.50	0.999593
2.60	0.999764
2.70	0.999866
2.80	0.999925
2.90	0.999959
3.00	0.999978

$$(x_1 - x_2)^3 \begin{bmatrix} a \\ b \\ c \\ d \end{bmatrix} = \tag{B.5}$$

$$\begin{bmatrix} -2 & 2 & (x_1 - x_2) & (x_1 - x_2) \\ 3(x_1 + x_2) & -3(x_1 + x_2) & -(x_1 + 2x_2)(x_1 - x_2) & -(2x_1 + x_2)(x_1 - x_2) \\ -6x_1x_2 & 6x_1x_2 & x_2(x_1 - x_2)(2x_1 + x_2) & x_1(x_1 - x_2)(x_1 + 2x_2) \\ x_2^2(3x_1 - x_2) & x_1^2(x_1 - 3x_2) & -x_1x_2^2(x_1 - x_2) & -x_1^2x_2(x_1 - x_2) \end{bmatrix} \begin{bmatrix} y_1 \\ y_2 \\ w_1 \\ w_2 \end{bmatrix}$$

The program Quadfit was written to determine the coefficients for an arbitrary number of cubic spline interpolations to the error function values. The program was written in Symantec's Think Pascal and run on a Macintosh LC475. The error function for values of x from -3 to +3 were divided into 12 segments and a set of 12 equations were generated to calculate the erf(x) for any value of x. The interpolated values agreed with the tabulated values to the fourth decimal place which was a sufficient accuracy for the calculations of this thesis.

```
program Quadfit;

 type
  data = array[1..100] of real;
  coeff = array[1..30] of real;

 var
  infile, outfile: text;
  Name, Save, Menu: string;
  i, j, subdiv: integer;
  incr, factor: real;
  x1, x2, y1, y2, w1, w2: real;
  a, b, c, d: coeff;
  xpoints, ypoints: data;

 procedure Searchy (x: real; var y: real; xpts, ypts: data);
  var
   k: integer;
 begin
  k := 0;
  repeat
   k := k + 1;
  until xpts[k] = x;
  y := ypts[k];
 end;

 procedure Calcderiv (x: real; var w: real);
```

```
 begin
  w := (2 / Sqrt(Pi)) * Exp(-x * x);
 end;

begin

 Writeln('This program is specifically written to');
 Writeln('fit the erf in the region -3 to +3');
 Writeln('You will be asked to open the appropriate file.');
 Writeln('Hit Return to continue');
 Readln;

 Name := Oldfilename(Menu);
 Open(infile, Name);
 for i := 1 to 81 do
  begin
   Read(infile, xpoints[i]);
   Read(infile, ypoints[i]);
   if i < 81 then
    Readln(infile);
  end;


 Writeln('How many subdivisions for the quadfit?');
 Readln(subdiv);

 Writeln('You will be asked for a filename to save the data as');
 Writeln('File format will be:number of subdivisions followed by the');
 Writeln('coefficients for the same number of cubic equations.');
 Writeln('Hit Return to continue.');
 Readln;

 Save := Newfilename(Menu);
 Open(outfile, Save);
 Writeln(outfile, subdiv);

 incr := 6 / subdiv;
 x1 := -3;
 x2 := x1 + incr;
 for j := 1 to subdiv do
  begin
   Searchy(x1, y1, xpoints, ypoints);
   Searchy(x2, y2, xpoints, ypoints);
   Calcderiv(x1, w1);
   Calcderiv(x2, w2);
   Factor := 1 / ((x1 - x2) * (x1 - x2) * (x1 - x2));
   a[j] := Factor * (-2 * y1 + 2 * y2 + (x1 - x2) * (w1)
           + (x1 - x2) * (w2));
   b[j] := Factor * (3 * (x1 + x2) * y1 - 3 * (x1 + x2) * y2
           - (x1 + 2 * x2) * (x1 - x2) * w1
           - (2 * x1 + x2) * (x1 - x2) * w2);
   c[j] := Factor * (-6 * x1 * x2 * y1 + 6 * x1 * x2 * y2
           + x2 * (x1 - x2) * (2 * x1 + x2) * w1
           + x1 * (x1 - x2) * (x1 + 2 * x2) * w2);
   d[j] := Factor * (x2 * x2 * (3 * x1 - x2) * y1
```

```
            + x1 * x1 * (x1 - 3 * x2) * y2
            - x1 * x2 * x2 * (x1 - x2) * w1
            - x1 * x1 * x2 * (x1 - x2) * w2);
   Writeln(outfile, a[j] : 5 : 6, ' ', b[j] : 5 : 6, '  ',
            c[j] : 5 : 6, ' ', d[j] : 5 : 6);

   x1 := x2;
   x2 := x2 + incr;
  end;
 Close(infile);
 Close(outfile);
end.
```

B.2 Fickian Distributions

The theoretical distributions of Section 6.4.1 were computed using the following program written in Symantec's Think Pascal and run on a Macintosh LC475. The program uses the cubic equations determined in Section B.1 to interpolate between the values of erf(x) given in Table B.1 allowing for the rapid calculation of concentrations distributions based on Equations 6.7 or 6.8. The program listing here is specific for the case of diffusion into a limited region but the same program can be used for the case of diffusion out of a limited region by substituting Equation 6.7 in procedure CalcDiff.

```
program Diffusion_Curve;
 type
  dataarray = array[1..2, 1..128] of real;
  theoretical = array[1..2, 1..1000] of real;
  many1 = array[0..9] of string[1];
  many2 = array[0..99] of string[2];
  coeff = array[1..50] of real;
 var
  ext1: many1;
  ext2: many2;
  incr, Diff, dincr, xprime1, xprime2: real;
  denom, erf1, erf2, chi2: real;
  subdiv, dnum: integer;
  a, b, c, d: coeff;
  x, conc, time, thickness, temp: real;
  segment: real;
  numpoints, n, m, j, k: integer;
  data: dataarray;
  diffcurve, swelled: theoretical;
  rootname, filename, period: string;


(*************************************************************)
```

```
(*Require the values of erf(x) to compute the diffusion curves. *)
(*Previously computed values of erf(x) are available in tables. *)
(*The previously determined cubic splines are incorporated in   *)
(*this program so that the erf of any value can be rapidly      *)
(*determined.                                                   *)
(****************************************************************)
 procedure Coefficients (var sd: integer; var aa, bb, cc, dd: coeff);
 begin
(*number of cubic splines used in the interpolation*)
  sd := 12;

(*Coefficients for each cubic spline*)

  aa[1] := 0.00311;
  bb[1] := 0.0277;
  cc[1] := 0.082357;
  dd[1] := -0.918224;

  aa[2] := 0.023045;
  bb[2] := 0.17404;
  cc[2] := 0.440291;
  dd[2] := -0.626543;

  aa[3] := 0.090917;
  bb[3] := 0.575578;
  cc[3] := 1.231973;
  dd[3] := -0.10635;

  aa[4] := 0.161688;
  bb[4] := 0.902506;
  cc[4] := 1.735056;
  dd[4] := 0.151537;

  aa[5] := 0.020344;
  bb[5] := 0.509449;
  cc[5] := 1.372974;
  dd[5] := 0.041168;

  aa[6] := -0.299353;
  bb[6] := 0.025082;
  cc[6] := 1.128379;
  dd[6] := 0;

  aa[7] := -0.299353;
  bb[7] := -0.025082;
  cc[7] := 1.128379;
  dd[7] := 0;

  aa[8] := 0.020344;
  bb[8] := -0.509449;
  cc[8] := 1.372974;
  dd[8] := -0.041168;

  aa[9] := 0.161688;
  bb[9] := -0.902506;
  cc[9] := 1.735056;
```

```
  dd[9] := -0.151537;

  aa[10] := 0.090917;
  bb[10] := -0.575578;
  cc[10] := 1.231973;
  dd[10] := 0.10635;

  aa[11] := 0.023045;
  bb[11] := -0.17404;
  cc[11] := 0.440291;
  dd[11] := 0.626543;

  aa[12] := 0.00311;
  bb[12] := -0.0277;
  cc[12] := 0.082357;
  dd[12] := 0.918224;
 end;

(*****************************************************************)
(*Computes extension strings from 000 to 999 for output files   *)
(*****************************************************************)
 procedure Extensionstrings (var e1: many1; var e2: many2);
  var
   i, j, k: integer;
   Period: string;
 begin
(*The following prepares arrays to compute*)
(*file extensions from 000 to 999 *)

  for i := 0 to 9 do
   e1[i] := Chr(i + 48);
(* Ord('0') = 48, Ord('9') = 57 for the Mac LC475*)

  k := 0;
  for i := 0 to 9 do
   for j := 0 to 9 do
    begin
     e2[k] := concat(e1[i], e1[j]);
     k := k + 1;
    end;
 end;

(*****************************************************************)
(*Determines in which segment the distance xx belongs, the cubic*)
(*spline for the erf calculation and returns the value of erf(xx)*)
(*****************************************************************)
 function Quad_erf (xx: real; sdv: integer;
  aaa, bbb, ccc, ddd: coeff): real;
  var
   step: real;
   lowerlevel, upperlevel: real;
   j: integer;
 begin
  if (xx < -3) or (xx > 3) then
   begin
    if xx < -3 then
```

```
    Quad_erf := -1.0;
   if xx > 3 then
    Quad_erf := 1.0;
  end

 else

  begin
   step := 6 / sdv;
   j := 1;
   lowerlevel := -3;
   upperlevel := lowerlevel + step;

   while upperlevel <= 3 do
    begin
     if (xx >= lowerlevel) and (xx <= upperlevel) then
      begin
      Quad_erf := aaa[j] * xx * xx * xx + bbb[j] * xx * xx
       + ccc[j] * xx + ddd[j];
      end
     else
      j := j + 1;
     lowerlevel := upperlevel;
     upperlevel := upperlevel + step;

    end;
  end;
end;

(*****************************************************************)
(*Asks for various parameters such as number of points and the  *)
(*time and the diffusion coefficients for the calculation       *)
(*****************************************************************)
 procedure GetInfo (var gidiff, gidincr, gitime, githick: real;
  var ginum, gidnum: integer; var gidata: dataarray;
  var giname: string);
  var
   Name, Menu: string;
   j: integer;
   temp1, temp2, temp3: real;
   infile: text;

 begin
  Writeln('This program calculates a water distribution assuming
   Fickian diffusion');
  Writeln;
  Writeln('Enter in the number of points in the distribution');
  Readln(ginum);
  Writeln;
  Writeln('Enter in:  start value for diffusion coefficient (space)
   increment (space) # increments');
  Readln(gidiff, gidincr, gidnum);
  Writeln;
  Writeln('Enter in the original thickness of the tablet');
  Readln(githick);
  Writeln('Enter in the time in seconds for the file you are about
```

```
   to open');
  Readln(gitime);

  Name := Oldfilename(menu);
  Open(infile, Name);
  for j := 1 to ginum do
   begin
    Readln(infile, temp1, temp2, temp3); (*temp3 is the error*)
    if temp1 > 0 then
     begin
      gidata[1, j] := temp1; (*distance*)
      gidata[2, j] := temp2
     end;
   end;
  Writeln('Enter in the rootname for the saved files.  Hit Return');
  Readln;
  giname := Newfilename(menu);
 end;

(*****************************************************************)
(*Calculates the concentration distribution based on Fickian     *)
(*into a limited region for the water distributions or out of a *)
(*limited region for the polymer and drug distributions          *)
(*****************************************************************)
procedure CalcDiff (cdDiff, cdtime, cdthick, cdsegment: real;
  cdsubdiv: integer; var cddiffcurve: theoretical;
  aa, bb, cc, dd: coeff);
  var
   denom, x, xprime1, erf1, xprime2, erf2, Co: real;
   i: integer;
 begin
  Co:=1; (*for normalized water concentrations*)
  denom := Sqrt(4 * cdDiff * cdtime);
  x := 0;
  i := 1;
  repeat
   begin
    xprime1 := (cdthick - x) / denom;
    erf1 := Quad_erf(xprime1, cdsubdiv, aa, bb, cc, dd);
    xprime2 := (cdthick + x) / denom;
    erf2 := Quad_erf(xprime2, cdsubdiv, aa, bb, cc, dd);

(*distance*)
    cddiffcurve[1, i] := x;
(*concentration for the distance*)
    cddiffcurve[2, i] := 0.5 * Co * ((1 - erf1) + (1 - erf2));
(*would use cddiffcurve[2, i] := 0.5 * Co * (erf1 + erf2) for*)
(*diffusion out of a limited region*)
    x := x + cdsegment;
    i := i + 1;
   end;
  until x > 1;
 end;

(*****************************************************************)
(*Compares the theoretical and actual distributions and computes*)
```

```
(*the values of chi2                                                    *)
(************************************************************)
 procedure Compare (compnum: integer; cdiffcurve: theoretical;
  csegment: double; cdata: dataarray; var cchi2: double);
  var
   i, j: integer;
   m, b, cdtest: double;
   test: boolean;

 begin
  cchi2 := 0;
  cdtest := 0;
  test := false;
  for i := 1 to compnum do
   begin
    j := 0;
    repeat
     j := j + 1;
     if (cdata[1, i] >= cdiffcurve[1, j]) and
      (cdata[1, i] <= cdiffcurve[1, j + 1]) then
      begin
       test := true;
       m := (cdiffcurve[2, j] - cdiffcurve[2, j + 1])
         / (cdiffcurve[1, j] - cdiffcurve[1, j + 1]);
       b := cdiffcurve[2, j] - m * cdiffcurve[1, j];
       cdtest := m * cdata[1, i] + b;
      end
     else
      test := false;
    until test = true;
    cchi2 := cchi2 + (cdata[2, i] - cdtest) * (cdata[2, i] - cdtest);
   end;
 end;

(************************************************************)
(*Outputs the theoretical concentrations distribution and the   *)
(*value of the diffusion coefficient and resulting chi2 of the  *)
(*comparison between the experimental and theoretical distributions*)
(************************************************************)
procedure WriteFile (wfname: string; wfsegment: real;
  wfdiffcurve: theoretical; wfdiff, wfchi2: real);
  var
   k: integer;
   tempname: string;
   outfile: text;
   temp: real;
 begin
  Open(outfile, wfname);
  Writeln(outfile, '    ', '    ',
   wfdiff : 10 : 10, '  ', wfchi2 : 10 : 10);
  k := 1;
  temp := 0;
  repeat
   Writeln(outfile, wfdiffcurve[1, k] : 3 : 3, '    ',
    wfdiffcurve[2, k] : 3 : 3);
   k := k + 1;
```

```
   temp := temp + wfsegment;
  until temp > 1;

  Close(outfile);
 end;

(*****************************************************************)
(*Main program that calls the procedures                         *)
(*****************************************************************)
begin
(*the following setup various arrays that will be used in the *)
(*calculations and the outputting of the data files*)
 Coefficients(subdiv, a, b, c, d);
 Extensionstrings(ext1, ext2);

(*require various parameters to perform the calculation*)
 GetInfo(Diff, dincr, time, thickness, numpoints, dnum, data, rootname);

 j := 0;
 k := 0;
 period := '.';
 segment := 0.005;

(*loop for incrementing the diffusion coefficient*)
 for n := 1 to dnum do
  begin

(*calculates the theoretical concentration distribution*)
   CalcDiff(Diff, time, thickness, segment, subdiv,
    diffcurve, a, b, c, d);

(*determines the chi2 value*)
   Compare(numpoints, diffcurve, segment, data, chi2);

(*increments the extension counters for the output file*)
   if j = 99 then
    begin
     k := k + 1;
     j := -1;
    end;
   j := j + 1;

(*outputs data to the file and to the screen*)
   filename := concat(rootname, period, ext1[k], ext2[j]);
   Writeln(filename : 50, ' ', Diff : 12 : 12, '    ', chi2 : 10 : 10);
   WriteFile(filename, segment, diffcurve, Diff, chi2);

(*increments the diffusion coefficient*)
   Diff := Diff + dincr;
  end;
end.
```

B.3 Segmented Tablet Model

The theoretical distributions of Section 6.4.2 were computed using the following program written in Symantec's Think Pascal and run on a Macintosh LC475. The program calculates the theoretical water distribution into the dry tablet using Equation 6.9 and then determines the degree of swelling for each segment, the new position of each segment and the resulting polymer weight percent concentration for the segment using Equations 6.12 and 6.13. An initial polymer concentration of 97% ensured that the resulting distribution contained 166 mg of polymer regardless of the degree of swelling. The factor for the swelling is included in procedures Swelling and DoSum and can be easily modified.

```
program conc;
 type
  dataarray = array[1..2, 1..128] of double;
  theoretical = array[1..2, 1..800] of double;
  many1 = array[0..9] of string[1];
  many2 = array[0..99] of string[2];
  coeff = array[1..50] of double;
 var
  ext1: many1;
  ext2: many2;
  thickness, time: double;
  diff, diffincr, distincr, dtemp: double;
  alpha, alphaincr, atemp: double;
  chi2: double;
  diffcurve, swelled: theoretical;
  numpoints, diffnum, alphanum: integer;
  a, d, j, k, ratio: integer;
  rootname, filename, period: string;
  data: dataarray;

(*****************************************************************)
(*prepares arrays to compute file extensions from 000 to 999     *)
(*****************************************************************)
procedure Extensionstrings (var e1: many1; var e2: many2);
  var
   i, j, k: integer;
   Period: string;
 begin
  for i := 0 to 9 do
   e1[i] := Chr(i + 48);
(* Ord('0') = 48, Ord('9') = 57 for the Mac LC475*)

  k := 0;
  for i := 0 to 9 do
   for j := 0 to 9 do
    begin
     e2[k] := concat(e1[i], e1[j]);
     k := k + 1;
```

```
    end;
 end;

(*****************************************************************)
(*Reads in the various parameters required for the calculations *)
(*****************************************************************)
procedure GetInfo (var gidiff, gidincr, gialpha, giaincr,
  gitime, githick: double; var ginum, gidnum, gianum: integer;
  var gidata: dataarray; var giname: string);
  var
   Name, Menu: string;
   j: integer;
   temp1, temp2, temp3: double;
   infile: text;
 begin
  Writeln('This program calculates a water distribution assuming
   Fickian diffusion');
  Writeln('and then uses it to calculate the swelling of the polymer');
  Writeln;
  Writeln('Enter in the number of points in the distribution');
  Readln(ginum);
  Writeln;
  Writeln('Enter in the water diffusion coefficient, the increment
   and the number of  increments');
  Readln(gidiff, gidincr, gidnum);
  Writeln;
  Writeln('Enter in the alpha factor, alpha increment and number
   of  increments');
  Readln(gialpha, giaincr, gianum);
  Writeln;
  Writeln('Enter in the original thickness of the tablet');
  Readln(githick);
  Writeln;
  Writeln('Enter in the time in seconds for the file you are
   about to open');
  Readln(gitime);

  Name := Oldfilename(menu);
  Open(infile, Name);
  for j := 1 to ginum do
   begin
    Readln(infile, temp1, temp2, temp3); (*temp3 is the error*)
    if temp1 > 0 then
     begin
      gidata[1, j] := temp1; (*distance*)
      gidata[2, j] := temp2
     end;
   end;
  Writeln('Enter in the rootname for the saved files.  Hit Return');
  Readln;
  giname := Newfilename(menu);
 end;

(*****************************************************************)
(*Calculates the theoretical water distribution                  *)
(*****************************************************************)
```

```
procedure Calculation (hh, tt, DD, xincr: double;
 var tempresults: theoretical; cratio: integer);
 var
  x, incr, temp1, temp2, temp3, BigSum, conc, water: double;
  m, n, posneg, points: integer;
begin
 x := xincr;
 m := 0;
 repeat
  Bigsum := 0;
  m := m + 1;
  (*the sum converged before n=10 under the conditions of *)
  (*the experiments in this thesis*)
  for n := 0 to 10 do
   begin
    if n mod 2 = 0 then
     posneg := 1
    else
     posneg := -1;
    temp1 := posneg / (2 * n + 1);
    temp2 := cos((2 * n + 1) * Pi * x / (2 * hh));
    temp3 := exp(-(2 * n + 1) * (2 * n + 1) * Pi * Pi * dd * tt
     / (4 * hh * hh));
    Bigsum := (temp1 * temp2 * temp3) + Bigsum;
   end;

  conc := 1 - (4 / Pi) * Bigsum;
  tempresults[1, m] := x;
  tempresults[2, m] := conc;

  x := x + xincr;
 until m = cratio;
end;

(*****************************************************************)
(*Performs the sum of the previous segment swellings to compute *)
(*the new distance for the current segment                       *)
(*****************************************************************)
function DoSum (dssegment, dsalpha: double; dsi: integer;
 dsdiffcurve: theoretical): double;
 var
  m: integer;
  Sum: double;
begin
 Sum := 0;
 m := 0;
 repeat
  m := m + 1;
  Sum := Sum + dssegment * ((dsalpha/ (1 - dsdiffcurve[2, m])) - 1);
 until m = dsi;
 DoSum := Sum;
end;

(*****************************************************************)
(*Calculates the new distance and concentration for each segment*)
(*based on the theoretical concentration of water               *)
```

```
(*************************************************************)
 procedure Swell (sratio: integer; ssegment, salpha: double;
  sdiffcurve: theoretical; var sswelled: theoretical);
  var
   j: integer;
   sfactor: double;
 begin
  j := 0;
  repeat
   j := j + 1;
   sswelled[1, j] := sdiffcurve[1, j] +
    DoSum(ssegment, salpha, j, sdiffcurve);
   sswelled[2, j] := 97 * (1 - sdiffcurve[2, j]) / salpha;
  until j = sratio;
 end;

(*************************************************************)
(*Compares the theoretical and actual distributions and computes*)
(*the values of chi2                                         *)
(*************************************************************)
 procedure Compare (compnum: integer; cdswelled: theoretical;
  csegment: double; cdata: dataarray; var cchi2: double);
  var
   i, j: integer;
   m, b, cdtest: double;
   test: boolean;
 begin
  cchi2 := 0;
  cdtest := 0;
  test := false;
  for i := 1 to compnum do
   begin
    j := 0;
    repeat
     j := j + 1;
     if (cdata[1, i] >= cdswelled[1, j]) and
      (cdata[1, i] <= cdswelled[1, j + 1]) then
      begin
       test := true;
       m := (cdswelled[2, j] - cdswelled[2, j + 1])
        / (cdswelled[1, j] - cdswelled[1, j + 1]);
       b := cdswelled[2, j] - m * cdswelled[1, j];
       cdtest := m * cdata[1, i] + b;
      end
     else
      test := false;
    until test = true;
    cchi2 := cchi2 + (cdata[2, i] - cdtest) * (cdata[2, i] - cdtest);
   end;
 end;

(*************************************************************)
(*Writes the swelled distribution and the various parameters  *)
(*to an output file                                          *)
(*************************************************************)
procedure WriteFile (wfname: string; wnumpoints: integer;
```

```
  wfswelled: theoretical; wfdiff, wfalpha, wfchi2: double);
  var
   k: integer;
   outfile: text;
 begin
  Open(outfile, wfname);
  Writeln(outfile, '    ', '    ', wfdiff : 10 : 10, '  ',
   wfalpha : 10 : 10, ' ', wfchi2 : 10 : 10);
  for k := 1 to wnumpoints do
   Writeln(outfile, wfswelled[1, k] : 8 : 8, '  ',
    wfswelled[2, k] : 6 : 6);
  Close(outfile);
 end;

(*****************************************************************)
(*Main Program.  Contains the counters for incrementing the values*)
(*of the diffusion coefficient and the swelling factor alpha.    *)
(*Calls the procedures required to calculate the theoretical     *)
(*water distribution and then swell the tablet according to the *)
(*amount of water present and the swelling factor                *)
(*****************************************************************)
begin
 Extensionstrings(ext1, ext2);
 GetInfo(Diff, diffincr, alpha, alphaincr, time, thickness,
  numpoints, diffnum, alphanum, data, rootname);
 distincr := 0.001;
 period := '.';
 ratio := Round(thickness / distincr) - 1;
 Writeln(rootname);
 Writeln(' #    ', '    Diff    ', '   alpha   ', '     chi2    ');
 d := 0;
 repeat
  dtemp := diff + d * diffincr;
  Calculation(thickness, time, dtemp, distincr, diffcurve, ratio);
  a := 0;
  repeat
   atemp := alpha + a * alphaincr;
   Swell(ratio, distincr, atemp, diffcurve, swelled);
   Compare(numpoints, swelled, distincr, data, chi2);
   if j = 99 then
    begin
     k := k + 1;
     j := -1;
    end;
   j := j + 1;
   filename := concat(rootname, period, ext1[k], ext2[j]);
   Writeln(concat(ext1[k], ext2[j]), '          ', dtemp : 10 : 10,
    '       ', atemp : 3 : 3, '     ', chi2 : 10 : 10);
   WriteFile(filename, ratio, swelled, dtemp, atemp, chi2);
   a := a + 1;
  until a = alphanum;
  d := d + 1;
 until d = diffnum;
end.
```